Bacterial Danger Sensing Protects Against Bacteriophage Predation

Dissertation

zur Erlangung des Grades eines

Doktor der Naturwissenschaften

(Dr. rer. nat.)

des Fachbereichs Biologie

der Philipps-Universität Marburg

Vorgelegt von

Sanika Vaidya

aus Ahmedabad, Indien

Marburg, Mai 2021

Bacterial Danger Sensing Protects Against Bacteriophage Predation

Dissertation

for Obtainment of a

Scientific Doctorate

(Dr. rer. nat.)

submitted to the Faculty of Biology,

Philipps University, Marburg

by

Sanika Vaidya

from Ahmedabad, India

Marburg, May 2021

Die vorliegende Dissertation wurde von November 2016 bis Mai 2021 am Max-Planck Institut für terrestrische Mikrobiologie unter Leitung von Prof. Dr. Knut Drescher angefertigt.

Vom Fachbereich Biologie der Philipps-Universität Marburg (Hochschulkennziffer 1180) als Dissertation angenommen am

Erstgutachter: Prof. Dr. Knut Drescher
Zweitgutachter: Dr. Lennart Randau

Tag der Disputation: 02 Juli 2021

To my parents,
who encouraged me to pursue my dreams

and

to my teachers,
who showed me the way.

Erklärung

Ich versichere, dass ich meine Dissertation mit dem Titel:

Bacterial Danger Sensing Protects Against Bacteriophage Predation

selbstständig und ohne unerlaubte Hilfe angefertigt und ich mich dabei keiner anderen als der von mir ausdrücklich bezeichneten Quellen und Hilfsmittel bedient habe.

Diese Dissertation wurde in der jetzigen oder einer ähnlichen Form noch bei keiner anderen Hochschule eingereicht und hat noch keinen sonstigen Prüfungszwecken gedient.

Marburg, 12 Mai 2021

Sanika Vaidya

Declaration of Originality

I, Sanika Vaidya, hereby declare that the work presented in this thesis, titled:

Bacterial Danger Sensing Protects Against Bacteriophage Predation

is my own work and has been performed without the help of third parties and only with the described sources and resources. Any work carried out by anyone other than myself, be it published or unpublished, has been acknowledged and clearly credited in the relevant places. Any resources or ideas that are from the work of others has been referenced and a full bibliography can be found at the end of the thesis. This thesis has not yet been submitted to any examining authority in the same or a similar form.

Marburg, 12 Mai 2021

Sanika Vaidya

Contents

Abstract

Bacterial adaptability to unfavourable conditions, in the environment or in their eukaryotic hosts, is essential for survival and proliferation. Bacteria also have to frequently contend with bacteriophages (simply termed phages) that pose a serious threat to bacterial survival. Phages are natural predators of bacteria and utilise bacterial cells as a host for replication and subsequently, release their progeny by lysing bacterial cells. Bacteria show augmented resilience against changing environmental conditions when they exist as matrix-embedded communities, termed biofilms. This matrix comprises of secreted polysaccharides and proteins that encase bacterial cells, making them more adept at surviving phage attack as compared to their planktonic counterparts. Although biofilm formation has been shown to be an advantage in bacterial survival against phage predation, the mechanism of how bacteria sense the presence of biotic stresses, such as phages, and how they initiate biofilm formation as a response is unknown.

To investigate phage-bacteria interactions, the model organism *Vibrio cholerae* was used. *V. cholerae* is a human pathogen, responsible for causing the disease cholera. *V. cholerae* cells form biofilms to survive in their aquatic environment, as well as in the human host. Furthermore, in both of these environments, *V. cholerae* cells encounter phages that have been shown to constrict the growth of *V. cholerae* communities and contribute to their evolution. One of the lytic phages that was co-isolated with *V. cholerae*, responsible for infecting a range of *V. cholerae* strains, called Vibriophage N4, was used as the viral agent in this study.

The results described in this thesis show that *V. cholerae* actively forms biofilms in response to the exposure of Vibriophage N4. This bacterial response was neither caused by the selection of phage resistant mutants, nor by hyper matrix-producing mutants. A combined approach of proteomics and transcriptomics uncovered that cells initiated the production of biofilm matrix components upon phage exposure. Biofilm matrix production was also confirmed using fluorescence confocal microscopy. When embedded in the biofilm matrix, *V. cholerae* cells were protected from phage predation. However, phage infection was successful at early time points prior to biofilm formation, and counterintuitively, biofilm formation was always preceded by initial cell lysis. This led to the hypothesis that phage-induced cell lysis was necessary for bacteria to elicit a biofilm response. By exposing *V. cholerae* cells to sonicated bacterial lysates, it was confirmed that biofilm formation in *V. cholerae* was triggered not by the phages themselves, but by a component of lysed bacterial cells. Moreover, this biofilm-inducing factor was found to be general to lysates obtained from various Gram-negative and -positive bacteria. By identifying the cellular fraction from which the biofilm-inducing factor originated, the signal for inducing biofilm formation was determined to

be peptidoglycan. The detection of peptidoglycan fragments from lysed cells served as an indirect signal for the presence of lysis-inducing entities (such as phages), and therefore, this signalling was referred to as bacterial danger sensing. Transcriptomics was used to characterise the bacterial response to peptidoglycan and consequently, genes related to the production of an intracellular secondary messenger molecule, c-di-GMP, were found to be upregulated. Additionally, genes encoding biofilm matrix components were also upregulated, similar to the proteome and transcriptome profile of cells that survived phage infection. The production of c-di-GMP and biofilm matrix in *V. cholerae* cells during peptidoglycan exposure was visualised by fluorescence confocal microscopy. As c-di-GMP has been known to play a crucial role in inducing bacterial biofilm formation, it was likely that peptidoglycan exposure induced biofilm formation in *V. cholerae via* c-di-GMP. Peptidoglycan was also found to be a relevant signal for inducing biofilm formation in *Pseudomonas aeruginosa*, suggesting that danger sensing could be conserved in bacteria. These results demonstrate how danger sensing induces bacterial biofilm formation to facilitate a rapid and general response to protect cells against phages, and potentially, other lytic stresses.

Zusammenfassung

Die Anpassungsfähigkeit von Bakterien an ungünstige Bedingungen, in der Umwelt oder in ihren eukaryotischen Wirten, ist für das Überleben und die Vermehrung von Bakterien essentiell. Bakterien sind häufig Bakteriophagen (einfach als Phagen bezeichnet) ausgesetzt, die eine ernsthafte Bedrohung für das bakterielle Überleben darstellen. Phagen sind natürliche Predatoren von Bakterien, da sie Bakterienzellen als Wirt für die Replikation nutzen und anschließend ihre Nachkommenschaft durch Lyse der Wirtszelle freisetzen. Bakterien zeigen eine erhöhte Widerstandsfähigkeit gegenüber sich ändernden Umweltbedingungen, wenn sie als zelluläre Gemeinschaft, eingebettet in selbst produzierter Matrix, leben. Solche bakteriellen Gemeinschaften werden auch als Biofilme bezeichnet. Die Matrix besteht aus sekretierten Polysacchariden und Proteinen, welche die Bakterienzellen umhüllen und sie im Vergleich zu planktonischen Zellen schützen, Phagenangriffe zu überleben. Obwohl sich die Biofilmbildung als Vorteil für das Überleben von Bakterien gegen Phagenbefall erwiesen hat, ist der Mechanismus, wie Bakterien die Anwesenheit von biotischen Stressfaktoren wie Phagen wahrnehmen und wie sie die Biofilmbildung als Reaktion darauf initiieren, unbekannt.

Um die Interaktionen zwischen Phagen und Bakterien zu untersuchen, wurde der Modellorganismus *Vibrio cholerae* verwendet. *V. cholerae* ist ein humaner Krankheitserreger und verursacht die Krankheit Cholera. *V. cholerae*-Zellen bilden Biofilme, um sowohl in ihrer aquatischen Umgebung als auch im menschlichen Wirt zu überleben. Darüber hinaus treffen *V. cholerae*-Zellen in diesen beiden Habitaten auf Phagen, die nachweislich das Wachstum von *V. cholerae*-Gemeinschaften einschränken und deren Evolution beeinflussen. Einer der lytischen Phagen, der mit *V. cholerae* co-isoliert wurde und für die Infektion einer Reihe von *V. cholerae*-Stämmen verantwortlich ist, genannt Vibriophage N4, wurde in dieser Studie als virales Agens verwendet.

Die in dieser Arbeit beschriebenen Ergebnisse zeigen, dass *V. cholerae* aktiv Biofilme als Reaktion auf die Exposition mit Vibriophage N4 bildet. Diese bakterielle Reaktion wurde weder durch die Selektion von phagen-resistenten Mutanten, noch durch Hypermatrix-produzierende Mutanten verursacht. Ein kombinierter Ansatz von Proteomik und Transkriptomik deckte auf, dass die Zellen die Produktion von Biofilm-Matrix-Komponenten nach Phagen-Exposition initiierten. Die Biofilm-Matrix-Produktion wurde auch mittels konfokaler Fluoreszenzmikroskopie bestätigt. V. cholerae-Zellen waren vor Phagen geschützt, solange sie in die Biofilm-Matrix eingebettet waren. Infektion durch Phagen war jedoch möglich solange noch keine Biofilme gebildet wurden, und kontraintuitiv ging der Biofilmbildung immer eine initiale Zelllyse voraus. Dies führte zu der Hypothese, dass die Phagen-induzierte Zelllyse für die Bakterien notwendig ist,

um eine Biofilm-Antwort hervorzurufen. Indem *V. cholerae*-Zellen Bakterienlysaten ausgesetzt wurden, konnte bestätigt werden, dass die Biofilmbildung in *V. cholerae* nicht durch die Phagen selbst, sondern durch eine Komponente lysierter Bakterienzellen ausgelöst wurde. Darüber hinaus wurde festgestellt, dass dieser Biofilm-induzierende Faktor allgemein für Lysate aus verschiedenen gramnegativen und -positiven Bakterien gilt. Durch die Identifizierung der zellulären Fraktion, aus der der Biofilm-induzierende Faktor stammte, wurde Peptidoglykan als das Signal zur Induktion der Biofilmbildung entdeckt. Das Erkennen von Peptidoglykanfragmenten aus lysierten Zellen diente als indirektes Signal für die Anwesenheit von lyse-induzierenden Entitäten (wie z. B. Phagen), weshalb es sich bei diesem Phänotyp um eine bakterielle Erkennung von Gefahr handelt. Mit Hilfe der Transkriptomik wurde die bakterielle Reaktion auf Peptidoglykan charakterisiert, und es wurde festgestellt, dass Gene, die mit der Produktion eines intrazellulären sekundären Botenmoleküls, c-di-GMP, zusammenhängen, hochreguliert sind. Zusätzlich wurden auch Gene, die für Komponenten der Biofilm-Matrix kodieren, hochreguliert, ähnlich dem Proteom- und Transkriptom-Profil von Zellen, die eine Phagen-Infektion überlebt haben. Die Produktion von c-di-GMP und Biofilm-Matrix in *V. cholerae*-Zellen während der Peptidoglykan-Exposition wurde mittels konfokaler Fluoreszenzmikroskopie visualisiert. Da bekannt ist, dass c-di-GMP eine entscheidende Rolle bei der Induktion der bakteriellen Biofilmbildung spielt, war es wahrscheinlich, dass die Peptidoglykan-Exposition die Biofilmbildung in *V. cholerae* über c-di-GMP reguliert. Peptidoglykan erwies sich auch als relevantes Signal für die Induktion der Biofilmbildung in *Pseudomonas aeruginosa*, was darauf hindeutet, dass die Erkennung von Gefahren in Bakterien konserviert sein könnte. Diese Ergebnisse zeigen, wie Gefahren-Signale die bakterielle Biofilmbildung induziert, um eine schnelle und allgemeine Reaktion zum Schutz der Zellen gegen Phagen und möglicherweise andere lytische Belastungen zu ermöglichen.

Acknowledgements

I would like to thank Prof. Dr. Knut Drescher for giving me the opportunity to pursue a PhD in his laboratory. The past and current members of the group have provided invaluable contributions during the process of research and I am grateful for all that I have learnt working with these talented scientists! The scientific discussions that I have had with the following people were vital in the overall success (or sometimes, non-success) of tested theories: specifically, I would like to acknowledge Dr. Praveen K. Singh, Dr. Eric Jelli, Mads F. Hansen, and Dr. Kazuki Nosho, who contributed scientifically to the research described in this thesis. I would also like to mention Dr. Lucia Vidakovic, Daniel Rode, Violina Potlog, Dr. Raimo Hartmann, Dr. Carey Nadell, and Miriam Bayer with whom I've had the pleasure of working with over the past 4.5 years.

During my time as a PhD student, Marburg has become a second home and I am extremely grateful to my Marburg family. Neha, Praveen, Lucia, Keerthana, Miriam, and Daniel - I wouldn't have made it through without you guys! I am also grateful to my virtual support system: Matt, Spruha, Anja, Rachana, and Indrajit - thank you always being just a phone call away! A heartfelt thank you to my family in India and Europe, who have always been a source of inspiration and fun. Kaustubh-dada, your words of advice and encouragement always reinvigorated my scientific spirit! Vandana, Kaustubh, and Sameer - thank you for making home so much closer.

It is my belief that scientists are not born, they are cultivated. Thank you to my amazing teachers and mentors over the years who instilled in me a passion to become a scientist. Miss T, Mrs. Falguni De, Dr. Bindu Unnikrishnan, Dr. Sutirth Dey, Dr. Julia van Kessel, and Dr. Andrew Edwards - you saw something in me before I saw it myself and for this, I am eternally grateful.

The most important acknowledgment of all goes to my wonderful parents, who have supported and encouraged me all my life. Without your teachings, and your unwavering and unconditional love, I wouldn't be here today. I am what I am because of you.

List of Figures

List of Tables

Abbreviations

3D	three-dimensional
AHL	acyl-homoserine lactone
ATP	adenosine tri-phoshate
BHI	brain-heart infusion
CAI-1	cholera autoinducer-1
cAMP	cyclic adenosine 3'5'-monophosphate
CBASS	cyclic-oligonucleotide-based anti-phage signalling system
c-di-AMP	3'5'-cyclic di-adenosine monophosphate
c-di-GMP	3'5'-cyclic di-guanosine monophosphate
CFU	colony forming unit
cGAMP	3'3'cyclic GMP-AMP
cGMP	cyclic guanosine 3'5'-monophosphate
CSLC	carrier state life cycle
DGC	diguanylate cyclase
EI	enzyme I
EII	enzyme II
EOP	efficiency of plating
EPS	extracellular polymeric substances
FDR	false discovery rate
GMP	guanosine mono-phosphate
GTP	guanosine tri-phosphate
HCD	high cell density
HK	histidine kinase
LB	Luria-Bertani broth
LBD	ligand-binding domain
LCD	low cell density
LCMS	liquid chromatography–mass spectrometry
LPS	lipopolysaccharide
MCP	methyl-accepting chemotaxis protein
MOI	multiplicity of infection
NOD	nucleotide binding and oligomerisation domain
OMV	outer membrane vesicle
PASTA	penicillin-binding and Ser/Thr kinase-associated

PBS	phosphate buffered saline
PDE	phosphodiesterase
PDMS	polydimethylsiloxane
PEP	phosphoenolpyruvate
PFU	plaque forming unit
pGpG	linear di-GMP
(p)ppGpp	guanosine tetra- or penta-phosphate
PGRP	peptidoglycan recognition proteins
PTFE	poly-tetra-fluoro-ethylene
PTS	phosphotransferase system
QS	quorum-sensing
ROS	reactive oxygen species
RR	response regulator
SEM	scanning electron microscope
SOC	super optimal broth with catabolite repression
sRNA	small RNA
T4P	type IV pili
TA	toxin-antitoxin
TAE	tris-acetate-EDTA
TB	tryptone broth
TCS	two-component systems
TSB	tryptic soy broth
VPS	*Vibrio* polysaccharide
WT	wild type

1 Introduction

Before history and science, there were humans; and bacteria were there even before that. Being one of the earliest lifeforms on Earth, bacteria have all the requirements for life to fit into a single cell. The ability of bacteria to rapidly replicate, along with their ability to withstand extreme environments, is widely regarded to be the underlying cause of their ubiquity and diversity. There are estimated to be a total of 10^{30} bacteria on Earth (1), with more than a million different species found across a range of different environments (2). Their strength lies in numbers and therefore, in spite of their minuscule size, bacteria have been responsible for shaping biogeochemical cycles (3) and even influencing human history (4).

In our body, bacterial cells contribute half of our total cells (5) and most of those constitute our gut microbiome (6). The composition of our gut microbiome affects our health, behaviour and has even been shown to contribute to our personality (7, 8). In contrast, bacteria that release toxic compounds are called pathogens and are the cause of diseases such as pneumonia, tuberculosis, cholera, leprosy, and syphilis. Pathogens that are equipped with multiple antibiotic resistance mechanisms, called superbugs, cause complications in hospital-borne infections and can often be lethal. The connection between diseases and their causative bacterial agents was first identified by Robert Koch, when he cultured bacteria in his laboratory (9). His homogenous planktonic cultures became synonymous with prokaryotic life, which pinned bacteria as solitary creatures.

In recent years, however, there has been a paradigm shift in the way we study bacteria. With the advent of new technologies and broadening of subject horizons, studying bacterial phenomena has become an interdisciplinary field of research. Studies by multiple labs across the globe show us that bacteria are in fact, not solitary beings at all; but exist as communities in the environment, called biofilms. Bacteria in biofilms are embedded in a self-produced matrix and exhibit multicellular behaviour, distinct to their planktonic mode of life (10, 11). To traverse unfavourable environments and evade predation by other living entities, bacteria tune their transition from motile single cells to multicellular biofilms by sensing and responding to signals around them. Pathogenic bacteria such as *Vibrio cholerae*, *Salmonella enterica*, *Listeria monocytogenes*, *Acinetobacter baumannii*, and *Pseudomonas aeruginosa* are able to transition from their motile planktonic lifestyle to biofilms in order to efficiently survive and proliferate both in the human host, as well as in the aquatic environment (12). This thesis describes the role of a novel signal that promotes bacterial collective behaviour in order to aid bacterial survival during stressful conditions.

1.1 Bacterial biofilms

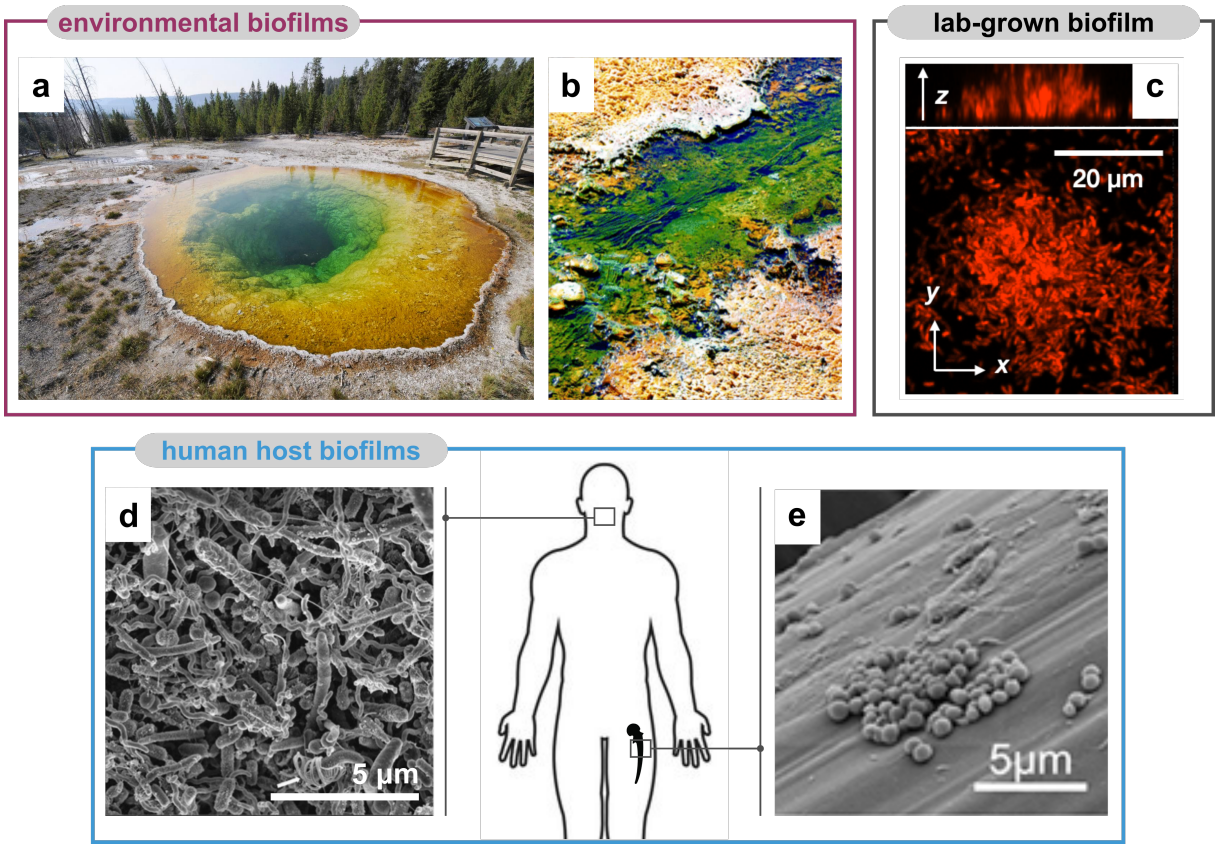

Figure 1.1: Schematic representing the ubiquity of bacterial biofilms in the natural environment and the human host. a, Bacterial biofilms can grow in extreme conditions, such as geothermal geyser basins, where the temperature is between 70-90 °C. Image is from Yellowstone National Park, USA. **b,** Biofilms in streams are beneficial for aquatic ecosystem maintenance (13). **c,** Confocal microscopy image of a *V. cholerae* biofilm grown in flow chambers under laboratory conditions. Biofilms are typically imaged one slice at a time (*xy*-plane) and all imaged slices are layered to construct the side view (z-projection). The scale bar measures $20\,\mu m$. **d,** Scanning Electron Microscope (SEM) image of a mixed species biofilm causing dental plaque (14). **e,** SEM image of a *S. aureus* biofilm formed on a surgical implant. Image is from ICFO, Spain. The scale bars measure $5\,\mu m$.

Bacteria are organisms that exist in communities, usually embedded in self-produced matrix and adhered to a surface, called biofilms (15). Biofilms constitute approximately 80% of all bacteria on Earth (16) and can comprise of multiple bacterial species that engage in a variety of complex multicellular interactions. Biofilms can be found in diverse environments (Figure 1.1a-b) such as acidic sulphuric caves in Italy (17), permanently cold and alkaline ikaite columns in Greenland (18), hydrothermal deep-sea vents (19, 20), and the hot springs of Yellowstone National Park (21). In the human host, bacterial biofilms most commonly manifest as subgingival dental plaque, catheter blockage, and implant contamination (15) (Figure 1.1d-e). Predominantly due to their ability to withstand antibiotic treatment, biofilm eradication is particularly challenging (22). Therefore, bacterial biofilms are often associated with persistent infections caused by multi-antibiotic resistant strains such as *Staphylococcus aureus* and *Pseudomonas aeruginosa* (23).

The structure of biofilms varies depending on the environmental conditions and bacterial species involved but all biofilms share a point of commonality, i.e., that they all contain extracellular polymeric substances (EPS), which is secreted by some or all bacterial cells in the biofilm (24). The presence of EPS around bacterial cells has been shown to account for the enhanced ability of biofilms to tolerate environmental stresses such as high temperature (25), pH (26), desiccation (27), as well as stresses incurred in the human host such as predation by immune cells (28) and antibiotics (29).

1.1.1 Studying bacterial biofilms

In order to uncover the mechanisms by which bacterial biofilms withstand environmental stresses, it is necessary to study their developmental processes with high spatial and temporal resolution. Microscopy-based approaches provide the best outlook for this approach (30–33). Fluorescent proteins or dyes (collectively, known as fluorophores) are used to visualise bacterial cells in a biofilm (34). Fluorescence microscopy is based on using fluorophores that absorb energy from the wavelength of light used for excitation, followed by the emission of a longer wavelength of light that is collected with a detector (usually a camera). In order to obtain three-dimensional (3D) images of bacterial biofilms with high spatial resolution, confocal microscopy is used. Confocal microscopes possess pinholes to reject out-of-focus light during specimen illumination, which results in greater image resolution, contrast, and reduced background noise (35). Therefore, the specimen is imaged one slice at a time, containing data corresponding to individual *xy*-planes. The image slices are subsequently compiled and processed to reconstruct a 3D image of the biofilm (Figure 1.1c).

Confocal microscopy typically generates a large volumes of data and therefore, relies on automated computer programs and software packages in order to extract biologically relevant information. For the quantification of the properties of biofilm-forming cells, a new software named *BiofilmQ* was developed by the Drescher research group (36). *BiofilmQ* was designed to analyse fluorescence images of biofilm-forming cells grown in various laboratory systems. Data generated for this thesis also contributed to conceptualisation of *BiofilmQ* and therefore, *BiofilmQ* was consequently used for the analysis of all acquired images described in this thesis.

1.1.2 Biofilm lifecycle

Using microscopy, cells of various bacterial species forming biofilms have been imaged. These images have revealed that even though there is a huge variation in the structure and composition of biofilms across different bacterial species, the general lifecycle of all biofilms constitutes three steps: attachment, maturation, and dispersal of bacterial cells from the biofilm (37). When bacterial cells encounter a surface *via* their flagella or type IV pili (T4P), they first reversibly, then irreversibly attach to the surface (38). The attachment phenomenon is aided by intracellular compounds like secondary messenger molecules and proteins (39). This process of mechanosensing (discussed further in section 1.4.4) drives the most well-studied initiation of biofilm formation (40). The clustering of dividing cells that are either adhered to each other or the surface (or both) results in the formation of a micro-colony. This rudimentary and homogenous structure is

followed by, or occurs in combination with the secretion of matrix components during further cell division. This step of biofilm maturation cements the bacterial cells together and differentiates the cells of the biofilm, contributing to the emergence of biofilm architecture (41). Signals originating from the environment or from within the biofilm trigger cellular dispersal from biofilms (42). Dispersing cells that have regained motility have the capability to re-attach to another surface to initiate the process all over again (43).

Our understanding of the different biofilm stages comes from studies done with bacteria such as *Vibrio cholerae*, *Escherichia coli*, *Pseudomonas aeruginosa*, and *Staphylococcus aureus*, which are considered model organisms. For this study, the model organism *Vibrio cholerae* was chosen.

1.2 *Vibrio cholerae*

Vibrio cholerae is a Gram-negative bacterium, responsible for causing cholera. It is an environmental pathogen that can enter the human host when ingested *via* contaminated food or water. In its aquatic environment, *V. cholerae* exists as biofilms, either as floating matrices or attached to a biotic or abiotic substratum (44). Biofilms play an important role not only in protection from environmental stresses, but also transmission into the human host, as ingestion of biofilms enables the intake of high numbers of pathogenic *V. cholerae* (45, 46). Furthermore, *V. cholerae* cells in the stool of a cholera patient have been found to possess a hyper-infectious phenotype and are present in biofilm-like clusters, which causes enhanced dissemination to new hosts (47, 48). The importance of its biofilm lifestyle for survival and pathogenicity accounts for the application of *V. cholerae* as a model organism to study biofilm formation.

1.2.1 Biofilm formation in *V. cholerae*

Biofilm formation is initiated by attachment by mannose-sensitive hemagglutinin (MSHA) pili, which move back and forth scanning the cells' immediate surroundings (49). When they encounter a surface, cells reversibly and then irreversibly attach *via* the action of the secretion of a matrix protein, called Bap1. The secretion of Bap1 at the cell-surface interface is thought to be necessary for initiation of micro-colony formation (50). The matrix of *V. cholerae* biofilms is sugar-rich, consisting nearly 50% of a polysaccharide called *Vibrio* polysaccharide (VPS) (51). *V. cholerae* produces other matrix proteins that are secreted at different stages of biofilm formation and play distinct roles in biofilm development. RbmA is major biofilm matrix protein, which accumulates on cells after the initial surface attachment and plays the role of a scaffolding protein to make 3D biofilms. The cells also secrete RbmC, which along with Bap1, makes the matrix more flexible as the cells grow and divide leading to biofilm maturation (52). The production of these matrix components have been found to be essential for intestinal colonisation in a human host, strongly indicating that biofilms play a role in *V. cholerae*'s virulence (53).

Biofilm formation in *V. cholerae* is regulated by environmental cues, inter-bacterial and intracellular signalling. Bacterial adaptation to nutrient fluctuations can be observed by changes in biofilm formation by phosphotransferase system (PTS) (54) (discussed further in section 1.4.2).

V. cholerae also recognises molecules released in the human host, such as polyamines, indole, and Ca^{2+} ions (46). Quorum sensing (QS) is one of the major regulators of biofilm formation in *V. cholerae* (discussed further in section 1.4.3). Changes in the concentration of intracellular secondary messenger molecules like c-di-GMP, cAMP and the stringent response signaling molecule (p)ppGpp directly influence biofilm formation (55–57) (discussed further in section **??**). Once the environmental signal is sensed, the regulation of biofilm formation in *V. cholerae* is governed by a coordinated combination of transcriptional activators such as VpsR and VpsT, repressors such as HapR, alternative RNA polymerase sigma factors such as RpoS, and small RNAs (sRNA) (52) (discussed further in section 1.4.6). Together, these signalling systems allow *V. cholerae* to rapidly modify its behaviour in order to adapt to changing environmental conditions.

1.2.2 Cholera

As a pathogen that spends most of its time outside the human host, *V. cholerae* has evolved the ability to transition between its environmental quiescent state and its pathogenic toxin-producing lifestyle. *V. cholerae* infection in the human gut results in watery diarrhoea leading to rapid dehydration, which, if untreated, can lead to fatal hypotonic shock (58).

Cholera as a disease was first described in the early 19^{th} century, primarily around the Indian subcontinent but later, spreading to Europe and North America (59). The first cholera pandemic occurred in Bengal, India, from 1817-1824 (60). However, it was not until the third pandemic, which occurred in Europe from 1839-1856, that the bacterium that caused cholera, *V. cholerae*, was isolated by Italian anatomist Filippo Pacini (61). In the same year, a British physician, John Snow, mapped a cholera outbreak in London and determined that the disease originated from a contaminated water source (62). The world has suffered seven cholera pandemics in the past 200 years, with the final pandemic still ongoing in countries of the Asian and African subcontinent (63). Typically, successive cholera pandemics are sparked by the emergence of a new genetically distinct, prevailing strain of *V. cholerae* (64). The different *V. cholerae* strains are classified into serotypes based on their cell surface lipopolysaccharide (LPS), specifically the O antigen. Bacteria of the serotype O1 are historically the most virulent (65). However, other serotypes called O139 and more recently emerged non-O1 and non-O139 serotypes have also been reported to possess toxicity (66, 67). The first six pandemics were caused by *V. cholerae* strains of the classical biotype, but the most recent pandemic is caused by a new strain, which has been commonly referred to as El Tor (64). The *V. cholerae* O1 El Tor strain C6706 was used as model organism in this study.

To this day, cholera is a deadly disease, especially in tropical and sub-tropical environments where large numbers of *V. cholerae* bloom periodically in communal water bodies (63). In regions of Asia and Africa, cholera is seasonal, responsible for the death of 93,000 people annually (68). In 2016, it was reported that although the number of cholera cases have decreased, the fatality rate had doubled from the previous year (World Health Organisation 2017). With the rise in antibiotic resistance world-wide, the development of alternative strategies for prophylaxis have become essential to combat disease. One of the more popular ideas is phage therapy, i.e. using host-specific lytic bacteriophages to infect and lyse bacteria at the site of infection (69).

1.3 Bacteriophages

Bacteriophages (or simply, phages) are viruses, comprised of DNA (or in rare cases, RNA) encapsulated in a proteinaceous coat, that utilise bacterial transcriptional and translational machinery to replicate (70, 71). Phages are natural predators of bacteria; bacteria encounter them in their natural environment, as well as in the human host. In fact, it has been estimated that phages outnumber bacteria by a factor of ten (72). Therefore, phages are an important biotic stress that bacteria contend with in order to survive.

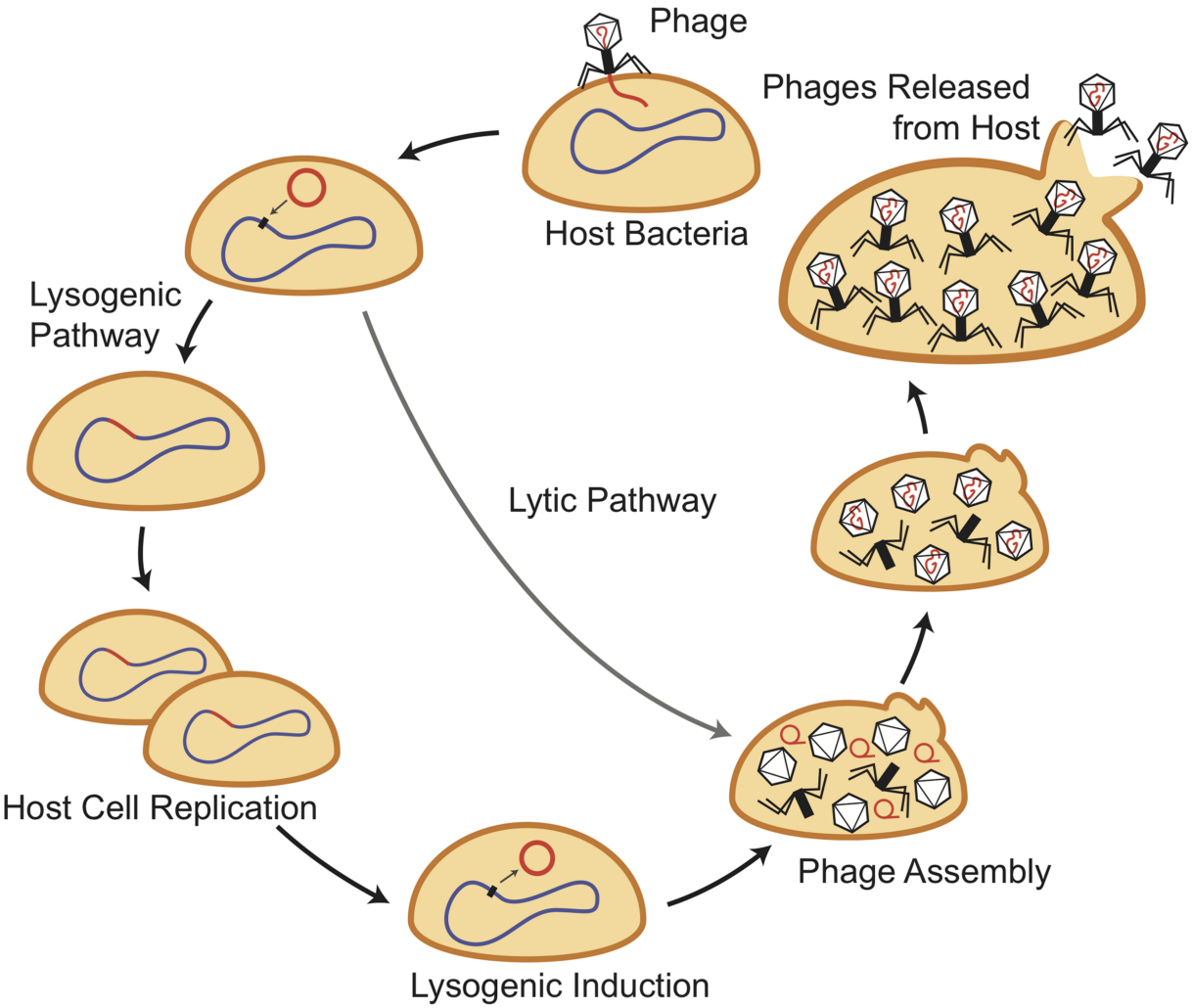

Figure 1.2: Bacteriophage lifecycles. Phages inject their genetic material into a bacterial cell (yellow) to initiate infection. Lysogenic phages can insert their genomes (red) into the host bacterial chromosome (blue) to become prophages. Lytic or lysogenic phages, following induction and excision from the bacterial chromosome, shut down bacterial machinery to produce phage proteins. After phage assembly, phage progeny are released from the host by bacterial cell lysis. Image is from Chiang *et al.*, 2019 (73).

1.3.1 Phage replication

Phages initiate infection by adsorbing onto receptors, which are typically on the bacterial outer membrane, LPS, or cellular appendages, and injecting their genetic material into the bacterial cell (74). Phages can follow either the lytic or lysogenic lifecycle (Figure 1.2). Phages that hijack

bacterial machinery to produce viral DNA and proteins, assemble progeny phages, and finally release them by bacterial lysis are called lytic phages (75). Lysis is achieved by phage-encoded enzymes called endolysins, which attack and break down peptidoglycan in the bacterial cell wall (76). On the other hand, some phages can insert their DNA into the bacterial chromosome so that their genetic material is conserved in the bacterial lineage during replication (77). These are called lysogenic phages or prophages, and have been known to encode virulence factors or antibiotic resistance genes that favour their integration into the bacterial chromosome (78, 79). Upon encountering certain environmental stresses or sensing signals related to bacterial host density, prophages can excise out of the bacterial chromosome and enter the lytic cycle to replicate and lyse their bacterial host (80, 81). However, phages do not only rely on lysis to release their progeny. Phages associated with some *Mycoplasma* species are extruded from the cell by budding through the bacterial cell membrane (82). Phages such as the CTX phage of *V. cholerae*, also known as filamentous phages, can be released from the cell by secretion, without causing cell lysis (83).

1.3.2 Vibriophages

Due to the narrow specificity of bacterial hosts, phages have been used to detect and classify bacterial strains. This method, called 'phage-typing', was originally used to trace the source of outbreaks of bacterial infections (84). In an early study performed using *E. coli*, seven phages (named T1 to T7) were described that replicated *via* the lytic lifecycle using different *E. coli* strains (85). Even today, these coliphages are used as a standard with which other phages are compared to in order to infer features related to phage morphology and infection. The T7 phage in particular, has been used a model to study the lytic phage infection cycle as it has a relatively wide host range and uses the bacterial LPS as its receptor (86). T7 has an icosahedral capsid (head) that is approx. $60\,\mathrm{nm}$ in diameter and made out of 415 copies of the protein Gp10 (87). T7 phages are characterised by a non-contractile tail, which is used to eject its DNA into the bacterial cell that it infects (88). T7 has a burst size, i.e., number of progeny phages released during one infection cycle, of 200 (89).

Phage-typing was used as a method to classify pathogenic *Vibrio* strains, responsible for causing cholera epidemics, by serotype. The first of such phage-typing schemes was developed in India in 1968 (90). Phages responsible for infecting *Vibrio* species, also known as Vibriophages, were isolated from contaminated seawater containing *V. cholerae* cells. In 1993, Vibriophages, named N4, S5, M4, D10 and S20 were isolated, which were used to distinguish classical biotypes from a new variant responsible for causing the recent cholera epidemic, called El Tor (91). In 2005, more phages were isolated from pond and sewage waters in India, called AS1, AS2 and AS3 (92). In the same year, Faruque and Mekalanos published the JSF series of environmental phages, which were isolated in Bangladesh (93). Lytic Vibriophages have also been isolated from water bodies in other countries including Malyasia and Mexico (94, 95). Other phage-typing schemes utilise phages isolated from cholera patients, like the VP series of phages isolated from the stool of an infected person in China in 1962 (96). More recently, three phages were isolated from cholera patients in Bangladesh, named ICP1 to ICP3, which were representative of a dominant

lineage of lytic Vibriophages specific to that area (97). Although so many Vibriophages have been isolated, little is known about their genomes and infection properties. Therefore, Vibriophages have been scrutinised for similarities in genome sequence and morphology. Vibriophages N4, VP3, and ICP3 have been deemed to be similar to the *E. coli* phage T7, and hence, are members of the 'T7-supergroup' (97–100).

Vibriophages have been known to play an important role in shaping *V. cholerae* communities over the course of its history. It has been suggested that the variety and abundance of these Vibriophages may be a hallmark of their continuous evolution *via* interactions with *V. cholerae* cells. Phage-bacterial interactions have been suggested to contribute to evolution of both bacterial cells as well as the bacteriophages (93). It remains unclear why the classical strain of *V. cholerae* diminished but the possibility of phages contributing to its selective elimination whilst enriching the El Tor biotype has not been ruled out (101). Previous studies have reported an inverse correlation between the titre of environmental phages and abundance of viable *V. cholerae* cells in aquatic environments (93). Bacterial predation by Vibriophages was discovered to play a role in mediating the self-limiting nature of the seasonal epidemics, as observed in Bangladesh (102). Therefore, understanding the relation between *V. cholerae* and Vibriophages is environmentally relevant and can shed light upon how their interaction affects bacterial pathogenesis. The presence of *V. cholerae* biofilms in the environment and the human host, along with the abundance of bacteriophages, suggests a high probability of interaction between biofilms and Vibriophages. In this study, I used Vibriophage N4, which was previously isolated from the waters of the Bay of Bengal by Chattopadhyay *et al.*, in 1993 (91), to infect *V. cholerae* O1 El Tor C6706, the causative agent of the previous cholera outbreak (66).

1.3.3 Anti-phage defence systems

The ubiquity of phages in environmental niches results in a continuous arms race between the bacterial prey and the phage predator (103). It is well-known that bacteria employ multiple defence strategies against phages, targeting different steps of the infection process. Bacteria can prevent phage entry by losing, blocking, or altering phage receptors (104). Upon entry, bacteria can cleave phage DNA using restriction modification (RM) mechanisms (105) or CRISPR-Cas systems (106, 107). In some cases, bacteria in communities employ QS-based signal transduction mechanisms to reduce the production of phage receptors, thus eluding phage infection (108). Sometimes, a few bacterial cells in a population increase the production of the toxins of a toxin-antitoxin system, which results in self-destruction and an abortive infection (109, 110). This altruistic method of resistance ensures that no phage progeny is released from the infected cell. However, phages often have counter methods to seize control of bacterial machinery (111, 112).

Biofilms act as a general defence strategy against lytic phage infection

The aforementioned defence systems, along with most phage-bacteria interactions, have been studied using planktonic bacterial cells in shaking liquid cultures. However, as bacteria prominently exist in biofilms, there is a gap of knowledge in how bacterial communities react to the presence of phages. Compared to planktonic cells, bacteria in matrix-embedded communities,

called biofilms, are more adept at surviving phage attack (113, 114). Bacterial biofilms have been thought to act as an arena for phage-bacterial interactions. The biofilm matrix has been described to shield cells from phage infection by preventing the diffusion of phage particles into the bacterial community (115). The presence of matrix has also been shown to contribute to phage protection by obscuring phage receptors on the bacterial surface (104). In fact, it has also been shown that the presence of phages leads to increased bacterial biofilm production, which subsequently contributes to augmented bacterial resilience to other stressors (116–118). The heterogenous distribution of matrix, bacterial cells, and phages gives rise to micro-niches that accommodate various phenotypes which are the outcome of the interplay between these three factors (119). The biofilm matrix can also provide a refuge for phages that remain dormant but have the capability to re-initiate lytic infection once conditions become favourable (120). Therefore, biofilm formation is generally assumed to be an eventuality of phage exposure or an advantage to combat phage infection. However, if the motivation to form biofilms is dependent on the presence of a stressor, such as phages, then it poses the question: what are the environmental cues that warn bacteria to bolster their defences by producing biofilm matrix? Bacteria possess an assortment of signalling systems to monitor their environment and regulate biofilm formation, which is discussed in the next section.

1.4 Bacterial signalling pathways

The ability of bacteria to adapt to changes in their environment accounts for their survival and proliferation across different habitats (121–123). Bacteria that evolved to survive in extreme conditions bear the hallmarks of modifying their genetic content by adaptive mutations (124). On the other hand, bacteria challenged with fluctuating biotic or abiotic factors utilise signalling pathways in order to rapidly respond to environmental cues (125–127). Bacterial signalling systems (Figure 1.3) consist of arrays of two-component systems (TCS), transcriptional regulators, and secondary messenger molecules that together, form a regulatory network allowing bacteria to tailor their response to effectively counter unfavourable environmental perturbations (128–130). Bacterial signalling responses are highly variable and are often determined by the nature of the stimulus. This section describes the variety of signals and sensory systems that bacteria employ to monitor their environment and regulate collective behaviour, particularly, biofilm formation.

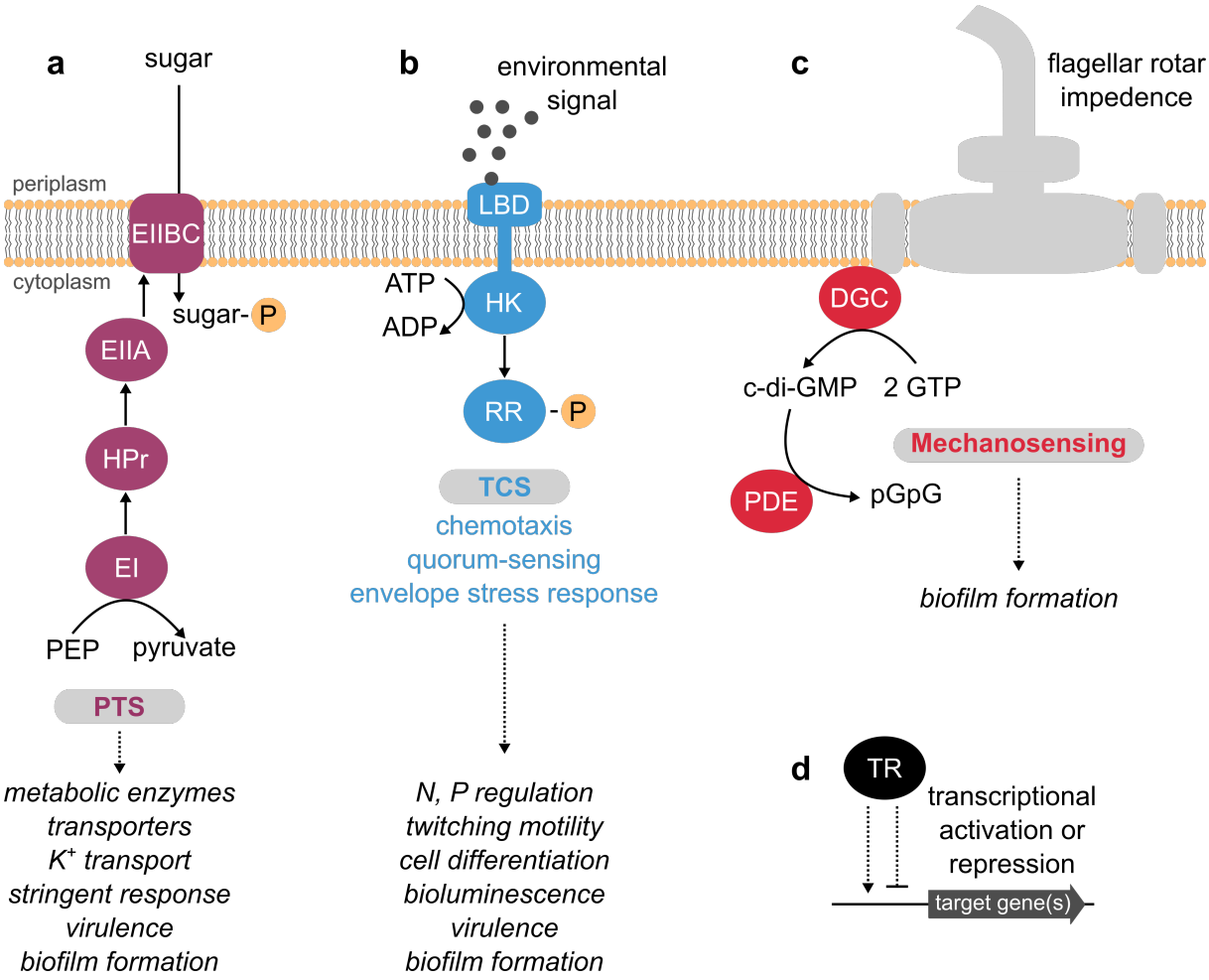

Figure 1.3: Schematic of the major bacterial signalling systems that contribute to biofilm formation a, Phosphotransferase system (PTS) transports extracellular sugars into the bacterial cytoplasm by phosphorylation, using PEP as the phosphoryl group donor. PTS consists of three protein complexes: enzyme I (EI), HPr, and enzyme II (EII), which is further divided into subunits A, B, and C. PTS is responsible for responding to changes in carbon source utilisation and regulates bacterial processes such as K^+ transport, stringent response, c-di-GMP production, virulence, and biofilm formation. **b, Two component systems (TCS)** sense environmental stimuli by the ligand-binding domain (LBD) of their membrane-associated histidine kinase (HK) receptor, causing it to autophosphorylate using ATP as the phosphoryl group donor. Phosphorylation of the response regulator (RR) by the HK is responsible for mediating cellular processes such as nitrogen (N) or phosphorus (P) regulation, twitching motility, cell differentiation, bioluminescence, virulence, and biofilm formation. **c, Mechanosensing** is the process during which the impedance of flagellar rotation, when a bacterium encounters a surface, causes bacteria to elicit a response. This is usually associated with production of secondary messenger molecules such as c-di-GMP by diguanylate cyclases (DGC), which regulates cellular processes such as biofilm formation. c-di-GMP can be degraded by phosphodiesterases (PDE). **d, Transcriptional factors**, which can regulated by all the aforementioned systems (or a component of the signalling pathway itself, e.g., response regulators), are responsible for either activating or repressing the expression of target genes in order to ultimately induce a bacterial response to the environmental stress.

1.4.1 Stress signals

Bacteria, regardless of their environment, are constantly exposed to cues that impact their growth and behaviour. Signals originating due to changes in environmental conditions that elicit a bacterial regulatory response, namely, changes in gene expression or adaptation of protein function, are called as 'stress signals' (25). In the human host as well as in the natural environment, bacteria commonly encounter abiotic stresses such as nutrient deprivation, temperature changes, or extreme pH (131, 132). Environmental changes constituting a change in nutrient composition not only affect bacterial metabolism, but also impact virulence traits (133). The PTS is responsible for recognising the availability of environmental sugars and regulating the corresponding metabolic adaptive response (134) (discussed in 1.4.2). Abiotic signals can have either a physical or chemical nature, which often determines the type of bacterial response induced. The recognition of chemical signals on bacterial surfaces usually induces responses involving TCS such as chemotaxis or QS (128) (discussed in 1.4.3). On the other hand, exposure to physical forces such as those exerted by surfaces or objects, results in bacterial mechanosensing (135) (discussed in 1.4.4). Along with enduring abiotic stresses, bacteria must also survive during biotic stresses such as predation by protists (136, 137), the immune system attack of eukaryotic hosts (28), invasion by other bacterial species (138), and most commonly, the presence of bacteriophages (108, 139). The presence of such biotic and abiotic stresses in the environment can sometimes translate to intracellular changes, so that the stress signal originates from within the cell itself. Accumulation of reactive oxygen species (ROS) (140), misfolded proteins (141), and heightened ion concentrations are examples of intracellular stress signals (142). Whether extracellular or intracellular, the sensing of signal(s) is crucial for initiating a response. Bacteria have a multitude of different systems that are specialised to sense and respond to various stress signals.

1.4.2 Phosphotransferase system (PTS)

The phosphoenolpyruvate (PEP) sugar phosphotransferase system (PTS) is responsible for transporting and phosphorylating sugars and other carbon sources across the bacterial membrane (143). PTS is conserved across bacterial species and largely consists of three protein complexes: enzyme I (EI), HPr, and enzyme II (EII). EII is further composed of three (or four) subunits that are associated with the membrane and specific for various sugar substrates, such as glucose, mannitol, and cellobiose (134). The phosphorylation of EI using PEP as a high energy phosphoryl donor initiates the PTS signal transduction cascade (144). The phosphoryl group is transferred from EI to HPr, through the various subunits of EII, and finally onto the sugar. The phosphorylated sugar is finally transported into the cytoplasm (145). Depending on the nutrient composition of its environment, bacteria can adapt to a preferred carbon source by mediating the phoshorylation level of its PTS components by a process called carbon catabolite regulation (146). Enzymes of the PTS can regulate cellular process by interacting with components of TCS, transcriptional regulators, catabolic enzymes, or transporters (147, 148). These interlinked regulatory circuits allow bacteria to use PTS as a mediator between sugar utilisation and cellular responses such as K^+ transport, stringent response, c-di-GMP production, virulence, and biofilm formation (134).

1.4.3 Two-component systems (TCS)

Bacteria use TCS to respond to changes in critical extracellular parameters as well as intracellular physiology. Bacterial TCS usually consist of a membrane-bound histidine kinase (HK) protein, which senses environmental signals, coupled with a corresponding response regulator (RR), which is responsible for mediating a cellular response (149). HK proteins, while conserved across the bacterial kingdom, possess highly variable sensory input domains (150). Signal transduction occurs by stimulus-mediated alterations in the transmembrane regions or by binding of signal molecules to cytoplasmic autokinase domains (151). Binding of the signal to ligand-binding domains (LBD) of HK sensors causes a conformational change that triggers them to autophosphorylate by utilising one molecule of adenosine tri-phoshate (ATP) (152). The phosphate group is transferred to a RR, which subsequently initiates the bacterial response to the sensed environmental signal (153).

As bacteria have to constantly monitor their environment, almost every known regulatory pathway in bacteria includes a TCS, making them essential for bacterial adaptive responses (154, 155). Cellular metabolic processes including nitrogen assimilation (156, 157), phosphate regulation (158), and sugar transportation (159) are controlled by their corresponding TCS. The transition of sessile to motile state is mediated by a flagellar switch system, which also incorporates a TCS (160). Secretion of virulence factors by pathogens such as *V. cholerae* are regulated by TCS that help the bacterium assess its cellular state as well as its micro-environment in order to efficiently administer toxins to its host whilst avoiding detection by the immune system (161). Additionally, bacteria also possess a network of specialised TCS that have evolved to respond frequently encountered signals in their environment. These are discussed in the following paragraphs.

Chemotaxis

A specialised TCS, called chemotaxis, is used by bacteria to orient their motility according to environmental cues (162). Chemosensing enables bacterial cells to sense and swim up or down gradients of specific chemical attractants and repellents, respectively, which include certain amino acids, sugars, and metal ions (150). Bacteria monitor their environment using a plethora of chemoreceptors, averaging to about 14 chemoreceptor-related genes per bacterial genome (163). In addition to motility, chemosensory systems have also been implicated in other bacterial processes such as regulation of twitching motility (164), cell differentiation (165), biofilm formation (166, 167) and pathogenicity (168).

Quorum sensing (QS)

Bacteria use cell-to-cell communication systems, called quorum sensing (QS), to collectively modify their behaviour in response to changes in cell density and species composition of their surrounding microbial community. QS is initiated by sensing of extracellular signalling molecules, which are often self-secreted, called autoinducers (169). As the bacterial cell density increases, autoinducers accumulate in the microbial population (170). *V. cholerae* produces acyl-homoserine lactones (AHL), called cholera autoinducer-1 (CAI-1), which are sensed by membrane-bound HK proteins as QS receptors, that are part of a TCS (171). CAI-1 molecules are synthesised by CqsA and sensed by the HK protein CqsS (172). In addition to AHL, another QS system, which is conserved across various Gram-negative species, senses a furanosyl borate diester known as AI-2, for inter-species communication (173). AI-2 is synthesised by LuxS and is sensed by the HK protein LuxPQ (174). In recent years, other inter-species and inter-kingdom QS signals have been identified such as (nor)epinephrine (175), DPO (176), and ethanolamine (177). In total, it has been shown that *V. cholerae* possesses four parallel QS receptors CqsS, LuxPQ, CqsR, and VpsS (178). At low cell densities (LCD), which correlates with a low concentration of autoinducers, all four HK receptors autophosphorylate and transfer the phosphoryl group to a common RR protein, called LuxO, *via* the intermediary protein LuxU (Figure 1.4). Phosphorylation of the LuxO leads to a synchronised change in the global genetic expression on a community-wide level (170). Phosphorylated LuxO, together with the alternative sigma factor σ^N, activates the transcription of four sRNAs, which are responsible for the inhibition of translation of the major transcriptional regulator HapR. When HapR is repressed, the transcription of the biofilm-related genes take precedence, with VpsR acting as the transcriptional activator of matrix-encoding genes at the *vps* loci. The activity of VpsR depends on another transcriptional factor VpsT, and can also be influenced by intracellular signalling molecules such as c-di-GMP (Figure 1.5). HapR repression allows for the accumulation of AphA (179), which is a transcriptional regulator that controls the expression of genes required for virulence (180) and natural competence (181). At high cell density (HCD), when the levels of autoinducers increase, the QS receptors function as phosphatases, leading to a dephosphorylation of LuxO. During this state, HapR accumulates and mediates the repression of biofilm matrix genes (182). This results in dispersal of cells from the biofilm (182, 183). Overall, QS is responsible for regulating many different bacterial processes such as bioluminescence production, biofilm formation, secondary metabolite production, competence for DNA uptake, and virulence factor production (184).

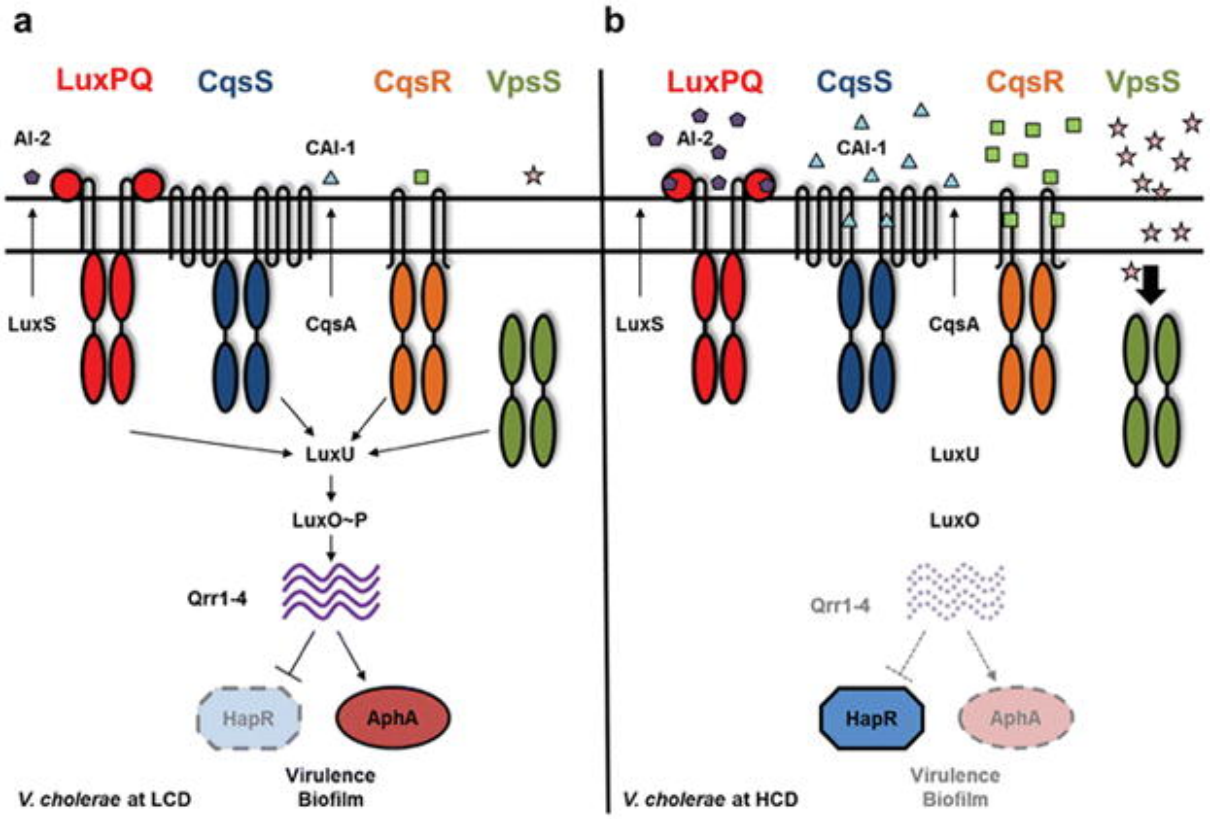

Figure 1.4: The *V. cholerae* quorum sensing (QS) system. a, At low cell density (LCD), autoinducer levels are low and the QS receptors LuxPQ, CqsS, CqsR and VpsS act as kinases, which initially autophosphorylate and subsequently transfer the phosphoryl group to LuxO *via* LuxU. Phosphorylated LuxO promotes transcription of four small RNAs called Qrr1-4, which in turn activate translation of AphA and inhibit production of HapR. At LCD, genes required for biofilm formation and virulence factor production predominate. **b,** At high cell density (HCD), autoinducer levels are high and the QS receptors behave as phosphatases, leading to a dephosphorylation of LuxO. Thus, LuxO is no longer active and Qrr transcription is repressed. HapR is made at this state while AphA is not produced. Reciprocal expression of these two regulators leads to repression of biofilm formation and virulence factor production. Image is from Jung *et al.*, 2016 (178).

1.4.4 Mechanosensing

Analogous to the constant presence of chemical cues, due to their small size, bacteria are also under constant exposure to physical forces, such as those exerted by gravity, liquid shear, or surfaces. These mechanical cues cause a perturbance in cell membrane or cellular appendages like flagella or pili, which initiates a biological response *via* a process called 'mechanosensing' (185). Bacteria use flagella or pili for motility in a fluid or across a surface, respectively. Flagella are long, whip-like filaments that range from 1-9 μm in length (186). *V. cholerae* has a single flagellum that is made up of protein subunits called FlaA (187). Flagellar rotation is driven by the flagellar motor apparatus, which consists of membrane-embedded stators and a transmembrane rotor (188). Flagellar stators employ a proton motive force (as is the case in *P. aeruginosa*) or a sodium motive force (as is in the case in *V. cholerae*) (189). While the central role of a flagellum is motility, it also plays an integral role in surface-sensing which is mediated by interference in

its rotation by a proximal surface (135). Impedance of flagellar rotation onsets the production of secondary messenger molecules like c-di-GMP and is usually the first step for biofilm formation (190).

1.4.5 Cyclic nucleotides as secondary messenger molecules

Bacteria use secondary messenger molecules to relay and amplify information from membrane-bound sensors to macromolecular regulatory systems by binding to RNA targets, transcription factors, or other receptor proteins (191). These nucleotide secondary messengers play a fundamental role in cellular growth, development, and metabolism (130). Cyclic mononucleotides such as cyclic adenosine 3'5'-monophosphate (cAMP) and cyclic guanosine 3'5'-monophosphate (cGMP) are universal signalling nucleotides prevalent across the prokaryotic kingdom (192). Bacteria also produce stringent response alarmones guanosine tetra- and penta-phosphate ((p)ppGpp) in response to nutrient and osmotic stresses (193). Cyclic dinucleotides such as 3'5'-cyclic di-guanosine monophosphate (c-di-GMP) and 3'5'-cyclic di-adenosine monophosphate (c-di-AMP) are important secondary messengers that control numerous responses in bacteria, including motility, biofilm formation, and virulence (194, 195).

c-di-GMP was first discovered in Moshe Benziman's laboratory in 1987 (196), but its potential as a key regulator in pathogenesis became only evident after its discovery in major pathogens such as *S. enterica* (197), *E. coli* (198), *P. aeruginosa* (167), and *V. cholerae* (55). In *V. cholerae*, c-di-GMP levels change in response to the presence of an environmental stimulus such as surface contact or a chemotactic gradient (199). c-di-GMP levels are regulated by the activity of diguanylate cyclases (DGC), which are c-di-GMP producers, and phosphodiesterases (PDE), which are c-di-GMP degraders (200). DGCs possess a GGDEF domain, which catalyses the conversion of two guanosine tri-phosphate (GTP) molecules into one c-di-GMP molecule (201). On the other hand, PDEs possess an EAL or HD-GYP domain, which catalyses the reverse process of degrading one molecule of c-di-GMP into one molecule of linear di-GMP (pGpG) or two guanosine monophosphate (GMP) molecules, respectively (202, 203). c-di-GMP is an important regulator of gene expression (204). In *V. cholerae*, c-di-GMP is an important regulator of biofilm formation. *V. cholerae* possesses a multitude of known as well as putative proteins responsible for regulating intracellular levels of c-di-GMP (205). High cellular levels of c-di-GMP promote enhanced transcription of genes involved in biofilm formation, by promoting VpsT-mediated transcriptional activation of *vps* genes (Figure 1.5) (52). c-di-GMP can also be sensed by receptor proteins, such as those possessing a PilZ domain, or by c-di-GMP-responsive riboswitches (206, 207). The striking signal diversity of input and output specificity of c-di-GMP questions how several signalling pathways can function in parallel if they all use the same diffusible messenger molecule. Recently, it has been hypothesised that bacteria achieve this flexibility by monitoring local intracellular pools of c-di-GMP along with global c-di-GMP levels (208).

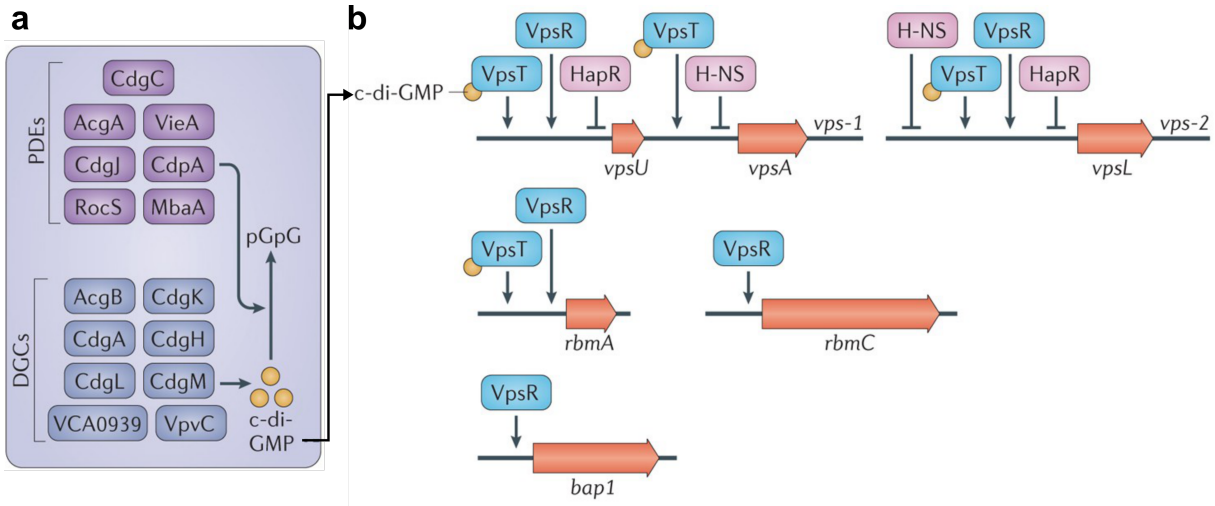

Figure 1.5: The role of c-di-GMP in *V. cholerae* biofilm regulation. **a,** Known diguanylate cyclases (DGC) and phosphodiesterases (PDE) involved in the production and degradation of c-di-GMP, respectively. **b,** The binding of c-di-GMP to VpsT initiates transcription of *vps* genes, resulting in biofilm formation. VpsR is the master regulator of biofilm activation in *V. cholerae*. HapR and H-NS are responsible for repressing the transcription of *vps* genes. Image is modified from Teschler *et al.*, 2015 (52).

Recently, a novel hybrid cyclic nucleotide 3'3'-cyclic GMP-AMP (cGAMP) was discovered as a secondary messenger molecule that regulates chemotaxis and intestinal colonisation in *V. cholerae* (209). cGAMP is synthesised by DncV, and binds to CapV, which activates it and causes degradation of the cell membrane (210). cGAMP signalling has been shown to primarily mediate an anti-phage defence system that is common in bacteria, called cyclic-oligonucleotide-based anti-phage signalling system (CBASS) (211). cGAMP signalling has also been shown to regulate biofilm formation in *E. coli* ECOR1, an animal commensal (212). Bacterial cGAMP is homologous to 2'3'-cGAMP, a eukaryotic innate immune signalling and antiviral response molecule, indicating that cyclic nucleotides are a conserved group of signalling molecules across different kingdoms (213, 214).

1.4.6 Transcriptional regulation

Transcriptional regulators couple the bacterial response to the environmental perturbation by influencing gene expression (129). The regulation of bacterial transcription is broadly performed by sigma factors (σ^N, σ^S, σ^H, σ^F, σ^E, and σ^{fecI}), which recruit RNA Polymerase to initiate transcription (215); and transcription factors (216), which are proteins with DNA-binding domains that interact with promoter sequences to either activate or repress transcription. Small ligands can also affect transcription, either by interacting directly with the translational machinery, as is in the case of ppGpp (217), or by modulating the DNA-binding activity of the transcriptional factor, as is how allolactose controls the activity of the Lac repressor (218). When phosphorylated by their corresponding HK, RR can also bind to gene promoters to initiate a cellular response (152). Bacteria have over 300 transcriptional factors, out of which seven are the major regulators of bacterial genetic expression, responsible for controlling over 50% of gene regulation (219). Bacteria use these general transcriptional factors (CRP, FNR, IHF, Fis, ArcA, NarL, and

Lrp) to respond to changes in their surroundings that they face most often such as nutrient starvation, oxygen starvation, phage infection, and switch to anaerobic respiration (129). Most other transcription factors have only one DNA-binding location and play a role in specific responses to environmental cues, idiosyncratic to each bacterial species (220). The proteins described in the previous sections that regulate biofilm formation in *V. cholerae*, namely HapR, AphA, VpsR, and VpsT, are among those specialised transcriptional regulators which are responsible for targeted control of gene expression.

1.4.7 Other forms of bacterial genetic regulation

Canonically, proteins have been considered the major subunits of bacterial genetic regulation due to their involvement in known bacterial signalling pathways as sensors, response regulators, sigma factors, or transcriptional factors. Other than proteins, bacteria also use cyclic nucleotides, small RNA (sRNA), or riboswitches to efficiently elicit a stress response (130, 221, 222). Furthermore, it has also been shown that lipids present in outer membrane vesicles (OMVs) from Gram-negative bacteria or in the cell wall of Gram-positive bacteria also play a role during bacterial stress responses (223, 224). The plethora of factors that bacteria use in response to stress make bacterial gene regulation an interesting and complex area of study.

1.5 Motivation

The outcome of abiotic stresses such as nutrient deprivation, temperature changes, or extreme pH often manifests in an increased secretion of proteins and carbohydrates that facilitates cellular adhesion (225). Bacteria in biofilms show augmented resilience against changing environmental conditions (27, 226, 227) and exposure to antibiotics (228, 229). Therefore, biofilms themselves have been considered to be a general response to various types of stresses (230). Biofilms also offer protection against bio-antagonists such as predatory protists (136, 137), the immune system of eukaryotic hosts (28), invading external bacterial species (138), and bacteriophages (108, 115, 139). As described in section 1.4, bacteria use a multitude of signalling pathways to sense unfavourable changes in their environment and induce biofilm formation. The battery of elements involved in bacterial gene regulation have been elucidated for responses to abiotic stresses. However, little is known about how bacteria sense and respond to biological agents that threaten their survival. Phages that require bacterial cell lysis in order to propagate, i.e., lytic phages, pose the greatest threat to bacterial survival. Considering that phages outnumber bacteria and have been found to co-exist with bacteria in the same niche (described in section 1.3), it suggests that bacteria may have evolved signalling systems to sense and respond to damages incurred during lytic phage infection. Moreover, the predominance of bacterial existence in biofilms (described in section 1.1) sets the stage for the involvement of bacterial collective behaviour as a phage defence system (discussed in section 1.3.3). Together, these facts raise the question: how do bacterial communities respond to the presence of lytic phages?

1.6 Thesis outline

As discussed in the previous sections, it is clear that bacteria possess complex signalling systems to sense and initiate a regulatory response to environmental changes. Furthermore, these social prokaryotes also exhibit collective behaviour such as biofilm formation to effectively adapt to various stresses. The most extreme form of stress faced by a bacterium is exposure to lysis-causing entities, such as bacteriophages. The following chapters in this thesis demonstrate how bacteria use group behaviour to survive lytic stress.

In **chapter 2**, *V. cholerae* was used as a model organism to understand how bacteria respond to lytic phage exposure. Vibriophage N4 was used to test the ability of *V. cholerae* to withstand phage exposure. Consequently, I found that although *V. cholerae* cells were initially susceptible to infection by Vibriophage N4, the formation of biofilms enabled bacterial survival during the continuous presence of phages.

In **chapter 3**, biofilm formation as a general response to lysed bacterial cells was explored. I discovered that biofilm formation was triggered by sensing peptidoglycan fragments that were released from lysed cells. Sensing this 'danger signal' resulted in increased cellular c-di-GMP levels and biofilm matrix production in *V. cholerae*. Peptidoglycan as a danger signal was found to be conserved in other bacteria as well. These results led to the conclusion that biofilm formation facilitates a quick and general bacterial hideaway in response to the presence of lysis-causing stressors.

2 | Biofilm formation protects *Vibrio cholerae* from lytic phage attack

Bacteriophages are the natural predators of bacteria. They constrict the growth of their prey and thus, are responsible for shaping bacterial populations everywhere (231). However, bacteria have also been known to coexist with phages, sometimes even in the same ecological niche. A good example of bacteria-phage coexistence is that of *Vibrio cholerae* and Vibriophages; *V. cholerae* encounters phages, both in the aquatic environment, as well as the human host (232, 233). *V. cholerae* is an interesting model organism, not only because of its medical relevance as a pathogen, but also due to its tendency to exhibit group behaviours that are essential for its ability to cause infection and dissemination from the host. Collective behaviour in *V. cholerae* is typically governed by quorum sensing (QS), which senses bacterial cell density in order to induce a global change in gene expression (182). QS regulates a number of bacterial behaviours including virulence, biofilm formation, and susceptibility to bacteriophages, in order to ensure the survival and proliferation of its population (46). Therefore, to study bacteria-phage interactions in bacterial communities, I chose the bacterium *V. cholerae* as a model organism. To infect *V. cholerae*, I selected Vibriophage N4 as the viral agent for this study. Vibriophage N4 has a relatively wide host range for infection in *V. cholerae* O1 El Tor strains (91). This phage was chosen for its similarity to the *E. coli* phage T7 and as it was one of the few phages whose genome has been sequenced (99).

Studying bacterial-phage dynamics involves the characterisation of the lytic infection process of the phage in its bacterial host. In previous studies that describe Vibriophage N4 infection, the authors propagated the phage in the *V. cholerae* O1 El Tor strain MAK 757 (99). This strain was isolated in 1937, before the seventh pandemic (which started in 1961). In this study, the most recent *V. cholerae* O1 El Tor strain called C6706, which was isolated during the seventh pandemic in 1991 (234) was used. Therefore, I first had to test for the compatibility between *V. cholerae* C6706 and Vibriophage N4. To understand how *V. cholerae* C6706 cells interacted with Vibriophage N4, I performed basic phage experiments to characterise the infection process.

Phage-bacterial interactions have traditionally been studied in the laboratory using batch culture systems. Such shaking liquid culture set-ups were optimal for identifying the features of phages during their propagation in their bacteria hosts. The thorough mixing in batch cultures creates a uniform distribution of predator and prey which in turn, fosters an increased amount

of phage-bacterial encounters, thus increasing the probability of infection (103, 235). However, such a system is not necessarily the best representation of a bacterial niche. Recently, the use of microfluidic chambers that have a continuous flow system, called microfluidics, have gained popularity due to their ability to serve as a proxy for bacterial environments (236). Such systems are also useful for live-imaging of bacterial phenotypes at a single-cell level (237). In this chapter, I used a combination of batch culture and microfluidics to characterise the effects of Vibriophage N4 exposure on *V. cholerae* cells. Using batch cultures, I was able to assess the impact of phage exposure on a population-level. On the other hand, using a microfluidics flow system enabled the investigation of bacterial behaviour during phage exposure on a single-cell level. This method of growth was used to visualise and quantify bacterial biofilm formation, similar to previous studies (32, 115). Growing cells in a microfluidics flow system under a constant supply of fresh growth medium ensured reduced effects of media fluctuations and accumulation of bacterial secondary metabolites and waste products. Moreover, cells grown in a microfluidic chamber were assured a uniform supply of oxygen as compared to a batch culture.

When Vibriophage N4 was added to a culture of *V. cholerae*, I found that bacteria utilised collective behaviour to survive phage infection. Using a combination of microfluidic and confocal microscopy, I discovered that *V. cholerae* C6706 cells form biofilms in response to phage exposure. Further, techniques such as bacterial genetic engineering, proteomics, and transcriptomics were implemented to identify that bacterial biofilm formation was a not a result of genetic selection, but rather, a regulatory response to phage exposure.

The results described in this chapter have contributed to a paper (238), pending publication. The experiments described in this chapter were performed by myself. Bacterial strains were constructed either by myself or were used from the Drescher laboratory strain collection (see section 5.1.1). Biofilm quantification was performed using a custom script written by Eric Jelli. Treatment of bacterial samples and liquid chromatography–mass spectrometry (LCMS) for proteomics was performed by Timo Glatter. RNA isolation for transcriptomics was performed by Kazuki Nosho. Data analyses were performed by myself. The experiments were designed and conceptualised by Praveen K. Singh and myself, and the project was initiated by Knut Drescher.

2.1 Vibriophage N4 infection in *V. cholerae* O1 El Tor strains

Phage infection depends on many factors, one of which is the genotype and serotype of the bacterial cell it encounters. To identify a suitable bacterial host for Vibriophage N4 (Figure 2.1a), six *V. cholerae* strains of different genotypes, grown to exponential phase in Luria-Bertani (LB) medium, were exposed to Vibriophages and incubated at $37\,^{\circ}\mathrm{C}$ for $8\,\mathrm{h}$. Phage infection was monitored by measuring optical density at 600 nm (OD_{600}) of the bacterial culture. Vibriophage N4 was able to successfully infect *V. cholerae* strains C6706, N16961, A15512, DRC-193A, and E7946, which was seen as a decrease in OD_{600} (Figure 2.1b). These strains are clinical isolates and all belong to the *V. cholerae* O1 serotype family. Vibriophage N4 was unable to infect *V. cholerae* V52, which is an environmental strain of the O37 serotype. All the strains that were infected showed bacterial re-growth after phage infection (this phenomenon is discussed in 2.2).

Thus, Vibriophage N4 infected a variety of *V. cholerae* strains, but only those of the O1 serotype. For this study, the *V. cholerae* strain C6706 was chosen as the bacterial host for Vibriophage N4.

Phage infection in *V. cholerae* strain C6706 was also visualised by performing a plaque assay. Here, a suspension of lyophilised Vibriophage N4 was spotted on a lawn of *V. cholerae* C6706 cells, and incubated overnight at 37 °C. The appearance of a zone of clearance, also known as plaques, was indicative of successful infection (Figure 2.1c).

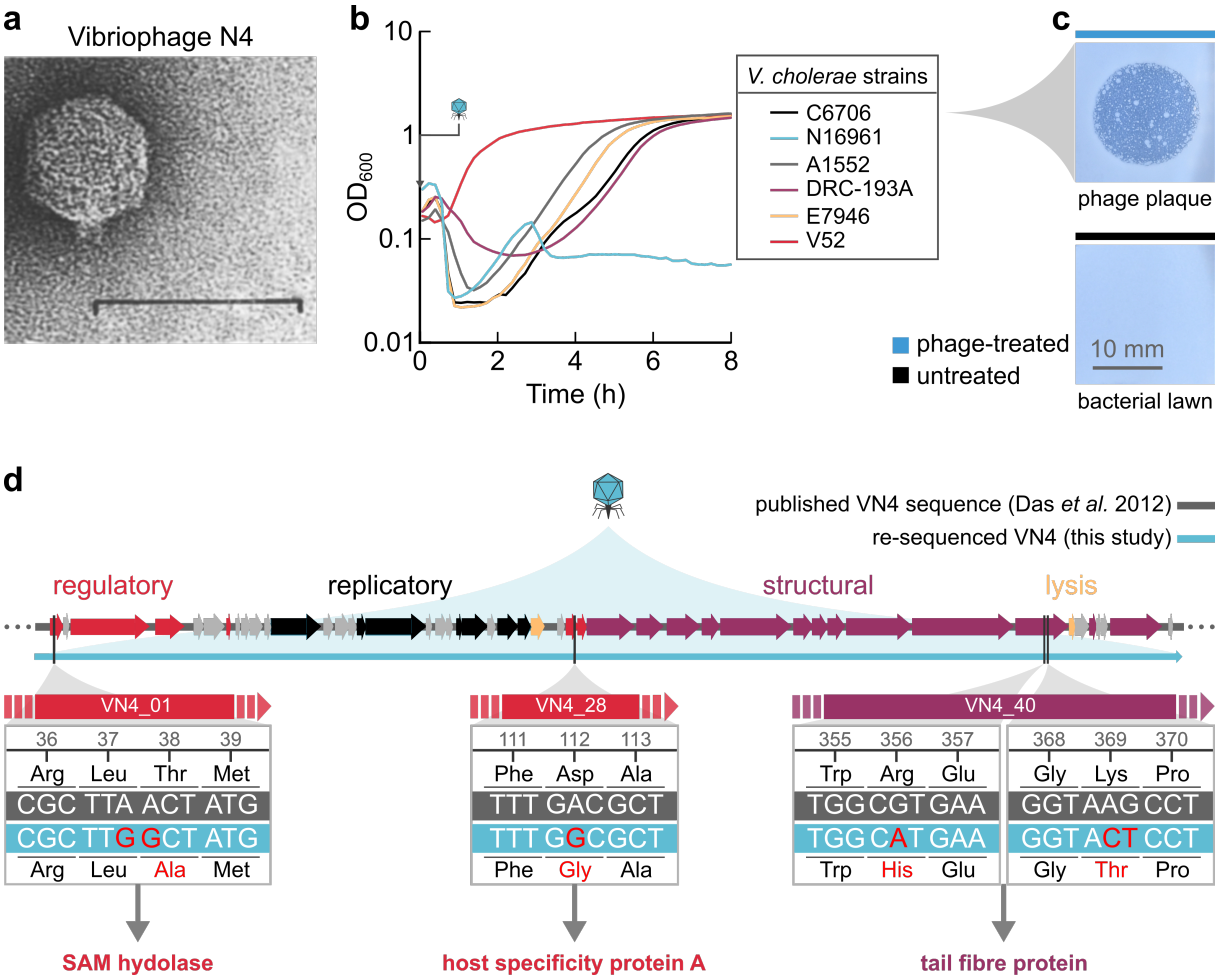

Figure 2.1: Vibriophage N4 infection in bacterial host *V. cholerae* O1 El Tor C6706 and subsequent phage genome sequencing. **a,** Scanning electron microscope (SEM) images of Vibriophage N4. Image is from Chattopadhyay *et al.*, 1993 (91). **b,** Change in culture density (represented by OD_{600}) over time of *V. cholerae* WT strains exposed to Vibriophage N4 (MOI = 1) at 0 h (grey arrow). All strains except V52 were susceptible to infection by Vibriophage N4. **c,** Phage infection of *V. cholerae* O1 El Tor C6706 cells spread on LB agar, incubated overnight at 37 °C. Spotting of Vibriophages resulted in plaque formation (blue); spotting of LB only did not affect the bacterial lawn (black). **d,** Sequence alignment of published Vibriophage N4 (VN4) genome (grey line) and re-sequenced genome of phage progeny obtained by propagating in *V. cholerae* O1 El Tor C6706 cells (blue line). Gene classes represented by coloured titles correspond to coloured genes on the genome (99). Dots at the beginning and end of the sequence represent a continuation of the sequence, as VN4 has a circular genome. Magnified regions of the sequence show inconsistencies between the published DNA sequence and re-sequenced genome along with the consequences on the translated peptides.

To ensure that there were no mutations in the phage DNA during infection (which could have happened as I used a host that was different from the original propagating strain), I sequenced the DNA of the Vibriophage N4 progeny that were obtained from infecting *V. cholerae* C6706 cells. Comparing the sequenced phage genome to the published sequence (99) showed six base-pair mismatches at various loci. These mismatches could have been caused due to mutations acquired during infection in C6706 or else, might not be mutations at all, but rather discrepancies in the existing sequence. Out of the six, one mismatch caused a silent mutation (Leu^{37} in VN4_01). The other five resulted in four amino acid substitutions in three different proteins of Vibriophage N4 (Figure 2.1d). Keeping these modifications in mind, it is possible that Vibriophage N4 had a modified genome after infecting *V. cholerae* C6706 cells. However, these amino acid substitutions were not studied further as the phage was able to cause extensive lysis in the host. Therefore, I proceeded with characterising the infection of Vibriophage N4, using *V. cholerae* C6706 as a propagating strain.

2.2 *V. cholerae* uses collective behaviour to survive phage infection

Due to the dearth of knowledge available for interactions between *V. cholerae* C6706 and Vibriophage N4, I performed necessary optimisation experiments in order to identify culture conditions for efficient phage infection. After ascertaining that Vibriophage N4 could infect *V. cholerae* C6706 cells, I proceeded to test different parameters that could affect phage susceptibility such as growth medium, temperature, bacterial growth phase, and multiplicity of infection (MOI). Cultures of *V. cholerae* C6706 cells were grown to exponential phase and subsequently exposed to Vibriophage N4 lysates in a multi-well plate, in which the cell culture density (OD_{600}) was measured every $10\,\mathrm{min}$. Observations from the shaking culture experiments showed either infection, no infection, or attenuated infection. A decrease in OD_{600} was indicative of successful phage infection. In some cases, bacterial growth slowed after exposure to phages without cell lysis, which is termed here as attenuated infection. The different media tested included minimal media such as M9, and rich media such as tryptone broth (TB), LB, and brain-heart infusion (BHI). Phage infection was successful when bacteria and phages were cultured in rich media but no cell lysis was observed when a minimal medium was used (Figure 2.2a). A slight decrease in OD_{600} was observed when a high titre of phages (MOI = 10) was added to cells cultured in M9. However, the decrease in OD_{600} was <0.01, which was near the detection limit of the platereader. Therefore, it was not clear whether the decrease of OD_{600} resulted in cell lysis and/or phage propagation during attenuated infection. The incubation temperature had an impact on the phage susceptibility of bacteria for all growth media. Bacteria grown at $37\,^{\circ}\mathrm{C}$ showed the steepest decrease in culture OD_{600} after phage addition. Bacterial lysis was also seen in cultures grown at $28\,^{\circ}\mathrm{C}$ but the decrease was less pronounced[1]. For infections in rich media, the phage-bacterial ratio or MOI appeared to be independent of the outcome of phage infection when cells were grown at $37\,^{\circ}\mathrm{C}$; but at $28\,^{\circ}\mathrm{C}$, only the maximum MOI of 10 was able to cause successful infection. For all future phage-bacteria co-incubation experiments, *V. cholerae* C6706 cells were cultured in LB and incubated at $37\,^{\circ}\mathrm{C}$. An MOI of 1 was selected for all liquid culture experiments.

[1] graphs of phage infection in *V. cholerae* cells under different growth conditions are in Appendix (Figure A1)

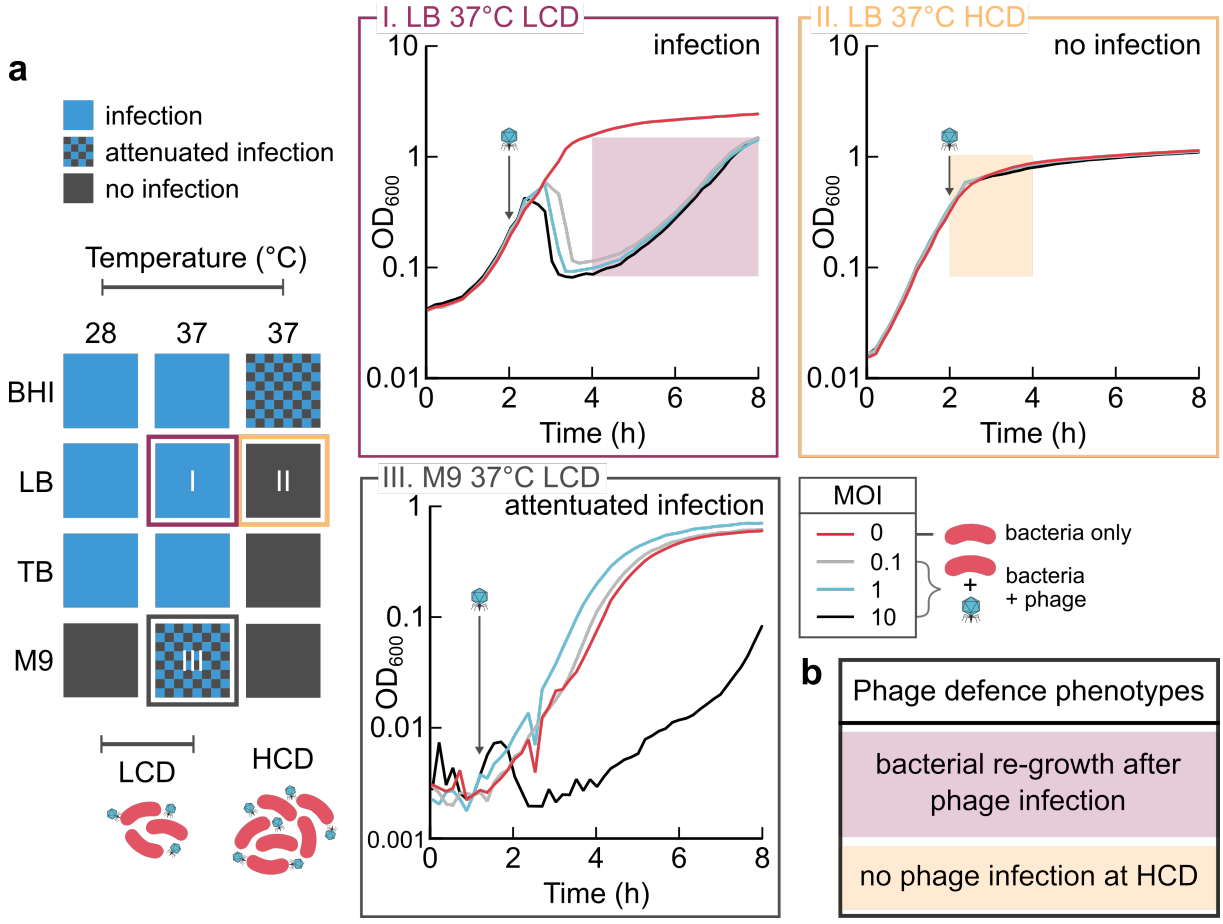

Figure 2.2: Optimising culture conditions for Vibriophage N4 infection in *V. cholerae* C6706. **a,** Summary table of results of phages added to *V. cholerae* C6706 cultures grown in different media, temperatures, and bacterial growth phase (LCD is low cell density and HCD is high cell density), infected with Vibriophage N4 at a multiplicity of infection (MOI) = 10. Selected conditions are indicated by coloured boxes which correspond to the graphs on the right. (I.) Bacteria infected in LB 37 °C LCD showed a decrease in OD_{600} during phage-induced lysis, followed by a subsequent increase in OD_{600}, indicating bacterial re-growth after phage infection. (II.) Phage infection in LB 37 °C HCD was unsuccessful. (III.) Phage infection in M9 37 °C LCD was attenuated; cells were not susceptible to phage infection except at a MOI=10. Coloured lines in each graph correspond to different MOIs (0, 0.1, 1, 10) as indicated in the legend. MOI of 0 refers to a bacteria only (no phage) control. Graphs of all conditions are in Appendix (Figure A1). **b,** Summary of the two phage defence phenotypes observed as shown in the respective shaded purple and yellow boxes above.

From the results of experiments done in rich media versus minimal media, it was apparent that the type of nutrients available to bacteria appeared to impact the maximum cell culture density at which cells were still susceptible to phage infection. Therefore, I tested phage infection at low cell density (LCD), i.e., early exponential phase; or high cell density (HCD), i.e., late exponential phase. I observed that cells at LCD re-grew after an initial round of phage-induced lysis. I also observed that cells at HCD were not susceptible to phage infection. From these initial set of experiments designed to identify optimal conditions for Vibriophage N4 infection in cultures of *V. cholerae* C6706, I discovered two anti-phage bacterial phenotypes (Figure 2.2b): (1) evasion of phage predation after initial phage infection when bacteria are at LCD by bacterial re-growth,

and (2) protection against phage infection when bacteria are at HCD. This chapter focuses on the bacterial dynamics of how *V. cholerae* cells cope with lytic phage attack after undergoing phage-induced lysis.

2.3 *V. cholerae* shows re-growth after phage infection

When *V. cholerae* cells were exposed to phages at LCD, the cells lysed due to phage infection, which was followed by an increase in OD_{600}, 2 h after phage infection (Figure 2.3a). I reasoned that the proliferation of bacterial cells could be due to the selection of genetic mutants during phage infection, which would result in the growing population to consist of phage-resistant mutants. To test if the surviving cells were resistant to phage infection, bacteria were isolated from a phage-treated culture by streaking on LB agar plates (Figure 2.3b) and individual colonies were inoculated in fresh LB along with phages. Surprisingly, I found that these bacterial cells were susceptible to phage infection and showed a similar phenotype of lysis and re-growth (Figure 2.3c). Thus, *V. cholerae* cells that survived Vibriophage N4 attack were not genetically resistant to phage infection.

As the bacterial cells that re-grew were still susceptible to phage infection, it was possible that bacteria utilised a defence system to actively lower the phage count in the medium. It is known that phages can be inactivated by compounds released from bacterial cells (239, 240). To test if the reason for bacterial growth post-infection was due to the inactivation of phages, the supernatants of bacterial cultures of *V. cholerae* cells exposed to Vibriophage N4 (MOI = 1) were plated to enumerate the titre of active phages over time. Here, the culture supernatant was first filtered though a $0.22\,\mu\mathrm{m}$ membrane to eliminate bacteria and subsequently plated on a bacterial lawn on LB agar at different timepoints. After overnight incubation of the plates at $37\,^{\circ}\mathrm{C}$, plaques formed on the bacterial lawn. Phages were enumerated by counting the plaque-forming units (PFU). For the same timepoints, bacterial numbers were also enumerated by plating bacteria (after washing to remove phages) and counting the colony-forming units (CFU). We observed that the PFU increased 10-fold, whereas the CFU decreased 100-fold during phage infection. Thereafter, the amount of phages remained constant during the time of increasing number of bacterial cells (Figure 2.3d). These observations indicated that the cells that survived phage infection could grow and divide normally even in the presence of active phages. So, considering that both phages and bacteria were active and susceptible to infection, it suggested the presence of a transient external or internal factor that could limit phage infection in order to enable bacteria growth.

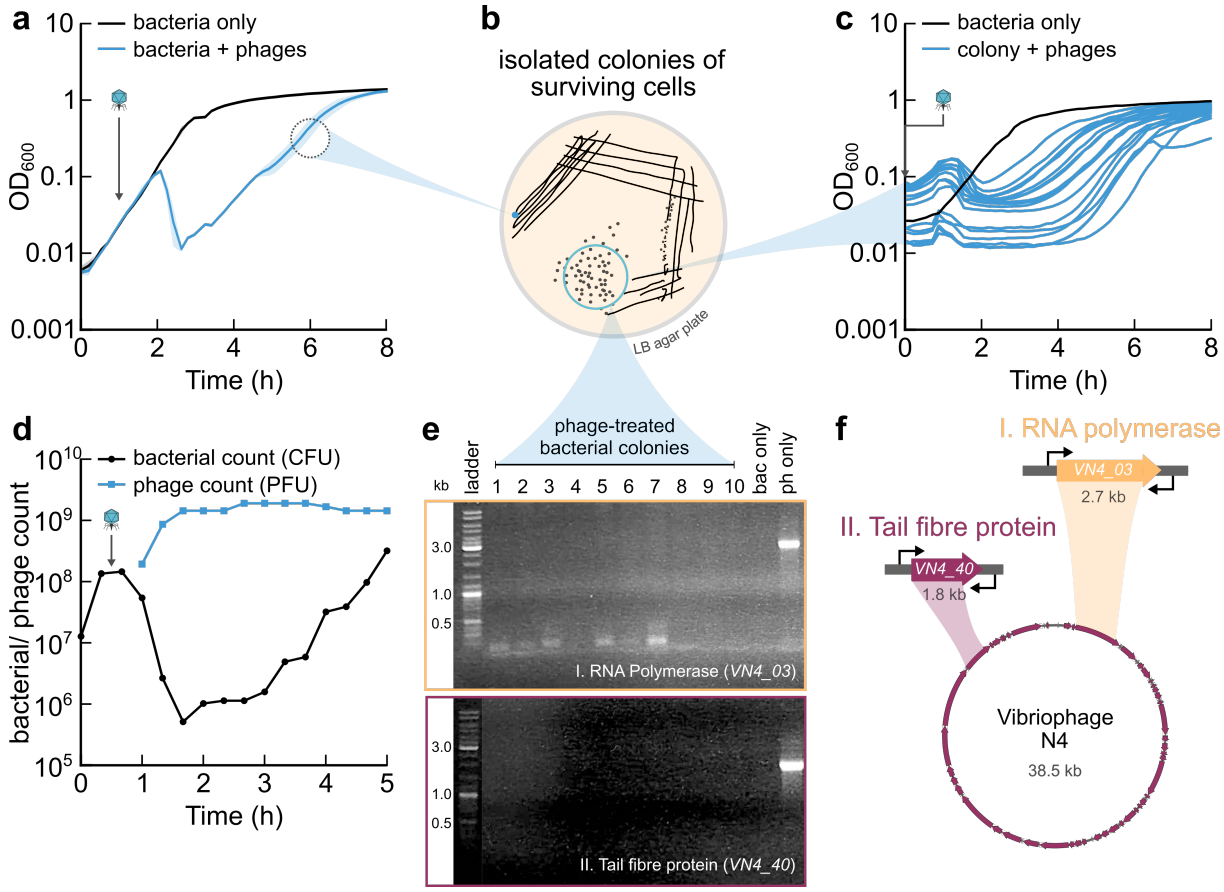

Figure 2.3: *V. cholerae* cells that survived phage infection were not genetically resistant and did not possess any phage DNA. a, Change in culture density (OD_{600}) of *V. cholerae* cells exposed to Vibriophage N4 over time showed bacterial re-growth after phage infection (blue line). Phages were added (MOI=1) to a growing bacterial culture during early log phase, at 1 h (grey arrow), incubated at 37 °C. The bacteria only control (black line) showed normal logarithmic growth followed by stationary phase. Lines represent the mean of three biological replicates and the shaded regions depict the standard deviation. **b,** Bacterial cells that survived phage infection were streaked out on an LB plate and incubated overnight at 37 °C to obtain isolated colonies. **c,** Individual colonies were grown in LB and incubated at 37 °C. Cells from these logarithmically growing cultures were co-incubated with phages (MOI = 1) at 0 h (grey arrow) and the bacterial OD_{600} was tracked over time. Each blue line represents one colony tested for susceptibility to phage infection. Cells from all colonies showed infection followed by re-growth. Fresh *V. cholerae* WT cells were used for the bacteria only control (black line). **d,** Bacterial colony-forming units (CFU, black line) and phage plaque-forming units (PFU, blue line) were enumerated of a bacterial culture that was exposed to phages. The phage count (PFU) increased 10-fold whereas the bacterial count (CFU) decreased 100-fold during phage infection, after which the phage count remained constant during bacterial re-growth. **e,** Agarose gel image showing colony PCR results of cells from phage-treated isolated colonies. No amplicons were obtained from a PCR performed with primers for phage-specific genes (shown in panel f). The bacteria-only lane contained the product of a colony PCR of *V. cholerae* WT cells (negative control). Phages were used as a crude template for a PCR with the same primers (positive control). **f,** Primers used for the colony PCR aimed to amplify phage-specific genes that encode for RNA polymerase (I) or tail fibre protein (II). The expected sizes of the amplified DNA fragments are listed below the gene, which correspond to the sizes of the DNA bands of the phage only lane in the agarose gel image (shown in panel e).

Conserving bacterial hosts is essential for sustainable phage proliferation. Phages that can remain dormant in bacteria without causing lysis by integrating into the bacterial chromosome are called lysogenic phages or prophages (77). However, lytic phages that cannot integrate into bacterial chromosomes due to absence of essential genes required for lysogeny can also sometimes survive inside bacterial cells as plasmid-like circular phage DNA, called episomes or psuedolysogens (241, 242). The presence of these episomes in a bacterial population induces a carrier state life cycle (CSLC), which describes a mixture of bacteria and phages coexisting in a state of equilibrium (243). Bacterial strains exhibiting CSLC are resistant to superinfection (244, 245). To test for the presence of phage DNA in bacterial cells during re-growth, we performed a colony PCR using bacterial cells from 10 isolated colonies from a phage-treated culture and oligonucleotides that targeted sites of phage DNA encoding essential phage proteins (Figure 2.3f). During PCR, no DNA fragments were amplified (Figure 2.3e). This indicated that Vibriophage N4 did not inject its DNA into *V. cholerae* cells.

2.4 Exposure to Vibriophage N4 results in biofilm formation

As the bacterial cells that re-grew were not resistant to phage infection, I hypothesised that the presence of a physical barrier masking phage receptors on the bacteria could have permitted cells to evade phage infection. It has been shown that the accumulation of dead cells forms a barrier between live cells and the lysis-inducing biological agent to protect uninfected cells (246). Biofilm-dwelling cells have also been known to be protected against phage infection as the matrix substances mask bacterial surface receptors (104). To test if such kinds of collective behaviour imparted protection against phage infection, I imaged *V. cholerae* cells during the phase of re-growth using brightfield microscopy. Interestingly, I observed that *V. cholerae* cells formed aggregates during the initiation of bacterial re-growth after phage infection (Figure 2.4).

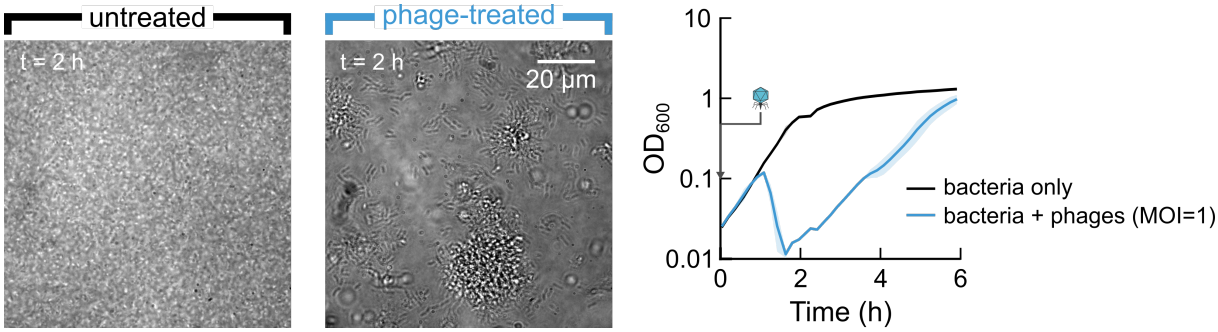

Figure 2.4: *V. cholerae* formed aggregates during Vibriophage N4 exposure in liquid culture experiments. Brightfield images of *V. cholerae* cells sampled from a shaking liquid culture 2 h after the addition of purified phages (MOI = 1) show the presence of aggregates in the phage-treated condition (blue), whereas cells that were not exposed to phages (untreated; black) were in a homogenous suspension.

To visualise the process of phage-induced biofilm formation, I used confocal microscopy to image *V. cholerae* cells (constitutively expressing *sfGFP*) inoculated in microfluidic chambers during a continuous influx of Vibriophage N4 virions for $8\,\mathrm{h}$. Exposing *V. cholerae* cells to phages resulted in an initial decrease of bacterial biomass (similar to liquid culture experiments, Figure 2.3a), with the minimum biomass measured at $2\,\mathrm{h}$ from the initiation of phage inflow. Similar to our observations in the liquid culture system, we observed that during the course of the population-wide phage-induced lysis, there were a few cells that did not lyse but continued to multiply, forming biofilms over the following $6\,\mathrm{h}$, in spite of the constant exposure to phages (Figure 2.5a). In comparison, bacterial cells that were grown in the absence of phages showed a gradual increase in biomass, forming a lawn, as cells proliferated across the surface of the microfluidic chamber.

To analyse and quantify this bacterial response to phage exposure, the acquired images was quantified using a specialised in-house developed software to analyse different aspects of biofilms, called *BiofilmQ* (36). Global changes in bacterial biomass were inferred by measuring the total volume of fluorescent bacterial cells (hereafter, referred to as 'biovolume') attached to the surface of the microfluidic chamber over time. *V. cholerae* cells that were not exposed to phages (untreated) showed an increase in bacterial biovolume and maintained a constant level after saturating the surface of the microfluidic channel (Figure 2.5c). Phage-treated chambers showed a decrease in biovolume during phage infection followed by an increase in biovolume during biofilm formation. This was different from the increase in OD_{600} that we observed when bacteria and phages were incubated in liquid culture (Figure 2.4). OD_{600} measurements were unable to convey a increase in bacterial biomass when cells were in aggregates. By measuring fluorescence of cells in microfluidic chambers, we overcame this caveat and gained a more accurate representation of the bacterial response to phage exposure.

Biofilms are defined as matrix-embedded bacterial communities that show growth and expansion in three dimensions (15). Making use of this salient feature of biofilms, we quantified the growth of bacterial cells in the z-direction, i.e., the biofilm height. Biofilm formation was measured by calculating a parameter we termed as biofilm biovolume fraction. Here, the amount of bacterial biomass present $3\,\mu\mathrm{m}$ above the surface ($H > 3\,\mu\mathrm{m}$) was divided by the total biomass for each imaged position. This parameter was used to quantify the biofilm-forming ability of *V. cholerae* cells in response to phage exposure. Bacterial cells exposed to phages showed an increase in the biofilm biovolume fraction from the third hour of phage exposure, which temporally coincided with the growth of cells as biofilms after the majority of cells had been lysed (Figure 2.5c). In the absence of phages, the growth of bacterial cells was limited to less than $3\,\mu\mathrm{m}$ in height, and thus this condition showed low values (< 0.1) of their biofilm biovolume fraction. Thus, exposure to lytic phages resulted in an initial lysis of *V. cholerae* cells, followed by a recovery of bacterial growth in the form of biofilms.

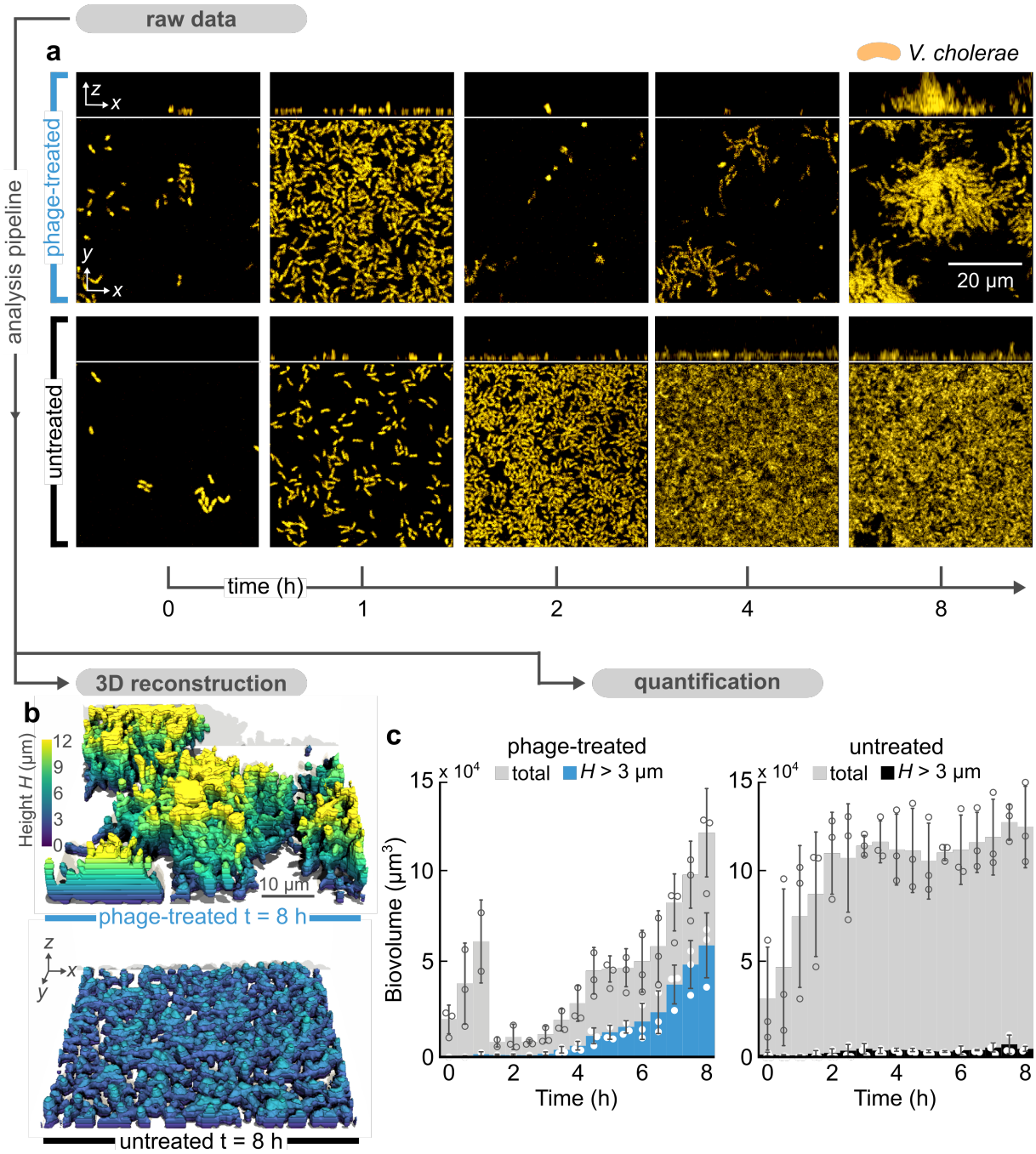

Figure 2.5: *V. cholerae* cells survived the lytic attack of Vibriophage N4 by growing as biofilms. a, Confocal image time series of *V. cholerae* cells (yellow), constitutively expressing *sfGFP*, under the control of a chromosomal P_{tac} promoter, exposed to a continuous flow of Vibriophage N4 virions (10^6 PFU mL^{-1}, blue) or untreated (black) over 8 h. Bacterial cells exposed to phages show an initial decrease in total biomass during phage infection, followed by growth as biofilms in the presence of a continuous flow of phages. In the absence of phages, cells grow as a lawn to confluently cover the surface of the flow chamber. **b,** Rendered images of phage-treated (blue) or untreated (black) *V. cholerae* cells after 8 h. Cells are coloured according to their height H above the bottom surface of the microfluidic chamber. **c,** Quantification of the total biovolume (grey bars) and fraction of biovolume with height $H > 3\,\mu$m of bacterial cells over 8 h in the presence (blue bars) or absence (black bars) of Vibriophage N4 (10^6 PFU mL^{-1}). Biovolume represents the volume (μm^3) occupied by fluorescent bacterial cells. Bars are mean values with points (open grey circles or white closed circles for total or $H > 3\,\mu$m biovolume, respectively) denoting 3 biological replicates and error bars indicate the standard deviation.

2.5 Phage titre influences the size of the resulting biofilms

In shaking liquid cultures, I observed that the time taken for phage infection and re-growth was influenced by the MOI (Figure 2.2). To test whether the concentration (titre) of phages exposed to *V. cholerae* cells affected biofilm formation in microfluidic chambers, bacterial cells were exposed to varying titres of Vibriophage N4. We observed that increasing the phage titre resulted in increasing values of the maximum biofilm biovolume fraction. The biofilm biovolume fraction was dependent on the concentration of phages supplied in the microfluidic chamber until a phage titre of $10^6\,\mathrm{PFU\,mL^{-1}}$, after which it plateaued at a maximum value of 0.55 for a phage titre of $10^8\,\mathrm{PFU\,mL^{-1}}$ (Figure 2.6). This indicated that the extent of biofilm formation was dependent on the amount of phages supplied in the chamber.

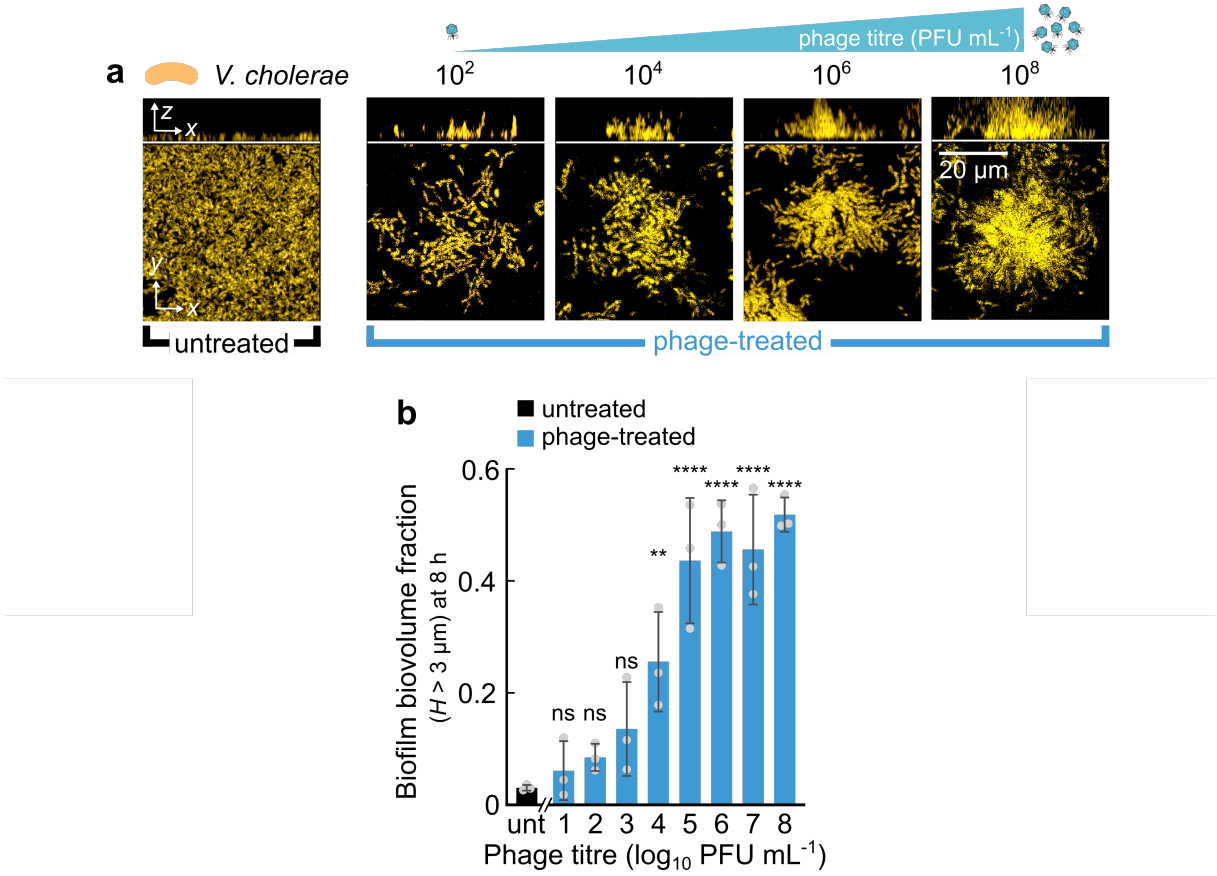

Figure 2.6: Biofilm formation in *V. cholerae* increased with increasing titre of Vibriophage N4. a, Confocal images of *V. cholerae* cells constitutively expressing *sfGFP* (yellow) after $8\,\mathrm{h}$ in the absence (untreated, black) or presence (phage-treated, blue) of varying phage titres. **b,** 3D biofilm formation increased with increasing phage titre. Biofilm biovolume fraction was quantified as the sum of the biovolume with height $H > 3\,\mu\mathrm{m}$ divided by the total biovolume. Bars are mean values with points denoting 3 biological replicates and error bars indicate the standard deviation. Statistical significances were calculated relative to the untreated condition using a one-way ANOVA with Bonferroni's correction (ns = not significant, ** = $p < 0.01$; **** = $p < 0.0001$).

2.6 Phage-induced biofilm formation is independent of bacterial cell density

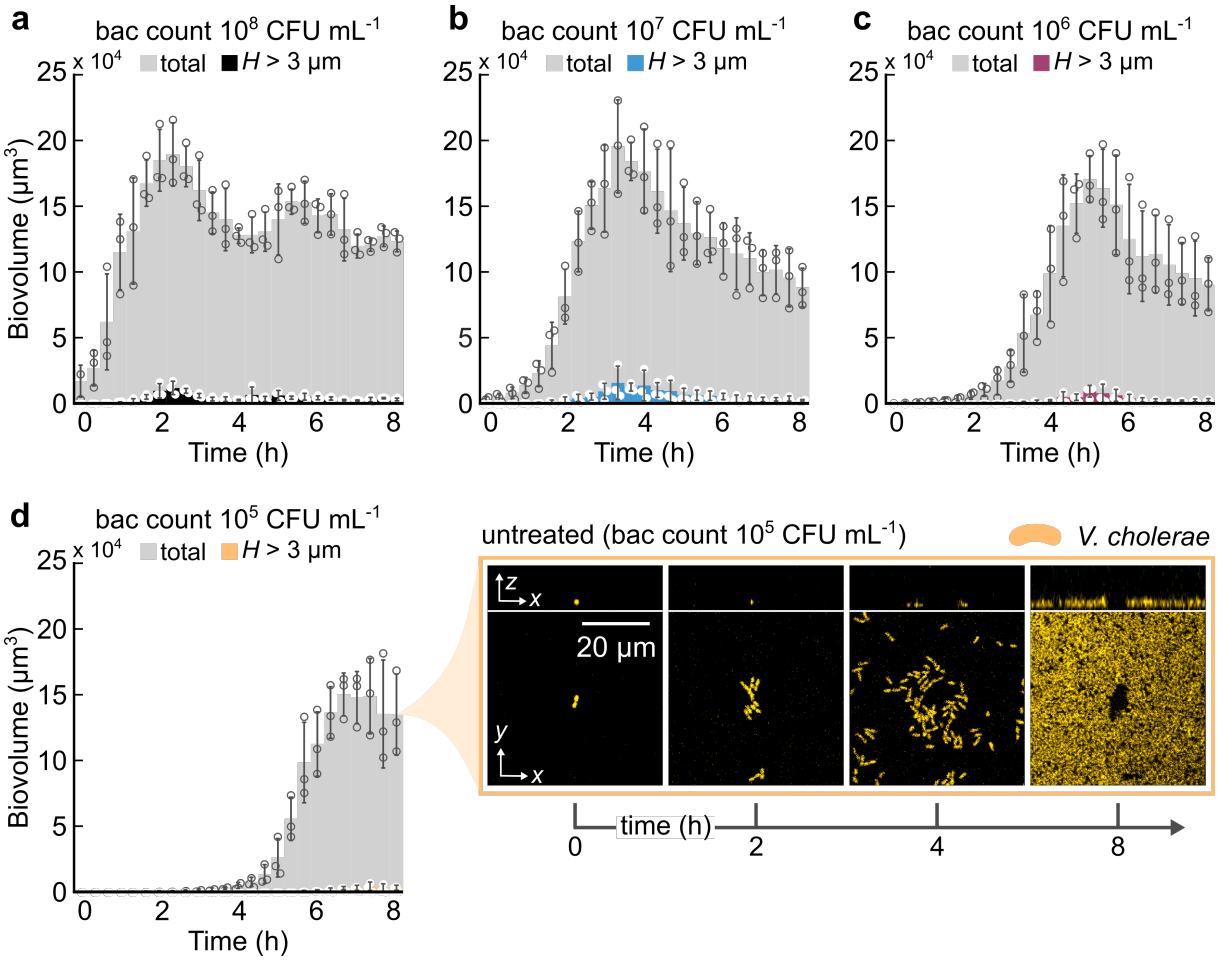

Figure 2.7: *V. cholerae* cells at LCD did not produce biofilms in the absence of phages. Quantification of the total biovolume (grey bars) and fraction of biovolume with height $H > 3\,\mu m$ (coloured bars) of bacterial cells diluted to varying starting concentrations during continuous flow of LB (no phages) over $8\,h$: **a,** $10^8\,CFU\,mL^{-1}$ (black; represents the same condition as Figure 2.5 untreated), **b,** $10^7\,CFU\,mL^{-1}$ (blue), **c,** $10^6\,CFU\,mL^{-1}$ (purple), **d,** $10^5\,CFU\,mL^{-1}$ (yellow) did not show biofilm formation. The inset depicts a confocal image time series of *V. cholerae* cells (yellow), constitutively expressing *sfGFP*, inoculated at an initial density of $10^5\,CFU\,mL^{-1}$, grown in the absence of phages. No biofilm formation in the absence of phages indicated that biofilm formation in the presence of phages could not be explained by bacterial cells being at LCD. Bars are mean values with points (open grey circles or white closed circles for total or $H > 3\,\mu m$ biovolume, respectively) denoting 3 biological replicates and error bars indicate the standard deviation.

As *V. cholerae* cells form biofilms at LCD (182), it was possible that the decrease in bacterial numbers during phage infection caused biofilm formation. To test whether biofilm formation during phage treatment was solely due to *V. cholerae* being at LCD, microfluidic chambers were inoculated with a varying number of bacterial cells (10^5-$10^8\,CFU\,mL^{-1}$) and grown in the absence of phages. For all other experiments in microfluidic chambers, an initial bacterial inoculation

density of $10^8\,\mathrm{CFU\,mL^{-1}}$ was used. Biofilm formation was not observed in any condition (Figure 2.7). Therefore, in the absence of phages, *V. cholerae* cells did not form biofilms. This confirmed that biofilm formation was not a facet of the cells being at LCD after phage infection.

2.7 Biofilm-forming cells are not phage-resistant mutants nor matrix hyper-producers

As phage infection did not result in complete killing of the bacterial population, it was possible that the resultant biofilms were made of mutants that were genetically resistant to phage infection or programmed to constitutively secrete matrix components. To test the susceptibility of surviving cells to phage infection, biofilm-dwelling *V. cholerae* cells were harvested from phage-treated microfluidic chambers and re-exposed to phages. Bacterial cells were collected by scraping of biofilms that were adhered to the glass surface of the channel and washing in fresh LB to create a suspension of homogeneously distributed single cells (Figure 2.8a). These bacteria were then exposed to phages and phage infection was monitored by measuring the OD_{600} of the bacterial culture. Bacterial susceptibility to phage infection was confirmed by a decrease in OD_{600} (Figure 2.8b). It was impossible to eliminate phage particles completely from the bacterial suspension during collection and therefore, we also saw a decrease in OD_{600} when only harvested cells were inoculated in fresh LB. Thus, the biofilms formed during phage treatment were not made up of genetically resistant cells.

In response to environmental stress, *V. cholerae* has been known to exhibit rugosity, i.e., a high-matrix production phenotype. Rugose strains are characterised by their wrinkled colony morphology on agar plates as well as their increased secretion of *Vibrio* polysaccharide (VPS) (247, 248). To test for the presence of rugose variants in the biofilms formed after phage infection, cells were collected from phage-treated microfluidic chambers (Figure 2.8a) and plated on LB agar plates. None of the observed colonies showed a rugose phenotype (Figure 2.8c). When the individual colonies were tested for their susceptibility to phage infection, I found that the resultant colonies consisted of both sensitive and resistant strains. Due to the presence of phages that were collected along with the harvested bacterial cells, phage-resistant mutants could have arisen by natural selection during the prolonged exposure of phages on the LB agar plates. To quantify the extent of biofilm formation of the cells from the sample colonies, I inoculated individual colonies in LB using 96-well plates and performed a crystal violet assay. The phage-resistant mutants showed a genetic predisposition to grow as biofilms to a greater extent as compared to the WT. However, colonies composed of cells that remained susceptible to phage infection showed low biofilm formation, similar to the WT (Figure 2.8d). This suggested that resistance to phage infection was coupled with an increase in biofilm production in bacterial cells that were exposed to phages for a prolonged duration of time. However, this selection was not relevant in the time frame of the experiment and hence, could not explain biofilm formation in microfluidic channels as the majority of cells harvested from the channel were still susceptible to phage infection. Thus, the cells that constituted phage-induced biofilms were not genetically programmed to form biofilms.

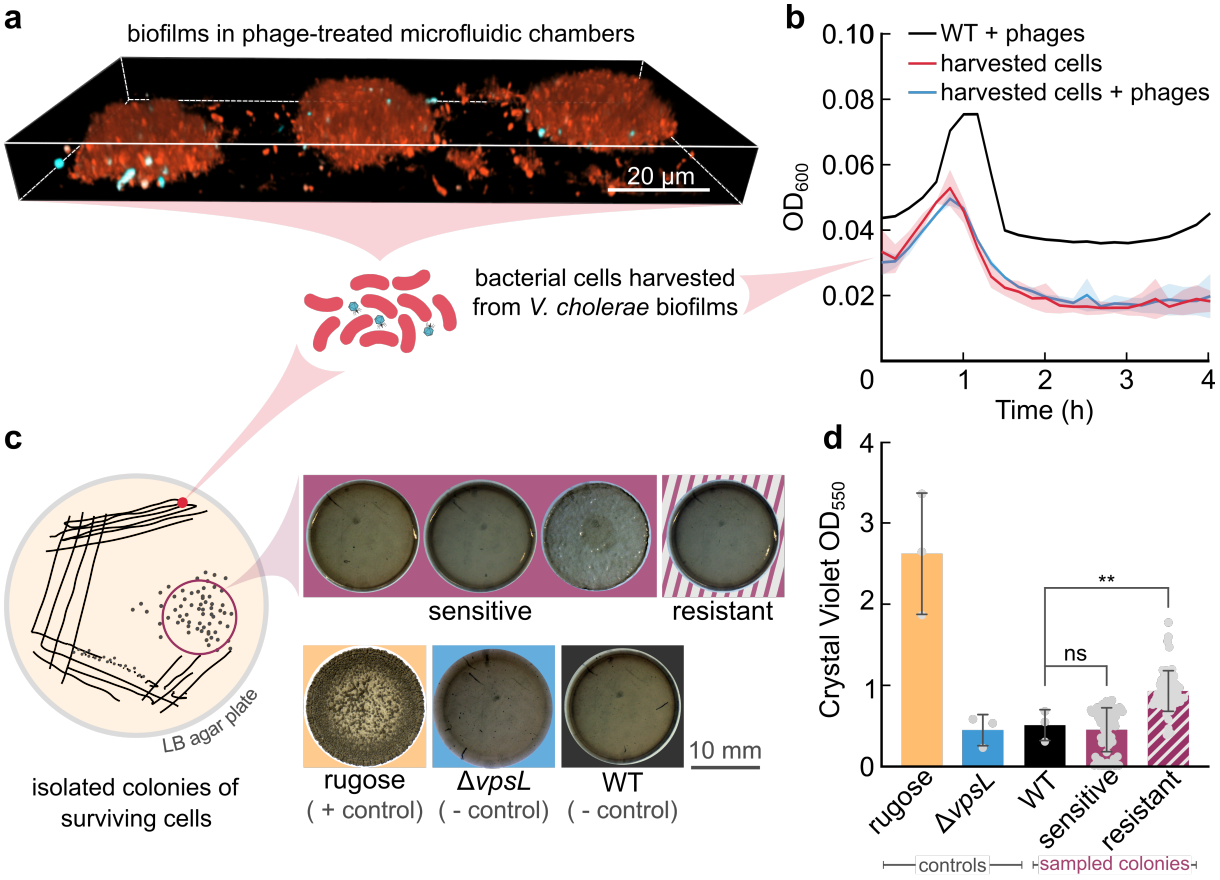

Figure 2.8: Biofilms formed in phage-treated conditions were not composed of resistant cells nor matrix hyper-producers. **a,** Bacterial cells were harvested from biofilms formed by *V. cholerae* cells in response to $8\,\mathrm{h}$ of Vibriophage N4 exposure ($10^6\,\mathrm{PFU\,mL^{-1}}$). Cells were vortexed and washed twice with LB to remove matrix components and phages respectively, from the medium. **b,** Bacterial cells were subsequently transferred to a 96-well plate and inoculated with fresh Vibriophage N4 virions ($10^6\,\mathrm{PFU\,mL^{-1}}$, blue) or LB only (red). The plate was incubated at $37\,^{\circ}\mathrm{C}$ shaking for $4\,\mathrm{h}$ during which cell density measurements (OD_{600}) were taken every $10\,\mathrm{min}$. As a positive control, exponentially growing *V. cholerae* cells (not exposed to phages) were also inoculated with fresh phages (black), and showed successful phage infection. Both the untreated and phage-treated wells also showed a decrease in cell density, indicating that biofilm-dwelling *V. cholerae* cells were still susceptible to phage infection (the untreated condition still had a few phages that could not be reliably removed from harvested bacterial cells). Lines represent the mean of three biological replicates and shaded regions indicate the standard deviation. **c,** Harvested *V. cholerae* cells were streaked out on multiple LB agar plates. The isolated colonies of surviving cells (purple) were imaged using a stereomicroscope and compared to controls. *V. cholerae* WT cells (not exposed to phages, black) and cells lacking in VPS production (Δ*vpsL*, blue), which showed smooth colony morphologies, were used as negative controls. On the other hand, a matrix hyper-producing strain of *V. cholerae* (rugose, yellow), which showed a wrinkled colony morphology, was used as a positive control. All colonies formed from bacteria that were harvested from phage-induced biofilms showed a smooth morphology, similar to the negative controls. Bacteria from colonies were tested for their ability to survive phage infection and marked as sensitive (solid purple) or resistant (purple-grey striped). Both sensitive and resistant colonies showed a smooth colony morphology. **d,** A crystal violet assay was used to quantify the extent of biofilm formation of the isolated colonies of harvested cells, along with the control strains. The rugose strain (yellow) showed high matrix production as compared to the WT (black) and Δ*vpsL* strain (blue), as has been described previously in literature (248). There was a disparity in ...

Figure 2.8: ... the matrix production of the tested colonies; some showing matrix production similar to the WT, but less than the rugose strain. The matrix production of these two subpopulations corresponded with their susceptibility to phage infection. Although all tested cells showed a smooth colony morphology, the ones susceptible to phage infection were indistinguishable from the WT with respect to matrix production. Bars are mean values with points denoting sampled data for each condition and error bars indicate standard deviation. Statistical significances between the sampled colonies and the WT control were calculated using a Student's t-test (ns = not significant; ** = $p < 0.01$).

2.8 A multi-omics approach to characterise the bacterial response to phage exposure

As the exposure to Vibriophage N4 did not result in genetic mutants that could impart resistance to *V. cholerae* cells against phage infection, I hypothesised that biofilm matrix production could be responsible for bacterial protection against phage infection (104, 115). Therefore, to test if genes related biofilm formation or regulation were induced during phage infection, I used a multi-omics approach. To identify the genes that played a role in phage-induced biofilm formation, I measured differential protein and gene expression using mass spectrometry (proteomics) and RNA-Seq (transcriptomics), respectively, for bacterial cells that were exposed to phages (MOI = 1) for $1\,\mathrm{h}$ compared to untreated cells. In this way, the proteome and transcriptome profile of *V. cholerae* cells that were the precursors of the resultant biofilms was compared to the cells that had never been exposed to phages, in order to identify the pathways that were important for biofilm formation after phage exposure. To collect sufficient biomass of cells after phage infection, *V. cholerae* cells were grown and infected with Vibriophage N4 in large batch cultures. Samples were collected from a culture of *V. cholerae* cells at $OD_{600} = 0.4$ (untreated), just prior to phage addition, and then $1\,\mathrm{h}$ after phage addition, when the OD_{600} had decreased to 0.1 (phage-treated) as a result of phage-induced bacterial lysis (Figure 2.9a). The amount of culture volume was adjusted in order to keep the number of harvested bacterial cells constant.

Proteomics analysis revealed that proteins responsible for biofilm matrix production were significantly more abundant (>3-fold) in phage-treated cells as compared to untreated cells (Figure 2.9b). These included proteins that have been described to contribute to VPS production, namely, VpsI (VC0925), VpsK (VC0927), and VC0937. A matrix component that is known to be important during early stages of biofilm formation, Bap1 (VC1888), was also more abundant in phage-treated cells as compared to untreated cells (52). Similarly, transcriptomics analysis also indicated that genes encoding biofilm matrix proteins were significantly upregulated (>2-fold) in phage-treated cells as compared to untreated cells (Figure 2.9c). Genes encoding proteins responsible for VPS production (53) belonging to the *vps*-I cluster (*vc0917-vc0927*) and *vps*-II cluster (*vc0934-vc0937*) were upregulated (>4-fold). Moreover, genes encoding important matrix proteins such as *vc0928* (*rbmA*), *vc0930* (*rbmC*), and *vc1888* (*bap1*) also showed higher expression (>4-fold). In addition to genes encoding matrix components, I also observed an increase of biofilm regulators in both analyses. Phage-treated cells showed an increased abundance of VpsR (VC0665), which is known to activate biofilm formation in a c-di-GMP-dependent manner

(249). Transcriptomics analysis showed an increase in transcript levels of *vca0952* (*vpsT*) as well as *vc0916* (*vpsU*), which together are responsible for regulating the production of matrix proteins (53). Together, these two omics approaches confirmed that exposure to Vibriophage N4 induced a biofilm formation response. However, in addition to biofilm activators, proteomics analysis showed that phage exposure also resulted in the expression of an important biofilm repressor, HapR (VC0583) (182). This represents a unique bacterial state, in which opposing regulators are expressed but biofilm formation nevertheless prevails.

There were 268 proteins that showed fold changes >3 in phage-treated cells compared to untreated cells[2]. Out of these, 39 proteins were transporters, 51 proteins were related to cellular metabolism, 47 proteins were involved in other cellular processes (such as cell division, translation, DNA repair, peptidoglycan biosynthesis, etc.), and 54 proteins had unknown functions. The remaining 77 proteins are discussed in the following paragraphs. There were 60 genes that showed differential gene expression, i.e., >2-fold upregulation[3]. Out of these, 5 genes encoded transporters, 6 genes were related to cellular metabolism, 8 genes were involved in other cellular processes (such as proteases, envelope proteins, and CTX prophage expression), and 11 genes had unknown functions. The remaining 30 genes are discussed in the following paragraphs.

Proteins corresponding to subunits of fructose-specific enzyme II (EII) of the phosphotransferase system (PTS), i.e., VC1821, VC1822, and VC1826, showed a fold-change of >4 in response to phage exposure. PtsP (VC0672), which corresponds to enzyme I (EI) of the PTS, also was more abundant in phage-treated cells. Interestingly, the transcriptomics analysis also showed that genes encoding components of the same PTS pathway, including *vc1820*, *vc1821*, and *vc1826* were upregulated. Therefore, phage exposure induced, the production of the fructose-specific PTS components on a transcriptional and translational level.

Cells that were exposed to phages showed increased production of chemotaxis-related proteins as compared to cells in the untreated condition. These proteins included methyl-accepting chemotaxis-like proteins (chemoreceptors) such as VC0216, VC1298, VC1859, VC1868, Mlp24 (VC2161), VC2439, VCA0663, and Mlp43 (VCA1069). CheV proteins CheV-2 (VC2006) and CheV-3 (VC2202), which are responsible for coupling the CheA histadine kinase (HK) to the chemoreceptors (250), also showed increased production after phage exposure. Other HK proteins, responsible for sensing environmental signals, such as VarS (VC2453) and CqsS (VCA0522), also showed increased production in phage-treated cells. CqsS is responsible for sensing QS autoinducers that are produced by CqsA (VCA0523) (182), which also showed a large fold-change (>40) in cells that were exposed to phages. HK such as *carS* (*vc1319*), *vc1349*, and *cqsR* (*vc1831*) also showed higher transcript levels in phage-treated cells compared to untreated cells. HK proteins typically instigate a bacterial response by phosphorylating their corresponding response regulator (RR) (153). Here, I observed that a gene encoding a RR produced during LCD and *V. cholerae* biofilm formation, *aphA* (*vc2647*) was upregulated 2.5-fold in phage-treated cells. However, it remains unclear how these genes and proteins play a role in bacterial signalling during phage exposure.

[2]all proteins showing differential increased expression listed in Appendix Table A1
[3]all genes showing differential upregulation listed in Appendix Table A2

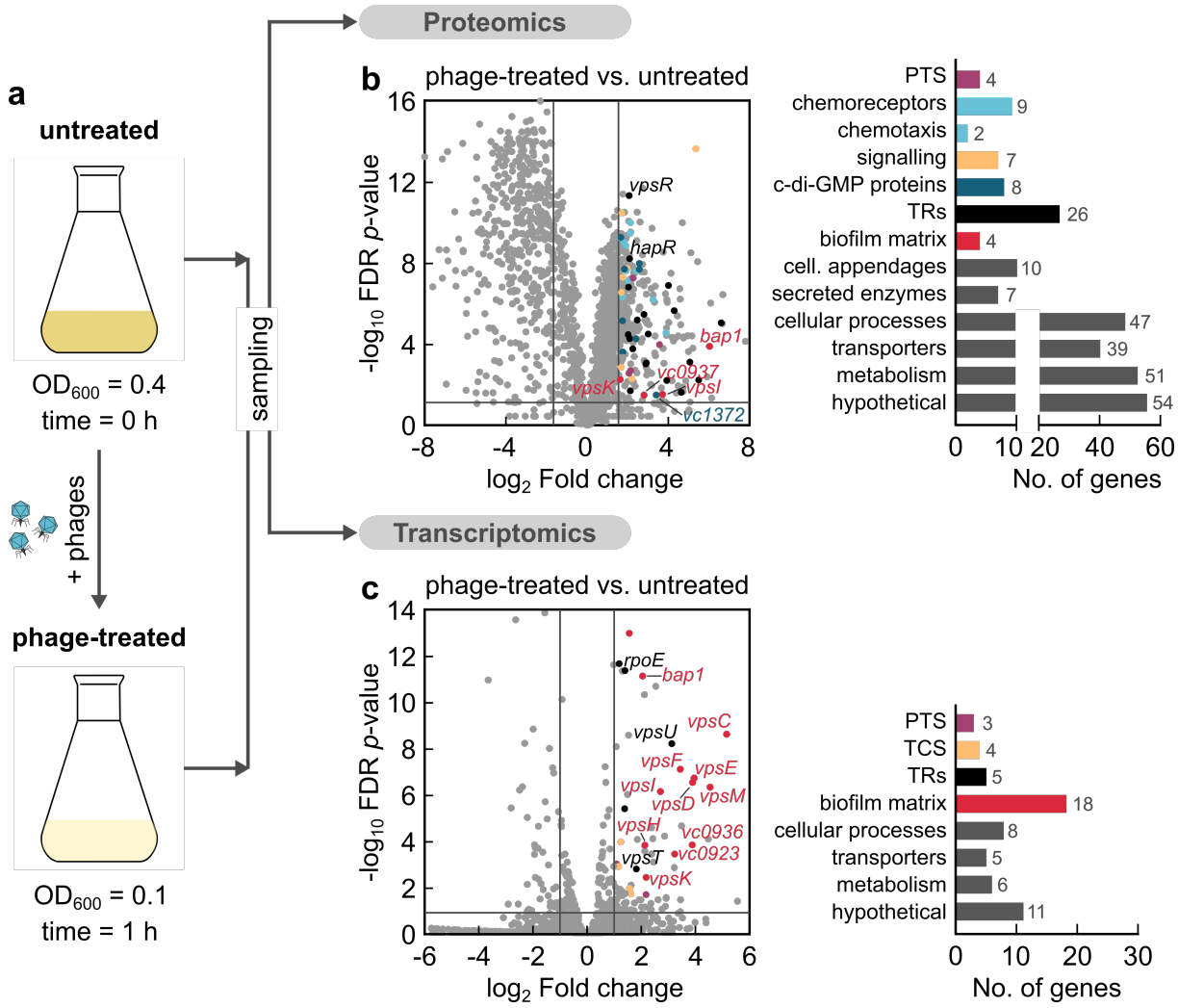

Figure 2.9: Proteomics and transcriptomics of *V. cholerae* exposed to Vibriophage N4 uncovered that proteins and genes linked to biofilm matrix production were differentially expressed. a, *V. cholerae* WT cells grown in a shaking liquid culture to exponential phase (OD_{600} = 0.4) were infected with Vibriophage N4 (phages; MOI = 1) for 1 h at 37 °C with shaking. Phage infection resulted in clearing of the bacterial culture (OD_{600} = 0.1). In order to perform proteomics (**b**) and transcriptomics (**c**), bacterial cells were sampled before and after phage infection, representing the untreated and phage-treated condition, respectively. Volcano plots depict differentially regulated proteins (**b**) or genes (**c**) during phage treatment that were identified by comparing the proteome or transcriptome, respectively, of *V. cholerae* WT phage-treated cells to untreated cells. Proteins with absolute fold changes of ≥ 3 and a false discovery rate (FDR) corrected *p*-value of ≤ 0.05 were considered to be differentially expressed (**b**). Genes with absolute fold changes of ≥ 2 and a FDR-corrected *p*-value of ≤ 0.05 were considered to be differentially expressed (**c**). Proteins (**b**) or genes (**c**) showing increased expression were functionally categories (coloured dots) using a combination of annotations from UniProt (251), KEGG (252), and MicrobesOnline (253). Colours correspond to the colours of the adjacent bar graph, which is a quantification of the number of proteins or genes differentially upregulated for each mentioned category.

Bacteria employ cyclic nucleotides as secondary messenger molecules to influence transcriptional regulation (191). The proteomics analysis showed that proteins related to cGAMP production, CapV (VC0178) and DncV (VC0179), showed increased fold-changes (>3) in response to phage

exposure. Proteins related to c-di-GMP, which is a major regulator of biofilm formation and virulence in *V. cholerae* (205), also showed differential expression. Diguanylate cyclases (DCG), such as VC1372, VCA0049, and CdgF (VCA0956) showed high fold changes (10.6, 5.3, and 3.2, respectively), indicating that cellular levels of c-di-GMP may increase in response to phage exposure. However, phosphodiesterases (PDE) such as CdpA (VC0130), CdgJ (VC0137), RocS (VC0653) were also expressed. This suggests a more complex regulation of c-di-GMP. In addition, proteins that bind c-di-GMP, such as PlzC (VC2344) and PlzD (VCA0042), showed increased production in cells that were exposed to phages. PlzC and PlzD have been shown to influence cellular motility (205). The proteomics analysis strongly indicates the involvement of cyclic nucleotides such as cGAMP and c-di-GMP during phage-induced biofilm formation.

Overall, the combined proteomics and transcriptomics analyses of *V. cholerae* cells during phage exposure provided data that uncovered the involvement of various groups of bacterial genes during phage protection. It was clear from both methods that *V. cholerae* cells actively initiated biofilm matrix production during phage exposure. Furthermore, the potential role of bacterial signalling pathway components such as PTS, two-component systems (TCS), and cyclic nucleotides was revealed. The mechanism of how phage exposure induces biofilm formation in *V. cholerae* is further explored in the next sections.

2.9 Visualisation of biofilm matrix production during phage exposure

Matrix production is the hallmark of biofilm formation and therefore, it was necessary to visualise biofilm matrix production spatiotemporally during phage infection. For this, I exposed *V. cholerae* cells expressing the gene encoding the fluorescent protein mRuby2, under the control of the promoter of *vps* genes (P_{vpsL}-*mRuby2*) to Vibriophage N4 in microfluidic chambers. The bacterial cells also produced the fluorescent protein sfGFP constitutively (P_{tac}-*sfGFP*), which was used to normalise for cellular fluorescence levels. After population-wide phage-induced lysis, some cells started to produce mRuby2, which was an indicator of *vps* transcription, and consequently initiated biofilm formation (Figure 2.10a). These experiments showed that the transcription of matrix-encoding genes initiated very quickly after cell lysis. In the untreated condition, there were a few *V. cholerae* cells that showed mRuby2 production in the initial timepoints. However, these cells did not form biofilms and showed decreased fluorescence levels over time. mRuby2 production was quantified by plotting kymographs that depict changes in the level of *vps*-regulated fluorescence normalised by the constitutive fluorescence (indicated by the colourmap) across the height of the bacterial biofilm (y-axis) and over time (x-axis). These kymographs showed that *V. cholerae* cells transcribed *vps* genes during micro-colony formation (Figure 2.10b) while fresh phages were constantly supplied.

Along with *Vibrio* polysaccharide (VPS), the biofilm matrix protein RbmA also plays a major role in *V. cholerae* biofilm formation (52). Using anti-His antibodies conjugated to a fluorescent dye, the abundance of RbmA (with a polyhistidine-tag) was visualised during Vibriophage N4 exposure. Immunofluorescence staining showed that RbmA forms shells around the cells secreting it. *V. cholerae* cells exposed to phages produced RbmA during phage infection and these cells formed biofilm colonies over time (Figure 2.11a). RbmA shell formation was also seen for a few cells in the untreated condition but these cells did not form biofilms or continue producing RbmA during cell division over the period of the experiment. RbmA shells were quantified spatiotemporally by plotting the intensity of fluorescent anti-His antibodies (indicated by the colourmap) across the height of the bacterial biofilm (y-axis) and over time (x-axis). These kymographs showed that *V. cholerae* cells produced RbmA during phage-induced biofilm formation (Figure 2.11b).

Visualising the expression of major matrix components VPS and RbmA confirmed that *V. cholerae* cells initiated biofilm formation as a response to phage exposure.

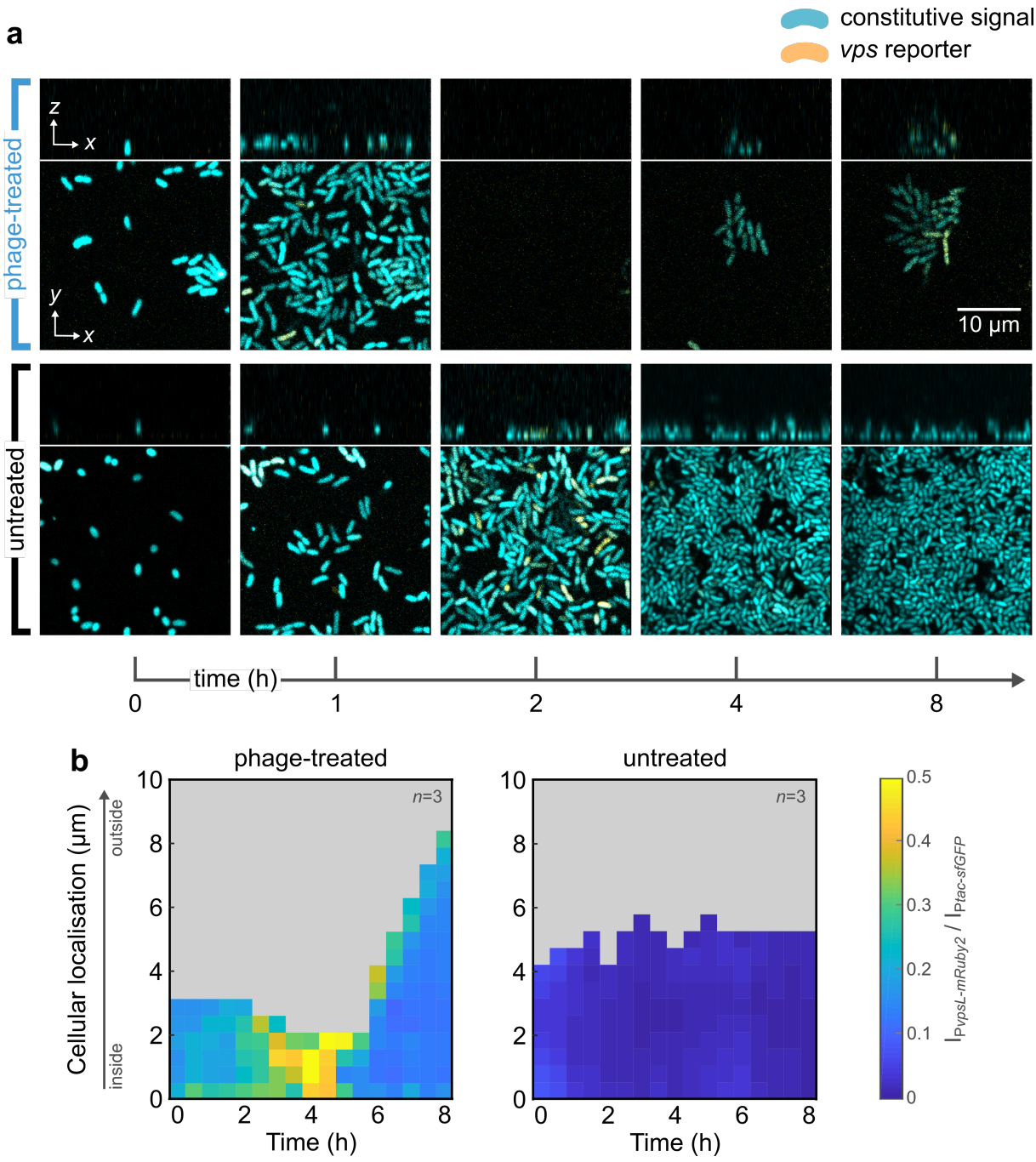

Figure 2.10: *V. cholerae* cells express *vps* genes in response to phage exposure. a, Confocal image time series of *V. cholerae* cells constitutively expressing *sfGFP* (cyan), under the control of the P_{tac} promoter, and mRuby2 (yellow), under the control of the P_{vpsL} promoter, exposed to a continuous flow of Vibriophage N4 ($10^6\,\mathrm{PFU\,mL^{-1}}$, blue) or untreated (black) over $8\,\mathrm{h}$. Bacterial cells exposed to phages show transcription from the *vps* promoter during phage exposure. In the absence of phages, only a few cells show *vps* transcription, but do not develop into biofilms. **b,** Visualisation of the spatiotemporal dynamics of the *vps* operon transcription in the presence or absence of Vibriophage N4 ($10^6\,\mathrm{PFU\,mL^{-1}}$). The fluorescence of the *vps* transcriptional reporter (P_{vpsL}-*mRuby2*) was normalised by the fluorescence intensity of a constitutive reporter (P_{tac}-*sfGFP*). Each pixel in these kymographs is coloured according to the ratio of fluorescence expression at a given time and spatial position in the biofilm. Fluorescence expression values were averaged over all cells with similar distances from the outer biofilm boundary facing the liquid medium. Kymographs are representative of $n = 3$ different biofilms.

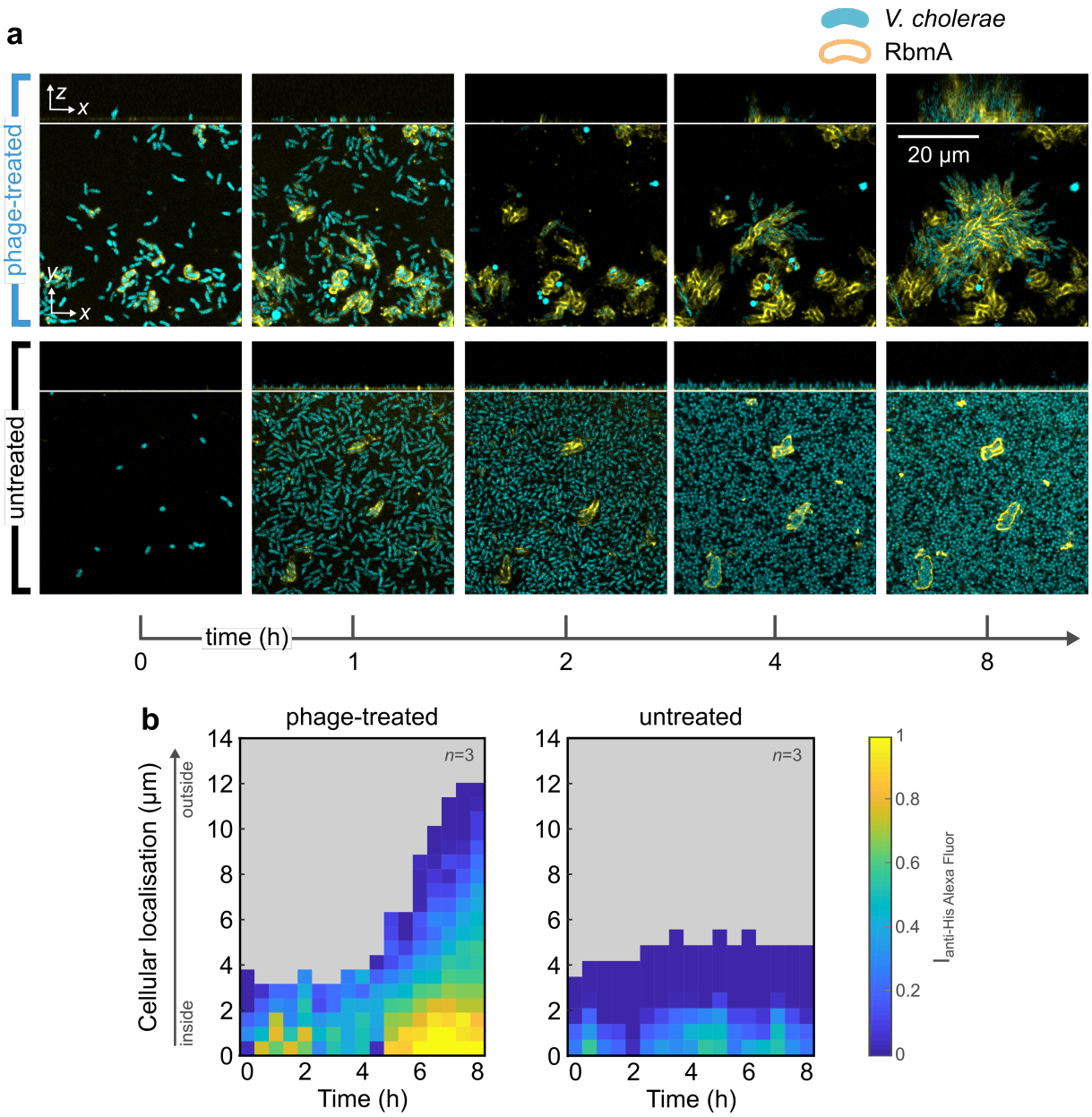

Figure 2.11: *V. cholerae* cells produced RbmA in response to phage exposure. a, Confocal image time series of *V. cholerae* cells constitutively expressing *sfGFP* (cyan), under the control of a P_{tac} promoter, exposed to a continuous flow of Vibriophage N4 ($10^6\,\mathrm{PFU\,mL^{-1}}$, blue) or untreated (black) over $8\,\mathrm{h}$. Bacterial cells exposed to phages showed RbmA production (yellow shells), visualised by using fluorescent anti-His Alexa Fluor antibodies that conjugate with polyhistidine-tagged RbmA, during phage-induced biofilm formation. In the absence of phages, only a few cells showed RbmA production, but did not develop into biofilms. **b,** Visualisation of the spatiotemporal dynamics of RbmA production in the presence or absence of Vibriophage N4 ($10^6\,\mathrm{PFU\,mL^{-1}}$). The fluorescence expression of the anti-His Alexa Fluor antibody at a given time and spatial position in the biofilm. Fluorescence expression values were averaged over all cells with similar distances from the outer biofilm boundary facing the liquid medium. Kymographs are representative of $n = 3$ different biofilms.

2.10 Construction of a fluorescent phage infection reporter

In order to study how phages influenced bacterial behaviour, a tool to distinguish infected and uninfected cells was required. For this, I developed a fluorescent reporter to enable spatiotemporal visualisation of phage infection. This reporter relied on the introduction of a phage-regulated promoter into the bacterial genome so that when a bacterial cell was infected by a phage, the promoter would be recognised by the phage RNA polymerase and subsequently would initiate transcription of the regulated gene. For the efficient functioning of this reporter, a strong phage promoter was required, along with a fast-folding fluorescent protein that had a maturation time less than the time required for one lytic cycle.

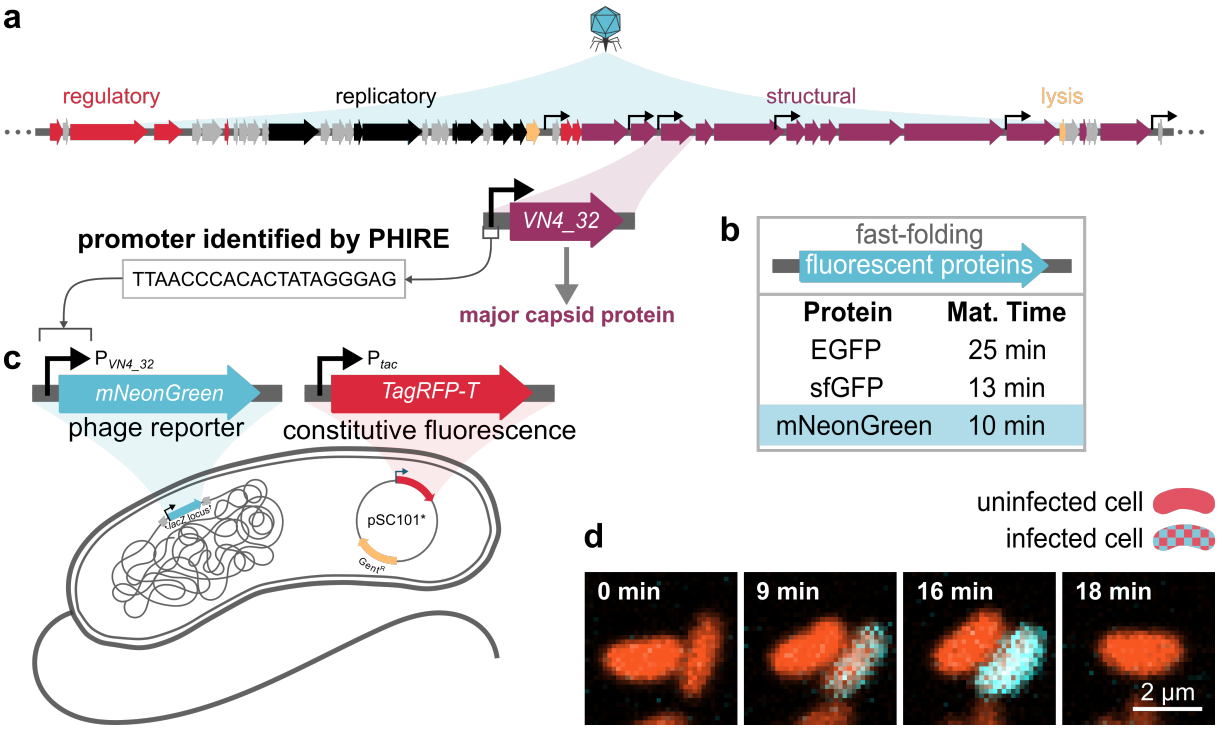

Figure 2.12: Construction of a fluorescent reporter to visualise infection by Vibriophage N4 in *V. cholerae* cells. a, Results of the bioinformatic analysis performed on the Vibriophage N4 genome by PHIRE (254) showing the positions of the phage promoter regulating the transcription of the gene encoding the major capsid protein (encoded by *VN4_32*). **b,** Table of fast-folding green fluorescent proteins and their maturation times as measured in *E. coli* (255). **c,** Schematic of the constructed bacterial fluorescent phage reporter system. The phage reporter consists of the phage promoter (P_{VN4_32}) followed by *mNeonGreen* (blue) inserted at the *lacZ* of the *V. cholerae* chromosome. The constitutive fluorescent marker consists of the P_{tac} promoter followed by *TagRFP-T* (red), which was cloned onto a low-copy plasmid (pSC101*) with a $Gent^R$ marker (yellow). **d,** Confocal microscopy image series depicting the production of mNeonGreen (cyan) during phage infection, followed by cell lysis. All cells produce TagRFP-T (red).

Although the genome of Vibriophage N4 has been sequenced (99), it has not been annotated with promoter regions. I used an online genetic tool called PHIRE (254) for performing *in silico* genome analysis of Vibriophage N4 to identify and annotate promoter regions. As capsid proteins are one of the most abundant proteins synthesised during phage replication, I chose the promoter regulating the transcription of the capsid gene *VN4_32*. Furthermore, the bioinformatics analysis revealed that this promoter was repeated at several positions and was the most abundant promoter in the phage genome (Figure 2.12a). Therefore, I chose the promoter P_{VN4_32} for the phage reporter.

The next step was to find a fast-folding bright fluorescent protein. After comparing the brightness and maturation time of different fluorescent proteins described in bacterial cells (255), mNeonGreen was chosen as a readout for the expression of the selected phage promoter (256) (Figure 2.12b). The fluorescent reporter was constructed by amplifying the selected phage promoter, fusing it upstream to the gene encoding mNeonGreen, and then inserting the fragment into the *V. cholerae* chromosome at a neutral locus (Figure 2.12c). Thus, when a *V. cholerae* cell was infected by Vibriophage N4, the promoter would be recognised by the phage RNA polymerase and mNeonGreen would be produced (Figure 2.12d). To visualise all cells, bacteria produced the red fluorescent protein TagRFP-T constitutively.

2.11 Visualisation of phage infection during biofilm formation

To characterise the process of biofilm formation during phage exposure, the constructed phage reporter was used to track the progress of phage infection spatiotemporally. When *V. cholerae* cells harbouring the phage reporter system (Figure 2.12) were imaged during Vibriophage N4 exposure, I observed rampant phage infection in the bacterial population during the first $2\,\mathrm{h}$, which was quantified by an increase in mNeonGreen fluorescence. However, the phages were unable to kill the entire bacterial population. The cells that did not get infected acted as the pioneering cells of the resulting biofilms (Figure 2.13a). These cells started to divide as their neighbouring cells lysed around them. Quantifying the occurrence of infected cells during biofilm growth by plotting kymographs, showed that *V. cholerae* cells were infected prior to biofilm formation (Figure 2.13b). The kymographs also revealed that there was no subsequent phage infection during biofilm growth. Phage infection was observed only prior to bacterial biofilm dispersal at $8\,\mathrm{h}$. Therefore, *V. cholerae* cells were infected by Vibriophage N4 virions and subsequently, biofilm formation was initiated. These observations indicated that biofilm formation was always preceded by phage infection and bacterial lysis, suggesting that phage infection could be vital for subsequent biofilm formation. The phage reporter also revealed that biofilm-dwelling cells were protected from phage infection.

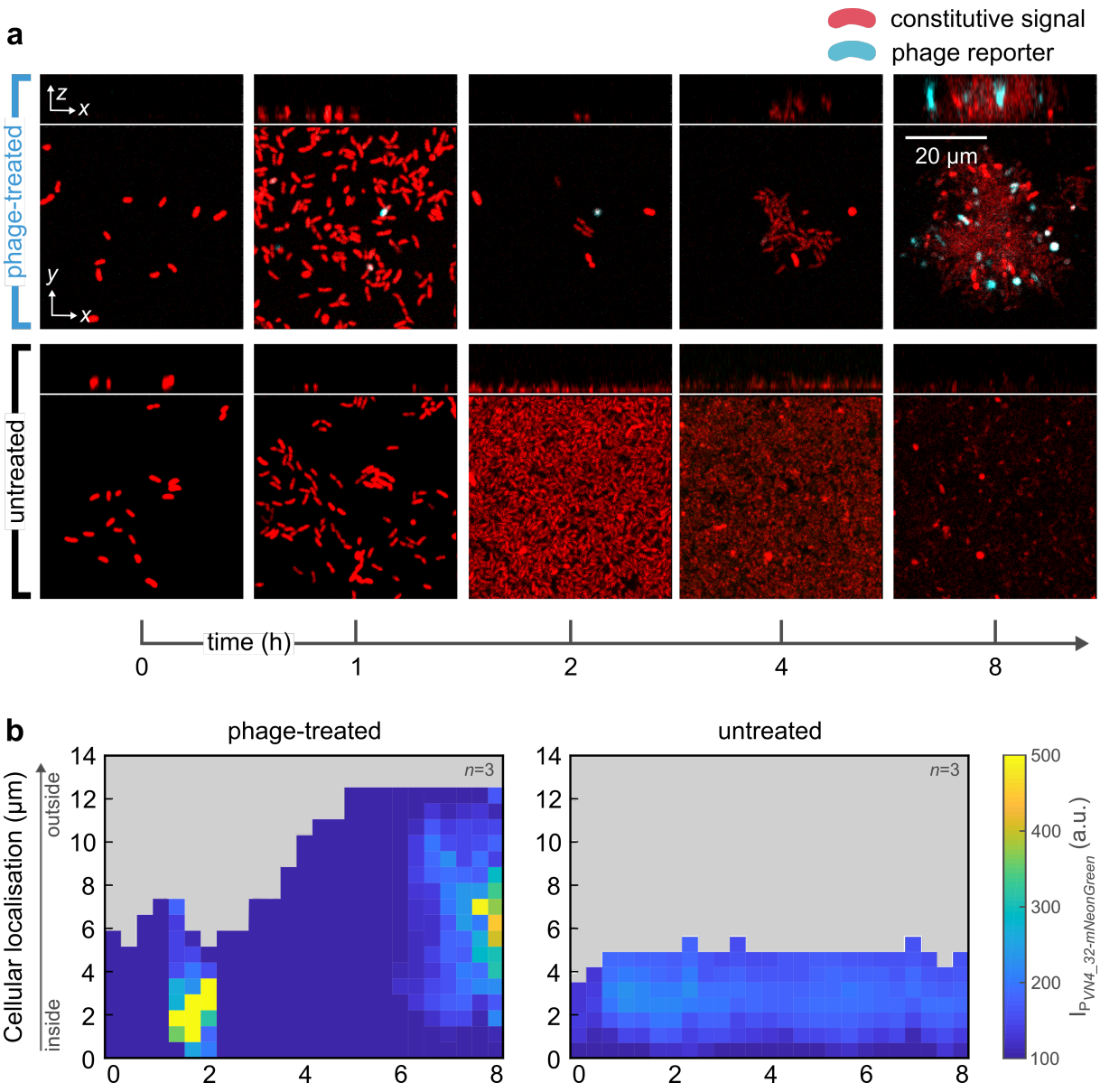

Figure 2.13: *V. cholerae* cells in biofilms were protected from infection by Vibriophage N4. **a,** Confocal image time series of *V. cholerae* cells constitutively expressing TagRFP-T (red), under the control of a P_{tac} promoter, and mNeonGreen (cyan) under the control of the phage promoter (P_{VN4_32}) exposed to a continuous flow of Vibriophage N4 (blue; $10^6\,\mathrm{PFU\,mL^{-1}}$) or untreated (black) over $8\,\mathrm{h}$. Bacterial cells exposed to phages showed the production of mNeonGreen during the first cycle of phage infection. However, after biofilm formation was initiated by cells that were not infected by Vibriophage N4, there was no more production of mNeonGreen until biofilm dispersal at $8\,\mathrm{h}$. In the absence of phages, cells grew as a lawn and did not produce mNeonGreen. **b,** Visualisation of the spatiotemporal dynamics of phage infection in the presence or absence of Vibriophage N4 ($10^6\,\mathrm{PFU\,mL^{-1}}$). Each pixel in these kymographs is coloured according to the fluorescence expression of P_{VN4_32}-*mNeonGreen* at a given time and spatial position in the biofilm. Fluorescence expression values were averaged over all cells with similar distances from the outer biofilm boundary facing the liquid medium. Kymographs are representative of $n = 3$ different biofilms.

Conclusion

The results described in this chapter confirmed that *V. cholerae* cells were susceptible to Vibriophage N4 infection and facilitated its propagation by cell lysis (Figure 2.1). The described series of experiments performed to study phage-bacterial interactions revealed that *V. cholerae* cells evade Vibriophage N4 infection by utilising one or more types of group behaviour (Figure 2.2). During phage exposure, most bacterial cells were lysed but the few that cells survived became the pioneering cells that formed biofilms (Figure 2.5). Furthermore, it was confirmed that bacterial cells, which formed biofilms during phage exposure, were not phage-resistant mutants nor matrix hyper-producers (Figure 2.8). Therefore, *V. cholerae* actively initiated the production of matrix components when exposed to Vibriophage N4. The production of biofilm matrix components was confirmed by transcriptomics and proteomics (Figure 2.9). *V. cholerae* cells were also imaged to visualise and confirm biofilm matrix production during phage exposure (Figure 2.10, 2.11).

The biofilms that were formed during phage exposure protected bacterial cells from phage infection. While embedded in the matrix, biofilm-dwelling cells could replicate in their gated communities in spite of the presence of active phages in their environment (Figure 2.13). Therefore, forming biofilms enabled survival of the bacterial population, although at a cost of the initial lysis of cells. As biofilm formation occurred only after lysis of the majority of cells in the microfluidic chamber, I hypothesised that this initial sacrifice of bacterial cells was necessary for initiating biofilm formation. This also raised the question of whether uninfected cells sensed the lysis of their neighbours, ultimately activating a genetic pathway that induced biofilm formation. Proteomics uncovered the potential role of bacterial signalling pathway components such as PTS and c-di-GMP, which could be involved in the regulatory response that resulted in bacterial biofilm formation (Figure 2.9a). The signal that induces biofilm formation in *V. cholerae* cells during phage exposure is further explored in the next chapter.

3 | Bacterial danger sensing triggers biofilm formation

Being unicellular organisms, bacteria have to continuously fend off attacks from predators in order to survive. At such times, intra-species cooperation becomes crucial to outcompete bio-antagonists that threaten bacterial survival such as bacteriophages and non-self bacteria deploying toxins or other bactericidal compounds (257, 258). As they coexist in the same niche, interactions between phages and bacteria are one of the most common encounters in the environment (72). However, the mechanism of how bacteria sense and respond to predatory biological agents (including, but not limited to phages) is not well-understood. These biological agents, especially lytic phages, are often responsible for bacterial cell lysis, which releases previously intracellular components into the extracellular millieu of intact bacterial cells. Analogous to innate immunity in multicellular organisms, it has been suggested that bacteria must have also evolved systems to sense and respond to exogenous self or non-self molecules that are indicative of the presence of a lytic threat (259). The ability to sense these 'danger signals' would be vital to induce a defence response to ultimately ensure bacterial survival. Although the idea of bacterial danger sensing has been suggested, such immunostimulatory molecules have not yet been identified for bacterial systems.

In the previous chapter, I discovered that *Vibrio cholerae* cells responded to phage exposure by producing matrix components and growing as biofilms. By using a fluorescent reporter (Figure 2.12), infection was visualised during phage exposure (Figure 2.13). As biofilm formation was always preceded by an initial cycle of phage-induced bacterial lysis (Figure 2.5) and as the extent of biofilm formation was dependent on the phage titre that the bacterial cells were exposed to (Figure 2.5), I hypothesised that phage infection, but not the phages themselves, was responsible for the biofilm formation response. This chapter describes the process of characterisation of the biofilm-inducing signal during lytic phage exposure. Similar to the experiments described in the previous chapter, here I also used a microfluidic flow system to grow and expose *V. cholerae* to bacterial cell lysates. Interpretations were made on the basis of image analysis that was performed using *BiofilmQ*, as described previously (see section 2.4). Transcriptomics was used to elucidate the genetic pathway leading to biofilm induction. Here, biofilm formation is discussed as a general stress response to sensing 'danger' in a bacterial cell's microenvironment.

The results described in this chapter have contributed to a paper (238), pending publication.

The described experiments were performed by myself with the help of Mads F. Hansen, who constructed and collected data related to the *V. cholerae* Δ*trxA* mutant, and Violina Potlog, who collected data related to the response of *V. cholerae* cells exposed to isolated peptidoglycan. Bacterial strains were constructed either by myself or were used from the Drescher laboratory strain collection (see section 5.1.1). Biofilm quantification was performed using a custom script written by Eric Jelli. The bacterial sample preparation and RNA isolation for transcriptomics was performed by Kazuki Nosho. Data analyses were performed by myself. The experiments were designed and conceptualised by Praveen K. Singh and myself, and the project was initiated by Knut Drescher.

3.1 Phage-induced cell lysis is necessary for biofilm formation in *V. cholerae*

From observations described in the previous chapter, I hypothesised that biofilm formation occurred in response to a stimulus (or stimuli) incurred after phage infection. The stimulus could have been directly related to the presence of phages, i.e., docking of phages on the bacterial surface, shutting down of bacterial translational machinery, or some other cue introduced by the physical presence of the phage on or inside the bacterium. However, as about 90% of the initial population lysed due to phage infection (Figure 2.3a), I reasoned that the physical presence of phages on or in the bacteria was not responsible for bacterial biofilm formation. In order to confirm this, purified Vibriophage N4 virions were heat-treated to obtain inactivated phages that could not infect bacterial cells (260, 261). Exposing *V. cholerae* cells to inactivated phages did not result in cell lysis or biofilm formation (Figure 3.1a). This confirmed that bacterial biofilm formation was not a result of the presence of the phage bodies.

To reproduce a condition in which phages could adhere to bacterial cells, inject DNA, but not complete their lytic cycle, a *V. cholerae* Δ*trxA* mutant was constructed. Vibriophage N4 is member of the T7 supergroup and its polymerases share some (approx. 60%) similarity to the polymerases of phage T7 (99). The DNA polymerase of T7 phages requires host-encoded thioredoxin to increase processivity and assemble a functional replisome (261, 262). Hence, Δ*trxA* mutants possess population-level immunity to T7-like phages (263–266). Therefore, although being susceptible to Vibriophage N4 infection, it was expected that the *V. cholerae* Δ*trxA* mutant would not support completion of the phage lytic cycle. Accordingly, it was observed that the adsorption of the phages to the bacterial cell surface was not affected by the *trxA* deletion, however, no phage progeny were produced (Figure 3.1b). This was also confirmed by measuring the relative efficiency of plating (EOP), i.e., the titre of the phage on a given bacterial strain compared to the maximum titre observed, of the wild type (WT) and the Δ*trxA* mutant. The low EOP of the Δ*trxA* mutant indicated that phage infection was interrupted and therefore, significantly fewer phage plaques were observed on the bacterial lawn (Figure 3.1c). Growth curves of bacterial cells in liquid shaking cultures infected with Vibriophage N4 with a multiplicity of infection (MOI of 0.2 or 2) also indicated that the phages were incapable of causing a decrease in optical density measured at $600\,\mathrm{nm}$ (OD_{600}) in the Δ*trxA* mutant (Figure 3.1d). At a high MOI, phage exposure

caused a delay in growth, indicating that infection was successful, but could not account for lysis of bacterial cells. When exposed to phages in microfluidic channels, the Δ*trxA* mutant did not show biofilm formation (Figure 3.1e), supporting the hypothesis that cell lysis was essential to initiate a biofilm response. Furthermore, there was a negative correlation between the number of surviving cells 1 h post-phage exposure and extent of biofilm formation 7 h later. Unlike the WT, for which <0.01% cells survived after phage exposure, the Δ*trxA* mutant did not show an overall reduction in cell count when exposed to phages for 1 h (Figure 3.1f).

Phage infection results in lysis of bacterial cells which releases phage progeny into the micro-environment along with a multitude of bacterial cell wall fragments, proteins, metabolites and other internal cellular components that are subsequently exposed to neighbouring intact cells. I hypothesised that one or more of these cellular components served as the stimulus for biofilm formation. To test this, *V. cholerae* cells were exposed to phage-free cell lysate (generated by sonicating a highly concentrated culture of *V. cholerae* cells). I observed that that both the WT and the Δ*trxA* mutant could produce biofilms in response to lysate exposure (Figure 3.1g). This concluded that biofilm formation was triggered by a component of the bacterial cell lysate and was independent of phages.

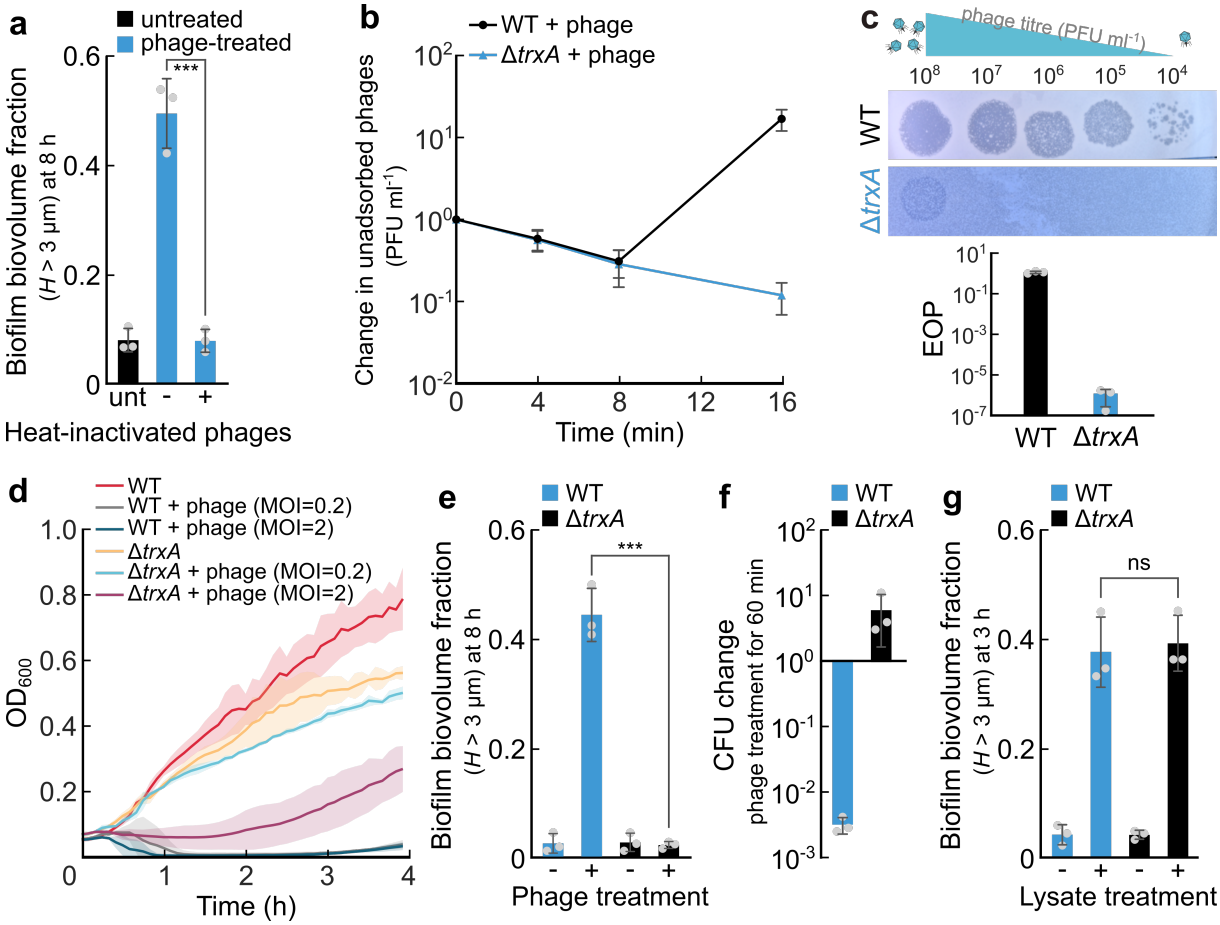

Figure 3.1: Bacterial lysis caused due to Vibriophage N4 infection was necessary for biofilm formation in *V. cholerae*. a, Biofilm formation, quantified as the biofilm biovolume fraction (the sum of the biovolume with height $H > 3\,\mu m$ divided by the total biovolume) at $8\,h$, for cells exposed to LB only (untreated, black) or to Vibriophage N4 (phage-treated, blue) virions that were active ($10^6\,PFU\,mL^{-1}$) or inactive after heat-treatment ($80\,°C$ for $20\,min$). Bacterial cells exposed to active phages formed biofilms whereas cells exposed to heat-inactivated phages did not form biofilms, similar to the untreated condition. **b,** A phage adsorption curve of *V. cholerae* wild-type (WT) and Δ*trxA* cells exposed to Vibriophage N4. A *V. cholerae* Δ*trxA* mutant was resistant to phage infection. Bacterial cultures were sampled every $4\,min$ and unabsorbed phage particles were enumerated by plaque-forming unit (PFU) assays. Phage adsorption to the bacterial cells was unaffected by the *trxA* knockout, but the number of progeny phages produced after $16\,min$ was approx. 100-fold diminished in the Δ*trxA* strain as compared to the WT. Points represent the mean of 3 biological replicates and errorbars indicate the standard deviation. **c,** A severely decreased efficiency of plating (EOP) of the Δ*trxA* mutant as compared to the WT indicated that bacterial lysis was attenuated by deleting the *trxA* gene. Plaque images are representative of 3 biological replicates. **d,** Growth curves in shaking liquid cultures wherein bacterial cells were infected at $0\,h$ and at an MOI = 0.2 or 2 indicated that Vibriophage N4 was incapable of causing a decrease in optical density in the Δ*trxA* mutant (blue line), but instead caused a significant delay of growth at high MOI (purple line). In comparison, WT cells were strongly susceptible to phage infection, even at low MOIs (grey and dark blue lines represent an MOI = 0.2 and 2, respectively). Lines represent the mean of 3 biological replicates and shaded regions indicate the standard deviation. **e,** WT cells displayed biofilm formation after $8\,h$ of phage exposure ($10^6\,PFU\,mL^{-1}$) whereas the Δ*trxA* mutant did not. Both strains did not form 3D biofilms without phage exposure. **f,** Following $60\,min$ of phage exposure, the bacterial colony-forming unit (CFU) count dropped substantially for the WT due to phage-induced lysis, whereas the Δ*trxA* mutant was unaffected (MOI = 1). **g,** Both the WT and Δ*trxA* mutant formed biofilms …

Figure 3.1: ... when exposed to a lysate obtained by sonication of WT *V. cholerae* cells (10^{10} lysed cells mL^{-1}) for $3\,\mathrm{h}$. Bars are mean values with points denoting 3 biological replicates and error bars indicate the standard deviation. Statistical significances were calculated using a Student's t-test (ns = not significant; *** = $p < 0.001$).

3.2 Sonicated bacterial lysate induces biofilm formation in *V. cholerae*

When *V. cholerae* cells were exposed to sonicated *V. cholerae* cell lysate, I observed that bacterial cells initiated biofilm formation within $2\,\mathrm{h}$ of exposure, with the maximum biofilm height at $3\,\mathrm{h}$ post-lysate induction (Figure 3.2a-b). The time required for lysate-mediated induction, i.e., $2\,\mathrm{h}$, was also the same amount of time that bacteria required to establish biofilms after phage infection (Figure 2.5). I also found that, similar to phage exposure (Figure 2.6), the extent of biofilm formation was directly related to the concentration of the bacterial lysate (Figure 3.2c-d). Thus, *V. cholerae* produced biofilms as a response to cell lysate in a dose-dependent manner. This suggested that *V. cholerae* cells sensed 'danger' in the form of lysed bacterial cells to initiate a biofilm defence response.

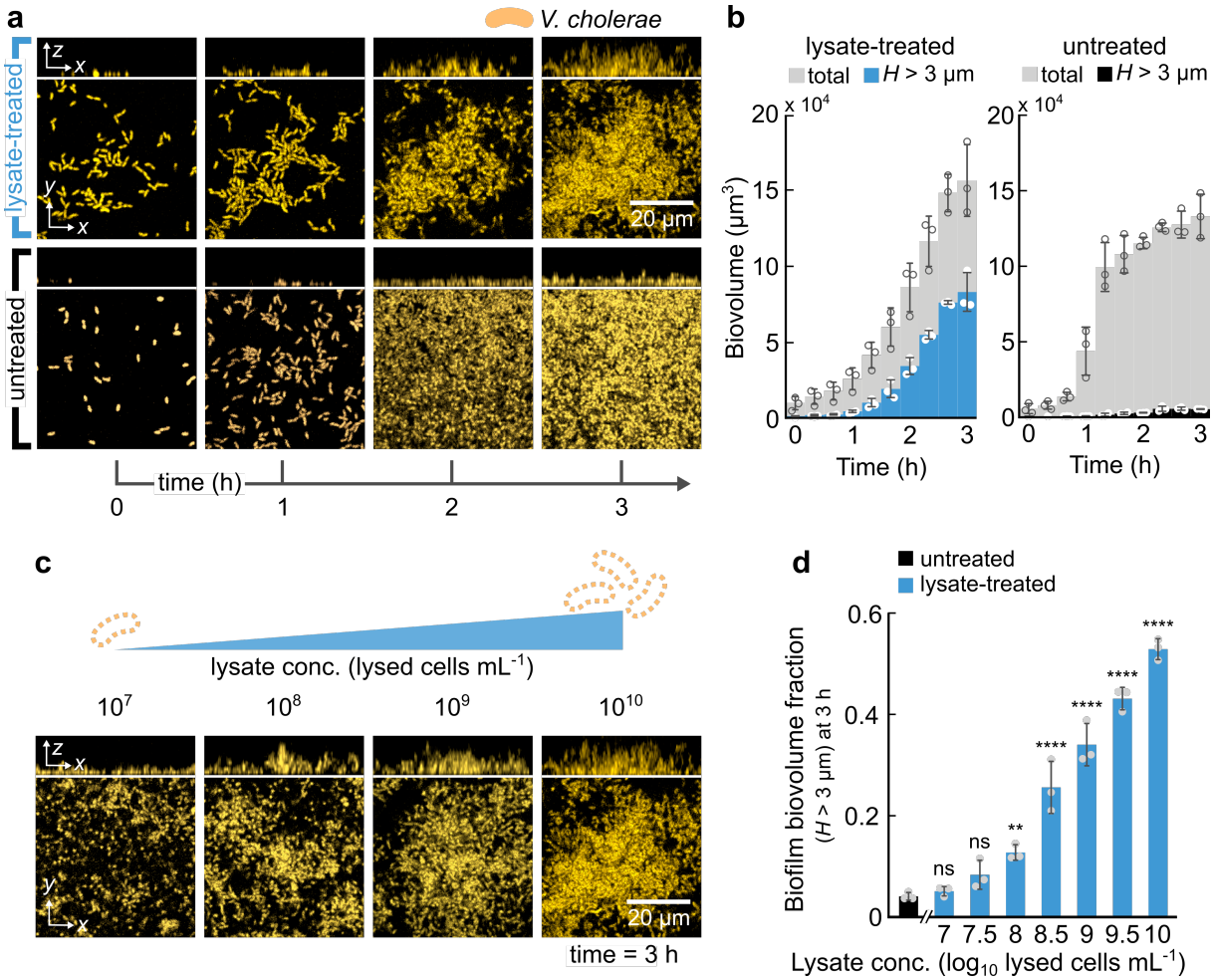

Figure 3.2: Bacterial cell lysate induced biofilm formation in *V. cholerae*. **a,** Confocal image time series of *V. cholerae* cells (yellow), constitutively expressing *sfGFP*, under the control of a chromosomal P_{tac} promoter, exposed to a continuous flow of sonicated lysate of *V. cholerae* cells (blue, 10^{10} lysed cells mL^{-1}) or untreated (black) over $3\,\mathrm{h}$. Bacterial cells exposed to bacterial cell lysate showed biofilm growth. In the absence of lysate, cells grew as a lawn to confluently cover the surface of the flow chamber. **b,** Quantification of the total biovolume (grey bars) and fraction of biovolume with height $H > 3\,\mu\mathrm{m}$ (coloured bars) of bacterial cells over $3\,\mathrm{h}$ in the presence (blue) or absence (black) of a sonicated lysate of *V. cholerae* cells (10^{10} lysed cells mL^{-1}). **c,** Confocal images of *V. cholerae* cells (yellow), constitutively expressing *sfGFP*, under the control of a chromosomal P_{tac} promoter, exposed to varying concentrations of sonicated lysate of *V. cholerae* cells $3\,\mathrm{h}$ after the start of lysate exposure. Exposing bacterial cells to increasing concentrations of sonicated lysate resulted in an increase in the maximum biofilm height (seen in the z-projection). **d,** Biofilm formation increased with exposing cells to increasing concentrations of a sonicated lysate of *V. cholerae* cells. Biofilm formation was quantified by calculating the biovolume fraction, which is the sum of the biovolume with height $H > 3\,\mu\mathrm{m}$ divided by the total biovolume. Bars are mean values with points (open grey circles or white closed circles for total or $H > 3\,\mu\mathrm{m}$ biovolume, respectively) denoting 3 biological replicates and error bars indicate the standard deviation. Statistical significances were calculated relative to the untreated condition using a one-way ANOVA with Bonferroni's correction (ns = not significant; ** = $p < 0.01$; **** = $p < 0.0001$).

3.3 Bacterial lysate does not influence bacterial attachment or growth

As exposure to lysed bacterial cells resulted in biofilm formation in *V. cholerae* cells, it was tempting to assume that bacterial cells sensed a biofilm-inducing signal from the exposed lysate. However, it was first necessary to rule out that bacterial biofilm formation was not an artefact caused due to alterations in bacterial surface attachment. Bacterial cell lysates are a variegated mixture of broken cellular components. Therefore, it was possible that the presence of lysate in microfluidic flow chambers modified the surface and influenced bacterial attachment, which then indirectly caused bacterial biofilm formation. In order to test this, a sonicated lysate of *V. cholerae* cells was flowed into chambers of a microfluidic device for $1\,\mathrm{h}$ prior to bacterial cell inoculation. When *V. cholerae* cells were subsequently inoculated into the chamber, the LB medium replaced the lysate in the chamber barring those components that were already adhered to the surface of the microfluidic chamber. However, pre-treating the microfluidic chamber surface with lysate, alone, was not sufficient to induce biofilm formation in *V. cholerae* (Figure 3.3a). As controls, non-treated microfluidic chamber surfaces and surfaces treated with LB for $1\,\mathrm{h}$ were also inoculated with *V. cholerae* cells. In all conditions, *V. cholerae* cells exposed to LB only (untreated) did not form biofilms whereas flowing lysate into the microfluidic chambers during the course of the experiment triggered biofilm formation. Therefore, lysate exposure did not induce biofilm formation in *V. cholerae* by influencing bacterial surface attachment.

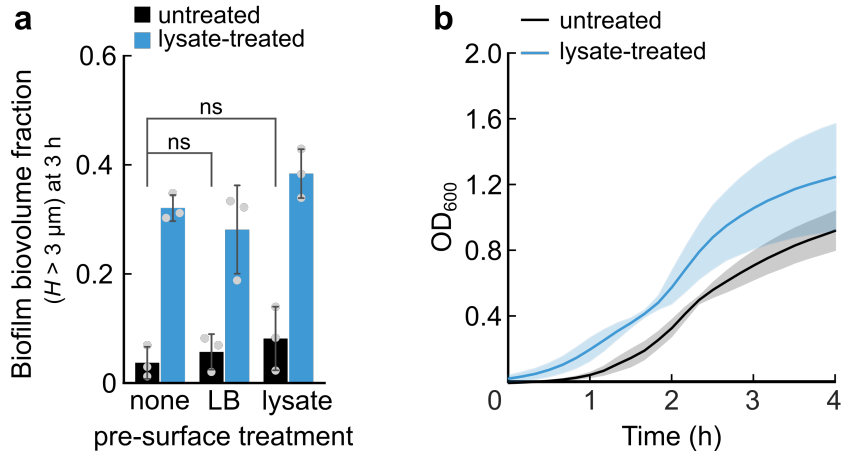

Figure 3.3: Exposing *V. cholerae* cells to bacterial cell lysate did not influence bacterial attachment nor restrict growth. a, 3D biofilm formation of *V. cholerae* cells exposed to sonicated lysates of *V. cholerae* cells (10^{10} lysed cells mL^{-1}, blue) or untreated (black), which were inoculated in microfluidic chambers whose surfaces were not pre-treated, or pre-treated with LB or lysate. Pre-treating the surface of microfluidic chambers with lysate did not induce bacterial biofilm formation. Biofilm formation was quantified by calculating the biovolume fraction, which is the sum of the biovolume with height $H > 3\,\mu\mathrm{m}$ divided by the total biovolume. Bars are mean values with points denoting 3 biological replicates and error bars indicate the standard deviation. Statistical significances were calculated using a one-way ANOVA with Bonferroni's correction (ns = not significant). **b,** Growth curves in liquid cultures wherein *V. cholerae* cells, at a starting $\mathrm{OD}_{600} = 0.04$, were inoculated in LB (untreated, black) or a sonicated lysate of *V. cholerae* cells (10^9 lysed cells mL^{-1}, blue). Exposure to lysate did not decrease bacterial growth rate. The ratio of bacterial cells to lysate was kept consistent with the starting conditions of the microfluidic experiments. Lines represent the mean of 3 biological replicates and shaded regions indicate the standard deviation.

Another factor that influences bacterial biofilm formation is regulation by quorum sensing (QS), which is dependent on cell density. However, results from the previous chapter show that bacterial cell density has no effect on biofilm formation (Figure 2.7). Along with changes in cell density, changes in bacterial growth rate have also been linked to biofilm formation (267, 268). To test if the exposure to lysate affected bacterial growth, *V. cholerae* cells were grown in a solution of sonicated *V. cholerae* cells and the optical density at $600\,\mathrm{nm}$ (OD_{600}) was measured periodically. The observations from this experiment confirmed that *V. cholerae* cells did not grow slower in lysate as compared to LB only (Figure 3.3b). In fact, bacterial cells appeared to grow slightly faster in lysate than LB only, which was unsurprising as bacteria were provided with additional nutrients that they could recycle from lysed cells and use as an energy source (269).

3.4 Visualisation of biofilm matrix production during bacterial lysate exposure

As biofilm formation in response to lysate exposure was not a facet of an alteration in bacterial attachment or growth, it suggested that danger sensing triggered biofilm formation. Matrix production is the hallmark of biofilm formation and therefore, it was necessary to visualise biofilm matrix production spatiotemporally during lysate exposure. For this, I exposed *V. cholerae* cells producing the fluorescent protein mRuby2 under the control of the promoter of *vps* genes (P_{vpsL}-*mRuby2*) to sonicated lysate of *V. cholerae* cells in microfluidic chambers. The bacterial cells also produced the fluorescent protein sfGFP constitutively (P_{tac}-*sfGFP*), which was used to normalise for cellular fluorescence levels. Increase in the mRuby2 fluorescence signal indicated that *V. cholerae* cells initiated the transcription of *vps* genes within the first hour of lysate exposure (Figure 3.4a). In the untreated condition, there were a few *V. cholerae* cells that showed mRuby2 production in the initial timepoints. However, these cells did not form biofilms and showed decreased fluorescence levels over time. mRuby2 production was quantified by plotting kymographs that depict changes in the level of *vps*-regulated fluorescence normalised by the constitutive fluorescence (indicated by the colourmap) across the height of the bacterial biofilm (y-axis) and over time (x-axis). These kymographs showed that *V. cholerae* cells transcribed *vps* rapidly during lysate exposure (Figure 3.4b).

The production of RbmA was also visualised during lysate exposure using anti-His antibodies conjugated to a fluorescent dye. Immunofluorescence staining showed that RbmA (with a polyhistidine-tag) formed shells around *V. cholerae* cells that were exposed to sonicated lysate (Figure 3.5a). RbmA shell formation was also seen for a few cells in the untreated condition but these cells did not form biofilms over the period of the experiment. The increase in fluorescence intensity of the anti-His antibodies can be explained by non-specific binding or accumulation. RbmA shells were quantified spatiotemporally by plotting the intensity of fluorescent anti-His antibodies (indicated by the colourmap) across the height of the bacterial biofilm (y-axis) and over time (x-axis). These kymographs showed that *V. cholerae* cells produced RbmA during lysate-induced biofilm formation (Figure 3.5b).

Visualising the expression of major matrix components *Vibrio* polysaccharide (VPS) and RbmA confirmed that *V. cholerae* cells initiated biofilm formation as a response to lysate exposure.

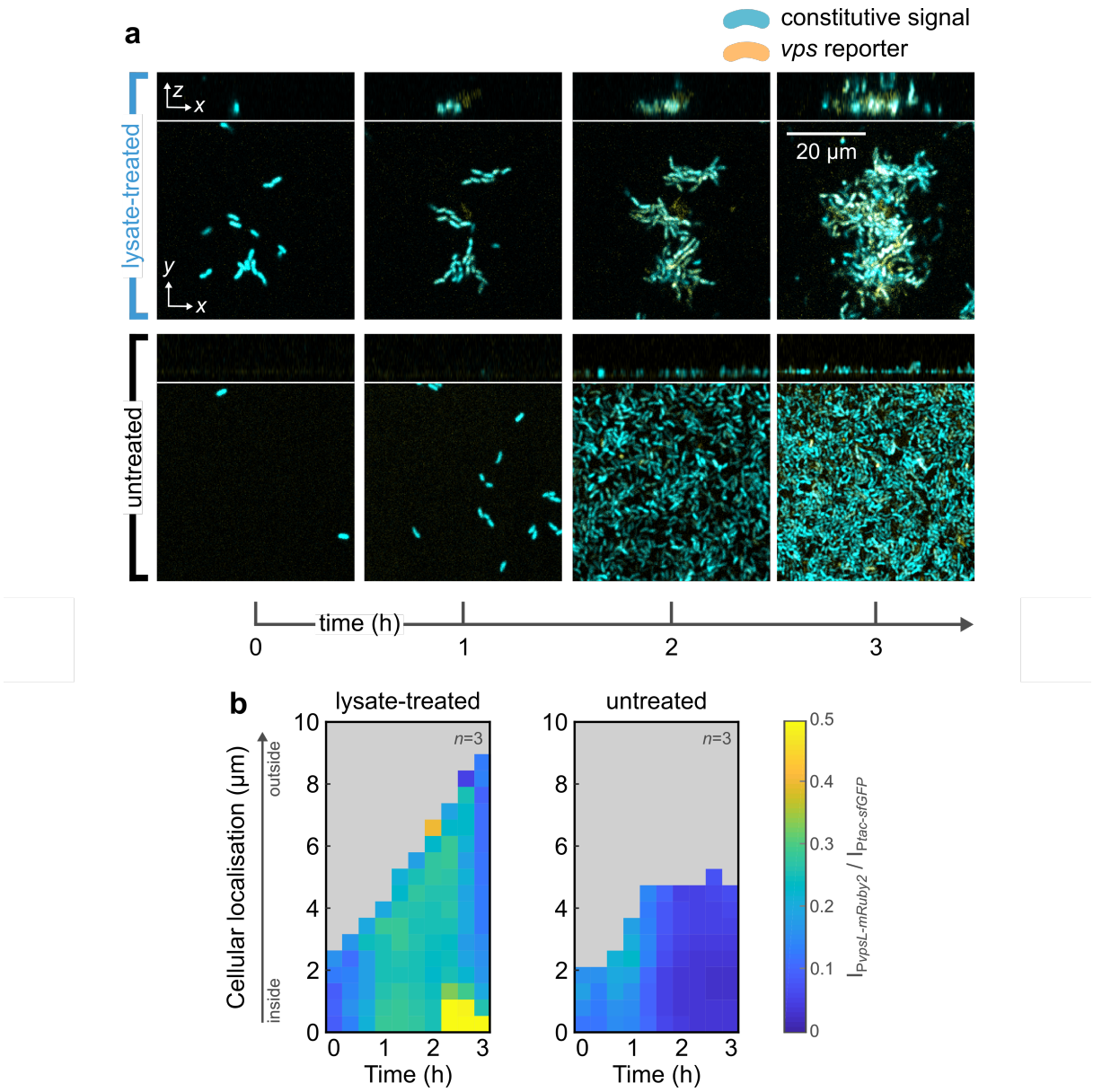

Figure 3.4: *V. cholerae* cells expressed *vps* genes in response to lysate exposure. a, Confocal image time series of *V. cholerae* cells constitutively expressing *sfGFP* (cyan), under the control of a P_{tac} promoter, and *mRuby2* (yellow), under the control of the P_{vpsL} promoter, exposed to a continuous flow of sonicated lysate of *V. cholerae* cells (blue, 10^{10} lysed cells mL^{-1}) or untreated (black) over $3\,\mathrm{h}$. Bacterial cells exposed to lysate showed transcription of *vps* genes whereas in the absence of lysate, only a few cells showed transcription from the *vps* promoter, but did not develop into biofilms. **b,** Visualisation of the spatiotemporal dynamics of *vps* operon transcription in the presence or absence of sonicated lysate of *V. cholerae* cells (10^{10} lysed cells mL^{-1}). The fluorescence of the matrix gene reporter (P_{vpsL}-*mRuby2*) was normalised by the fluorescence intensity of a constitutive reporter (P_{tac}-*sfGFP*). Each pixel in these kymographs is coloured according to the ratio of fluorescence expression at a given time and spatial position in the biofilm. Fluorescence expression values were averaged over all cells with similar distances from the outer biofilm boundary facing the liquid medium. Kymographs are representative of $n = 3$ different biofilms.

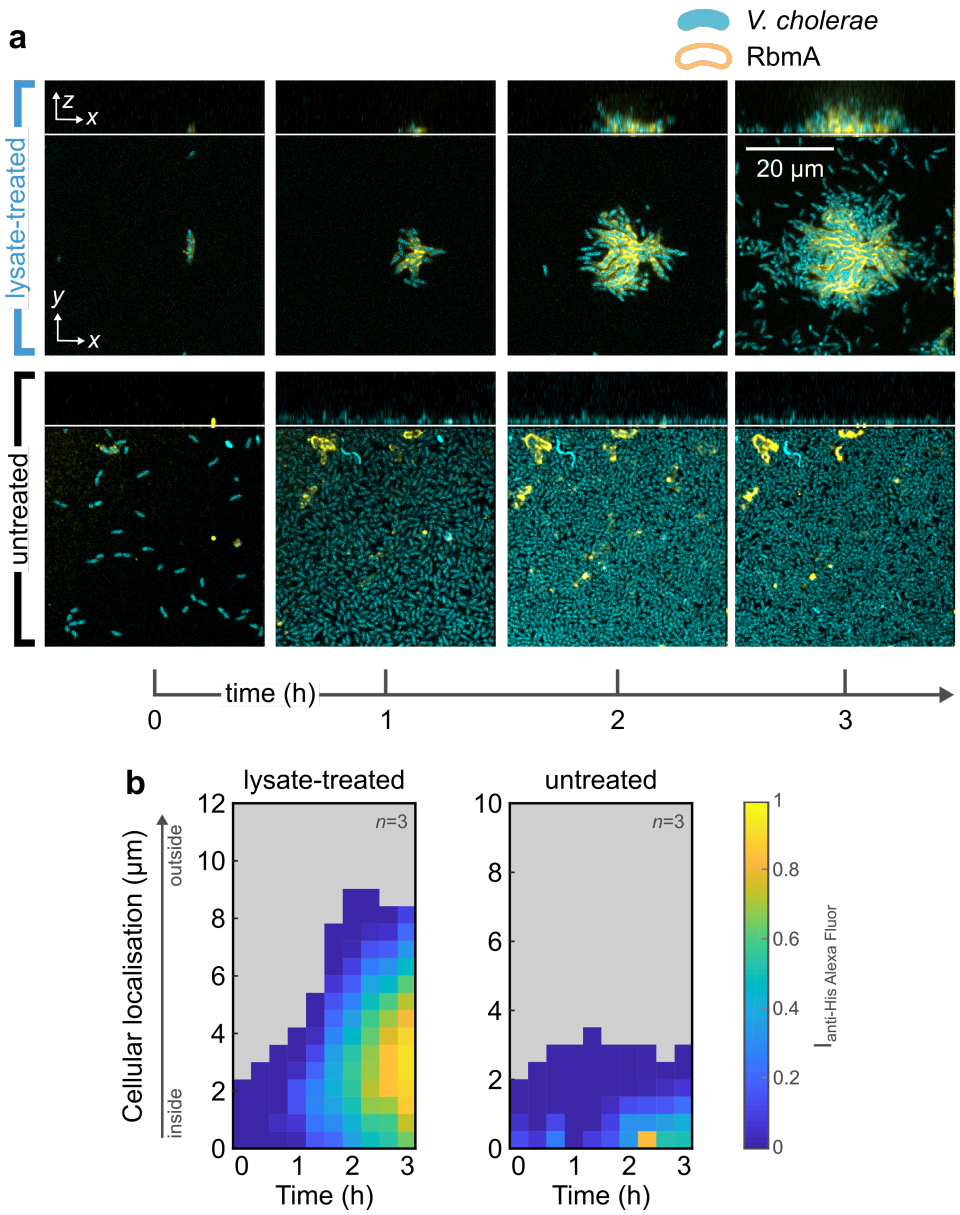

Figure 3.5: *V. cholerae* cells produced RbmA in response to lysate exposure. a, Confocal image time series of *V. cholerae* cells constitutively expressing *sfGFP* (cyan), under the control of a P_{tac} promoter, exposed to a continuous flow of sonicated lysate of *V. cholerae* cells (blue, 10^{10} lysed cells mL^{-1}) or untreated (black) over $3\,\mathrm{h}$. Bacterial cells exposed to lysate showed RbmA production (yellow shells), visualised by using fluorescent anti-His Alexa Fluor antibodies that conjugate with polyhistidine-tagged RbmA, during lysate-induced biofilm formation. In the absence of lysate, only a few cells showed RbmA production, but did not develop into biofilms. **b,** Visualisation of the spatiotemporal dynamics of RbmA production in the presence or absence of sonicated lysate of *V. cholerae* cells (10^{10} lysed cells mL^{-1}). The fluorescence expression of the anti-His Alexa Fluor antibody at a given time and spatial position in the biofilm. Fluorescence expression values were averaged over all cells with similar distances from the outer biofilm boundary facing the liquid medium. Kymographs are representative of $n = 3$ different biofilms.

3.5 VPS production is essential for lysate-induced biofilm formation

Apart from VPS and RbmA, which are the two major matrix components of *V. cholerae* biofilms, *V. cholerae* also produces matrix proteins RbmC and Bap1 (52). To explore the role of the various biofilm matrix components during lysate sensing, *V. cholerae* cells lacking different genes responsible for producing different matrix components were exposed to a sonicated lysate of WT *V. cholerae* cells. Single deletion mutants of matrix-related genes such as Δ*vpsL* and Δ*rbmA* showed a defect in biofilm formation when exposed to bacterial lysate (Figure 3.6). Out of the two, the Δ*vpsL* mutant did not form biofilms at all, as compared to the Δ*rbmA* mutant, which was still capable of making rudimentary biofilms during lysate exposure. The other two matrix components RbmC and Bap1 did not appear to be crucial for the biofilm response during danger sensing as their respective mutants (Δ*rbmC* and Δ*bap1*, respectively) were still capable of producing biofilms in response to lysate exposure. Overall, these observations indicated that *V. cholerae* used the two major components of the biofilm matrix, i.e., VPS and RbmA, to produce biofilms during lysate exposure, with VPS being the essential component without which the cells were not able to form biofilms.

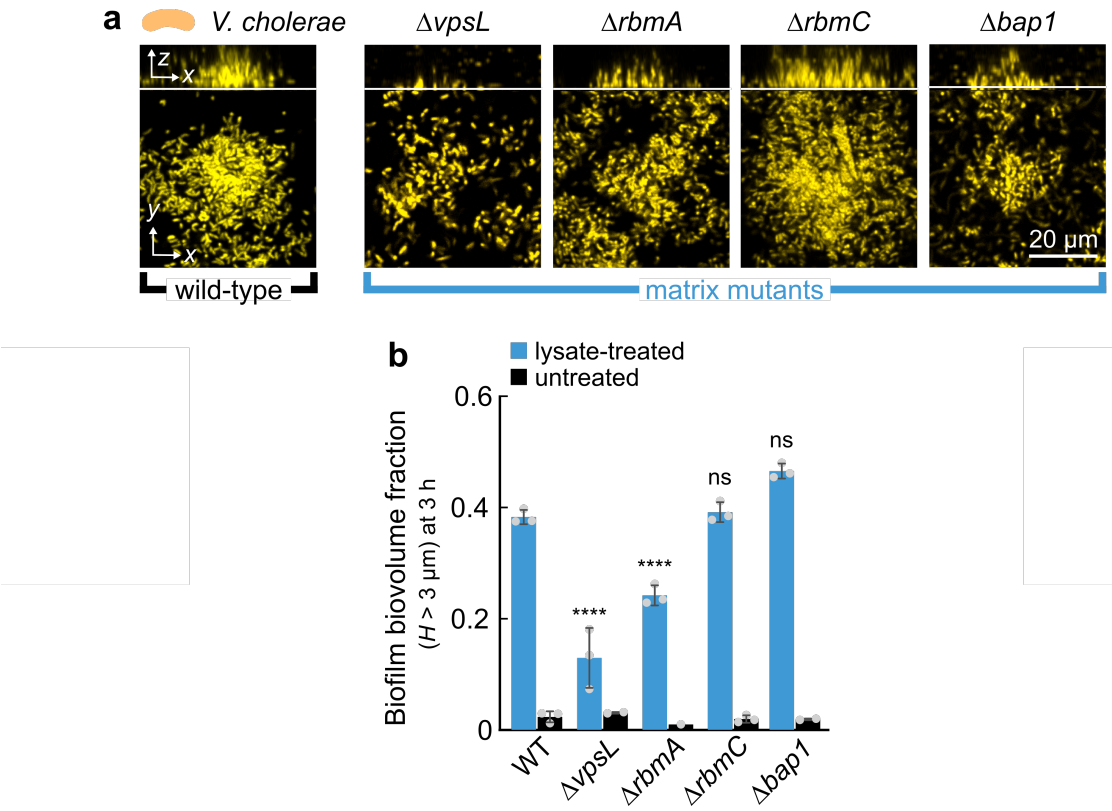

Figure 3.6: VPS and RbmA were essential for biofilm formation in response to bacterial lysate exposure in *V. cholerae*. a, Confocal images of *V. cholerae* wild-type (WT, black) cells or cells lacking different components of the biofilm matrix (blue), namely, VPS (Δ*vpsL*), RbmA (Δ*rbmA*), RbmC (Δ*rbmC*), or Bap1 (Δ*bap1*), constitutively expressing *sfGFP* (yellow), after $3\,\mathrm{h}$ of lysate exposure (10^{10} lysed cells mL^{-1}). **b,** 3D biofilm formation of *V. cholerae* WT or matrix deletion mutants exposed to sonicated lysates of *V. cholerae* WT cells (10^{10} lysed cells mL^{-1}). The Δ*vpsL* and Δ*rbmA* mutants showed strongly reduced biofilm formation during lysate exposure, calculating the biovolume fraction, which is the sum of the biovolume with height $H > 3\,\mu\mathrm{m}$ divided by the total biovolume. Bars are mean values with points denoting 3 biological replicates and error bars indicate the standard deviation. Statistical significances of the lysate-treated conditions were calculated relative to the WT using a one-way ANOVA with Bonferroni's correction (ns = not significant, **** = $p < 0.0001$).

The previously described results show that *V. cholerae* cells respond to lysate by forming biofilms. Moreover, biofilm formation was not caused by secondary effects of modified bacterial attachment. Together, these data suggested that *V. cholerae* cells sensed a component of the bacterial lysate that induces biofilm formation. The following sections describe the process of identifying the biofilm-inducing compound responsible for bacterial danger sensing.

3.6 The biofilm-inducing compound is general

Considering that many components of bacterial cells are conserved across different phyla, I tested if biofilm formation was a general response to lysates from other bacterial species. Lysates from other Gram-negative bacteria such as *Escherichia coli* and *Pseudomonas aeruginosa*, and Gram-positive bacteria such as *Bacillus subtilis* and *Staphylococcus aureus* were prepared by sonication. *V. cholerae* cells were exposed to different lysates separately and their biofilm biovolume fraction was measured after $3\,\mathrm{h}$ of exposure. I observed that exposure to lysates from other bacterial species also yielded biofilm formation in *V. cholerae* cells (Figure 3.7), indicating that the biofilm-inducing compound was general to all bacterial cells.

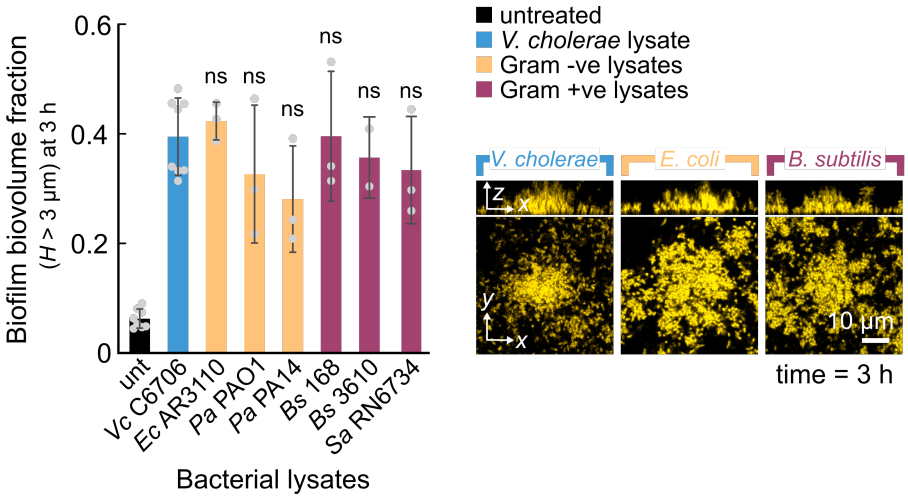

Figure 3.7: Biofilm formation in *V. cholerae* was triggered by a compound that is conserved across different bacterial species. Exposure to sonicated lysates (10^{10} lysed cells mL^{-1}) of various strains of Gram-negative (*Vc* = *Vibrio cholerae*; *Ec* = *Escherichia coli*; *Pa* = *Pseudomonas aeruginosa*) or Gram-positive (*Bs* = *Bacillus subtilis*; *Sa* = *Staphylococcus aureus*) species triggered *V. cholerae* cells to grow into 3D biofilms over $3\,\mathrm{h}$. Biofilm formation was quantified by calculating the biovolume fraction, which is the sum of the biovolume with height $H > 3\,\mu\mathrm{m}$ divided by the total biovolume. Bars are mean values with each point denoting one biological replicate and error bars indicate the standard deviation. Statistical significances were calculated relative to the *Vc* lysate using a one-way ANOVA with Bonferroni's correction (ns = not significant). Confocal images show the $3\,\mathrm{h}$ timepoint demonstrating the formation of *V. cholerae* 3D biofilms in response to the exposure of lysates made from *V. cholerae* cells (blue), *E. coli* cells (yellow), or *B. subtilis* cells (purple), with yellow cells representing *V. cholerae* cells constitutively producing sfGFP.

3.7 Bacterial cell wall fragments induce biofilm formation

To further narrow the search for the biofilm-inducing signal, I filtered the *V. cholerae* cell lysate through membrane filters of various sizes prior to exposing them to intact *V. cholerae* cells. The biofilm-inducing capability of the filtered lysates appeared to diminish with the decreasing pore size of the filter, with lysates composed of molecules less than 30 kDa unable to induce biofilm formation (Figure 3.8a). The biofilm-forming capability of lysates that contained differently sized molecules suggested the involvement of a bacterial biopolymer as the signal.

With information regarding the nature and size of the biofilm-inducing signal, I proceeded to investigate the cellular location from where it could have originated. For this, I created a lysate from *V. cholerae* spheroplasts to test for intracellular components as a signal. In parallel, I also isolated the murein sacculus (peptidoglycan) from the *V. cholerae* cell wall. Testing these two fractions for their ability to induce biofilm formation showed that exposure to the cell wall fraction resulted in a high biofilm biovolume fraction, similar to the whole cell lysate (Figure 3.8b). Overall, I observed that *V. cholerae* initiated biofilm formation in response to one or more components present in lysed bacterial cells. The biofilm-inducing compound was conserved across both Gram-negative and -positive bacteria and was most likely a polymer or part of one. Although the observations suggested that there might be some biofilm formation induced by compounds present in the cell interior (as the spheroplast lysate could also induce biofilm formation, albeit reduced), most of the biofilm induction could be explained by a component of the bacterial cell wall.

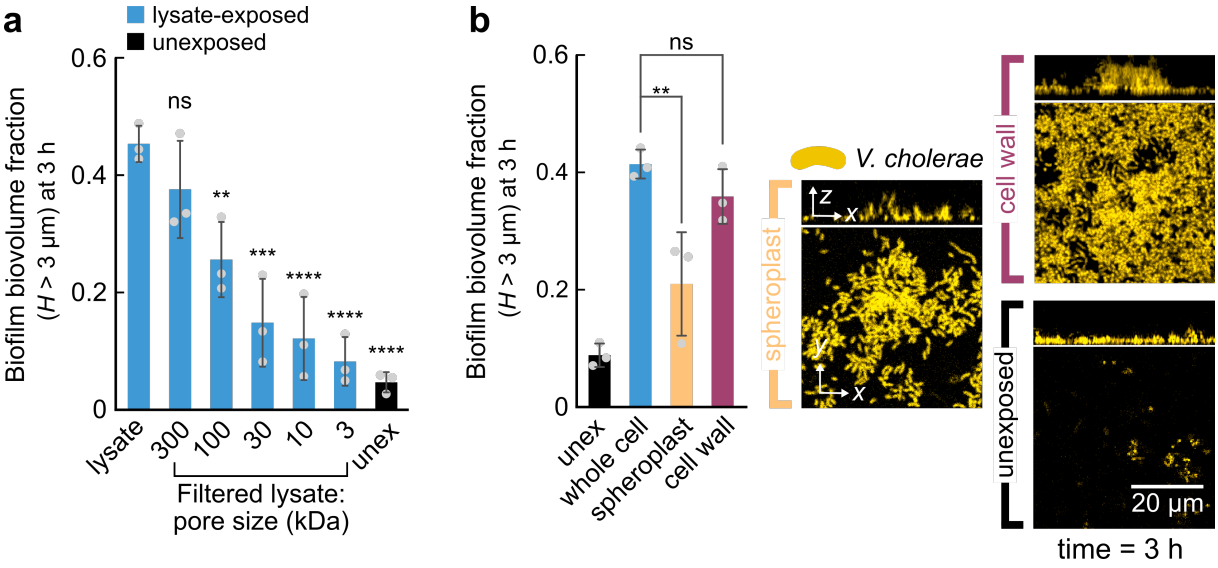

Figure 3.8: Bacterial cell wall fragments triggered biofilm formation in *V. cholerae*. a, Fractions of a *V. cholerae* lysate obtained by passing lysates through differently sized filters (3-300 kDa) resulted in decreasing biofilm-inducing capability with decreasing filter pore size. Crude lysate was obtained by sonicating 10^{10} lysed cells mL^{-1}, followed by sterilisation using a $0.2\,\mu\mathrm{m}$ filter. **b,** Comparison of biofilm-induction capability of different lysate fractions: lysate of whole cells (blue), lysate of cells that lacked a cell wall (spheroplasts, yellow), or cell wall fragments purified from a lysate of whole cells (purple). Cell wall fragments induced biofilm formation similar to a whole cell lysate. All lysates were made from a starting bacterial culture concentration of $10^{10}\,\mathrm{CFU\,mL}^{-1}$. Confocal images show the $3\,\mathrm{h}$ timepoint demonstrating the formation of *V. cholerae* 3D biofilms in response to the exposure of lysates made from whole cells and cell wall fraction of *V. cholerae* cells (blue). *V. cholerae* did not form 3D biofilms when exposed to spheroplast lysate (blue) or in the untreated condition (black). Yellow cells represent *V. cholerae* cells constitutively producing sfGFP. Biofilm formation was quantified by calculating the biovolume fraction, which is the sum of the biovolume with height $H > 3\,\mu\mathrm{m}$ divided by the total biovolume. Bars are mean values with points denoting 3 biological replicates and error bars indicate the standard deviation. Statistical significances were calculated using a one-way ANOVA with Bonferroni's correction (ns = not significant; ** = $p < 0.01$; *** = $p < 0.001$; **** = $p < 0.0001$).

3.8 Lysate-induced biofilm formation is not caused by DNA, RNA or proteins

As the spheroplast lysate also induced biofilm formation to a certain extent, the possibility of an intracellularly located biofilm-inducing signal could not be ruled out. To test for the presence of such a compound, I treated a *V. cholerae* cell lysate with DNase, RNase, or proteinase K prior to *V. cholerae* cell exposure. Treated lysates induced biofilm formation similar to an untreated control (Figure 3.9a). This indicated that the biofilm-inducing compound in a bacterial lysate was not DNA, RNA, or proteins. As a commonly reported compound that is responsible for forming a scaffold that preludes biofilm formation is extracellular DNA (eDNA) (270), whether eDNA played a role in lysate-induced biofilm formation was further examined by exposing *V. cholerae* cells. However, I found that *V. cholerae* cells exposed to eDNA were unable to form biofilms (Figure 3.9b), thus cementing the claim that eDNA did not play a role in lysate-induced biofilm formation in *V. cholerae*.

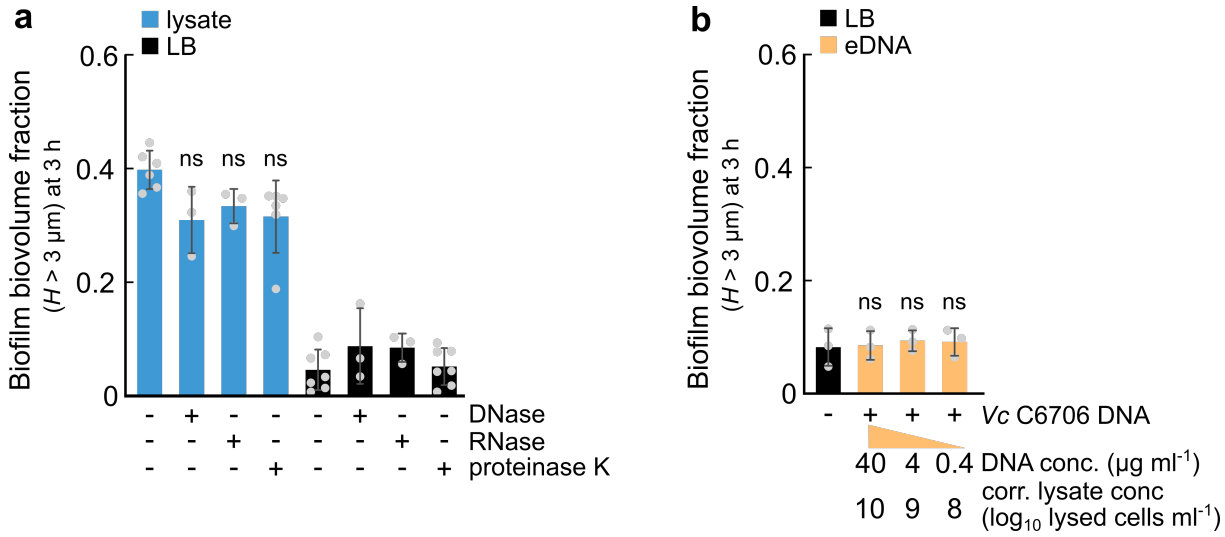

Figure 3.9: Biofilm induction in *V. cholerae* was not caused by DNA, RNA or proteins. a, *V. cholerae* cells were exposed to sonicated lysates of *V. cholerae* cells (10^{10} lysed cells mL^{-1}, blue) treated with DNase ($1\,\mathrm{U\,mL}^{-1}$ at 37 °C for 30 min), RNase ($1\,\mu\mathrm{g\,mL}^{-1}$ at 37 °C for 30 min), or proteinase K ($20\,\mu\mathrm{g\,mL}^{-1}$ at 37 °C for 60 min). The enzyme treatments did not diminish the biofilm-inducing capability of the lysate. As controls, these enzyme treatments were also performed in LB only (black). However, the presence of these enzymes did not induce bacterial biofilm formation in the absence of lysate. **b,** *V. cholerae* cells that were exposed to varying concentrations of extracellular DNA (eDNA, yellow), isolated from *V. cholerae* cells, did not show biofilm formation, similar to the untreated condition (black). The amount of DNA ($\mu\mathrm{g\,mL}^{-1}$) was estimated for the number of cells that were lysed in the corresponding *V. cholerae* cell lysates. Biofilm formation was quantified by calculating the biovolume fraction, which is the sum of the biovolume with height $H > 3\,\mu\mathrm{m}$ divided by the total biovolume. Bars are mean values with each point denoting one biological replicate and error bars indicate the standard deviation. Statistical significances were calculated using a one-way ANOVA with Bonferroni's correction (ns = not significant).

3.9 Peptidoglycan fragments rapidly trigger biofilm formation

As peptidoglycan is the major component of Gram-negative cell walls, and is conserved across all bacterial species, I hypothesised that peptidoglycan fragments or one of its components was responsible for inducing biofilm formation in *V. cholerae*. To test this, I exposed *V. cholerae* cells to purified peptidoglycan at a concentration of $300\,\mu\mathrm{g\,mL^{-1}}$, which corresponded to 10^{10} lysed cells $\mathrm{mL^{-1}}$, the amount of cells lysed in the most concentrated lysate solution (see Methods section 5.1.14 for estimation of peptidoglycan in lysate). Similar to lysate exposure, *V. cholerae* cells formed biofilms during $3\,\mathrm{h}$ of peptidoglycan exposure (Figure 3.10a). Also similar to lysate, I confirmed that peptidoglycan exposure did not affect bacterial growth (Figure 3.10b). Furthermore, peptidoglycan digested with lysozyme did not induce biofilm formation, which indicated that peptidoglycan acted as a signal for biofilm formation (Figure 3.10c). Solidifying this claim, I observed that the biofilm formation response was dependent on the concentration of peptidoglycan supplied in the microfluidic chambers (Figure 3.10d). Together, these observations revealed that *V. cholerae* cells respond to high concentrations of peptidoglycan in their immediate environment, either in the form of a pure compound or as fragments originating from lysed cells, which ultimately act as a signal to trigger bacterial biofilm formation.

Interestingly, I observed that the presence of the signal (i.e., peptidoglycan) was not required during the entire $3\,\mathrm{h}$ of the experiment. Pulsing bacterial cells with peptidoglycan for $5\,\mathrm{min}$, after which only growth medium was supplied, still resulted in biofilm formation at the end of $3\,\mathrm{h}$ (Figure 3.10e). Thus, *V. cholerae* rapidly sensed peptidoglycan fragments and committed to biofilm formation thereafter.

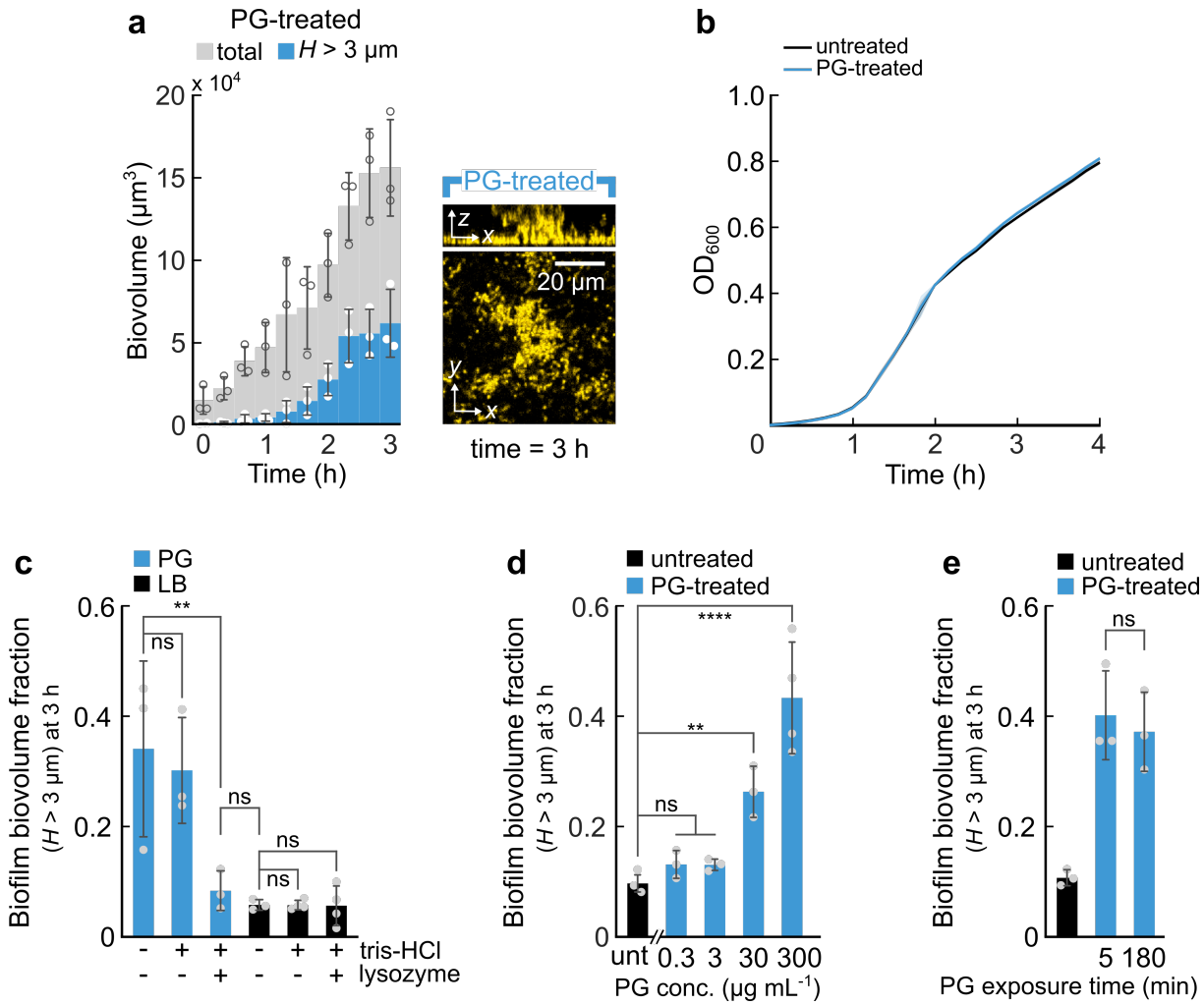

Figure 3.10: Peptidoglycan fragments triggered biofilm formation in *V. cholerae*. **a,** Quantification of the total biovolume (grey bars) and fraction of biovolume with height $H > 3\,\mu m$ (coloured bars) of bacterial cells over $3\,h$ of exposure to pure peptidoglycan (PG, $300\,\mu g\,mL^{-1}$, blue). Confocal image shows the $3\,h$ timepoint demonstrating the formation of 3D biofilms in the PG-treated condition, with yellow cells representing *V. cholerae* cells constitutively producing sfGFP. **b,** Growth curves in liquid cultures wherein *V. cholerae* cells, at a starting OD_{600} = 0.04, were inoculated in LB (untreated, black) or PG ($30\,\mu g\,mL^{-1}$, blue). Exposure to PG did not decrease bacterial growth rate (the lines for untreated and PG-treated overlap). The ratio of bacterial cells to PG was kept consistent with the starting conditions in the microfluidic experiments. Lines represent the mean of 3 biological replicates and shaded regions indicate the standard deviation. **c,** Lysozyme-digested peptidoglycan did not induce biofilm formation. *V. cholerae* cells were exposed to PG ($300\,\mu g\,mL^{-1}$, blue) either untreated or treated with lysozyme ($1\,mg\,\mu L^{-1}$ at $37\,°C$ for $30\,min$). As controls, cells were also exposed to medium only (LB, black) that was also untreated or treated with lysozyme with the same conditions. The buffer required for lysozyme activity, i.e., $10\,mm$ Tris-HCl, did not affect the biofilm or lawn formation of the PG or LB conditions, respectively. **d,** Biofilm formation after $3\,h$ of PG exposure increased with increasing concentration of PG (blue). **e,** Exposure of *V. cholerae* cells to PG ($300\,\mu g\,mL^{-1}$, blue) for $5\,min$ followed by $175\,min$ of LB, or $180\,min$ (continuous flow) induce similar levels of biofilm formation. Biofilm formation was quantified by calculating the biovolume fraction, which is the sum of the biovolume with height $H > 3\,\mu m$ divided by the total biovolume. Bars are mean values with points denoting 3 biological replicates and error bars indicate the standard deviation. Statistical significances were calculated using a one-way ANOVA with Bonferroni's correction (ns = not significant; ** = $p < 0.01$; **** = $p < 0.0001$).

3.10 Transcriptomics during peptidoglycan exposure

To understand how exposure to peptidoglycan triggers biofilm formation in *V. cholerae*, I measured differential gene expression using RNA-Seq for bacterial cells in microfluidic chambers that were exposed to peptidoglycan ($300\,\mu g\,mL^{-1}$) for $10\,min$ compared to cells supplemented with medium only (untreated) for the same duration of time. Transcriptomics analysis revealed that genes responsible for the production of VPS, such as *vps*-I cluster (*vc0917-vc0927*), were upregulated more than 2-fold in peptidoglycan-treated cells as compared to untreated cells (Figure 3.11a). Genes of the *vps*-II cluster (*vc0934-vc0939*) were also upregulated. However, the *rbm* cluster genes (*vc0928-vc0933*) the encode matrix proteins such as RbmA and RbmC, responsible for biofilm structure maintenance, were not significantly upregulated. Thus, transcriptomics confirmed that peptidoglycan exposure caused an upregulation of matrix-related genes.

As matrix-related genes were upregulated approximately 2-fold, I reasoned that genes involved in the regulatory response to peptidoglycan exposure, which triggered matrix gene transcription, would show higher fold changes. I found that there were 325 genes that were upregulated more than 2-fold in peptidoglycan-treated cells as compared to untreated cells[1]. Out of these, 170 genes encoded transporters or were related to metabolism (Figure 3.11b). The *cel* operon (*vc1281-vc1285*), which encodes genes related to the uptake of cellobiose (and its related compounds) *via* the phosphotransferase system (PTS) was upregulated more than 2-fold in response to peptidoglycan exposure. I also observed an increased expression of chemotaxis-related genes in cells that were exposed to peptidoglycan. These genes included those encoding methyl-accepting chemotaxis-like proteins such as *vc0216*, *vc0282*, *vc1248*, *vc1298*, *vc1535*, *vc1868*, *vca0031*, *vca0979*, *vca1034*, and *vca1069*. Genes that belong to chemotaxis cluster I (*vc1400-vc1403*) and cluster III (*vca1088-vca1096*) were also upregulated. Chemotaxis-related genes are often associated with CheY-like response regulators that modify gene expression depending on their phosphorylation state (271, 272). I found 8 response regulators that were upregulated more than 2-fold in peptidoglycan-treated cells: *cheY2* (*vc1396*), *vc1081*, *vc1082*, *vc1086*, *vc1087*, *vc1157*, *vca1086*, and *cheY4* (*vca1096*). Bacteria also use transcriptional regulators (TR) to modify gene expression. We saw an upregulation of 7 TRs, 2 of which are master regulators of biofilm formation, namely RpoS (*vc0534*) and HapR (*vc0583*). Genes encoding other transcriptional regulators linked to biofilm formation such as AphA (*vc2647*), VpsT (*vca0952*), VpsR (*vc0665*) were however, not significantly upregulated. The other upregulated TRs included CadC (*vc0278*), TfoX (*vc1153*), RstR1 (*vc1455*), RstR2 (*vc1464*), *vc1588*, and *vca0542*.

As the trigger for biofilm formation required only $5\,min$ of peptidoglycan exposure, I hypothesised that *V. cholerae* utilises rapid intracellular signalling to upregulate the expression of matrix genes. In many bacterial species, including *V. cholerae*, cyclic nucleotides, such as c-di-GMP, are employed to rapidly respond to environmental changes (205). Moreover, c-di-GMP regulation is tightly linked to biofilm formation (273). I found that 6 genes encoding diguanylate cyclases (DCG) (*vc1067*, *vc1370*, *vc1372*, *vc1376*, *vc1593*, and *vca0848*) were upregulated during pep-

[1] all differentially upregulated genes are listed in Appendix Table A3

tidoglycan exposure. Therefore, I hypothesised that a peptidoglycan-induced upregulation of DGCs increases cellular c-di-GMP levels, ultimately resulting in biofilm formation. This is explored further in the next section 3.11.

Previous studies have shown that bacterial danger-sensing can induce not only defensive factors, such as matrix production, but also offensive factors that aid in bacterial warfare against the source of threat (274, 275). The RNA-Seq data showed that in addition to the 11 genes linked to matrix production, there were 16 genes related to the production of other effectors that were also upregulated more than 2-fold. These included genes encoding the extracellular nuclease XDS (*vc2621*), haemolysin (*vca0219*), proteases PrtV (*vca0223*) and HapA (*vca0865*), toxin co-regulated pilus (*vc0829-vc0837*), and motility-associated killing proteins (*vca0880-vca0883*). However, the role of these effectors in *V. cholerae* danger-sensing is yet to be elucidated.

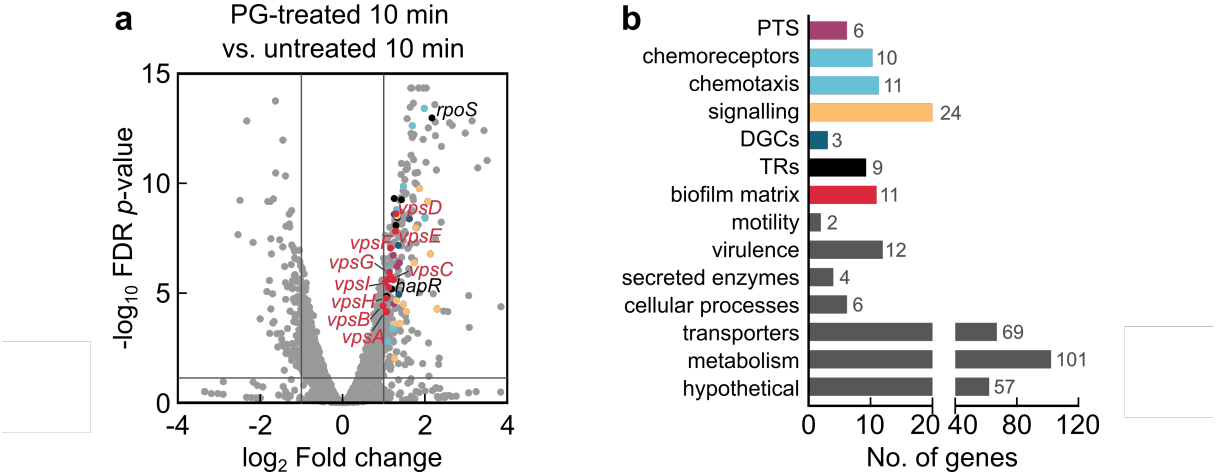

Figure 3.11: RNA-Seq of *V. cholerae* cells exposed to peptidoglycan uncovered that genes linked to c-di-GMP and biofilm matrix production were upregulated. a, Differentially regulated genes during peptidoglycan (PG, $300\,\mu g\,mL^{-1}$) treatment were identified by comparing the transcriptome of *V. cholerae* cells that were exposed to pure PG for $10\,min$ and untreated cells exposed to LB only for $10\,min$. Genes with absolute fold changes of > 2 and a false discovery rate (FDR) corrected p-value of < 0.05 were considered to be differentially expressed. Upregulated genes were functionally categorised (coloured dots) using a combination of annotations from UniProt (251), KEGG (252), and MicrobesOnline (253). Colours correspond to the colours of the bar graph in **b,** which is a quantification of the number of genes differentially upregulated for each mentioned category. All differentially upregulated genes are listed in Appendix Table A3.

3.11 Peptidoglycan exposure results in increased cellular c-di-GMP levels

As genes encoding c-di-GMP-producing proteins (DGCs) were upregulated during peptidoglycan exposure, I hypothesised that peptidoglycan exposure leads to an increase in cellular c-di-GMP levels. To visualise changes in cellular c-di-GMP levels during peptidoglycan exposure, I adapted a previously described riboswitch-based fluorescent reporter to visualise changes in cellular c-di-GMP levels (276). Here, the production of sfGFP was regulated by three tandem riboswitches (Bc3 to Bc5) that respond to c-di-GMP (*bc3-5-sfGFP*) (Figure 3.12a). Thus, when c-di-GMP levels are high, its binding to the riboswitches cause a conformational change, which results in the transcription of *sfGFP* (276). To prevent the accumulation of the fluorescent protein, *sfGFP* was cloned with a degradation tag (277). Bacterial cells also produced mRuby3 constitutively (P_{tac}-*mRuby3*). The functionality of this reporter was validated by transforming the plasmid, containing the reporter and constitutive fluorescence, into *V. cholerae* strains with low (Δ4DCG) or high (Δ2PDE) cellular c-di-GMP levels. Δ4DCG is short for Δ*cdgD*Δ*cdgK*Δ*cdgH*Δ*cdgL*, which is a quadruple deletion mutant of four DGCs, namely, CdgD (encoded by *vca0697*), CdgK (encoded by *vc1104*), CdgH (encoded by *vc1067*), and CdgL (encoded by *vc2285*). The lack of four proteins responsible for producing c-di-GMP causes this strain to have an inherent property of low cellular c-di-GMP levels. Δ2PDE is short for Δ*rocS*Δ*cdgJ*, which is a double deletion mutant of phosphodiesterases (PDE), namely, RocS (encoded by *vc0653*) and CdgJ (encoded by *vc0137*). The lack of two proteins responsible for degrading c-di-GMP causes this strain to have an inherent property of high cellular c-di-GMP levels. The low and high c-di-GMP level strains harbouring the reporter plasmid were imaged and the fluorescent intensity levels of the c-di-GMP reporter was measured in these two strains, and compared with the WT. I found that the Δ4DCG mutant showed low levels of sfGFP fluorescence as compared to the WT, whereas the Δ2PDE showed higher levels as compared to the WT (Figure 3.12b). This confirmed that the fluorescent intensity levels of the c-di-GMP reporter ($I_{bc3\text{-}5\text{-}sfGFP}$) were directly proportional to the cellular c-di-GMP levels.

When *V. cholerae* cells were exposed to peptidoglycan, the fluorescence levels of sfGFP increased after $40\,\mathrm{min}$ of exposure, indicating that peptidoglycan exposure caused an increase in cellular c-di-GMP levels (Figure 3.12c-d). This increase was not observed in the untreated condition.

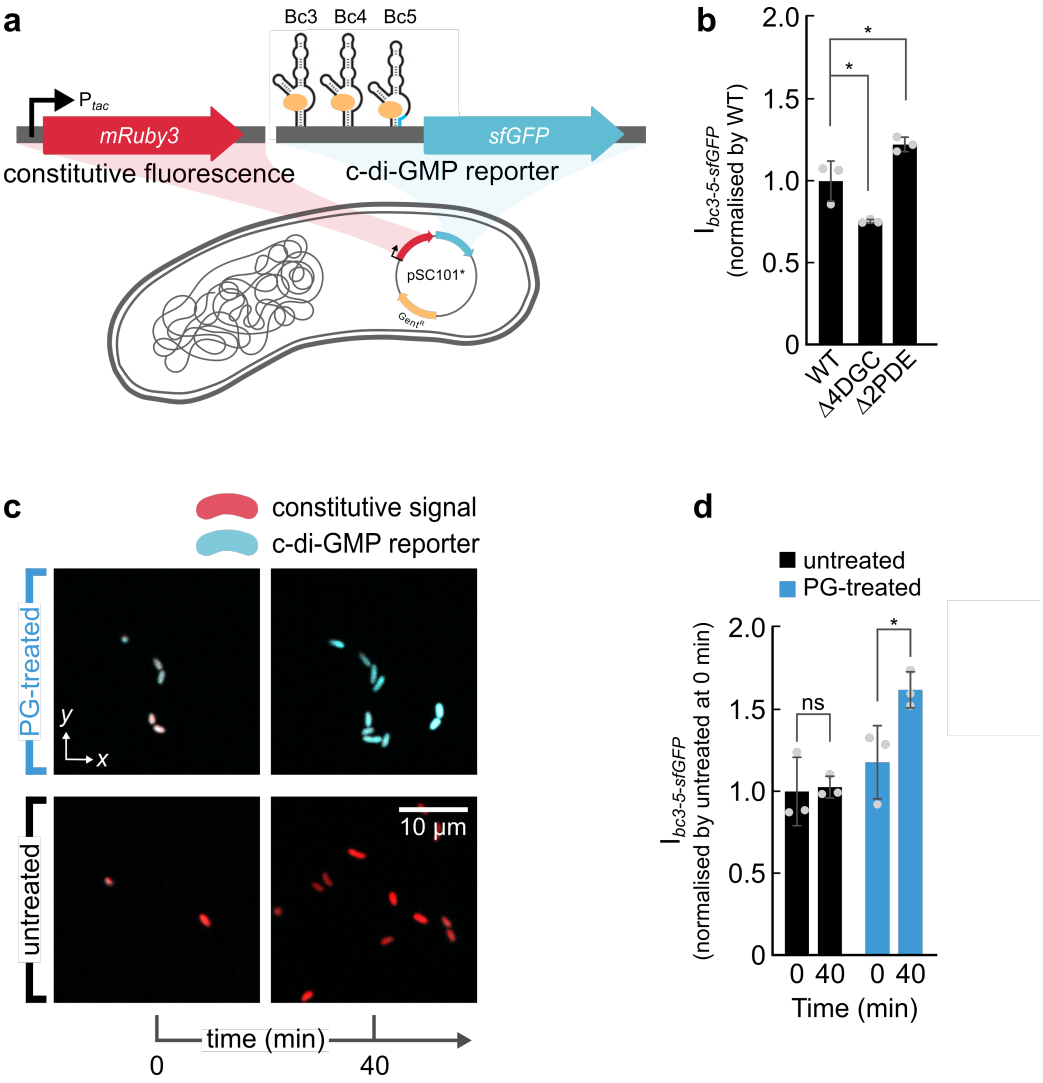

Figure 3.12: Cellular levels of c-di-GMP increased when *V. cholerae* cells were exposed to peptidoglycan. a, Schematic of the constructed bacterial fluorescent c-di-GMP reporter system. Triple tandem riboswitches (Bc3-5) permit transcription of *sfGFP* (blue) when c-di-GMP molecules (yellow) are bound. This *bc3-5-sfGFP* fragment was cloned onto a low copy-number plasmid (pSC101*) with a Gent^{R} marker (yellow) along with *mRuby3* (red), with the entire fragment under the control of a P_{tac} promoter. **b,** Quantification of the fold-change in fluorescent intensity levels of the c-di-GMP reporter ($I_{bc3\text{-}5\text{-}sfGFP}$ normalised by the WT levels) in *V. cholerae* wild-type (WT) cells, compared to cells lacking four proteins responsible for producing c-di-GMP (Δ4DCG) or two proteins responsible for degrading c-di-GMP (Δ2PDE). The cellular c-di-GMP levels were expected to be intermediate, low, and high for the WT, Δ4DCG mutant, and Δ2PDE mutant, respectively. Measurement of the sfGFP fluorescence levels indicated that the fluorescent intensity levels of the c-di-GMP reporter corresponded proportionally with the expected cellular c-di-GMP levels. **c,** Confocal images of *V. cholerae* WT cells constitutively expressing mRuby3 (red) and sfGFP (cyan), in response to increasing c-di-GMP levels exposed to a continuous flow of peptidoglycan (PG, $300\,\mu g\,mL^{-1}$, blue) or untreated (black) over $40\,min$. Bacterial cells exposed to PG showed production of sfGFP, which did not occur in the untreated condition. **d,** Quantification of the fold-change in fluorescent intensity levels of the c-di-GMP reporter ($I_{bc3\text{-}5\text{-}sfGFP}$ normalised by cellular levels in the untreated condition at $0\,min$) in *V. cholerae* WT cells exposed to PG ($300\,\mu g\,mL^{-1}$, blue) or untreated (black) immediately ($0\,min$) or $40\,min$ after the initiation of PG flow in the microfluidic chamber. A significant increase in sfGFP levels in PG-treated ...

Figure 3.12: ... cells indicated that PG exposure resulted in an increase in cellular c-di-GMP levels. sfGFP fluorescence levels remained constant in the untreated condition. Bars are mean values with points denoting 3 biological replicates and error bars indicate the standard deviation. Statistical significances were calculated either using a one-way ANOVA with Bonferroni's correction (panel **b**) or a Student's t-test (panel **d**), respectively (ns = not significant; * = $p <$ 0.05).

3.12 Visualisation of biofilm matrix production during peptidoglycan exposure

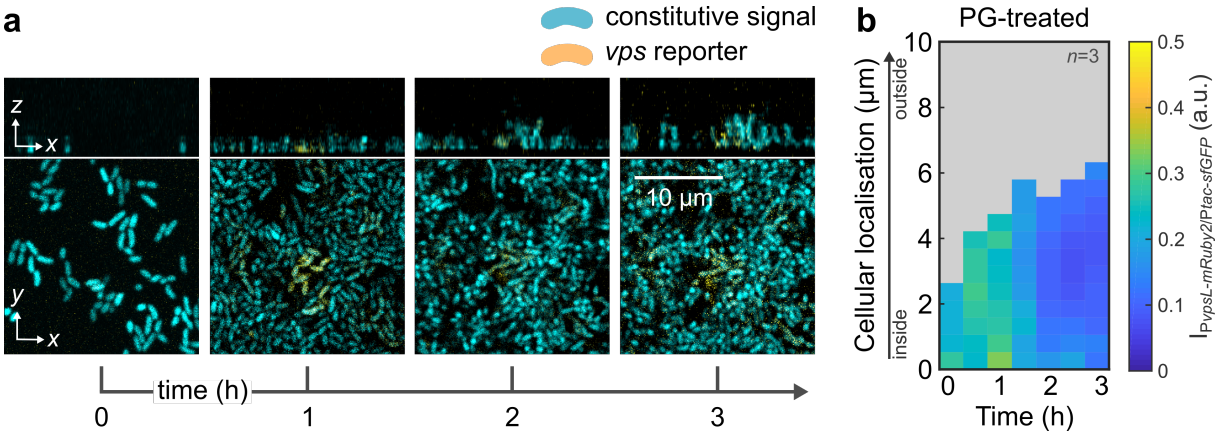

Figure 3.13: *V. cholerae* cells expressed *vps* genes in response to peptidoglycan exposure. **a,** Confocal image time series of *V. cholerae* cells constitutively expressing *sfGFP* (cyan), under the control of the P_{tac} promoter, and *mRuby2* (yellow), under the control of the P_{vpsL} promoter, exposed to a continuous flow of peptidoglycan (PG, $300\,\mu g\,mL^{-1}$). Bacterial cells exposed to PG showed transcription of *vps* genes. The untreated condition was the same as Figure 3.4. **b,** Visualisation of the spatiotemporal dynamics of *vps* operon transcription during PG exposure ($300\,\mu g\,mL^{-1}$). The fluorescence of the matrix gene reporter (P_{vpsL}-*mRuby2*) was normalised by the fluorescence intensity of a constitutive reporter (P_{tac}-*sfGFP*). Each pixel in these kymographs is coloured according to the ratio of fluorescence expression at a given time and spatial position in the biofilm. Fluorescence expression values were averaged over all cells with similar distances from the outer biofilm boundary facing the liquid medium. Kymographs are representative of n = 3 different biofilms.

Transcriptomics analysis of *V. cholerae* cells exposed to peptidoglycan showed that *vps* genes, encoding the major matrix component VPS, were differentially upregulated as compared to untreated cells (Figure 3.11). To confirm this, *vps* gene expression was visualised spatiotemporally by exposing *V. cholerae* cells producing the fluorescent protein mRuby2 under the control of the promoter of *vps* genes (P_{vpsL}-*mRuby2*) to peptidoglycan in microfluidic chambers. The bacterial cells also expressed the fluorescent protein sfGFP constitutively (P_{tac}-*sfGFP*), which was used to normalise for cellular fluorescence levels. Increase in the mRuby2 fluorescence signal indicated that *V. cholerae* cells initiated the transcription of *vps* genes within the first hour of peptidoglycan exposure (Figure 3.13a). From figure 3.4, it is already known that untreated cells do not express mRuby2, nor form biofilms. mRuby2 production was quantified by plotting kymographs that depict changes in the level of *vps*-regulated fluorescence normalised by the constitutive fluo-

rescence (indicated by the colourmap) across the height of the bacterial biofilm (y-axis) and over time (x-axis). These kymographs showed that *V. cholerae* cells transcribed *vps* rapidly during peptidoglycan exposure (Figure 3.13b).

3.13 Peptidoglycan is a conserved danger-signal

The previously described results identified the signal for inducing biofilm formation in *V. cholerae* to be peptidoglycan. As *V. cholerae* cells were able to produce biofilms in response to bacterial lysates made from other bacteria, it seemed prudent to test the inverse as well, i.e., do other bacteria also sense peptidoglycan and initiate biofilm formation? To test this, I exposed *E. coli* and *P. aeruginosa*, constitutively expressing sfGFP, to peptidoglycan in microfluidic chambers. Interestingly, I found that *P. aeruginosa* cells were able to form biofilms in response to peptidoglycan exposure, whereas *E. coli* cells were not (Figure 3.14). Similar to *V. cholerae*, these bacterial species did not form biofilms in the absence of peptidoglycan exposure. These observations suggested that peptidoglycan is a conserved signal that has the capability to induce biofilm formation in other bacteria, such as *P. aeruginosa*.

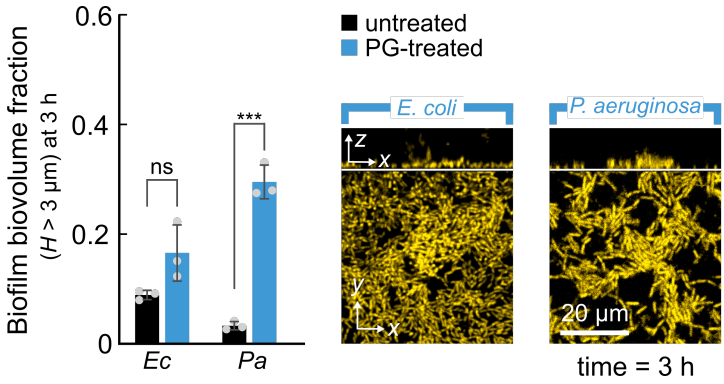

Figure 3.14: *P. aeruginosa* cells formed biofilms in response to peptidoglycan exposure. Exposure to peptidoglycan (PG, $300\,\mu g\,mL^{-1}$, blue) triggered *P. aeruginosa* cells (*Pa*) to grow into 3D biofilms over $3\,h$. Biofilm formation was quantified by calculating the biovolume fraction, which is the sum of the biovolume with height $H > 3\,\mu m$ divided by the total biovolume. Biofilm formation was not observed when *E. coli* cells (*Ec*) were exposed to PG. *P. aeruginosa* or *E. coli* cells did not form biofilms in the absence of PGN (untreated, black). Bars are mean values with each point denoting one biological replicate and error bars indicate the standard deviation. Statistical significances were calculated using Student's t-tests (ns = not significant; *** = $p <$ 0.001). Confocal images show the $3\,h$ timepoint demonstrating the formation of 3D biofilms in *P. aeruginosa*, but not *E. coli*, with yellow cells representing bacterial cells constitutively producing sfGFP.

Conclusion

The results described in this chapter confirmed that *V. cholerae* cells responded to components of lysed bacterial cells *via* a novel method of bacterial signalling, hereby referred to as danger sensing. Biofilm formation was a result of bacterial lysis during phage infection, but not due to the presence of the phages themselves (Figure 3.1). This was further demonstrated by the fact that cellular lysis caused by factors other than phages (here, sonicated lysate was used as a proxy) also induced biofilm formation (Figure 3.2). Soluble components of the bacterial lysate triggered biofilm formation in *V. cholerae* by a sensory system, and not by limiting bacterial attachment or growth in microfluidic chambers (Figure 3.3). During the search for identifying the biofilm-inducing compound in the bacterial lysate, I found that the inducer was conserved across various Gram-negative and -positive bacterial species, and had a size of 30 kDa or more (Figure 3.7). While eDNA has been shown to be a crucial player in scaffolding of biofilms, I found that eDNA did not play a role in lysate-induced biofilm formation in *V. cholerae* (Figure 3.9). By exposing *V. cholerae* cells to crude cell wall extracts and purified peptidoglycan, I discovered that peptidoglycan fragments served as the signal for danger-sensing, which triggered biofilm formation (Figure 3.10). Using transcriptomics, the involvement of bacterial signalling systems such as PTS and chemotaxis were unveiled (Figure 3.11). The transcriptomics analysis also suggested that *V. cholerae* cells might use secondary messenger molecules such as c-di-GMP for regulating the cellular response to peptidoglycan exposure. To investigate the role of c-di-GMP in bacterial danger-sensing, I constructed a fluorescent reporter to visualise changes in cellular c-di-GMP levels during peptidoglycan exposure. Using the reporter, it was confirmed that peptidoglycan exposure caused an increase in cellular c-di-GMP levels (Figure 3.12). *V. cholerae* cells produced the major biofilm matrix components VPS and RbmA during lysate (Figure 3.4-3.5) and peptidoglycan exposure.

I also found that peptidoglycan induced biofilm formation in other bacteria such as *P. aeruginosa*. In this study, peptidoglycan as a biofilm-inducing signal was only tested with the Gram-negative bacteria *P. aeruginosa* and *E. coli*. Its role in Gram-positive bacteria and other Gram-negative bacteria is yet to be explored. The presence of biofilm formation as a regulatory response to peptidoglycan exposure suggested that danger sensing could be conserved across various bacterial species. Overall, I observed that biofilm formation facilitated a quick bacterial hideaway and therefore, played a crucial role in protecting bacteria from phage predation and potentially, other lytic stresses.

4 | Discussion

This thesis describes a novel signal used by bacteria to sense danger in their surroundings and protect themselves against phage predation by forming biofilms. The biofilm formation phenotype presented in Chapter 2 can be explained by the characterisation of the danger signal as well as the discovery of the signalling pathway, as described in Chapter 3. Typically, when phages infect bacterial cells *via* their lytic lifecycle, it results in the lysis of the bacterial host. Therefore, it was surprising to observe that *Vibrio cholerae* cells actively produced biofilms during phage exposure. Furthermore, biofilm formation was confirmed to be a regulatory response, and not due to the selection of phage-resistant or matrix hyper-producer mutants (as described in Chapter 2). Bacterial cells embedded in the biofilm matrix were protected against phage infection, as has been reported previously (104, 115). Although it has been shown that a low-level of phage predation resulted in biofilm formation in bacterial species such as *Staphylococcus aureus*, *Escherichia coli* and *Pseudomonas aeruginosa* (116–118), the mechanism of how cells increased biofilm matrix production has not been described. Understanding that the initial outcome of phage infection, i.e., cell lysis, was essential to ensure protection on a bacterial population-level played a pivotal role, which led to the discovery of bacterial danger sensing. Previous studies have shown the involvement of cell lysis (either spontaneous, or phage-induced) in bacterial biofilm formation (278–280). However, in these bacteria, extracellular DNA (eDNA) was described to be instrumental for bacterial biofilm formation by acting as a scaffolding substance that contributed to shaping biofilm architecture (281, 282). In this study, it was clear that eDNA did not play a role and that biofilm matrix genes were transcriptionally upregulated by sensing a soluble component from lysed bacterial cells, which was identified to be peptidoglycan (as described in Chapter 3). Combining the results from Chapters 2 and 3, I propose a model for danger sensing in *V. cholerae* in which bacterial cells sense peptidoglycan fragments from lysed cells and induce biofilm matrix production, with c-di-GMP playing the role as the relay messenger molecule (Figure 4.1).

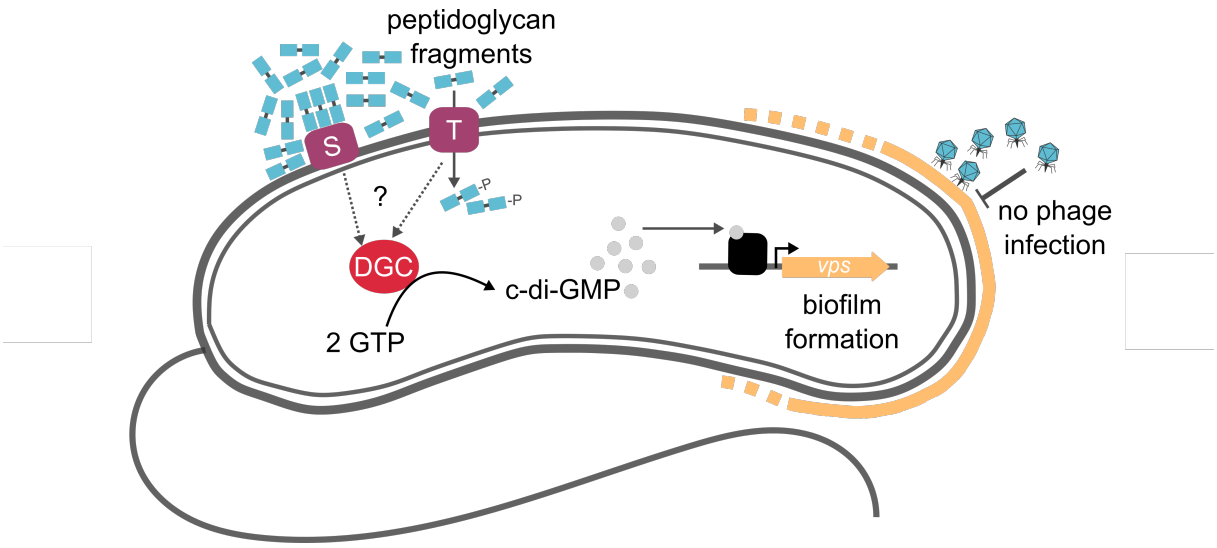

Figure 4.1: Danger sensing in *V. cholerae* leads to biofilm formation. Schematic of danger sensing, which is initiated by sensing peptidoglycan (PG) fragments in the bacterial extracellular environment. Extracellular PG fragments could be detected by a sensor (purple, S) present on the bacterial outer membrane (discussed in section 4.1). It is also possible that PG could be taken up by an active transport system (purple, T), such as the phosphotransferase system (PTS). Sensing of PG leads to the production of c-di-GMP (grey), *via* the activation of diguanylate cyclase (DGC, red), and biofilm formation by initiating the transcription of biofilm matrix genes (yellow). *V. cholerae* cells embedded in biofilm matrix are protected from phage infection.

While this model explains how biofilm formation occurs during phage infection (or other lytic stresses), there remain many unanswered questions regarding the danger sensing regulatory pathway: How do *V. cholerae* cells sense peptidoglycan fragments? How does peptidoglycan-sensing result in increased c-di-GMP levels? Although it has been shown that c-di-GMP leads to biofilm formation in *V. cholerae via* the transcriptional regulator VpsT (205), the presence of this regulation is needed to be confirmed in order to confirm the role of c-di-GMP as the intracellular signalling molecule responsible for signal relay. The avenues for the elucidation of the sensor and regulatory system, along with implications of the signal and the sensory system as a bacterial defence system against stresses that cause bacterial cell lysis are discussed in the following sections.

4.1 Necrosignals and their receptors

In this work, peptidoglycan was identified as a signal for danger sensing in *V. cholerae*. This signal was found to also induce biofilm formation in other bacteria such as *P. aeruginosa*. Compounds that are indicative of cellular damage but do not cause harm themselves have been referred to as danger signals or 'necrosignals' (259, 283). However, not many such compounds have been found. It is possible that there are other unidentified compounds in bacterial lysates that could also function as necrosignals. A recent study identified a periplasmic protein ArcA as a necrosignal that stimulated the expression of efflux pumps to aid in bacterial survival during antibiotic exposure (283). Other studies have proposed that volatile organic compounds released from eukaryotic cells could provide bacteria with warning of incoming predators from a distance

(284, 285). However, these compounds have not been identified and their role in bacterial danger sensing have not been described.

In order for danger sensing to efficiently operate, bacterial cells must be able to sense these signals at all times, suggesting that the receptors for these necrosignals must be constitutively produced. This would permit bacteria to continuously monitor their environment for impending predators. However, the constitutive expression of proteins on the outer surface of bacteria could be costly for the cell, especially if predators such as bacteriophages utilise this protein as a receptor to initiate infection. Bacteria have been known to adjust the levels of outer membrane proteins depending on their cell density in order to prevent phage infection (286). Therefore, it is more probable that bacterial outer membrane proteins that have other metabolic or transport functions are utilised as a receptor for sensing necrosignals. This was the case in the ArcA-dependent danger sensing study, where the receptor was identified as TolC, an outer membrane efflux pump (283). On the other hand, the Gac/Rsm signalling pathway, which was involved in distinguishing lysed kin or non-kin cells of *P. aeruginosa*, comprises of a two-component system (TCS) GacS/GacA, which is responsible for the transition between biofilm and planktonic lifestyle of the bacteria (287, 288). Here, the danger signal is sensed by an orphan sensor kinase RetS, which modulates GacS activity (287). Although the Gac TCS is conserved in many γ-proteobacteria (289) and has a homolog in *V. cholerae* (290, 291), called VarS/VarA (encoded by *vc2453* and *vc1213*, respectively), its role in sensing peptidoglycan has not been explored in this work. However, VarA is known to repress biofilm formation in *V. cholerae* (292). Therefore, it may not be involved in sensing peptidoglycan in *V. cholerae*. There could be other more promising candidates for sensing peptidoglycan, which are discussed in the following paragraphs.

While it might seem counterintuitive for bacteria to sense a component of their own cell wall as a danger signal, sensing peptidoglycan has proven to be very effective in the eukaryotic world. Detecting the presence of bacterial pathogens is essential for survival of eukaryotic cells (293). For plant cells or cells of the human immune system, sensing peptidoglycan is vital for adequately eliciting immune responses (294). Bacterial peptidoglycan is sensed by surface receptors such as peptidoglycan recognition proteins (PGRP), nucleotide binding and oligomerisation domain (NOD)-like receptors, proteins with penicillin-binding and Ser/Thr kinase-associated (PASTA) domains, or proteins with lysin motif (LysM) domains (295). All these surface receptors share homology as they comprise of pattern-specific repeats that bind peptidoglycan (294). However, only LysM domains have been found to be conserved across all kingdoms of life (296). Proteins containing LysM domains have been described in bacteria, but only as regulators of cell wall synthesis and recycling (297, 298). By a homology search, I found that *V. cholerae* possesses proteins containing LysM domains. Out of these, some proteins are located on the cell surface and contain additional domains related to signalling such as a CACHE domain, for signal-binding, and GGDEF domain, for regulation of c-di-GMP levels (Table 4.1). Future work could test these promising candidate proteins for their involvement in sensing peptidoglycan.

Table 4.1: Proteins containing LysM domains and signalling domains in *V. cholerae*

Locus	Protein	Function
VC0047	TsaP	putative type IV pilus protein
VC0998	FimV	type IV pilus assembly protein
VC1406	Mlp16	methyl-accepting chemotaxis-like protein
VCA0101	YjcC-2	putative c-di-GMP PDE
VCA0220	HlyB	methyl-accepting chemotaxis-like protein
VCA1069	Mlp43	methyl-accepting chemotaxis-like protein
VCA1077		serine/threonine protein kinase Pkn1

Results from Chapter 3 indicate that bacterial cells initiate biofilm formation only in response to high levels of extracellular peptidoglycan. This could indicate that peptidoglycan binds non-specifically to receptors on the cell surface. The transcriptomics analysis revealed numerous chemoreceptors and components of the chemotaxis clusters I and III that were upregulated during peptidoglycan exposure. One interesting differentially upregulated gene was *vca1069*, which encodes the methyl-accepting chemotaxis-like protein Mlp43, containing a LysM domain. Other upregulated genes encoding chemoreceptors were *vc0216* (Mlp2) and *vc0282*. Genes from chemotaxis clusters I and III that were upregulated included *vc1248*, *vc1868*, and *vca0031*. The functions of these genes are not described but they all have been shown to be upregulated during bacterial monolayer formation (299). In *V. cholerae*, only proteins in chemotaxis cluster II regulate flagellar rotation (272). The role of the other two clusters, I and III, remains unknown (300). Proteins involved in bacterial chemotaxis systems have been shown to influence biofilm formation in some bacteria (301–305). This has been well-described in the Wsp chemosensory system of *P. aeruginosa*, wherein the CheY-like response regulators have been shown to possess or interact with proteins with GGDEF domains (306). This results in the production of c-di-GMP, which then causes an increase in biofilm matrix production (167). In fact, c-di-GMP has been shown to act as an à la carte component used by bacterial cells to mediate between various cellular processes including chemotaxis and biofilm formation (307–309). Considering that these systems were strongly upregulated during peptidoglycan exposure (as found by the transcriptomics analysis), the identified chemoreceptors and chemotaxis-related genes could be a promising lead to identifying the receptor and regulation mechanism of sensing peptidoglycan.

In the context of bacterial danger sensing, it is possible that *V. cholerae* cells take up peptidoglycan as it is present in excess in the environment, and its accumulation inside the bacterial cell serves as the actual signal, responsible for eliciting a bacterial response. Proteomics and transcriptomics revealed that components of the phosphotransferase system (PTS) were observed to be upregulated in response to phages, as well as peptidoglycan exposure, respectively. PTS has been known to mediate sugar utilisation and cellular responses such as biofilm formation

(134). This, along with the aforementioned hypotheses are possible leads to uncover how the necrosignal peptidoglycan is sensed.

4.2 Genetic regulation during bacterial danger sensing

The transcriptomics analysis of peptidoglycan-treated cells compared to untreated cells, and proteomics analysis of phage-treated cells compared to untreated cells revealed that transcriptional regulators like HapR and RpoS were produced during exposure to phages and peptidoglycan, which typically leads to biofilm dispersal in *V. cholerae* (183). This result was paradoxical to what is expected during peptidoglycan or phage exposure as the presence of HapR or RpoS generally represses biofilm formation (182). However, the studies that have elucidated the regulatory role of HapR have been done either in minimal media (183) or in shaking liquid cultures (182). The combined effect of rich media and presence of a surface to which bacterial cells adhered to, might have influenced the activity of these regulators. Moreover, the omics techniques do not offer spatial information, but provide a measurement for the bulk of bacterial cells collected. Phage infection eliminated a large population of *V. cholerae* cells, leaving only a few cells behind, which were responsible for eliciting the biofilm response. When *V. cholerae* cells were exposed to peptidoglycan, it is possible that not every single cell exhibited danger sensing and initiated biofilm formation. Therefore, it might be possible that the increase of the transcriptional regulators HapR and RpoS in non-biofilm forming cells masks their absence in cells that participated in biofilm formation.

The observations from proteomics and transcriptomics suggest that biofilm formation in *V. cholerae* as a response to peptidoglycan exposure could be induced *via* a pathway that circumvents the HapR-mediated repression of *vps* genes. According to previous studies, it has been shown c-di-GMP activates VpsT and VpsR, which then upregulate the transcription of biofilm matrix genes (52). Thus, in the presence of high levels of c-di-GMP, this process has been shown to take precedence over transcriptional repression by HapR (310). Another study showed that RpoS was upregulated during bacterial monolayer formation (299). As the transcriptome of *V. cholerae* cells was characterised after only $10\,\mathrm{min}$ of peptidoglycan exposure, it suggests that RpoS could be necessary for initial biofilm formation. However, these hypotheses require further investigation in order to disentangle the regulatory genetic circuitry in play during bacterial danger sensing. Genes related to the production of a recently discovered secondary messenger molecule, cGAMP, were also upregulated during peptidoglycan and phage exposure. However, the role of these signalling components during bacterial danger sensing and biofilm formation is yet to be explored.

4.3 Defensive and offensive effectors to oppose bacterial predators

Danger sensing involves the sensing of a self or non-self-derived cue and initiating a response that protects the bacterial cells against the antagonistic agent by producing defensive or offensive effectors, or both (259). In this study, bacterial danger sensing resulted in the production of biofilms, which served as a defensive strategy to ensure bacterial survival during phage exposure. Other studies also demonstrate that biofilm formation, caused as a result of exposure to

phages (116–118), sub-lethal concentrations of antibiotics (311), or low Mg^{2+} ions (312) (which were indicative of lysed cells), constitutes a defensive strategy to protect bacteria from multiple stresses (313). On the other hand, danger sensing has also been shown to initiate the secretion of offensive factors to aid eliminating the predator. Bacteria such as *P. aeruginosa*, expressing the Gac/Rsm pathway, have been shown to express offensive factors to contend with competing bacterial species (274, 275). These factors include the production of secreted enzymes (289), antimicrobial peptides (314), secreted toxins (315), deployment of the type VI secretion system (316), and many other chemical or mechanical weapons (317). In response to the exposure of toxin-producing bacterial competitors, bacteria have been shown to exhibit mass lysis in order to deliver high doses of their own toxins while keeping a subpopulation safe from competing species (318). Such kind of bacterial antagonism has been presented to be a result of competition sensing (319). Competition sensing has been proposed to detect harm caused by other cells in order to invoke a physiological response that counter-attacks the competing species by securing bactericides other anti-microbial peptides. This type of ecological competition could be relevant not only against other microbes but also against phages, or even the immune cells of human host. In this study, the transcriptomics analysis of peptidoglycan-treated cells compared to untreated cells revealed 16 differentially upregulated genes that were related to the production of secreted enzymes such as the nuclease XDS (encoded by *vc2621*), haemolysin (encoded by *vca0219*), proteases PrtV (encoded by *vca0223*) and HapA (encoded by *vca0865*), and virulence factors such as the toxin co-regulated pilus (encoded by *vc0829-vc0837*), and motility-associated killing proteins (encoded by *vca0880-vca0883*). These offensive factors would enable primed cells on the frontlines of bacterial communities to efficiently contend with predators to survive during such ecological competition.

4.4 Danger sensing as a component of bacterial innate immunity

Bacteria have evolved to adapt to changing environmental conditions either by accumulating genetic modifications or else, incorporating and utilising signalling systems to sense and respond to stresses (described in section 1.4). In particular, bacteria have been shown to use TCS to sense threats to bacterial survival indirectly, by detecting damage to their cell wall. Bacteria can therefore respond to agents that cause cell damage by invoking organised stress responses such as membrane stress (320, 321), SOS response (322), and oxidative stress response (140, 323). These are generally employed as defence systems against lytic agents such as antibiotics or phages, which prevent, repair or abort damage to the bacterial cell (324). However, in this study I observed that the majority of *V. cholerae* cells could not prevent phage infection when they were initially co-incubated with Vibriophage N4. Furthermore, I discovered that intact bacteria used peptidoglycan fragments as a signal to activate danger sensing. It is important to note here that peptidoglycan itself does not cause harmful effects to bacterial cells. Sensing of such a general exogenous compound, originating from damaged clonemates, has, to my knowledge, not previously been described.

The idea of danger sensing, proposed by Joseph Mougous, suggests that bacteria detect and respond to threats posed by biotic antagonists (such as phages or competing bacteria) *via* an in-

nate immune-like process (259). Here, the signal for danger sensing coincides with the presence of a bacterial predator but is independent of the biological entity itself. Moreover, the danger signal does not itself cause cellular damage. This completely encompasses the phenotype described in this study, and therefore, peptidoglycan is a signal for bacterial danger sensing. Here, phage infection was used as a biotic threat to study the bacterial response. However, peptidoglycan sensing could also occur during lysis caused by other forms of bacterial antagonism such as antimicrobial peptides (325), secreted toxins (326), deployment of the T6SS (327), and contact-dependent inhibition (328).

While this study is the first to describe a general signal for danger sensing, the concept of sensing and responding to bacterial antagonism has also been described by other publications. Out of these, the system that is most well-established is the TCS Gac/Rsm pathway in *P. aeruginosa* (289). Bacteria have been shown to recognise kin lysis and elicit an offensive (secretion of antimicrobials, extracellular proteases, T6SS induction) or defensive (QS autoinducers, EPS production) response *via* the Gac/Rsm pathway (287). This method of signalling has been shown to be conserved in many species of gamma-proteobacteria but the effectors that are regulated by the Gac/Rsm pathway vary across different bacterial species (289). Although the regulatory mechanism has been described for this pathway, the signal still remains elusive. For closely related bacterial species, proteins have been shown to act as the necrosignal to elicit a defensive response against competing species (283). These described danger sensing systems have been shown to be species-specific. However, in multi-species biofilms or in situations where mass cell lysis takes place, species-specificity would become irrelevant as there would be a higher probability of imminent danger. Under such short-range interactions, high doses of a signal could serve as an indication for the presence of lytic stressors (284, 329). It is also therefore, unsurprising that such kind of danger sensing would induce a general stress response such as biofilm formation, which has been shown to protect cells from a variety of biotic and abiotic stresses (230).

The ability to recognise exogenous molecules that are indicative of the presence of a threat is characteristic of the innate immune response in eukaryotic systems (330). Such immunostimulatory molecules include components of the arriving predator (in the case of human immune cells, this is usually the cell wall of pathogenic bacteria, called PAMPs) or fragments of self that indicate the presence of damaged cells (DAMPs) (293). While danger sensing has been well-described in eukaryotes, the presence of such systems in prokaryotes have been concluded on the presumption that they would be the precursors from which the eukaryotic systems have evolved. The ubiquity of agents that have the ability to cause bacterial lysis, such as phages or competing bacterial species, suggests that bacteria might have evolved regulatory systems to sense and respond to damages incurred by its clonal neighbour. The presence of such bacterial systems is evident in this work, along with other studies (283, 287, 289, 311, 331, 332). As bacterial biofilm formation constitutes a general response to protect bacteria from impending threat, it is tempting to speculate that bacterial danger sensing represents a primitive form of innate immunity.

4.5 Coexistence of bacteria and bacterial predators

The need for danger sensing in bacteria could arise from the fact that bacteria often face predators such as lytic phages or eukaryotic host cells, or other competing bacteria. The presence of both bacteria and their predators in the environment is a reflection of biological coexistence. While it is clear from this context that predators benefit from their prey by utilising them for proliferation or as an energy source, it is also important to note that prey often reap advantages from their predators. Although seemingly counterintuitive, it has been shown that bacteria also benefit from keeping their predator phages alive (333). This phage sensitivity can manifest as enhanced bacterial resilience against other bacterial competitors. For example, it has been shown that phages can facilitate bacterial cell lysis to release bacteriocins that act as weapons against competing microbial species (334). Interestingly, phage-encoded toxins have been shown to act as a bacterial defence system against eukaryotic predators (335). Cell lysis caused by phages (or other factors) also releases DNA, which may be taken up by natural competence systems, leading to increased horizontal gene transfer (336). Acquisition of genes that impart antibiotic resistance, enhance bacterial toxicity, or immunity against other bacterial toxins contribute to widening of bacterial arsenal to aid in survival (337). This is exemplified by *V. cholerae*, which shows natural competence while growing on chitin (338). Competition studies of *V. cholerae* cells on chitin demonstrate that naturally competent bacterial cells use their type VI secretion system (T6SS) to actively acquire DNA from non-kin neighbours (339). It is possible that phage predation and danger sensing could also induce bacterial natural competence systems. In fact, the transcriptomcis analysis revealed that the gene encoding the natural competence regulator *tfoX (vc1153)* was enhanced during peptidoglycan exposure. However, this requires further investigation.

Overall, the advantages of phages are often difficult to perceive on a single-cell level as they typically cause population-wide lysis. However, this study, along with others (116, 117) have shown that phage exposure promotes bacterial biofilm formation, indicating that phages confer a population-level effect to enhance bacterial survival. Biofilms could provide a platform for playing out different bacterial and phage defence strategies (118). As observed in this study, matrix secretion constitutes a temporary protection strategy to preventing phage predation whilst keeping them at bay, but without eliminating them. This transient method of protection exhibits the relevance of coexistence of bacteria and bacterial predators. Other than phages, this biofilm mode-of-life also permits bacteria to coexist with other predators such as the obligate predatory bacterium *Bdellovibrio* spp. (340). The study of phage-bacteria dynamics, while complex, provides a rich tool for studying the multitude of outcomes arising from prey-predator interactions. Danger sensing is a new player in these dynamics and further exploration of bacterial danger sensing systems could contribute to a better understanding of their importance in bacterial coexistence with their predators in the environment.

5 Methods

5.1 Microbiological methods

5.1.1 Bacterial strains and growth conditions

All *Vibrio cholerae* strains used in this study are derivates of the wild-type clinical isolate O1 El Tor C6706 (341). *Escherichia coli* strains S17-λpir (342) and Top10 (Invitrogen) were used for cloning and maintaining plasmids used in the construction of genetically modified *V. cholerae* strains. Bacterial strains used for lysate preparation include *V. cholerae*, *E. coli*, *Pseudomonas aeruginosa*, *Bacillus subtilis*, and *Staphylococcus aureus*. Detailed lists of bacterial strains and plasmids used in this dissertation are listed in Table 5.1 and 5.2, respectively.

All bacterial strains (except *S. aureus*) were cultured in Luria Bertani (LB) medium at $37\,^{\circ}\mathrm{C}$ with shaking at $250\,\mathrm{RPM}$ to facilitate aeration. *S. aureus* strains were cultured in tryptic soy broth (TSB) medium at $37\,^{\circ}\mathrm{C}$ with shaking at $250\,\mathrm{RPM}$. Where required, the growth medium was supplemented with antibiotics of the following concentrations: gentamicin ($30\,\mu\mathrm{g\,mL^{-1}}$), ampicillin ($100\,\mu\mathrm{g\,mL^{-1}}$ for *E. coli* and $200\,\mu\mathrm{g\,mL^{-1}}$ for *V. cholerae*), or kanamycin ($50\,\mu\mathrm{g\,mL^{-1}}$ for *E. coli* and $100\,\mu\mathrm{g\,mL^{-1}}$ for *V. cholerae*). As *V. cholerae* is resistant to polymyxin B, this antibiotic was used at a concentration of $50\,\mu\mathrm{g\,mL^{-1}}$ (in combination with the antibiotics mentioned previously) for the selection of transformants after bacterial conjugation.

Single bacterial colonies from an LB agar plate were inoculated into $3\,\mathrm{mL}$ of fresh LB and grown with shaking overnight (approx. $16\,\mathrm{h}$) at $37\,^{\circ}\mathrm{C}$. The following day, overnight cultures were mixed with glycerol (final concentration 20%) and stored at $-80\,^{\circ}\mathrm{C}$. These bacterial freezer stocks were used for subsequent inoculation of overnight cultures. For experimentation, *V. cholerae* cells from an overnight culture were diluted 1:200 in $3\,\mathrm{mL}$ of fresh LB and grown with shaking until an optical density measured at a wavelength of 600 nm (OD_{600}) of 0.4 was reached. OD_{600}=0.4 corresponds to approx. $10^8\,\mathrm{CFU\,mL^{-1}}$.

Table 5.1: Bacterial strains used in this study

Identifier	Strain Description	Reference
	***Escherichia coli* cloning strains**	
S17-1 λ*pir*	Δ*lacU169* (φ*lacZ*Δ*M15*), *recA1*, *endA1*, *hsdR17*, *thi-1*, *gyrA96*, *relA1*, λ*pir*	(342)
Top10	*mcrA* Δ(*mrr-hsdRMS-mcrBC*) φ80 *lacZ* Δ*M15* Δ*lacX74* *deoR recA1 araD139* Δ(*ara-leu*)7697 *galU galK rpsL* *endA1 nupG*	Invitrogen
KDE84	pRK600, Cm^R	Lab stock
	***Vibrio cholerae* strains**	
KDV87	Wild-type DRC-193A (O1 El Tor, Sm^R)	(343)
KDV93	Wild-type E7946 (O1 El Tor, Sm^R)	(344)
KDV101	Wild-type N16961 (O1 El Tor, Sm^R)	(345)
KDV201	Wild-type C6706 (O1 El Tor, Sm^R)	(341)
KDV207	C6706 Δ*vpsL*	(237)
KDV428	C6706 *lacZ*::P_{tac}-*sfGFP*	(183)
KDV504	C6706 pNUT844, $Gent^R$	Lab stock
KDV941	Rugose C6706 $vpvC^{W240R}$	Lab stock
KDV969	C6706 Δ*vpsL* pNUT542, $Gent^R$	Lab stock
KDV970	C6706 Δ*rbmC* pNUT542, $Gent^R$	Lab stock
KDV986	C6706 *lacZ*::P_{VN4_32}-*sfGFP*	This study
KDV992	C6706 *lacZ*::P_{VN4_32}-*sfGFP*, pNUT1475, $Gent^R$	This study
KDV1156	Wild-type A1552 (O1 El Tor, Rif^R)	(346)
KDV1160	Wild-type V52	(347)
KDV1400	C6706 Δ*rbmA* pNUT542, $Gent^R$	Lab stock
KDV1600	C6706 Δ*bap1* pNUT542, $Gent^R$	Lab stock
KDV2151	C6706 *lacZ*::P_{tac}-*sfGFP*, *rbmA*::*rbmA-6xHis*	(348)
KDV2464	C6706 Δ*trxA*	This study
KDV2489	C6706 *lacZ*::P_{tac}-*sfGFP* Δ*trxA*	This study

KDV2971	C6706 pNUT3038, Gent^R	This study
	Bacterial strains used for lysate generation	
KDE474	*Escherichia coli* wild-type AR3110	(349)
KDP43	*Pseudomonas aeruginosa* wild-type PAO1	(350)
KDP44	*Pseudomonas aeruginosa* wild-type PA14	(351)
KDB1	*Bacillus subtilis* wild-type 168	Bacillus Genetic Stock Center (BGSC, Ohio State Univ.)
KDB2	*Bacillus subtilis* wild-type NCIB 3610	Bacillus Genetic Stock Center (BGSC, Ohio State Univ.)
KDM2	*Staphylococcus aureus* RN6734	(352)
	Other bacterial strains used	
KDE1469	*Escherichia coli* AR3110 *attB*::P$_{tac}$-*sfGFP*	Lab stock
KDP39	*Pseudomonas aeruginosa* PAO1 *attB*::P$_{tac}$-*sfGFP*	Lab stock

Table 5.2: Plasmids used in this study

Identifier	Origin, Marker	Plasmid Description	Reference
pNUT144	pR6K, Amp^R, Kan^R	pKAS32 with Kan^R	(353)
pNUT480	pR6K, Amp^R, Kan^R	pKAS32 with *lacZ*:P$_{tac}$-*sfGFP*:*lacZ*	(183)
pNUT542	pSC101*, Gent^R	pSC101* with P$_{tac}$-*sfGFP*	(183)
pNUT844	p15a, Gent^R	p15a with P$_{tac}$-*sfGFP*, P$_{vpsL}$-*mRuby2*	Lab stock
pNUT1027	pSC101*, Gent^R	pNUT542 with P$_{tac}$-*sfGFP* replaced by with P$_{tac}$-*mNeonGreen*	This study
pNUT1029	pSC101*, Gent^R	pNUT542 with P$_{tac}$-*sfGFP* replaced by with P$_{tac}$-*mRuby3*	(33)
pNUT1035	pR6K, Amp^R, Kan^R	pNUT144 with *lacZ*:P$_{tac}$-*mNeonGreen*:*lacZ*	This study
pNUT1442	pR6K, Amp^R, Kan^R	pNUT144 with *lacZ*:P$_{tac}$-*TagRFP-T*:*lacZ*	This study
pNUT1475	pSC101*, Gent^R	pNUT542 with P$_{tac}$-*sfGFP* replaced by with P$_{tac}$-*TagRFP-T*	This study

pNUT2259	pR6K, Amp^R, Kan^R	pNUT144 with *trxA* (*vc0306*) flanking regions for gene deletion	This study
pNUT2828	pSC101*, Gent^R	pNUT542 with P$_{tac}$-*sfGFP* replaced by P$_{tac}$-*mRuby3*, *bc3-5-sfGFP*	This study
pNUT3038	pSC101*, Gent^R	pNUT542 with P$_{tac}$-*sfGFP* replaced by P$_{tac}$-*mRuby3*, *bc3-5-sfGFP(LAA degradation tag)*	This study

5.1.2 Determination of bacterial numbers

The number of viable bacteria was measured before and after phage treatment or sonication to quantify the number of lysed cells. Additionally, to track cell numbers during phage exposure, bacteria were enumerated by serial dilution and plating. Bacterial cultures were ten-fold serially diluted (up to 10^{-8}) in LB. $100\,\mu L$ of the diluted bacterial culture was plated on LB agar plates using glass beads. Alternatively, bacterial counts were also determined by plating $10\,\mu L$ drops of various dilutions of the bacterial culture on different sections of an LB agar plate. The plates were incubated overnight at $37\,°C$. The following day, the colony forming units per mL ($CFU\,mL^{-1}$) were enumerated.

5.1.3 Amplification and purification of Vibriophage N4

V. cholerae O1 El Tor C6706 (KDV201) was used as the propagating strain for the Vibriophage N4 (ATCC 51352-B1). To test for compatibility between bacterial host and phage, lyophilised Vibriophage N4 was suspended in PBS and spotted on a lawn of *V. cholerae* O1 El Tor C6706 cells on an LB agar plate. The plate was incubated at $37\,°C$ overnight. The following day, the formation of a clear zone (plaque) on the bacterial lawn indicated successful phage infection. Phages were scraped from this plaque and suspended in LB. This phage suspension was mixed with glycerol (final concentration 40%) and stored at $-80\,°C$. This phage freezer stock was subsequently used for phage amplification by inoculation in bacterial culture.

Phage lysates were prepared as described previously (91). Briefly, cultures of *V. cholerae* O1 El Tor C6706 were grown in LB at $37\,°C$ until OD_{600}=0.4 and infected with phages (from a phage freezer stock). Bacteria and phages were co-incubated together at $37\,°C$ with shaking at $250\,RPM$ for $1\,h$ until the culture had cleared as a result of bacterial lysis and phage propagation. The lysate was filtered using a $0.22\,\mu m$ filter (Roth) and stored at $4\,°C$ or at $-80\,°C$ for long-term (>1 week) storage. The phage titre of the lysate was approx. $10^9\,PFU\,mL^{-1}$ (as determined by a plaque assay described in 5.1.4).

For infection experiments, purified phages were used. The phage particles were purified by the method as previously described (354) with the following modifications. Briefly, a phage lysate was prepared by growing bacterial cultures in Brain-Heart Infusion (BHI) until OD_{600}=1.2 and infecting with previously prepared phage lysate at a multiplicity of infection (MOI) of 0.1.

The prepared lysate was treated with DNase I ($1\,\mu g\,mL^{-1}$) for $30\,min$ at $37\,°C$ with shaking at $250\,RPM$. NaCl ($0.5\,\mu g\,mL^{-1}$) was added and the treated lysate was stored at $4\,°C$ for $1\,h$. The lysate was filtered using a $0.22\,\mu m$ filter (Roth) and 10% (w/v) PEG-6000 (Roth) was dissolved into the filtered lysate by gentle stirring. The lysate was stored for two days at $4\,°C$ in order to facilitate precipitation of phages (seen as whitish particles at the bottom). The precipitated phages were collected by centrifugation at $8000\,RPM$ (Eppendorf) for $15\,min$ and cooled to $4\,°C$. The pellet was resuspended in $5\,mL$ and stored at $4\,°C$. Phages were purified using a CsCl density gradient column. For this, a 62.5% CsCl solution was prepared by dissolving $25\,g$ of CsCl in $15\,mL$ of dH_2O. The column was prepared using the CsCl:PBS ratios described for the T7 *E. coli* phage in the T7 Select Novagen Manual. The CsCl solution was diluted in PBS to generate CsCl solutions with lower densities (41.67%, 31.25%, 20.83%). Next, the CsCl density gradient was generated by layering solutions of decreasing density ($2\,mL$ of each) using a Pasteur pipette in a $10\,mL$ polycarbonate centrifuge tube (Beckman Coulter). At the end, the phage suspension was added as the topmost layer of the column. The assembled CsCl density gradient column was centrifuged at 100,000 x *g* at $4\,°C$ for $24\,h$. No visible band of concentrated phages was observed but the layer in which the T7 phages would have been expected was taken for further purification. A 14000 MWCO membrane was equilibrated in first in dH_2O, then in PBS for $1\,h$ each. Subsequently, the membrane was filled with $500\,\mu L$ of the extracted phages and sealed on both sides using Eppendorf tubes. The CsCl was removed from the phage solution by dialysis with PBS overnight at $4\,°C$. The following day, dialysed phages were collected from the membrane and stored at $4\,°C$. The titre of the purified phages was approx. $10^{10}\,PFU\,mL^{-1}$ (as determined by a plaque assay described in 5.1.4).

5.1.4 Determination of phage titre

Phage concentration of lysates, purified phage solutions, or bacterial cultures was enumerated by performing a plaque assay. The phage-containing liquid was ten-fold serially diluted (up to 10^{-8}) in LB. $100\,\mu L$ of the diluted phage suspension was mixed together with $200\,\mu L$ of exponentially growing *V. cholerae* O1 El Tor C6706 (OD_{600}=0.4) and pipetted into $4\,mL$ of molten top agar (0.7% LB agar). The tube containing top agar and phages were vortexed briefly and then poured onto a 1.5% LB agar plate. Once the top agar solidified, the plate was incubated overnight at $37\,°C$. The following day, the plaque forming units per mL ($PFU\,mL^{-1}$) were counted and the phage titre was calculated.

5.1.5 Phage adsorption assay

To measure the number of phages adsorbed by bacteria, unadsorbed phages in the supernatant were quantified over time by performing multiple plaque assays during phage infection. Cultures of *V. cholerae* O1 El Tor C6706 were grown in LB at $37\,°C$ until OD_{600}=0.4 and then infected with purified phages at a MOI=0.001. Bacteria and phages were co-incubated together at $37\,°C$ with shaking at $250\,RPM$. $450\,\mu L$ of the culture was sampled at 0, 4, 8, and $16\,min$ after phages were added. Each sample was placed on ice and then immediately centrifuged at 10,000 x *g* for $2\,min$. The supernatants were transferred to fresh tubes, which were also placed on ice until all samples were collected. Phage-containing supernatants were ten-fold serially diluted (up to

10^{-3}) in PBS. The phage titre in the supernatants was calculated by measuring $\mathrm{PFU\,mL^{-1}}$ by performing a plaque assay (as described in 5.1.4). A decrease in the number of phages in the supernatant demonstrated by an increase in phages adsorption into bacteria. For each experiment, measurements were averaged from three LB agar plates per bacterial strain (technical replicates), and a total of three biological replicates were performed. Phage adsorption assays to compare the interaction between Vibriophage N4 and *V. cholerae* O1 El Tor C6706 wild-type or the corresponding Δ*trxA* mutant were performed by Mads Frederik Hansen.

5.1.6 Efficiency of plating (EOP) assay

To quantify the susceptibility of a bacterial strain to phage infection, relative efficiency of plating (EOP) assays were performed. Purified phages were ten-fold serially diluted (up to 10^{-8}) in LB. $10\,\mu\mathrm{L}$ of each phage dilution was spotted onto a lawn of *V. cholerae* O1 El Tor C6706 wild-type cells or Δ*trxA* mutant cells on an LB agar plate. The plates were incubated overnight at $37\,^{\circ}\mathrm{C}$. The following day, $\mathrm{PFU\,mL^{-1}}$ were counted for each spotted phage inoculum. EOP was calculated as the ratio of plaque count to the number of virions in the given spotted phage inoculum between the wild type and the mutant. For each experiment, measurements were averaged from five phage spots per bacterial strain (technical replicates), and a total of three biological replicates were performed. EOP assays to compare the susceptibility of *V. cholerae* O1 El Tor C6706 wild-type and the corresponding Δ*trxA* mutant to Vibriophage N4 were performed by Mads Frederik Hansen.

5.1.7 Monitoring bacterial growth and phage infection

Changes in $\mathrm{OD_{600}}$ during bacterial growth and phage infection under constant shaking was monitored using a shaking incubator platereader (Spark 10M, Tecan). An overnight culture of *V. cholerae* (incubated at $37\,^{\circ}\mathrm{C}$ and grown in LB) was subcultured into fresh LB, at a dilution ratio of 1:200, and incubated at $37\,^{\circ}\mathrm{C}$ with shaking at $250\,\mathrm{RPM}$ until an $\mathrm{OD_{600}}$=0.4. The cultures were subsequently back-diluted to $\mathrm{OD_{600}}$=0.05 and inoculated into individual wells of a plastic 96-well microtitre plate (82.1581.001, Sarstedt) with a total volume of $180\,\mu\mathrm{L}$ per well. Optical density and fluorescence intensity were measure every $10\,\mathrm{min}$ for 4 - $8\,\mathrm{h}$. The plates were incubated under constant shaking ($810\,\mathrm{RPM}$) in the platereader at $37\,^{\circ}\mathrm{C}$. Wells containing only media were used as blanks. To track phage infection, $10\,\mu\mathrm{L}$ of purified phages were pipetted into $170\,\mu\mathrm{L}$ of back-diluted bacterial culture. *V. cholerae* O1 El Tor C6706 cells were grown and infected in different media such as LB, BHI, Tryptone Broth (TB), or M9. Bacteria were co-incubated with phages at a MOI of 0.1, 1 or 10 (phage titres ranging from 10^8 to $10^{10}\,\mathrm{PFU\,mL^{-1}}$). Bacteria and phages were incubated at $28\,^{\circ}\mathrm{C}$ or $37\,^{\circ}\mathrm{C}$ to test for the effect of temperature on phage infection. To test the effect of lysate or peptidoglycan exposure on bacterial growth, $10\,\mu\mathrm{L}$ of sonicated lysate (diluted in LB) or purified peptidoglycan ($300\,\mu\mathrm{g\,\mu L^{-1}}$, Sigma) was mixed with $170\,\mu\mathrm{L}$ of back-diluted bacterial culture and incubated at $37\,^{\circ}\mathrm{C}$ under shaking conditions ($810\,\mathrm{RPM}$) for $4\,\mathrm{h}$.

5.1.8 Phage resistance test

To test if phage treatment resulted in the selection of genetic resistance, *V. cholerae* O1 El Tor C6706 cells that were exposed to Vibriophage N4 in liquid culture or in microfluidic chambers were harvested and re-exposed to phages. Bacterial cells in microfluidic chambers were collected by scraping from the glass bottom and PDMS top using a razor blade, and resuspended in fresh LB. Bacterial cells infected in liquid culture were sampled after re-growth of bacteria post phage infection. In both growth conditions, it was not possible to completely separate phages from the bacteria. However, centrifugation of the bacterial culture and washing the bacterial pellet with fresh LB twice significantly reduced the number of phages in the medium. These bacteria were co-incubated with or without fresh phages to test for their susceptibility to phage infection. Change in bacterial culture density was monitored using a platereader (as described in 5.1.7). The washed and resuspended bacteria were plated on LB agar plates and incubated overnight at $37\,^{\circ}\mathrm{C}$. The following day, isolated colonies that grew in the final streak were inoculated in fresh LB and co-incubated with phages to test for their susceptibility to phage infection. Change in bacterial culture density was monitored by measuring OD_{600} using a platereader (as described in 5.1.7).

5.1.9 Rugosity test

To test if phage treatment resulted in the selection of cells that were genetically programmed to produce high quantities of biofilm matrix (rugose), a rugosity test was performed by spotting phage-exposed bacterial cells onto LB agar plates. *V. cholerae* O1 El Tor C6706 cells that were exposed to Vibriophage N4 in microfluidic chambers were harvested, streaked out on LB agar plates (as described in 5.1.8), and incubated overnight at $37\,^{\circ}\mathrm{C}$. The following day, isolated colonies that grew in the final streak were inoculated in $200\,\mu\mathrm{L}$ of fresh LB and spotted on LB agar plates, which were incubated for three days at room temperature. To retain humidity, the plates were sealed with parafilm. As controls, overnight cultures of the *V. cholerae* wild type (KDV201), Δ*vpsL* (KDV207), and *vpvC*^{W240R} (rugose, KDV941) were also spotted on LB agar plates as two negatives and a positive control, respectively. High matrix production (rugosity) in *V. cholerae* manifests in the form of wrinkled and rough-looking bacterial colonies on LB agar (248). Colony morphology of the samples were visually compared to the smooth colonies of the wild type and Δ*vpsL* strain, and the wrinkled colonies of the rugose strain.

5.1.10 Crystal violet assay

To test the biofilm formation capability of bacteria that were exposed to phages, a crystal violet assay was performed as described previously (355), with the following modifications. *V. cholerae* O1 El Tor C6706 cells cells that were exposed to Vibriophage N4 in microfluidic chambers were harvested, streaked out on LB agar plates, and incubated overnight at $37\,^{\circ}\mathrm{C}$. The following day, isolated colonies that grew in the final streak were inoculated in $180\,\mu\mathrm{L}$ of fresh LB (in a 96-well microtitre plate). As controls, the *V. cholerae* wild type (KDV201), Δ*vpsL* (KDV207), and *vpvC*^{W240R} (rugose; KDV941) strains were also inoculated into individual wells of a 96-well microtitre plate from colonies on LB agar. These strains served as two negatives and a positive

control, respectively. For each strain, bacteria from a single colony were inoculated in triplicates. The microtitre plate was incubated at $37\,°C$ with shaking ($810\,RPM$) until OD_{600}=0.4. These cultures were then diluted 1:2000 in $150\,\mu L$ of fresh LB in another 96-well microtitre plate, which was incubated for biofilm growth at room temperature for $14\,h$. After this incubation period, the culture was discarded and the wells washed to remove any unattached bacterial biomass. A 0.1% solution of crystal violet in water was used to stain the surface-attached bacterial biomass. After $15\,min$ of incubation at room temperature, the crystal violet solution was discarded and the wells washed twice in clean water to remove any excess dye. The plates were left to dry upside down overnight at room temperature. The following day, 30% acetic acid was added to each well to solubilise the crystal violet and the optical density was measured at a wavelength of 550 nm (OD_{550}) using a platereader. For each measurement, the data were averaged from three wells (technical replicates) per experiment, and three independent biological replicates were performed.

5.1.11 Preparation of sonicated lysates

Along with *V. cholerae* (KDV201), other Gram-negative and Gram-positive bacteria such as *E. coli* (KDE474), *P. aeruginosa* (KDP43), *B. subtilis* (KDB2), and *S. aureus* (KDM2) were used to create sonicated lysates (bacterial strain details are provided in Table 5.1). All bacterial cultures were grown in LB medium (except *S. aureus*, which was grown in TSB) and incubated at $37\,°C$ with shaking. Bacterial overnight cultures were diluted 1:100 in their respective fresh growth medium and grown at $37\,°C$ with shaking until OD_{600}=0.4. These cells were washed twice with equal volumes of LB and then concentrated 100x into fresh LB. Sonication was performed using an ultrasonic probe (UP200St, Heilscher) with settings of 50% capacity (0.5 s on and 0.5 s off), 80% amplitude, 1 min intervals with 1 min rest for 45 min. Viable cells were enumerated by plating on LB agar before and after sonication to determine the number of cells that were lysed (as described in 5.1.2). Lysates prepared with the above-mentioned method usually yielded $\geq 99\%$ lysis (approx. 10^{10} lysed cells mL^{-1}). After sonication, the raw lysate was centrifuged (9000 x *g* for $10\,min$ at $4\,°C$) and filtered through a $0.22\,\mu m$ filter (Roth) to remove intact bacterial cells. Bacterial lysates were stored at $-80\,°C$.

To characterise the nature of the biofilm-inducing factor, sonicated lysates (made from *V. cholerae* cells) were treated with DNase ($1\,U\,mL^{-1}$ at $37\,°C$ for $30\,min$), RNase ($1\,\mu g\,mL^{-1}$ at $37\,°C$ for $30\,min$), or proteinase K ($20\,\mu g\,mL^{-1}$ at $37\,°C$ for $60\,min$) prior to incubation with KDV428 in microfluidic chambers. To characterise the size of the biofilm-inducing factor, sonicated lysates (made from *V. cholerae* cells) were filtered through membrane filters of varying pore sizes, 3 kDa, 10 kDa, 30 kDa, 100 kDa, 300 kDa (all from Merck Millipore) prior to incubation with KDV428 in microfluidic chambers.

5.1.12 Preparation of spheroplast lysate

Spheroplasts were prepared as described by Jyot *et al.*, 1999 (356) with minor modifications. Exponentially growing cells of *V. cholerae* O1 El Tor C6706 (KDV201) at OD_{600}=0.4 (grown in LB at $37\,°C$ were harvested by centrifugation at 5000 x *g* for $5\,min$. The cell pellet was washed with equal volume of LB once and then twice with $10\,mM$ Tris-HCl (pH 8.0). Cells were resuspended in

1/5th of the initial volume of spheroplasting buffer. This buffer solution is composed of $10\,\mathrm{m\ molar}$ Tris-HCl (pH 8.0) and $10\,\mathrm{mM}$ EDTA, containing 20% (w/v) sucrose. Lysozyme (Sigma) was added at a final concentration of $1\,\mathrm{mg\,\mu L^{-1}}$, and the cells were incubated at room temperature with gentle shaking for $3\,\mathrm{h}$. Spheroplasts were pelleted down by centrifugation at 16,000 x *g* for $10\,\mathrm{min}$ and suspended in 1/100th of the initial volume of LB. This suspension was immediately sonicated (as described in subsection 5.1.11) to obtain lysate.

5.1.13 Peptidoglycan isolation

Peptidoglycan from *V. cholerae* O1 El Tor C6706 (KDV201) cells was isolated as described by Dörr *et al.*, 2014 (357) with minor modifications. *V. cholerae* cells from an overnight culture (OD_{600}=4.0) were harvested by centrifugation at 5000 x *g* for $5\,\mathrm{min}$. The cell pellet was washed with equal volume of LB once and then resuspended in 1/10th of the initial volume of PBS. Resuspended cells were added drop-wise into $10\,\mathrm{mL}$ of boiling 10% SDS (in a waterbath), while continuously stirring. This suspension was boiled for $2\text{-}3\,\mathrm{h}$ (water was replenished to prevent drying). The lysed cell suspension was centrifuged at 1.1 x 10^5 RPM for $10\,\mathrm{min}$ at $20\,^{\circ}\mathrm{C}$. The pellet was washed with ddH_2O three times. Finally, the pellet was resuspended in 1/10th of the initial volume of LB and was immediately sonicated (as described in subsection 5.1.11) to obtain a crude extract of peptidoglycan fragments.

5.1.14 Purified peptidoglycan

Purified peptidoglycan (Sigma) was weighed using a fine scale and suspended in fresh LB at a final concentration of $300\,\mathrm{\mu g\,mL^{-1}}$. As peptidoglycan is not water-soluble, this suspension was sonicated (as described in subsection 5.1.11). After sonication, undissolved peptidoglycan was precipitated by centrifugation and the supernatant was used for the experiments.

5.2 Molecular biology techniques

5.2.1 Bacterial strain construction

Plasmid construction for *V. cholerae* strain modifications was carried out using standard molecular biology techniques (358). All enzymes for cloning were purchased from New England Biolabs or Takara Bio. Chromosomal modifications in the *V. cholerae* genome were carried out by homologous recombination using the suicide vector pKAS32, harboured in *E. coli*-λpir (359). All strains used for imaging constitutively expressed a fluorescent protein under control of the *tac* promoter (with the operator *lacO* deleted) at the *lacZ* site on the *V. cholerae* chromosome. For successful chromosomal integration of the suicide vector into the *V. cholerae* genome, two 1 kb long DNA fragments flanking the genomic region of interest were inserted into the pKAS32 vector using Gibson assembly (as described in 5.2.10). All reporter constructs were cloned onto a low copy number plasmid with a pSC101* origin of replication and a gentamicin resistance cassette, harboured in *E. coli* Top10 (Invitrogen). Plasmid construction was performed using restriction enzymes (used for the phage reporter described in 5.2.2) or Gibson assembly (all other constructs). Cloned plasmids constructed in their corresponding *E. coli* strains were introduced into *V. cholerae*

by conjugation (mating with Top10 strains required a helper *E. coli* strain harbouring the conjugation plasmid pRK600). Detailed cloning strategies are described in the following sub-sections. Primers were designed using the SnapGene software (from Insightful Science; snapgene.com). Oligos used for plasmid construction are listed in Table 5.3 and were commercially synthesised by Eurofins or Sigma Aldrich. All plasmid constructs that were created were verified by basic Sanger sequencing, which was carried out by Eurofins or Microsynth SeqLab.

Table 5.3: DNA oligonucleotides used in this study for plasmid construction. Sequences are given in the 5' →3' direction.

Identifier	Sequence
KDO719	ATCTTGATCCCCTGCGCCATC
KDO1519	CAAGTAGAAGCTCGTGTGATTGC
KDO1520	CCTTTGCTCACCATAATTTATTCTCCTTCTAAGATAATTG
KDO1534	GGGGTTAATTAACACATCCTGAATTAACCCACAC
KDO1535	TTTTGCGGCCGCTAGCTCTAGCAGGCC
KDO1599	GGCTTACCCGTCTTACTGTCC
KDO1968	ATTAATATTCCGGAGTATACGTAGCCGGC
KDO1969	AGGCCTAGGATGCATATGGCGG
KDO3441	TAATGCTTGCCAGCCCGCAGGCTG
KDO3442	AGGTATTTATTTATCGTGTTATTTATACAGTTCATCCATACCACCACCC
KDO3443	GGTATGGATGAACTGTATAAATAACACGATAAATAAATACCTATTTTTGGCACAC
KDO3445	CTTTTTATTTTGCCACTAGGAGGTGGTTGATGAG
KDO3446	TGCGGGCTGGCAAGCATTA
KDO3552	CTCTGCGATCCAGAGTCGACGCATG
KDO3080	CTACGTATACTCCGGAATATTAATCGCGCTAGACGAGTAATTGAATCCAG
KDO3090	GGAGTGAAAGATGAGTGACCTGTAATGAGTCAGACCGCCAAG
KDO3091	ACAGGTCACTCATCTTTCACTCCAATGTGATTTTC
KDO3092	CATATGCATCCTAGGCCTCACGTTTTTTCTGCGGTACATCACC
KDO3688	AGGATTCCTGATTTCCACAGTTCTC
KDO3689	TTATTACGCAGCTAAAGCATAATTTTCATCATTAGCAGC
KDO3690	AATGATGAAAATTATGCTTTAGCTGCGTAATAAGCTTGCCAGC

KDO3691	GAGAACTGTGGAAATCAGGAATCCT
KDO3769	CAACCACCTCCTAGTGGC
KDO3828	CGGGTACCGCTCGAGTTAATTGAGCTCGCTTGGACTCC

5.2.2 Construction of the phage reporter system

E. coli and *V. cholerae* strains used for the construction of the fluorescent phage reporter are listed in Table 5.1 and relevant primers in Table 5.3. For the phage infection reporter, the fragment P_{VN4_32}-*mNeonGreen* was constructed. To this end, the putative Vibriophage N4 promoter controlling transcription of the gene encoding phage major capsid protein (*VN4_32*) was amplified from phage DNA (directly from the phage lysate) using primers KDO1519 and KDO1520. The gene encoding for the fluorescent protein mNeonGreen was amplified from the plasmid pNUT1035. The two fragments were fused together by overlap PCR using primers KDO1534 and KDO1535. This P_{VN4_32}-*mNeonGreen* fragment was digested with restriction enzymes NheI (Cat-No. R3131S, New England Biolabs) and PacI (Cat-No. R0547S, New England Biolabs), and ligated into a similarly digested vector pNUT480 (conditions for digestion and ligation described in 5.2.11). The constructed plasmid was transformed into *E. coli* S17, yielding strain KDE1532. The plasmid contains homologous regions up- and down-stream of *lacZ*, which flank the P_{VN4_32}-*mNeonGreen* fragment on either side. The fragment was inserted into the *V. cholerae* genome at the *lacZ* site by transforming the constructed plasmid into KDV201 by conjugation (as described in 5.2.14), yielding strain KDV986.

For the expression of constitutive fluorescence in *V. cholerae*, the plasmid pNUT1475 was constructed. This plasmid has a pSC101* vector background and the gene encoding a red fluorescent protein TagRFP-T, downstream of a promoter P_{tac} lacking the *lacO* operator. The *TagRFP-T* fragment was amplified from the plasmid pNUT1442 using primers KDO1599 and KDO719, digested with BamHI (Cat-No. R3136S, New England Biolabs) and SacI (Cat-No. R3156S, New England Biolabs), and subsequently ligated with the backbone of a similarly digested plasmid pNUT1027. The assembled plasmid was transformed into *E. coli* Top10, yielding strain KDE1475. This plasmid with the constitutive red fluorescence protein was transformed into the previously constructed phage reporter by conjugation with strains KDV986 and KDE1475, to get the final strain KDV992.

5.2.3 Construction of the c-di-GMP fluorescent reporter

To generate the c-di-GMP reporter plasmid pNUT3038, which is a riboswitch-based fluorescent read-out for intracellular c-di-GMP levels (276), the DNA sequence encoding the naturally-occurring triple-tandem riboswitches Bc3-5 were amplified from the *Bacillus thuringiensis* subsp. chinensis CT-43 chromosome using oligos KDO3443 and KDO3769. The riboswitches were cloned upstream of *sfGFP*, which was amplified from pNUT480 using oligos KDO3445 and KDO3446, and overlapped with *bc3-5* using overlap extension PCR (as described in 5.2.7). For constitutive fluorescence, P_{tac}-*mRuby3* was amplified from pNUT1029 using oligos KDO3442 and KDO3552.

The two amplified fragments were cloned into a low copy-number plasmid with a pSC101* origin of replication and a gentamicin resistance cassette, whose backbone was amplified using oligos KDO3441 and KDO3828 from pNUT1029. The plasmid, named pNUT2828, was constructed using Gibson assembly (as described in 5.2.10). In order to visualise dynamic changes in c-di-GMP, a nucleotide sequence encoding the degradation tag with amino acid sequence LAA (277) was added to the *sfGFP* fragment. The primer KDO3688 had an overhanging sequence encoding the degradation tag, which was used along with KDO3689 to amplify the P_{tac}-*mRuby3-bc3-5-sfGFP* fragment from pNUT2828. The plasmid backbone of pNUT2828 was amplified with oligos KDO3690 and KDO3691. The two fragments were joined by Gibson assembly to create the final plasmid pNUT3038. This plasmid was harboured in an *E. coli* Top10 strain and introduced into KDV201 by conjugation to create the final strain KDV2971.

5.2.4 Creating the Δ*trxA* mutant

To delete chromosomal genes in *V. cholerae*, plasmids based on the suicide vector pKAS32 were generated for the respective gene. Briefly, the vector pNUT144 (a derivative of pKAS32) was amplified using oligos KDO1968 and KDO1969. 1 kb of the upstream and downstream flanking regions of the gene of interest were amplified with suitable oligos (listed in Table 5.3) using genomic DNA of KDV201. The final plasmid comprising of the amplified vector backbone and inserts was constructed by Gibson assembly (as described in 5.2.10). This method was used to generate the plasmid pNUT2259, which was introduced into KDV428 by conjugation to create the *V. cholerae* Δ*trxA* mutant, KDV2489. The construction of the Δ*trxA* mutant was performed by Mads Frederik Hansen.

5.2.5 Isolation of bacterial genomic DNA

Genomic DNA was isolated from $1\,\mathrm{mL}$ of a *V. cholerae* overnight culture using the NucleoSpin Tissue Kit (Macherey-Nagel). The manufacturer's protocol for bacterial extraction was followed during the isolation procedure.

5.2.6 Isolation of plasmid DNA

Plasmid DNA was isolated from $3\text{-}10\,\mathrm{mL}$ of an *E. coli* overnight culture using the NucleoSpin Plasmid EasyPure Kit (Macherey-Nagel). The manufacturer's protocol was followed during the isolation procedure.

5.2.7 Amplifcation of DNA by polymerase chain reaction (PCR)

DNA fragments were amplified using Q5 DNA polymerase (M0491L, New England BioLabs) or PrimeSTAR GXL DNA polymerase (Cat-No. R050A, Takara). The former was used for amplification of small fragments (<3 kb) and the latter for amplification of larger fragments (>3 kb), such as plasmid vector backbones. The composition of the reaction mixture and conditions for PCR with Q5 DNA Polymerase are described in Table 5.4 and 5.5, respectively. The composition of the reaction mixture and conditions for PCR with PrimeSTAR GXL DNA Polymerase are described in Table 5.6 and 5.7, respectively. When plasmid DNA was used as the template in a PCR reaction,

20 U of the restriction endonuclease DpnI (R0176L, New England Biolabs) were added to the completed PCR reaction mixture. After incubation for 1 h at 37°C, PCR products were purified or gel-extracted (as described in 5.2.9).

Table 5.4: PCR reaction mixture using PrimeSTAR GXL DNA polymerase

Reagent	Concentration
Q5 Reaction Buffer	1x
Q5 High GC Enhancer	1x
Primer forward	10 µM
Primer reverse	10 µM
dNTPs	0.2 mM
Q5 DNA polymerase	1 U
DNA template	50 ng genomic or plasmid DNA
Total volume	50 µL

Table 5.5: PCR program using Q5 DNA polymerase

Step	Temperature (°C)	Time (min)	Cycle
Initial Denaturation	98	2	1
Denaturation	98	0.5	30
Annealing	X	0.5	
Elongation	72	0.5/kb	
Final Elongation	72	10	1

X = T_m of lowest primer - 2 °C

Overlap extension PCR

Overlap extension PCR was used to join individual DNA fragments prior to plasmid assembly. DNA fragments were amplified from plasmid or genomic DNA using the protocol described above. For this PCR, oligonucleotides (primers) were designed so that each amplified DNA fragment consisted of a 5' overhang that was complementary to the 3' end of the other DNA fragment to be fused with. Complementary regions were 15-20 bp long with a melting temperature between 55-60 °C. After purification (as described in 5.2.9) of the individual fragments to be fused, two consecutive PCRs followed. In the first PCR, 0.1 pM of the purified DNA fragments served as the primers that generated the fused fragment. In the second PCR, oligonucleotides that bound to the beginning and end of the fused fragment were added to facilitate fragment amplification. The raw product from the first PCR was used as a template for the second PCR. The composition of the reaction mixture and the program for overlap extension PCRs are described in Table 5.8 and 5.9, respectively.

Table 5.6: PCR reaction mixture using PrimeSTAR GXL DNA polymerase

Reagent	Concentration
GXL Reaction Buffer	1x
Primer forward	$10\,\mu M$
Primer reverse	$10\,\mu M$
dNTPs	$0.2\,mM$
GXL DNA Polymerase	$0.63\,U$
DNA template	$50\,ng$ genomic or plasmid DNA
Total volume	$50\,\mu L$

Table 5.7: PCR program using PrimeSTAR GXL DNA polymerase

Step	Temperature (°C)	Time (min)	Cycle
Initial Denaturation	98	2	1
Denaturation	98	0.5	30
Annealing	X	0.5	
Elongation	68	0.5/kb	
Final Elongation	68	10	1

X = T_m of lowest primer - $2\,°C$

Colony PCR

Colony PCRs were performed to confirm genetic modifications. For *E. coli*, a small portion of a bacterial colony grown on LB agar (supplemented with antibiotics that select for the cloned plasmid) was used to prepare DNA for the PCR. For *V. cholerae*, transformant bacterial colonies were inoculated in $100\,\mu L$ of fresh LB in a microtitre plate and incubated at $37\,°C$ for $1\,h$ with or without shaking. After this incubation period, $1\,\mu L$ of the bacterial culture was used as the source of DNA for the colony PCR. DNA fragments were amplified using DreamTaq DNA polymerase (Cat-No. EP0702, Thermo Fischer Scientific). The composition of the reaction mixture and the program for overlap extension PCRs are described in Table 5.10 and 5.11, respectively.

5.2.8 Agarose gel electrophoresis

DNA amplification was confirmed by agarose gel electrophoresis. For this, a 1% solution of agarose in 1x Tris-acetate-EDTA (TAE) buffer was made (agarose was dissolved by heating). For visualisation of DNA, $5\,\mu L$ of the PCR product was mixed with $1\,\mu L$ of a fluorescent DNA binding dye (N313-Kit, VWR) prior to electrophoresis. The Gene Ruler DNA Ladder Mix (Cat-No. SM0331, Thermo Fischer Scientific) was used as the DNA ladder. The gel was run using a power pack (BioRad) that supplied 110 V of current for 18- $30\,min$. The agarose gels were imaged under UV-light in order to visualise the size-separated DNA fragments.

Table 5.8: Overlap extension PCR reaction mixture using PrimeSTAR GXL DNA polymerase

Reagent	PCR1 Concentration	PCR2 Concentration
GXL Reaction Buffer	1x	1x
Primer forward	0.1 pM DNA fragment 1	10 µM
Primer reverse	0.1 pM DNA fragment 2	10 µM
dNTPs	0.16 mM	0.2 mM
GXL DNA Polymerase	1 U	1 U
DNA template		10 µL PCR1 product
Total volume	50 µL	50 µL

Table 5.9: Overlap extension PCR program using PrimeSTAR GXL DNA polymerase

		PCR1		PCR2	
Step	**Temperature (°C)**	**Time (min)**	**Cycle**	**Time (min)**	**Cycle**
Initial Denaturation	98	2	1	2	1
Denaturation	98	0.5	13	0.5	30
Annealing	X	0.5		0.5	
Elongation	68	0.5/kb		0.5/kb	
Final Elongation	68	5	1	5	1

X = T_m of lowest primer - 2 °C

5.2.9 Purification of PCR products

PCR products were purified directly after the reaction or after running them on an agarose gel (as described in 5.2.8). PCR products were purified using the NucleoSpin Gel and PCR Clean-up Kit according to the protocol provided by the manufacturer (Macherey-Nagel). Following purification, DNA concentration was measured using a spectrophotometer (NanoDrop One, Thermo Fischer Scientific).

5.2.10 Plasmid construction by Gibson assembly

Suicide plasmids (pKAS32 background) and fluorescence marker expression plasmids (pSC101 background) were constructed by Gibson assembly. Similar to overlap PCR, oligonucleotides (primers) were designed so that each amplified DNA fragment consisted of a 5' overhang that was complementary to the 3' end of the other DNA fragment to be fused with. Complementary regions were 20-30 bp long with a melting temperature between 52-55 °C. Individual DNA fragments were amplified from plasmid or genomic DNA using Q5 or PrimeSTAR GXL DNA polymerase (as described in 5.2.7). Amplified fragments were run on an agarose gel (as described in 5.2.8) and purified by gel-extraction (as described in 5.2.9) to ensure maximum purity. Purified fragments were mixed with the Gibson assembly reaction mixture (360) on ice for one-step isothermal DNA

Table 5.10: Colony PCR reaction mixture using DreamTaq DNA polymerase

Reagent	Concentration
DreamTaq Reaction Buffer	1x
Primer forward	$10\,\mu M$
Primer reverse	$10\,\mu M$
dNTPs	$0.2\,mM$
DreamTaq DNA Polymerase	$0.5\,U$
DNA template	bacterial cells
Total volume	$10\,\mu L$

Table 5.11: PCR program using DreamTaq DNA polymerase

Step	Temperature (°C)	Time (min)	Cycle
Initial Denaturation	95	10	1
Denaturation	95	0.5	30
Annealing	X	0.5	
Elongation	72	1/kb	
Final Elongation	72	5	1

X = T_m of lowest primer - $2\,°C$

assembly. Here, $100\,ng$ of the vector along with equimolar concentrations of the fragments to be inserted were added to $7.5\,\mu L$ of the assembly master mixture in a total volume of $10\,\mu L$. The reaction mixture was placed at $50\,°C$ for $20\,min$ with gentle shaking at $350\,RPM$. After this incubation period, the reaction mixture was cooled on ice for $5\,min$ and the assembled plasmid was immediately transformed into chemically component *E. coli* cells by heat shock (as described in 5.2.12). Constructed plasmids were stored in their respective *E. coli* strain in the form of a freezer stock, stored at $-80\,°C$ (as described in 5.1.1). To verify the cloning, the plasmid was isolated (as described in 5.2.6) and the assembled region sequenced (as described in 5.2.13).

5.2.11 Plasmid construction using restriction enzymes

Plasmids used to construct the *V. cholerae* phage reporter (KDV992) were assembled using restriction enzyme digestion followed by ligation. Plasmid vectors were isolated from their respective *E. coli* (as described in 5.2.6) and fragments to be inserted were amplified from plasmid or genomic DNA using Q5 or PrimeSTAR GXL DNA polymerase (as described in 5.2.7). Amplified fragments were PCR purified (as described in 5.2.9). $100\,ng$ of the purified fragment and $300\,ng$ of the plasmid vector were digested (in separate reactions) with $20\,U$ each of the same two restriction enzymes in 1x CutSmart Buffer (Cat-No. B7204S, New England Biolabs) in a final volume of $20\,\mu L$. The reaction was incubated in a waterbath set at $37\,°C$ for $3\,h$. The vector and insert were purified separately (as described in 5.2.9). The digested fragments were ligated using $100\,ng$

of vector and $300\,\mathrm{ng}$ of the fragment to be inserted in a reaction mixture consisting of $400\,\mathrm{U}$ of T4 DNA Ligase (Cat-No. M0202S, New England Biolabs) in a 1x T4 DNA Ligase Reaction Buffer (Cat-No. B0202S, New England Biolabs), in a final volume of $20\,\mu\mathrm{L}$. The ligation mixture was incubated at room temperature overnight. The following day, $12\,\mu\mathrm{L}$ of the ligation mixture was transformed into chemically component *E. coli* cells by heat shock (as described in 5.2.12). Constructed plasmids were stored in their respective *E. coli* strain in the form of a freezer stock, stored at $-80\,^{\circ}\mathrm{C}$ (as described in 5.1.1). To verify the cloning, the plasmid was isolated (as described in 5.2.6) and the assembled region sequenced (as described in 5.2.13).

5.2.12 Preparation of chemically component bacteria and heat shock transformation

E. coli S17-λpir or Top10 cells were grown overnight at $37\,^{\circ}\mathrm{C}$ in LB with shaking at $250\,\mathrm{RPM}$. The following day, bacteria were subcultured (1:25) in $250\,\mathrm{mL}$ of fresh LB. Cells were grown at $37\,^{\circ}\mathrm{C}$ to OD_{600}=0.5 at which point the culture was chilled on ice for $10\,\mathrm{min}$. Once cooled, the bacterial culture was centrifuged (Eppendorf) for $5\,\mathrm{min}$ at 6000 x *g* at $4\,^{\circ}\mathrm{C}$. The bacterial pellet was resuspended in $100\,\mathrm{mL}$ of ice-cold $0.1\,\mathrm{M}$ $CaCl_2$ followed by incubation for $10\,\mathrm{min}$ on ice. Subsequently, the cells were centrifuged for $5\,\mathrm{min}$ at 6000 x *g* at $4\,^{\circ}\mathrm{C}$ and then resuspended in $5\,\mathrm{mL}$ of ice-cold $0.1\,\mathrm{M}$ $CaCl_2$/15% glycerol. These chemically competent cells were aliquoted and stored at $-80\,^{\circ}\mathrm{C}$ (as described in 5.1.1).

When required, an Eppendorf tube containing $100\,\mu\mathrm{L}$ of chemically component *E. coli* S17-λpir or Top10 cells were thawed on ice. $100\,\mathrm{ng}$ of assembled plasmid DNA (or $10\,\mu\mathrm{L}$ of the Gibson assembly reaction mixture) was added to the chemically component cells by gentle mixing and incubated on ice for $30\,\mathrm{min}$. Heat shock was applied by transferring bacteria into a waterbath set to $42\,^{\circ}\mathrm{C}$ for $45\,\mathrm{s}$ followed by incubation on ice for $2\,\mathrm{min}$. $900\,\mu\mathrm{L}$ of pre-warmed super optimal broth with catabolite repression (SOC) was added to the cells and incubated at $37\,^{\circ}\mathrm{C}$ for $2\,\mathrm{h}$ with shaking at $550\,\mathrm{RPM}$. After this, the cells were plated on LB agar supplemented with the appropriate antibiotic and incubated at $37\,^{\circ}\mathrm{C}$ overnight. The following day, transformants were verified by colony PCR (as described in 5.2.7).

5.2.13 DNA Sequencing

DNA sequencing was performed by basic Sanger sequencing, which was carried out by Eurofins Genomics or Microsynth SeqLab. Samples containing purified PCR products or isolated plasmid DNA were prepared according to the manufacturer's protocol. Sequencing results were analysed using the software SnapGene (GSL Biotech LLC, Chicago).

5.2.14 Bacterial conjugation

Transformation of plasmids into *V. cholerae* were performed by conjugation with the *E. coli* strain harbouring the relevant vector. For this, overnight grown *E. coli* S17-λpir harbouring a pKAS32 or pSC101 plasmid were washed once and concentrated 10x in LB medium. In case the plasmid was harboured in an *E. coli* Top10 strain, triparental mating was performed using a helper strain *E.*

coli S17-λpir containing the conjugative plasmid pRK600. $100\,\mu L$ of overnight grown *V. cholerae* cells were mixed with $50\,\mu L$ of concentrated *E. coli* cells spotted onto an LB agar plate, which was incubated at $37\,°C$ for 4-6 h. Bacteria from the giant colony were streaked out on an LB agar plate supplemented with polymyxin B ($50\,\mu g\,mL^{-1}$) along with kanamycin ($100\,\mu g\,mL^{-1}$ and ampicillin ($200\,\mu g\,mL^{-1}$) for transformation with a pKAS32 vector or gentamicin ($30\,\mu g\,mL^{-1}$) for transformation with a pSC101 vector. Plates were incubated overnight at $37\,°C$. For transformation with a pSC101 plasmid, the colonies on the streaked out LB plate obtained the following day were the final transformants. For transformation with a pKAS32 plasmid, further steps were required as described below.

The following day, two bacterial colonies were incubated in $1\,mL$ of LB medium supplemented with streptomycin ($5\,mg\,mL^{-1}$) and grown at $37\,°C$ for $4\,h$. Subsequently, bacteria were subcultured (dilution 1:20) into fresh LB supplemented with streptomycin at $37\,°C$ for $4\,h$. Bacterial cells from the second culture were diluted to 10^{-5} in LB prior to plating on LB agar supplemented with streptomycin using glass beads, which was incubated overnight at $37\,°C$. Growth in the presence of streptomycin selected for *V. cholerae* cells that underwent a second homologous recombination step and do not harbor the pKAS32 plasmid in their genome. For chromosomal insertions at the *lacZ* site, the diluted bacterial cells were plated on LB agar supplemented with streptomycin and X-gal ($40\,\mu g\,mL^{-1}$). X-gal was used for blue/white screening of transformant colonies on the following day. Positive transformants would have an interrupted *lacZ* gene and thus, could not express the β-galactosidase enzyme that is responsible for digesting X-gal into 5-bromo-4-chloro-3-hydroxyindole, which spontaneously dimerises into 5,5'-dibromo-4,4'-dichloro-indigo (an intensely blue compound). Therefore, after overnight incubation, large colonies (that were not blue, in case of *lacZ* screening) were tested for successful cloning by colony PCR (as described in 5.2.7). Positive transformants were re-streaked on LB agar and the plates were incubated overnight at $37\,°C$. The following day, a single colony was used to create an overnight culture which was used to create a freezer stock, stored at $-80\,°C$.

5.2.15 Isolation of phage DNA and sequencing

Phage DNA was isolated from $4\,mL$ of a Vibriophage N4 lysate using the Phage DNA Isolation kit (Cat. 46800, Norgen Biotek). The manufacturer's protocol was followed during the isolation procedure. The phage lysate was treated with $80\,U$ of DNaseI and incubated at room temperature for $15\,min$ to digest bacterial DNA present in the lysate. The enzyme was then inactivated by incubation at $75\,°C$. $1\,mL$ of lysis buffer with proteinase K ($16\,\mu g\,mL^{-1}$) was added to the treated lysate and incubated at $55\,°C$ for $30\,min$ to digest the phage capsid. $1.28\,mL$ of isopropanol was added to precipitate the phage DNA. The solution was then loaded onto a spin column to bind DNA, which was washed three times with wash solution A before eluting the DNA in $50\,\mu L$ of elution buffer. The lysis buffer, wash solution A, elution buffer and spin columns are components of the kit and their composition is proprietary. The extracted phage DNA of Vibriophage N4 was sequenced and assembled by the Max Planck-Genome-centre Cologne, Germany (http://mpgc.mpipz.mpg.de/home/). Sequencing results were analysed using the software SnapGene (GSL Biotech LLC, Chicago). PHIRE (254) was used to perform *in silico* analysis

on the Vibriophage N4 genome.

5.3 Microfluidic flow chamber assays

5.3.1 Construction of microfluidic flow chambers

Microfluidic flow chambers, made from polydimethylsiloxane (PDMS) and glass coverslips, as described previously (183), were $500\,\mu m$ wide, $100\,\mu m$ high and $7\,mm$ long. PDMS pieces were bonded to glass coverslips ($0.17\,mm$ thickness) using oxygen plasma. The microfluidic design contained either 4 or 8 channels of identical dimensions, which are independent from each other. The manufacturing process of these microfluidic channels guarantees highly reproducible channel dimensions and surface properties in the channels. Each microfluidic flow channel was connected with poly-tetra-fluoro-ethylene (PTFE) tubing to a syringe. The syringes were placed on a syringe pump (pico Plus, Harvard Apparatus) which was used to maintain a constant flow rate throughout the duration of the experiments.

5.3.2 Growth of bacterial cells in microfluidic chambers

V. cholerae cells were grown in LB medium overnight at $37\,°C$ with shaking. Day cultures were prepared by diluting an overnight culture 1:200 in fresh LB and incubating at $37\,°C$ under shaking conditions for $2\,h$. When required, gentamicin ($20\,\mu g\,mL^{-1}$) was supplemented in the growth medium. *V. cholerae* cells in exponential phase (OD_{600}=0.4) were inoculated into microfluidic flow chambers. The chambers were imaged on an inverted microscope, through the coverslip at the bottom of the channels. Following inoculation of the channels, the cells were given $1\,h$ to attach to the glass surface of the channel without flow. Channels were connected to syringes containing LB supplemented with purified Vibriophage N4, bacterial lysates, isolated DNA from *V. cholerae* cells or pure peptidoglycan (Sigma) *via* PTFE tubing. A flow of $100\,\mu L\,min^{-1}$ was initiated for $45\,s$ to wash away non-adherent cells. The flow rate was then set to $0.1\,\mu L\,min^{-1}$ until the end of the experiment, and the flow chambers were incubated in a $37\,°C$ incubator. Flow rates were controlled using a high-precision syringe pump (Harvard Apparatus).

5.3.3 Confocal microscopy

Immediately after initiation of the flow of media into the microfluidic device, *V. cholerae* cells were imaged using a confocal microscope every $20\,min$ for up to $8\,h$. Imaging was performed with a Yokogawa CSU confocal spinning disk unit mounted on a Nikon Ti-E inverted microscope using a 60x oil objective with numerical aperture 1.4 (Nikon) for biofilm biomass ratio quantification or 100x oil objective with numerical aperture 1.45 (Nikon) for spatiotemporal fluorescent reporter quantification. Fluorescent proteins were excited with a 488 nm laser (sfGFP) or a 552 nm laser (mRuby). The hardware was controlled by NIS Elements (Nikon). Images were captured by an Andor iXon EMCCD camera, cooled to $-70\,°C$. Images were acquired at low excitation light intensities with $90\,ms$ exposure time while amplifying the readout using the EM-gain of the camera. A Nikon perfect focus system (PFS) hardware autofocus was used to correct focus drift.

Image stacks were acquired at a spatial resolution of $63.2\,\mathrm{nm}$ (*xy*-plane) and $0.5\,\mu\mathrm{m}$ (along the z-axis).

5.3.4 Image analysis

All image analyses were performed with the software tool BiofilmQ (36). The acquired images were denoised by convolution, floating cells were suppressed and a top-hat filter of size 25 voxels was applied. For biofilm biomass quantification, the cells were distinguished from the background by an Otsu threshold set at 0.2. Subsequently, the total biovolume and the biofilm biovolume fraction (biovolume above $3\,\mu\mathrm{m}$ divided by the total biovolume) was calculated by a custom script written by Eric Jelli in MATLAB (MathWorks Version R2016b). For spatiotemporal quantification of fluorescent reporters, a similar threshold was applied based on the constitutive fluorescent marker and the images were further segmented into cubes with a side length of approx. $1\,\mu\mathrm{m}$. Fluorescence properties (mean intensity per object of one fluorescent channel or mean intensity ratio per object of two fluorescent channels) and distance to surface (biofilm boundary) with a voxel resolution similar to the segmented cube size were calculated for each imaged position. The parameter value of all cells with the same distance to the surface were average, resulting in a value that corresponded to the value of the respective pixel in the corresponding kymographs. This was performed for all distances to the surface and all time points imaged to construct kymographs for a given fluorescent parameter.

5.4 Proteomics

5.4.1 Sample collection for LCMS run

V. cholerae cells were grown in $500\,\mathrm{mL}$ cultures in $1\,\mathrm{L}$ Erlenmeyer flasks shaking at $37\,^{\circ}\mathrm{C}$, until OD_{600}=0.4 after which $5\,\mathrm{mL}$ of phage lysate ($10^9\,\mathrm{PFU\,mL^{-1}}$) was added. Samples were collected just prior to ($0\,\mathrm{h}$) and $1\,\mathrm{h}$ after phage addition. The cells were sampled by filtering $6\,\mathrm{mL}$ of culture through a $0.45\,\mu\mathrm{m}$ Durapore membrane filter (HVLP04700, Merck-Millipore) and washing with twice the amount of PBS. As the OD_{600}=0.1 at $1\,\mathrm{h}$ after phage addition, cells were collected from $24\,\mathrm{mL}$ of culture to normalise the cell count in the samples. The cells were snap frozen in liquid nitrogen and stored at $-80\,^{\circ}\mathrm{C}$. This sampling was repeated for 8 biological replicates.

The sample preparation for LCMS was performed according to the protocol provided by Dr. Timo Glatter. Frozen samples were thawed on ice, and the membrane filters (containing sampled cells) were submerged using $1\,\mathrm{mL}$ of lysis buffer consisting of 0.5% sodium deoxycholate (SDC) detergent, $100\,\mathrm{mm}$ ammonium bicarbonate buffer and $5\,\mathrm{mm}$ tris(2-carboxyethyl)phosphine hydrochloride (TCEP) and boiling at $90\,^{\circ}\mathrm{C}$ for $30\,\mathrm{min}$. Iodoacetamide was added at a 1:40 dilution and incubated at $25\,^{\circ}\mathrm{C}$ in the dark for $30\,\mathrm{min}$. To digest the proteins into peptides, $8\,\mu\mathrm{L}$ of trypsin was added and the samples were incubated at room temperature overnight. The following day, the membranes were washed with water and trifluoroacetic acid (TFA) was added at a final concentration of 1.5% to get a white precipitate. The supernatants containing the peptides were harvested and purified by solid phase extraction. The purified peptides were solubilised in 1%

TFA in preparation for LCMS. The LCMS run and protein quantification was performed by Dr. Timo Glatter as described in (361).

5.4.2 Proteomics analysis

Raw data files from the LCMS run were processed in MaxQuant (362). The *V. cholerae* N16961 from UniProt (3,788 entries) was used to define the search space for the built-in Andromeda search engine (251, 363). The label-free quantitation (LFQ) was enabled through the MaxLFQ algorithm (364). These generated LFQ values were used for further analyses of protein expression quantification. The data generated from MaxQuant was fed into a custom MATLAB program (MathWorks version R2016b), which was written by myself for this study. Protein results with less than 3 peptide hits were removed from the analysis. A principal component analysis (PCA) was performed to visualise the replicates across the different time points. The minimum LFQ expression value, rounded down to the nearest $\log_{10}$ value, was added to all the LFQ data so as to get rid of all the null expression values. This was done so that the null values were shifted to the minimum value to ensure that the fold-change could be correctly calculated. Next, the fold-change between protein expression values of two different time points was calculated and a Student's t-test was performed, which was corrected for false discovery rate (FDR), and graphed on a Volcano Plot. Differentially expressed proteins were taken as those with a fold-change ≥ 3 and those with a FDR-adjusted *p*-value ≤ 0.05.

5.5 Transcriptomics

5.5.1 Sample collection for RNA-Seq

To collect a sufficient amount of biomass for RNA-seq, I inoculated *V. cholerae* C6706 (KDV201) cells in microfluidic flow chambers in 6 separate identical chips. After peptidoglycan or LB (untreated) exposure for $10\,\mathrm{min}$, the microfluidic device was dismantled and a mixture of 50% (v/v) PBS, 47.5% EtOH, and 2.5% (v/v) phenol was flowed through all channels to terminate transcription and translation. Subsequently, bacterial biomass was collected by scraping cells off of the glass using a clean razor blade. $1\text{-}2\,\mathrm{mL}$ of cell suspensions were collected and supernatants were removed after centrifugation. Cells from each sample were suspended in $50\,\mu\mathrm{L}$ of lysozyme buffer which consisted of TE ($10\,\mathrm{mM}$ Tris, adjusted to pH 8.0 with HCl, $1\,\mathrm{mM}$ EDTA) and $20\,\mathrm{U}\,\mu\mathrm{L}^{-1}$ Ready-lyse lysozyme (Lucigen, R1804M). Those suspensions were immediately snap-frozen in liquid nitrogen and stored at $-80\,^{\circ}\mathrm{C}$ until RNA isolation was performed. This process was performed on three separate days, to obtain a three biological replicates for each of the two conditions.

5.5.2 RNA isolation and sequencing

Total RNA was extracted using the hot SDS/hot phenol method (365) with some modifications as follows. Cells were lysed at $65\,^{\circ}\mathrm{C}$ for $2\,\mathrm{min}$ in the presence of 1% (w/v) SDS. $6\,\mu\mathrm{L}$ of $1\,\mathrm{m}$ sodium acetate (pH 5.5) and $62.5\,\mu\mathrm{L}$ of Roti-Aqua-Phenol (Carl Roth, A980) were added to the lysate and incubated at $65\,^{\circ}\mathrm{C}$ for $8\,\mathrm{min}$. The whole mixture was transferred to a phase lock gel

tube (VWR, 733-2478), followed by the addition of $62.5\,\mu L$ chloroform (Sigma, C2432). The mixture was centrifuged at 15,000 RPM for $15\,min$ at $12\,°C$. The aqueous phase was transferred to a new tube. RNA was purified from this solution using Agencourt RNAClean XP Kit (Beckman Coulter, A63987). Samples were then treated with TURBO DNase (Thermo Fisher, AM2238) and quality-checked with TapeStation 4150 (Agilent, G2992AA). 150-$180\,ng$ of total RNA was used for rRNA depletion by the 'do-it-yourself' method (366). Sequencing library preparation was carried out using NEBNext Ultra II Directional RNA Library Prep with Sample Purification Beads (NEB, E7765S). Sequencing was carried out at the Max Planck Genome Centre (Cologne, Germany) using an Illumina HiSeq3000 with 150 bp single reads.

5.5.3 Transcriptomics analysis

The read files were imported into CLC Genomics Workbench v10.1.1 (Qiagen) and mapped to the *V. cholerae* reference genome (NCBI accession numbers: NC_002505.1 and NC_002506.1) using the 'RNA-Seq Analysis' function in the CLC software with standard parameters. Reads mapping to annotated coding sequences were counted, normalised (transcript per million, TPM) and transformed ($\log_2$). Differential expression between the conditions was tested using the 'Differential Expression for RNA-seq' command in the CLC software. Genes with a read count < 10 in any condition were excluded from analysis. Genes with a fold change ≥ 2 and a FDR-adjusted *p*-value ≤ 0.05 were defined as differentially expressed. Candidate genes were categorised by keyword enrichment using information imported from UniProt (251), KEGG (252), and MicrobesOnline (253).

5.6 Data representation and statistical analysis

Line graphs were plotted using the 'boundedline.m' function (367) using MATLAB. Bar graphs were plotted using Graphpad Prism v9, which was also used for performing all statistical tests indicated in figure legends. 3D renderation of bacterial cells was performed using Paraview (368). All figures in this dissertation were assembled using Inkscape 1.0.

Appendix

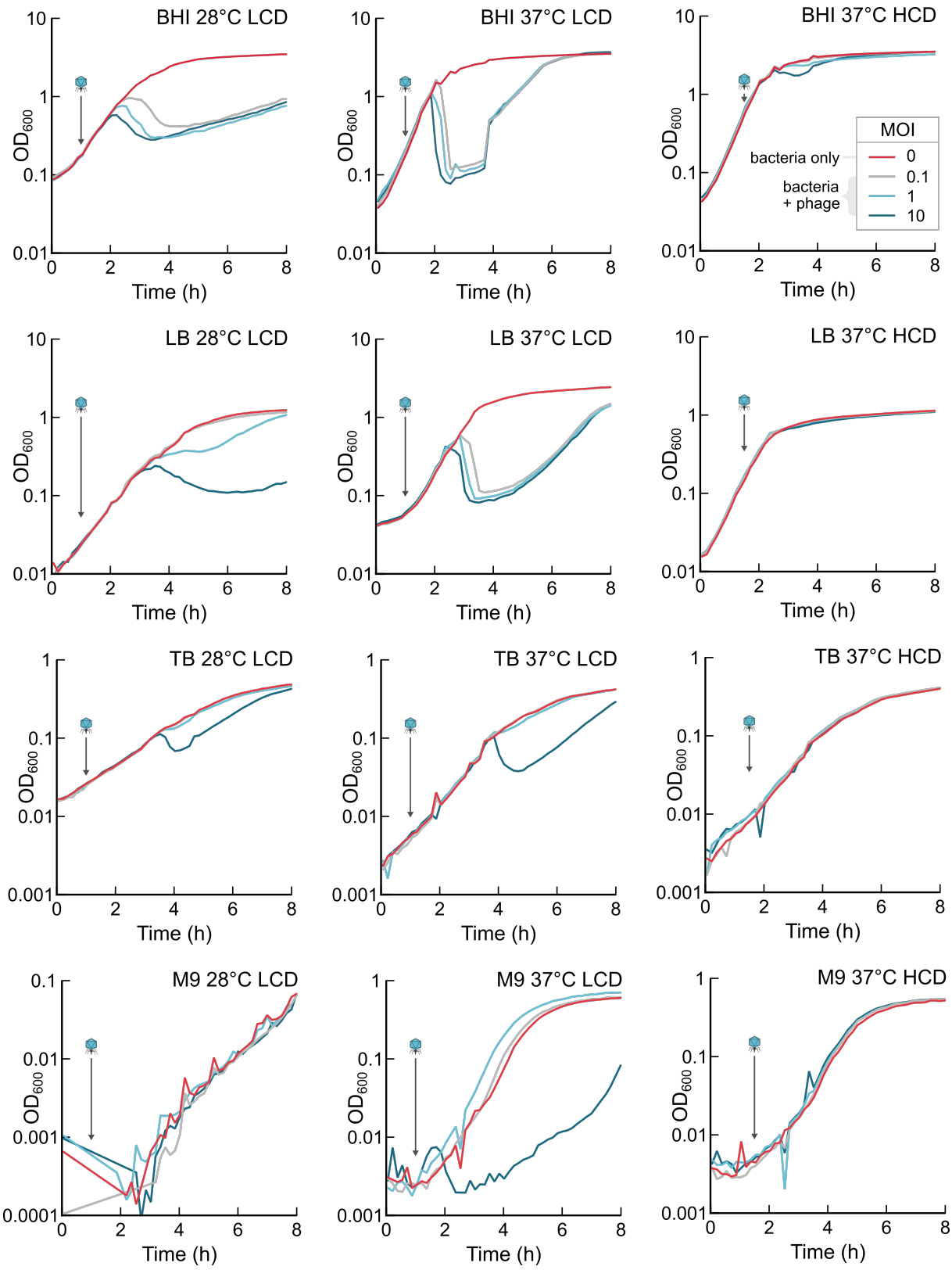

Figure A1: Vibriophage N4 infection in *V. cholerae* cells grown in different conditions. Bacteria infected in different media (top right of each graph) and cell density (LCD is low cell density and HCD is high cell density) with Vibriophage N4. The time at which the phages were added is indicated by a blue phage symbol and arrow. Phage infection was inferred by measuring bacterial culture density (OD_{600}) over $8\,h$. Coloured lines in each graph correspond to different MOIs (0, 0.1, 1, 10) as indicated in the legend. MOI of 0 refers to a bacteria only (no phage) control.

Appendix Table A1 : Differentially expressed proteins in phage-treated vs. untreated

Locus	Protein	Fold change	Function	Category
VC0672	ptsP	4.81	pts enzyme I	PTS
VC1821	frwBC	4.18	fructose pts enzyme II	PTS
VC1822	frwABC	11.83	fructose pts enzyme II	PTS
VC1826	fruA-1	4.39	fructose pts enzyme II	PTS
VC0216		3.94	methyl-accepting chemotaxis protein	chemoreceptor
VC2161	mlp24	3.74	methyl-accepting chemotaxis protein	chemoreceptor
VC2439		3.31	methyl-accepting chemotaxis protein	chemoreceptor
VC1298		4.38	methyl-accepting chemotaxis protein	chemoreceptor
VC1859		14.84	methyl-accepting chemotaxis protein	chemoreceptor
VC1898		5.38	methyl-accepting chemotaxis protein	chemoreceptor
VCA0663		4.39	methyl-accepting chemotaxis protein	chemoreceptor
VCA0773		4.34	methyl-accepting chemotaxis protein	chemoreceptor
VCA1069	mlp43	9.48	methyl-accepting chemotaxis protein	chemoreceptor
VC2006	cheV-2	3.49	RR	chemotaxis
VC2202	cheV-3	3.12	RR	chemotaxis
VC0035	srkA	3.39	stress response kinase	signalling
VC0178	capV	3.22	cGAMP protein	signalling
VC0179	dncV	3.27	cGAMP protein	signalling
VC1539		3.20		signalling
VC2453	varS	3.71	HK	signalling
VCA0522	cqsS	4.58	cai-1 sensor	signalling
VCA0523	cqsA	40.98	cai-1 synthase	signalling
VC0130	cdpA	3.39	PDE	c-di-GMP protein
VC0137	cdgJ	5.94	PDE	c-di-GMP protein
VC0653	rocS	3.35	PDE	c-di-GMP protein
VC1372		10.60	GGDEF family protein	c-di-GMP protein
VC2344	plzC	3.58	c-di-GMP binding	c-di-GMP protein
VCA0042	plzD	5.94	c-di-GMP binding protein	c-di-GMP protein
VCA0049		5.30	GGDEF family protein	c-di-GMP protein
VCA0956	vdcA cdgF	3.17	DCG	c-di-GMP protein
VC0068		8.05		transcriptional regulator
VC0161	ilvY	45.11		transcriptional regulator
VC0486		24.86		transcriptional regulator
VC0583	hapR	4.26	QS/ biofilm regulator	transcriptional regulator
VC0814		3.33		transcriptional regulator
VC1045		3.14	sigma70 factor	transcriptional regulator
VC1522		7.55		transcriptional regulator
VC1580		4.37		transcriptional regulator
VC1706	metR	97.37		transcriptional regulator
VC1741		16.06		transcriptional regulator
VC1825		7.41		transcriptional regulator
VC2007		3.16		transcriptional regulator
VC2337		6.96		transcriptional regulator
VC2692	cpxR	4.28	membrane stress	transcriptional regulator
VC2702	crbR	19.58	acetate switch	transcriptional regulator
VCA0011	malT	3.86		transcriptional regulator
VCA0056		3.56		transcriptional regulator
VCA0132	rbsR	4.07	ribose operon repressor	transcriptional regulator
VCA0182		4.11	erobic nitric oxide reductase transcriptional regul	transcriptional regulator
VCA0542		15.16		transcriptional regulator
VCA0575		6.95		transcriptional regulator
VCA0830		33.35		transcriptional regulator
VCA0964		5.54		transcriptional regulator

VCA0982		4.76		transcriptional regulator
VCA1020		3.30		transcriptional regulator
VC0665	vpsR	4.20	biofilm regulator	transcriptional regulator
VC0925	vpsI	13.04	biofilm matrix	biofilm
VC0927	cpsF vpsK	3.10	biofilm matrix	biofilm
VC0937		6.95	biofilm matrix	biofilm
VC1888	bap1	64.75	biofilm matrix	biofilm
VC0403	mshM	20.87	MSHA biogenesis	cellular appendages
VC0411	mshD	24.07	MSHA biogenesis	cellular appendages
VC0412		4.91	MSHA biogenesis	cellular appendages
VC0462	pilT	3.40	twitching motility	cellular appendages
VC2142	flaB	4.92	flagellin FlaB	cellular appendages
VC2143	flaD	3.87	flagellin FlaD	cellular appendages
VC2187	flaC	5.93	flagellin FlaC	cellular appendages
VC2188	flaA	3.31	flagellin FlaA	cellular appendages
VC2423	pilA	31.82	t4p subunit a	cellular appendages
VC2601	motX	7.90	sodium-type flagellar protein MotX	cellular appendages
VC0849	ratA	5.95	ribosome-associated toxin	secreted enzymes
VC1214	uvrC	4.11	exonuclease	secreted enzymes
VC1451	rtxA	7.66	toxin	secreted enzymes
VC2444	exeB	5.47	T2SS assembly	secreted enzymes
VC2445	exeA	4.02	T2SS assembly	secreted enzymes
VC2621	xds	9.17	extracellular nucelase	secreted enzymes
VCA0223	prtV	222.03		secreted enzymes
VC0014	recF	3.59	DNA repair	cellular processes
VC0036		3.60	FixG-related protein	cellular processes
VC0082	rmuC	3.37	DNA repair	cellular processes
VC0118		3.20	methyltransferase	cellular processes
VC0128	xerC	3.27	integrase/recombinase XerC	cellular processes
VC0148	ftsE	3.18	cell division ATP-binding protein FtsE	cellular processes
VC0149	ftsX	4.43	cell division protein FtsX	cellular processes
VC0159		3.55	RNA-binding protein	cellular processes
VC0221	mutM	7.84	DNA metabolism	cellular processes
VC0229	wavE	4.99	LPS biosynthesis	cellular processes
VC0447	djlA	3.86	DnaJ-related protein	cellular processes
VC0568	zapE	4.51	cell division	cellular processes
VC0574	petB	3.18	cytochrome B	cellular processes
VC0582	rsmI	3.73	ribosomal rna small subunit methyltransferase i	cellular processes
VC0661		4.01		cellular processes
VC0668	mutH	28.92	DNA repair	cellular processes
VC0812		14.48	helicase-related protein	cellular processes
VC0852	recN radB	34.53	DNA repair protein RecN	cellular processes
VC0990	rfaH	4.15	transcription antitermination protein	cellular processes
VC1144	clpA	3.49	clp protease	cellular processes
VC1153	tfoX	6.33	competence regulator	cellular processes
VC1386		3.85	heat shock protein 70	cellular processes
VC1407	rhlE-1	3.02	RNA helicase	cellular processes
VC1760		3.59	helicase	cellular processes
VC1847	ruvC	4.10		cellular processes
VC1912	lapB	4.01	LPS biosynthesis	cellular processes
VC1983		3.27	peptidase	cellular processes
VC1990		3.37	helicase	cellular processes
VC2017	mltG	7.51	endolytic murein transglycosylase	cellular processes
VC2061	parA	3.54	cell division	cellular processes
VC2180	hemA	3.64	glutamyl-tRNA reductase	cellular processes
VC2256	uppS	3.14	cell shape regulation	cellular processes

VC2428	zapD	7.55	cell division	cellular processes
VC2451	relA	3.25	stringent response	cellular processes
VC2463	lepA	3.00	translation	cellular processes
VC2525	lptC	4.16	LPS export system	cellular processes
VC2532		4.41	RNase adapter protein RapZ	cellular processes
VC2627		3.08	cell division, SPOR-domain	cellular processes
VC2711	recG spoV	3.80	helicase	cellular processes
VC2713	envZ	26.52	osmolarity sensor protein	cellular processes
VC2724	epsM	3.67	cholera toxin secretion protein EpsM	cellular processes
VC2734	epsC	3.01	cholera toxin secretion protein EpsM	cellular processes
VC2749	ntrC	3.95	nitrogen regulation	cellular processes
VCA0116	clpV	3.38	protease	cellular processes
VCA0198		3.52	DNA methyltransferase	cellular processes
VCA0270	dacA-2	10.23	PG biosynthesis	cellular processes
VCA1112	tmcA	4.67		cellular processes
VC0170		18.19		transporter
VC0541	cysA	3.33		transporter
VC0616		24.44		transporter
VC0617		67.89		transporter
VC0726	pstB-1	3.30	phosphate import	transporter
VC0905	metQ yaeC	3.94	lipoprotein YaeC	transporter
VC0907	metN	4.22	methionine import	transporter
VC0913	vexG	3.11	multidrug resistance protein	transporter
VC0914	vexH	4.91	multidrug resistance protein	transporter
VC0972	ompC	100.86	porin	transporter
VC0973		3.40	lipoprotein	transporter
VC0992		3.80	K ion transport	transporter
VC1092	oppB	4.85		transporter
VC1094	oppD	5.52		transporter
VC1095	oppF	5.45		transporter
VC1327	mglA	10.19		transporter
VC1673		9.06		transporter
VC1674		10.32	periplasmic linker protein	transporter
VC1675		3.35	multidrug resistance protein	transporter
VC1680	sapA	3.24		transporter
VC1683	sapD	3.01		transporter
VC1854	ompT	6.62	porin	transporter
VC2082	znuC	15.44	zinc transporter	transporter
VC2162	perM	7.72	permease	transporter
VC2215	copA	3.00	copper ion transport	transporter
VC2516	yrbB	3.80	sulphate transporter	transporter
VC2519	yrbE	3.99		transporter
VC2553		4.80		transporter
VCA0128	rbsA	17.52	ribose import	transporter
VCA0137	glpT	13.42	G3P transporter	transporter
VCA0205	dcuB	4.55	C4-dicarboxylate transporter, anaerobic	transporter
VCA0532		15.04		transporter
VCA0588		60.39		transporter
VCA0612	mscL	3.09	mechanosensitive channel	transporter
VCA0639	vexL	21.81		transporter
VCA0659		43.53		transporter
VCA0687	fbpC	19.05	iron transporter	transporter
VCA0867	ompW	24.12		transporter
VCA0977		3.39		transporter
VC0249	rfbL wbeL	3.33	rfbL protein	metabolism
VC0255		3.63	rfbT-related protein	metabolism

VC0262	galE-1	3.50	UDP-glucose 4-epimerase	metabolism
VC0348	hflX	3.12	GTP-binding protein HflX	metabolism
VC0390	metH	7.02	methionine synthase	metabolism
VC0550	oadA-1	10.07	oxaloacetate decarboxylase	metabolism
VC0786	dadA	13.38	D-amino acid dehydrogenase	metabolism
VC0788		3.52		metabolism
VC0866	mltF	3.11	murein lyase F	metabolism
VC0991	asnB	18.19	asparagine synthetase b	metabolism
VC1024	moaA	5.55	molybdenum cofactor biosynthesis protein A	metabolism
VC1040	cobA	3.19	cob(I)alamin adenosyltransferase	metabolism
VC1046	fadI hadHB	6.60	fatty acid metabolism	metabolism
VC1122	cfa	6.64	fatty acid metabolism	metabolism
VC1611	metA	4.64		metabolism
VC1717	smtA	4.60		metabolism
VC1727	glgC1	5.08		metabolism
VC1740		5.04		metabolism
VC1773	nanN	26.78		metabolism
VC1774	nanM	4.81		metabolism
VC1775	rpiR	7.01		metabolism
VC1781	nanE	20.74	n-acetylmannosamine-6-phosphate	metabolism
VC1783	nagA-2	13.76	n-acetylglucosamine-6-phosphate deacetylase	metabolism
VC1993	fadH	6.59	fatty acid metabolism	metabolism
VC2088	sdhB	3.57	TCA cycle	metabolism
VC2089	sdhA	3.33	TCA cycle	metabolism
VC2217	chb-2	4.32		metabolism
VC2332		3.39	acetyltransferase	metabolism
VC2373	gltB-1	7.20	glutamate synthase	metabolism
VC2438	glnE	3.83		metabolism
VC2616	aruD astD	16.24		metabolism
VC2617		22.44		metabolism
VC2628	aroB	3.22		metabolism
VC2646	ppc	3.91		metabolism
VC2657	frdB	3.08	TCA cycle	metabolism
VC2683	metB	8.26	cystathionine gamma-synthase	metabolism
VC2684	metL	6.32		metabolism
VC2685	metF	334.36		metabolism
VC2718	bioH	15.21	biotin biosynthesis	metabolism
VC2758	fadB	9.97	fatty acid metabolism	metabolism
VC2759	fadA	4.93	fatty acid metabolism	metabolism
VCA0208		3.11		metabolism
VCA0278	glyA-2	9.03		metabolism
VCA0657	glpD	8.94		metabolism
VCA0727	cobQ	3.46	cobyric acid synthase	metabolism
VCA0744	glpK	7.46		metabolism
VCA0747	glpA	6.69		metabolism
VCA0748	glpB	102.94		metabolism
VCA0749	glpC	36.93		metabolism
VCA0843	gapA-2	3.22	glyceraldehyde 3-phosphate dehydrogenase	metabolism
VCA0984	lldD	4.13		metabolism
VC0127		4.90		hypothetical
VC0131		5.69		hypothetical
VC0180		3.13		hypothetical
VC0204		30.96		hypothetical
VC0271		3.77		hypothetical
VC0353		5.15		hypothetical
VC0428		3.41		hypothetical

VC0429		3.90		hypothetical
VC0811		3.78		hypothetical
VC0880		6.04		hypothetical
VC0901		3.02		hypothetical
VC1197		3.36		hypothetical
VC1198		3.23		hypothetical
VC1210		22.36		hypothetical
VC1252		3.06		hypothetical
VC1291		3.97		hypothetical
VC1373		3.98		hypothetical
VC1377		3.23		hypothetical
VC1438		3.56		hypothetical
VC1606		3.05		hypothetical
VC1607		3.86		hypothetical
VC1865		70.05		hypothetical
VC1964		3.36		hypothetical
VC1965		4.48		hypothetical
VC1997		3.31		hypothetical
VC2009		26.83		hypothetical
VC2222		3.53		hypothetical
VC2334		4.28		hypothetical
VC2335		3.22		hypothetical
VC2346	smp	3.25		hypothetical
VC2497		3.81		hypothetical
VC2500		3.49		hypothetical
VC2556		26.45		hypothetical
VC2557		8.76		hypothetical
VC2610		12.63		hypothetical
VC2773		4.09		hypothetical
VCA0048		5.12		hypothetical
VCA0101		3.73		hypothetical
VCA0102		3.62		hypothetical
VCA0172		3.06		hypothetical
VCA0174		5.01		hypothetical
VCA0271		4.71		hypothetical
VCA0307		4.76		hypothetical
VCA0346		4.10		hypothetical
VCA0405		3.51		hypothetical
VCA0441		9.51		hypothetical
VCA0567	vxrC	7.64		hypothetical
VCA0628		6.09		hypothetical
VCA0790		23.71		hypothetical
VCA0793		25.82		hypothetical
VCA0922		5.84		hypothetical
VCA0958		35.70		hypothetical
VCA1072		14.99		hypothetical
VCA1085		3.02		hypothetical

Appendix Table A2 : Differentially upregulated genes in phage-treated vs. untreated

Locus	Gene	Fold Change	Function	Category
VC1820	frvA	4.65	fructose-specific enzyme IIA	PTS
VC1821	frwBC	2.2	fructose-specific enzyme IIB	PTS
VC1826	fruA-1	4.6	fructose-specific enzyme IIC	PTS
VC1319	carS	2.31	calcium-regulated sensor HK	TCS
VC1349		3.05	putative HK induced by vpsR	TCS
VC1831	cqsR	3.17	QS HK	TCS
VC2647	aphA	2.45	QS RR	TCS
VC0916	vpsU	8.98	biofilm regulator	transcriptional regulator
VC2464	rseC	2.7	sigma-E factor	transcriptional regulator
VC2466		2.35	anti-sigma-E factor	transcriptional regulator
VC2467	rpoE	2.72	sigma-E	transcriptional regulator
VCA0952	vpsT csgD	3.48	biofilm regulator	transcriptional regulator
VC0917	vpsA	19.27	biofilm matrix	biofilm
VC0918	vpsB	24.61	biofilm matrix	biofilm
VC0919	vpsC	36.31	biofilm matrix	biofilm
VC0920	vpsD	15.29	biofilm matrix	biofilm
VC0921	vpsE	15.87	biofilm matrix	biofilm
VC0922	vpsF	11.11	biofilm matrix	biofilm
VC0923		9.65	biofilm matrix	biofilm
VC0924	vpsH	4.52	biofilm matrix	biofilm
VC0925	vpsI	6.71	biofilm matrix	biofilm
VC0927	vpsK	4.66	biofilm matrix	biofilm
VC0928	rbmA	13.87	biofilm matrix	biofilm
VC0930	rbmC	7.43	biofilm matrix	biofilm
VC0934	vpsL	75.63	biofilm matrix	biofilm
VC0935	vpsM	23.86	biofilm matrix	biofilm
VC0936		15.09	biofilm matrix	biofilm
VC0937		21.63	biofilm matrix	biofilm
VC1888	bap1	4.24	biofilm matrix	biofilm
VCA0849	craA	2.87	adhesin	biofilm
VC0533	nlpD	2.28	lipoprotein with LysM domain	cellular processes
VC1454	rstA1	22.92	ctx phage production	cellular processes
VC1463	rstA2	9.55	ctx phage production	cellular processes
VC2694	sodA	2.02	superoxide dismutase, Mn	cellular processes
VC2724	epsM	2.39	cholera toxin secretion protein EpsM	cellular processes
VC2763	atpC	2.18	atp synthase	cellular processes
VCA0063	ptrB	2.83	protease II	cellular processes
VCA0644		2.62	NADH oxidase, putative	cellular processes
VC0906	metI	2.5		transporter
VC1566	varD	4.5	antibiotic efflux pump	transporter
VCA0064	hutR	4.97	iron transport	transporter
VCA0638		5.12		transporter
VCA0977		2.1		transporter
VC1042	fadL1	5.35	fatty acid metabolism	metabolism
VC1047	fadJ	3.74	fatty acid metabolism	metabolism
VC1146	grxA	2.15	glutaredoxin 1	metabolism
VC1827	manA-2 manA	6	mannose-6-phosphate isomerase	metabolism
VC2377	gltD-2 gltD	2.56	glutamate synthase	metabolism

VC2701	dsbD dipZ	2.92		metabolism
VC0438		5.62		hypothetical
VC1582		7.49		hypothetical
VC1607		3.2		hypothetical
VC2456		2.48		hypothetical
VCA0065		4.69		hypothetical
VCA0066		4.26		hypothetical
VCA0067		5.27		hypothetical
VCA0174		2.03		hypothetical
VCA0790		10.99		hypothetical
VCA0808		2.08		hypothetical
VCA1019		10.77		hypothetical

Appendix Table A3 : Differentially upregulated genes in peptidoglycan-treated vs. untreate

Locus	Gene	Fold change	Function	Category
VC_0917	vpsA	2.1	vps production operon I	biofilm matrix
VC_0918	vpsB	2.1	vps production operon I	biofilm matrix
VC_0919	vpsC	2.25	vps production operon I	biofilm matrix
VC_0920	vpsD	2.51	vps production operon I	biofilm matrix
VC_0921	vpsE	2.44	vps production operon I	biofilm matrix
VC_0922	vpsF	2.24	vps production operon I	biofilm matrix
VC_0923		2.18	vps production operon I	biofilm matrix
VC_0924	vpsH	2.21	vps production operon I	biofilm matrix
VC_0925	vpsI	2.12	vps production operon I	biofilm matrix
VC_0926	vpsJ	2.1	vps production operon I	biofilm matrix
VC_0938		2.03	vps production operon II	biofilm matrix
VC_0076	uspA	4.33	universal stress protein; defense against oxidative stress	cellular processes
VC_0510		3.47	DNA-repair protein RadC	cellular processes
VC_0706	vrp	2.71	ribosome-associated protein stationary phase	cellular processes
VC_1142	cspD	2.37	cold shock-like protein	cellular processes
VC_1290	polC	2.06	DNA polymerase III	cellular processes
VC_A0122	vasM	3.86	T6SS cluster	cellular processes
VC_0216	mlp2	2.49	methyl-accepting chemotaxis protein	chemoreceptor
VC_0282		3.96	methyl-accepting chemotaxis protein	chemoreceptor
VC_1248		9.02	methyl-accepting chemotaxis protein	chemoreceptor
VC_1298		3.24	methyl-accepting chemotaxis protein	chemoreceptor
VC_1535		2.36	methyl-accepting chemotaxis protein	chemoreceptor
VC_1868		2.31	methyl-accepting chemotaxis protein	chemoreceptor
VC_A0031		2.38	methyl-accepting chemotaxis protein	chemoreceptor
VC_A0979		4.01	methyl-accepting chemotaxis protein	chemoreceptor
VC_A1034		2.2	methyl-accepting chemotaxis protein	chemoreceptor
VC_A1069	mlp43	2.33	methyl-accepting chemotaxis protein	chemoreceptor
VC_1400		2.41	chemotaxis cluster I	chemotaxis
VC_1402	cheW	2.39	chemotaxis cluster I	chemotaxis
VC_1403		2.8	methyl-accepting chemotaxis protein; cluster I	chemotaxis
VC_A1088		2.14	methyl-accepting chemotaxis protein; cluster III	chemotaxis
VC_A1090	cheD	2.8	chemotaxis cluster III	chemotaxis
VC_A1091	cheR-3	2.63	chemotaxis cluster III	chemotaxis
VC_A1092		3.45	chemotaxis cluster III	chemotaxis
VC_A1093	cheW-2	4.92	chemotaxis cluster III	chemotaxis
VC_A1094	cheW-3	2.93	chemotaxis cluster III	chemotaxis
VC_A1095	cheA-3	4.22	chemotaxis cluster III	chemotaxis
VC_A1096	cheY-4	4.4	chemotaxis cluster III	chemotaxis
VC_1370		3.08	GGDEF domain protein	diguanylate cyclase
VC_A0720		2.06	guanylate cyclase-related protein	diguanylate cyclase
VC_A0848		2.56	GGDEF domain protein	diguanylate cyclase
VC_0025		2.8		hypothetical
VC_0038		2.27		hypothetical
VC_0180		3.57		hypothetical
VC_0181		4.1		hypothetical
VC_0182		2.31		hypothetical
VC_0183		2.31		hypothetical
VC_0508		3.01		hypothetical
VC_0509		3.31		hypothetical

VC_0569		2.22		hypothetical
VC_0884		2.51	acetyltransferase-related protein	hypothetical
VC_0957		4.71		hypothetical
VC_1035		2.76		hypothetical
VC_1066		2.01		hypothetical
VC_1116		4.26		hypothetical
VC_1322		2.25		hypothetical
VC_1323		2.02		hypothetical
VC_1324		21.92		hypothetical
VC_1326		8.46		hypothetical
VC_1333		3.56		hypothetical
VC_1334		7.92		hypothetical
VC_1466		14.41		hypothetical
VC_1472		3.01		hypothetical
VC_1510		4.08		hypothetical
VC_1514		3.16		hypothetical
VC_1518		2.88		hypothetical
VC_1539		2.04		hypothetical
VC_1645		2.9		hypothetical
VC_1772		2.7		hypothetical
VC_1804		2.5		hypothetical
VC_1933		2.62	putative oxidoreductase	hypothetical
VC_1991		7.05		hypothetical
VC_2318		2.35		hypothetical
VC_2340		2.58		hypothetical
VC_2357		2.47		hypothetical
VC_2554		2.86		hypothetical
VC_2615		7.39		hypothetical
VC_A0032		3.57		hypothetical
VC_A0078		2.48		hypothetical
VC_A0213		2.35		hypothetical
VC_A0224		5.51		hypothetical
VC_A0448		5.06		hypothetical
VC_A0465		2.22		hypothetical
VC_A0609		2.81		hypothetical
VC_A0628		2.2		hypothetical
VC_A0689		6.77		hypothetical
VC_A0834		3.49		hypothetical
VC_A0847		2.2		hypothetical
VC_A0957		2.07	malate synthase-related protein	hypothetical
VC_A0958		2.36		hypothetical
VC_A0961		2.09		hypothetical
VC_A0962		2.09		hypothetical
VC_A0963		2.15		hypothetical
VC_A0981		4.86		hypothetical
VC_A0994		2.61		hypothetical
VC_A1024		2.26		hypothetical
VC_A1054		3.11		hypothetical
VC_A1097		4.8		hypothetical
VC_0384	cysJ	4.92	sulphur metabolism	metabolism
VC_0385	cysI	4.43	sulphur metabolism	metabolism
VC_0386	cysH	3.96	sulphur metabolism	metabolism
VC_0391	lysC	3.98	aspartate kinase	metabolism
VC_0423		2.22	arginine deiminase	metabolism
VC_0432	mdh	2.09	malate dehydrogenase	metabolism
VC_0550	oadA1	2.15	oxaloacetate decarboxylase	metabolism

VC_0604	acnB	2.23	aconitate hydratase	metabolism
VC_0736	aceA	2.11	isocitrate lyase	metabolism
VC_0737	acuB	4.11	acetoin utilisation	metabolism
VC_0796	citC	5.89	citrate lyase	metabolism
VC_0797	citD	5.09	citrate lyase	metabolism
VC_0798	citE	2.57	citrate lyase	metabolism
VC_0799	citF	2.23	citrate lyase	metabolism
VC_0940	yitA	2.26	sulfate adenylyltransferase	metabolism
VC_0968	cysK	2.85	cysteine synthase A	metabolism
VC_1119		2	oxidoreductase	metabolism
VC_1120		2.14	fatty acid metabolism	metabolism
VC_1121		2.21	fatty acid metabolism	metabolism
VC_1122		2.01	fatty acid metabolism	metabolism
VC_1123		2.18	fatty acid metabolism	metabolism
VC_1124		2.19	fatty acid metabolism	metabolism
VC_1125		2.25	fatty acid metabolism	metabolism
VC_1190	purC	2	amino acid biosynthesis	metabolism
VC_1191	unfA	2.72	amino acid biosynthesis	metabolism
VC_1202	hutH	3.16	histadine metabolism	metabolism
VC_1203	hutU	3.16	histadine metabolism	metabolism
VC_1204	hutG	2.07	histadine metabolism	metabolism
VC_1205	hutI	2.08	histadine metabolism	metabolism
VC_1338	acnA	2.15	aconitate hydratase 1	metabolism
VC_1344	hppD	2.35	4-hydroxyphenylpyruvate dioxygenase	metabolism
VC_1492		2.53	arginine biosynthesis	metabolism
VC_1509	cobB	2.13	NAD-dependent deacetylase	metabolism
VC_1511	fdnI	3.9	formate dehydrogenase	metabolism
VC_1512	fdhB	4.25	formate dehydrogenase	metabolism
VC_1515		2.08	formate dehydrogenase	metabolism
VC_1516		2.64	Fe-S binding protein	metabolism
VC_1589	aldC	9.5		metabolism
VC_1590	alsS	16.77		metabolism
VC_1591		24.89		metabolism
VC_1592	acgA	2.95		metabolism
VC_1594	galM	3.06		metabolism
VC_1595	galK	3.01		metabolism
VC_1596	galT	3.36		metabolism
VC_1690		2.57	galactosidase	metabolism
VC_1704	metE	12.31		metabolism
VC_1727	glgC	3.58		metabolism
VC_1773	nanN	10.12		metabolism
VC_1774	nanM	12.94		metabolism
VC_1775	rpiR	3.18		metabolism
VC_1776	nanA	22.36		metabolism
VC_1777	siaM dctQ	30.84		metabolism
VC_1778	siaQ dctP	20.15		metabolism
VC_1779	dctP-1	30.66		metabolism
VC_1780		22.93		metabolism
VC_1781	nanE	28.04		metabolism
VC_1782	nanK	18.11		metabolism
VC_1783	nagA-2	12.63		metabolism
VC_1784	nanH	44.92		metabolism
VC_1786	radC	2.27		metabolism
VC_2084	sucD	2.92	succinate coA synthase	metabolism
VC_2085	sucC	2.85	succinate coA synthase	metabolism
VC_2086	sucB	2.06	succinate coA synthase	metabolism

VC_2089	sdhA	2.1	succinate dehydrogenase	metabolism
VC_2090	sdhD	2.04	succinate dehydrogenase	metabolism
VC_2092	gltA	2.28	citrate synthase	metabolism
VC_2341		2.16	fatty acid metabolism	metabolism
VC_2361	grcA	2.74	formate acetyl transferase-related protein	metabolism
VC_2374	gltD1	2.06	glutamate synthase	metabolism
VC_2377	gltD2	2.47	glutamate synthase	metabolism
VC_2544	fbp	2.22	fructose-1,6-bisphosphatase	metabolism
VC_2558	cysC	2.96	sulphate adenylate transferase	metabolism
VC_2559	cysN	3.86	sulphate adenylate transferase	metabolism
VC_2560	cysD	4.78	sulphate adenylate transferase	metabolism
VC_2561	cysG	5.88	sulphate adenylate transferase	metabolism
VC_2565	elaA	2.05		metabolism
VC_2616	aruD astD	6.67	succinylglutamate 5-semialdehyde dehydrogenase	metabolism
VC_2617		5.9	arginine/ornithine succinyltransferase	metabolism
VC_2618	argD	3.39		metabolism
VC_2669		2.05	5-carboxymethyl-2-hydroxymuconate delta isomerase	metabolism
VC_2738	pckA	3.52	phosphoenolpyruvate carboxykinase	metabolism
VC_A0136	glpQ	11.64	glycerophosphoryl diester phosphodiesterase	metabolism
VC_A0160	mtr	13.35	tryptophan transporter	metabolism
VC_A0161	tnaA	54.26	tryptophanase	metabolism
VC_A0269		2.23	decarboxylase	metabolism
VC_A0278	glyA2	2.43	serine hydroxymethyltransferase	metabolism
VC_A0610		2.7	sigma cross-reacting protein 27A	metabolism
VC_A0657	glpD	14.31	aerobic glycerol-3-phosphate dehydrogenase	metabolism
VC_A0688	phaC	5.27	polyhydroxyalkanoic acid synthase	metabolism
VC_A0690		5.29	acetyl-CoA acetyltransferase	metabolism
VC_A0691		4.78	acetoacetyl-CoA reductase	metabolism
VC_A0699	glgC	2.73	glucose-1-phosphate adenylyltransferase	metabolism
VC_A0744	glpK	12.56	glycerol kinase	metabolism
VC_A0747	glpA	11.22	anaerobic glycerol-3-phosphate dehydrogenase	metabolism
VC_A0748	glpB	5.97	anaerobic glycerol-3-phosphate dehydrogenase	metabolism
VC_A0749	glpC	5.77	anaerobic glycerol-3-phosphate dehydrogenase	metabolism
VC_A0798		2.06	CbbY family protein	metabolism
VC_A0827	phhB	2.2		metabolism
VC_A0828	phhA	2.49		metabolism
VC_A0829	acs-2	2.08		metabolism
VC_A0984	lldD	2.61	lactate dehydrogenase	metabolism
VC_1612	pilF	2.03	fimbrial biogenesis and twitching motility protein	motility
VC_2187	flaC	2.45	flagellin FlaC	motility
VC_1280	deaA	2.72	Chitin disaccharide deacetylase	pts system
VC_1281	celA	2.38	cellobiose-specific iib component	pts system
VC_1282	celB	2.38	cellobiose-specific iic component	pts system
VC_1283	celC	2.53	cellobiose-specific iia component	pts system
VC_1284	celF	2.29	6-phospho-beta-glucosidase	pts system
VC_1285	celR	2.07	carbohydrate deacetylase	pts system
VC_2621	xds	2.24	extracellular nuclease	secreted enzymes

VC_A0219	hlyA	6.36	haemolysin	secreted enzymes
VC_A0223	prtV	9.76	protease	secreted enzymes
VC_A0865	hapA	2.62	hemagglutinin/protease	secreted enzymes
VC_0178	capV	4.31	cGAMP-activated phospholipase	signalling
VC_0179	dncV	3.6	cGAMP synthase	signalling
VC_0533	nlpD	2.97	LysM-domain containg lipoprotein	signalling
VC_1050	rssB	2.44	CheY-like response regulator	signalling
VC_1080		3.37	histadine kinase phosphotransferase Hpt domain	signalling
VC_1081		3.77	CheY-like response regulator containing an HTH domain	signalling
VC_1082		2.59	CheY-like response regulator	signalling
VC_1083		6.06	chemotaxis protein CheC	signalling
VC_1084		4.37	histadine kinase	signalling
VC_1085		3.4	histadine kinase	signalling
VC_1086		2.84	response regulator; HapR-binding; EAL-domain	signalling
VC_1087		2.01	response regulator	signalling
VC_1156		2.58	histadine kinase regulating C4 dicarboxylate transport	signalling
VC_1157		3.66	CheY-like response regulator	signalling
VC_1314		3.23	di and tri-carboxylate transporter	signalling
VC_1315		2.68	histadine kinase	signalling
VC_1349		2.46	histadine kinase	signalling
VC_1710		2.98	EAL- domain protein; c-di-gmp binding	signalling
VC_1872		14.72	serine protein kinase PrkA	signalling
VC_1873		14.5		signalling
VC_1874		10.4		signalling
VC_A0523	cqsA	2.18	cai-1 autoinducer synthase	signalling
VC_A0719		2.21	sensor histide kinase	signalling
VC_A1086		2.17	response regulator	signalling
VC_0278	cadC	2.39	regulates lysine transport	transcriptional regulator
VC_0534	rpoS	4.51	sigma factor	transcriptional regulator
VC_0583	hapR	2.29	biofilm repressor	transcriptional regulator
VC_1153	tfoX	3.31	regulator of competence-specific genes	transcriptional regulator
VC_1455	rstR1	2.4	cryptic phage ctxphi transcriptional repressor rstr	transcriptional regulator
VC_1464	rstR2	2.46	represses expression of rstA2 (and ctxphi replication)	transcriptional regulator
VC_1465		2.88	DNA-binding domain	transcriptional regulator
VC_1588		2.06		transcriptional regulator
VC_A0542		2.7		transcriptional regulator
VC_0008		3.12	amino acid transporter	transporter
VC_0009		2.71	amino acid transporter	transporter
VC_0010		3.55	amino acid transporter	transporter
VC_0170		2.68	peptide transporter	transporter
VC_0171		4.74	peptide transporter	transporter
VC_0172		4.51	peptide transporter	transporter
VC_0173		4	peptide transporter	transporter
VC_0194	vexH	2.23	drug efflux pump	transporter
VC_0280	cadB	225.62	lysine transporter	transporter
VC_0281	cadA	402.65	lysine transporter	transporter
VC_0338		2.4	transporter	transporter
VC_0538	cysP	4.94	sulphate transporter	transporter
VC_0539	cysT	3.9	sulphate transporter	transporter
VC_0540	cysW	3.24	sulphate transporter	transporter
VC_0541	cysA	2.78	sulphate transporter	transporter

VC_0618		2.34	peptide transporter	transporter
VC_0784		2.92	sodium/alanine symporter	transporter
VC_0795	citS	3.23	citrate/sodium symporter	transporter
VC_0972	ompC	3.18	porin	transporter
VC_0973		2.6	lipoprotein	transporter
VC_1089		2.17	phosphonate transport system substrate-binding protein	transporter
VC_1091	oppA	2.58	oligotransport system	transporter
VC_1092	oppB	2.99	oligotransport system	transporter
VC_1093	oppC	3.21	oligotransport system	transporter
VC_1094	oppD	3.48	oligotransport system	transporter
VC_1095	oppF	4.19	oligotransport system	transporter
VC_1102		2.34	ABC transporter	transporter
VC_1103		2.4	ABC transporter	transporter
VC_1131		4.43	sodium antiporter	transporter
VC_1235		2.1	sodium/dicarboxylate symporter	transporter
VC_1279	opuD	2.31	bcct family transporter	transporter
VC_1325	mglB	17.31	galactoside ABC transporter	transporter
VC_1327	mglA	7.29	galactoside ABC transporter	transporter
VC_1328	mglC	6.05	galactoside ABC transporter	transporter
VC_1359		3.52	amino acid transporter	transporter
VC_1360		2.63	amino acid transporter	transporter
VC_1361		3.49	amino acid transporter	transporter
VC_1362		10.8	amino acid transporter	transporter
VC_1369		3.31	solute transporter	transporter
VC_1523		3.26	tungstate transporter	transporter
VC_1524		2.36	tungstate transporter	transporter
VC_1525		2.12	tungstate transporter	transporter
VC_1861		5.15	amino acid transporter	transporter
VC_1862		6.81	amino acid transporter	transporter
VC_1863		5.4	amino acid transporter	transporter
VC_1864		3.34	amino acid transporter	transporter
VC_2012		2.46	sodium-dependent transporter	transporter
VC_2076	feoC	2.02	iron transport	transporter
VC_2553		3.13	ABC transporter	transporter
VC_A0025		2.51		transporter
VC_A0083	emrD1	2.42	multidrug resistance protein	transporter
VC_A0127	rbsD	2.88	ribose transporter	transporter
VC_A0128	rbsA	3.02	ribose transporter	transporter
VC_A0129	rbsC	4.61	ribose transporter	transporter
VC_A0130	rbsB	17.14	ribose transporter	transporter
VC_A0131	rbsK	3.67	ribose transporter	transporter
VC_A0137	glpT	14.86	glycerol-3-phosphate transporter	transporter
VC_A0183	hmp	2.26	ferrisiderophore reductase	transporter
VC_A0684	uhpC	10.85	sugar phosphate sensor protein	transporter
VC_A0685		28.31	iron transport	transporter
VC_A0686		20.04	iron transport	transporter
VC_A0687	fbpC	11.44	iron transport	transporter
VC_A0759	artI	2.65	arginine transporter	transporter
VC_A0760	artP	2.19	arginine transporter	transporter
VC_A0867	ompW	3.2	outer membrane protein OmpW	transporter
VC_A0978		2.8	amino acid transporter	transporter
VC_A0983		2.69	lactate permease	transporter
VC_A1015	nhaD	2.69	sodium antiporter	transporter
VC_A1033		2.2	extracellular solute-binding protein	transporter
VC_0829	tcpB	2.8	toxin co-regulated pilus biosynthesis	virulence

VC_0830	tcpQ	2.06	toxin co-regulated pilus biosynthesis	virulence
VC_0831	tcpC	2.15	toxin co-regulated pilus biosynthesis	virulence
VC_0832	tcpR	2.84	toxin co-regulated pilus biosynthesis	virulence
VC_0833	tcpD	2.24	toxin co-regulated pilus biosynthesis	virulence
VC_0834	tcpS	2.62	toxin co-regulated pilus biosynthesis	virulence
VC_0835	tcpT	2.29	toxin co-regulated pilus biosynthesis	virulence
VC_0837	tcpF	2.06	toxin co-regulated pilus biosynthesis	virulence
VC_A0880	makD	8.39	motility associated killing	virulence
VC_A0881	makC	8.89	motility associated killing	virulence
VC_A0882	makB	2.63	motility associated killing	virulence
VC_A0883	makA	5.26	motility associated killing	virulence

Bibliography

[1] W. B. Whitman, D. C. Coleman, and W. J. Wiebe, "Prokaryotes: the unseen majority," *Proceedings of the National Academy of Sciences of the United States of America* **95**, pp. 6578–6583, Jun 1998.

[2] S. Louca, F. Mazel, M. Doebeli, and L. W. Parfrey, "A census-based estimate of Earth's bacterial and archaeal diversity," *PLOS Biology* **17**, p. e3000106, Feb 2019.

[3] J. A. Fuhrman, "Marine viruses and their biogeochemical and ecological effects," *Nature* **399**(6736), pp. 541–548, 1999.

[4] C. B. Cunha and B. A. Cunha, "Impact of plague on human history.," *Infectious disease clinics of North America* **20**, pp. 253–72, viii, Jun 2006.

[5] R. Sender, S. Fuchs, and R. Milo, "Revised Estimates for the Number of Human and Bacteria Cells in the Body," *PLOS Biology* **14**, p. e1002533, Aug 2016.

[6] A. B. Shreiner, J. Y. Kao, and V. B. Young, "The gut microbiome in health and in disease," *Current opinion in gastroenterology* **31**, pp. 69–75, Jan 2015.

[7] Y. Fan and O. Pedersen, "Gut microbiota in human metabolic health and disease," *Nature Reviews Microbiology* **19**(1), pp. 55–71, 2021.

[8] K. V.-A. Johnson, "Gut microbiome composition and diversity are related to human personality traits," *Human Microbiome Journal* **15**, p. 100069, 2020.

[9] R. Koch, "Die Ätiologie der Milzbrand-Krankheit, begründet auf die Entwicklungsgeschichte des Bacillus Anthracis," Robert Koch-Institut, 1876.

[10] C. D. Nadell, J. B. Xavier, and K. R. Foster, "The sociobiology of biofilms," *FEMS Microbiology Reviews* **33**, pp. 206–224, Jan 2009.

[11] D. Claessen, D. E. Rozen, O. P. Kuipers, L. Søgaard-Andersen, and G. P. van Wezel, "Bacterial solutions to multicellularity: a tale of biofilms, filaments and fruiting bodies," *Nature Reviews Microbiology* **12**(2), pp. 115–124, 2014.

[12] S. K. Desai and L. J. Kenney, "Switching Lifestyles Is an in vivo Adaptive Strategy of Bacterial Pathogens," *Frontiers in Cellular and Infection Microbiology* **9**(December), pp. 1–9, 2019.

[13] I. W. Sutherland, "The biofilm matrix–an immobilized but dynamic microbial environment.," *Trends in microbiology* **9**, pp. 222–227, May 2001.

[14] R. Holliday, P. M. Preshaw, L. Bowen, and N. S. Jakubovics, "The ultrastructure of subgingival dental plaque, revealed by high-resolution field emission scanning electron microscopy," *BDJ Open* **1**(1), p. 15003, 2015.

[15] L. Hall-Stoodley, J. W. Costerton, and P. Stoodley, "Bacterial biofilms: from the natural environment to infectious diseases.," *Nature reviews. Microbiology* **2**, pp. 95–108, Feb 2004.

[16] H.-C. Flemming and S. Wuertz, "Bacteria and archaea on Earth and their abundance in biofilms," *Nature Reviews Microbiology* **17**, pp. 247–260, Apr 2019.

[17] J. L. Macalady, D. S. Jones, and E. H. Lyon, "Extremely acidic, pendulous cave wall biofilms from the Frasassi cave system, Italy," *Environmental microbiology* **9**, pp. 1402–1414, Jun 2007.

[18] M. Schmidt, A. Priemé, and P. Stougaard, "Bacterial diversity in permanently cold and alkaline ikaite columns from Greenland," *Extremophiles* **10**(6), pp. 551–562, 2006.

[19] C. D. Taylor, C. O. Wirsen, and F. Gaill, "Rapid microbial production of filamentous sulfur mats at hydrothermal vents," *Applied and environmental microbiology* **65**, pp. 2253–2255, May 1999.

[20] B. Rasmussen, "Filamentous microfossils in a 3,235-million-year-old volcanogenic massive sulphide deposit.," *Nature* **405**, pp. 676–679, Jun 2000.

[21] S. M. Boomer, K. L. Noll, G. G. Geesey, and B. E. Dutton, "Formation of multilayered photosynthetic biofilms in an alkaline thermal spring in Yellowstone National Park, Wyoming.," *Applied and environmental microbiology* **75**, pp. 2464–2475, Apr 2009.

[22] J. C. Nickel, I. Ruseska, J. B. Wright, and J. W. Costerton, "Tobramycin resistance of Pseudomonas aeruginosa cells growing as a biofilm on urinary catheter material.," *Antimicrobial agents and chemotherapy* **27**, pp. 619–624, Apr 1985.

[23] E. Y. Trizna, M. N. Yarullina, D. R. Baidamshina, A. V. Mironova, F. S. Akhatova, E. V. Rozhina, R. F. Fakhrullin, A. M. Khabibrakhmanova, A. R. Kurbangalieva, M. I. Bogachev, and A. R. Kayumov, "Bidirectional alterations in antibiotics susceptibility in Staphylococcus aureus—Pseudomonas aeruginosa dual-species biofilm," *Scientific Reports* **10**(1), p. 14849, 2020.

[24] H.-C. Flemming, T. R. Neu, and D. J. Wozniak, "The EPS matrix: the "house of biofilm cells"," *Journal of bacteriology* **189**, pp. 7945–7947, Nov 2007.

[25] E. Z. Ron, "Bacterial Stress Response BT - The Prokaryotes: Prokaryotic Physiology and Biochemistry," pp. 589–603, Springer Berlin Heidelberg, Berlin, Heidelberg, 2013.

[26] J. L. Baker, R. C. Faustoferri, and R. G. J. Quivey, "Acid-adaptive mechanisms of Streptococcus mutans-the more we know, the more we don't.," *Molecular oral microbiology* **32**, pp. 107–117, Apr 2017.

[27] W.-S. Chang, M. van de Mortel, L. Nielsen, G. Nino de Guzman, X. Li, and L. J. Halverson, "Alginate production by Pseudomonas putida creates a hydrated microenvironment and contributes to biofilm architecture and stress tolerance under water-limiting conditions.," *Journal of bacteriology* **189**, pp. 8290–8299, Nov 2007.

[28] E. Roilides, M. Simitsopoulou, A. Katragkou, and T. J. Walsh, "How Biofilms Evade Host Defenses.," *Microbiology spectrum* **3**, Jun 2015.

[29] O. Ciofu and T. Tolker-Nielsen, "Tolerance and Resistance of Pseudomonas aeruginosa Biofilms to Antimicrobial Agents-How P. aeruginosa Can Escape Antibiotics.," *Frontiers in microbiology* **10**, p. 913, 2019.

[30] S. Schlafer and R. L. Meyer, "Confocal microscopy imaging of the biofilm matrix.," *Journal of microbiological methods* **138**, pp. 50–59, Jul 2017.

[31] M. Klausen, A. Heydorn, P. Ragas, L. Lambertsen, A. Aaes-Jørgensen, S. Molin, and T. Tolker-Nielsen, "Biofilm formation by Pseudomonas aeruginosa wild type, flagella and type IV pili mutants," *Molecular Microbiology* **48**, pp. 1511–1524, May 2003.

[32] F. Díaz-Pascual, R. Hartmann, M. Lempp, L. Vidakovic, B. Song, H. Jeckel, K. M. Thormann, F. H. Yildiz, J. Dunkel, H. Link, C. D. Nadell, and K. Drescher, "Breakdown of Vibrio cholerae biofilm architecture induced by antibiotics disrupts community barrier function," *Nature Microbiology* **4**(12), pp. 2136–2145, 2019.

[33] R. Hartmann, P. K. Singh, P. Pearce, R. Mok, B. Song, F. Díaz-Pascual, J. Dunkel, and K. Drescher, "Emergence of three-dimensional order and structure in growing biofilms," *Nature Physics* **15**(3), pp. 251–256, 2019.

[34] T. R. Neu and J. R. Lawrence, "Innovative techniques, sensors, and approaches for imaging biofilms at different scales.," *Trends in microbiology* **23**, pp. 233–242, Apr 2015.

[35] J. Jonkman, C. M. Brown, G. D. Wright, K. I. Anderson, and A. J. North, "Tutorial: guidance for quantitative confocal microscopy," *Nature Protocols* **15**(5), pp. 1585–1611, 2020.

[36] R. Hartmann, H. Jeckel, E. Jelli, P. K. Singh, S. Vaidya, M. Bayer, D. K. Rode, L. Vidakovic, F. Díaz-Pascual, J. C. Fong, A. Dragoš, O. Lamprecht, J. G. Thöming, N. Netter, S. Häussler, C. D. Nadell, V. Sourjik, Á. T. Kovács, F. H. Yildiz, and K. Drescher, "Quantitative image analysis of microbial communities with BiofilmQ," *Nature Microbiology* **6**(2), pp. 151–156, 2021.

[37] G. O'Toole, H. B. Kaplan, and R. Kolter, "Biofilm Formation as Microbial Development," *Annual Review of Microbiology* **54**, pp. 49–79, Oct 2000.

[38] C. R. Armbruster and M. R. Parsek, "New insight into the early stages of biofilm formation," *Proceedings of the National Academy of Sciences* **115**, pp. 4317 LP – 4319, Apr 2018.

[39] K. A. Floyd, C. K. Lee, W. Xian, M. Nametalla, A. Valentine, B. Crair, S. Zhu, H. Q. Hughes, J. L. Chlebek, D. C. Wu, J. Hwan Park, A. M. Farhat, C. J. Lomba, C. K. Ellison, Y. V. Brun,

J. Campos-Gomez, A. B. Dalia, J. Liu, N. Biais, G. C. L. Wong, and F. H. Yildiz, "c-di-GMP modulates type IV MSHA pilus retraction and surface attachment in Vibrio cholerae," *Nature Communications* **11**(1), p. 1549, 2020.

[40] R. Belas, "Biofilms, flagella, and mechanosensing of surfaces by bacteria.," *Trends in microbiology* **22**, pp. 517–27, Sep 2014.

[41] J. J. Schuster and G. H. Markx, "Biofilm Architecture BT - Productive Biofilms," pp. 77–96, Springer International Publishing, Cham, 2014.

[42] K. P. Rumbaugh and K. Sauer, "Biofilm dispersion," *Nature Reviews Microbiology* **18**(10), pp. 571–586, 2020.

[43] D. McDougald, S. A. Rice, N. Barraud, P. D. Steinberg, and S. Kjelleberg, "Should we stay or should we go: mechanisms and ecological consequences for biofilm dispersal.," *Nature reviews. Microbiology* **10**, pp. 39–50, Nov 2011.

[44] M. Alam, M. Sultana, G. B. Nair, R. B. Sack, D. A. Sack, A. K. Siddique, A. Ali, A. Huq, and R. R. Colwell, "Toxigenic Vibrio cholerae in the Aquatic Environment of Mathbaria, Bangladesh," *Applied and Environmental Microbiology* **72**, pp. 2849–2855, Apr 2006.

[45] R. Tamayo, B. Patimalla, and A. Camilli, "Growth in a Biofilm Induces a Hyperinfectious Phenotype in Vibrio cholerae," *Infection and Immunity* **78**, pp. 3560–3569, Aug 2010.

[46] J. G. Conner, J. K. Teschler, C. J. Jones, and F. H. Yildiz, "Staying Alive: Vibrio cholerae's Cycle of Environmental Survival, Transmission, and Dissemination," in *Virulence Mechanisms of Bacterial Pathogens, Fifth Edition*, **4**(2), pp. 593–633, American Society of Microbiology, 2016.

[47] S. M. Faruque, K. Biswas, S. M. N. Udden, Q. S. Ahmad, D. A. Sack, G. B. Nair, and J. J. Mekalanos, "Transmissibility of cholera: in vivo-formed biofilms and their relationship to infectivity and persistence in the environment.," *Proceedings of the National Academy of Sciences of the United States of America* **103**, pp. 6350–5, Apr 2006.

[48] A. T. Nielsen, N. A. Dolganov, T. Rasmussen, G. Otto, M. C. Miller, S. A. Felt, S. Torreilles, and G. K. Schoolnik, "A Bistable Switch and Anatomical Site Control Vibrio cholerae Virulence Gene Expression in the Intestine," *PLoS Pathogens* **6**, p. e1001102, Sep 2010.

[49] A. S. Utada, R. R. Bennett, J. C. N. Fong, M. L. Gibiansky, F. H. Yildiz, R. Golestanian, and G. C. L. Wong, "Vibrio cholerae use pili and flagella synergistically to effect motility switching and conditional surface attachment," *Nature Communications* **5**(1), p. 4913, 2014.

[50] V. Berk, J. C. N. Fong, G. T. Dempsey, O. N. Develioglu, X. Zhuang, J. Liphardt, F. H. Yildiz, and S. Chu, "Molecular Architecture and Assembly Principles of Vibrio cholerae Biofilms," *Science* **337**(6091), 2012.

[51] F. Yildiz, J. Fong, I. Sadovskaya, T. Grard, and E. Vinogradov, "Structural Characterization of the Extracellular Polysaccharide from Vibrio cholerae O1 El-Tor," *PLOS ONE* **9**, p. e86751, Jan 2014.

[52] J. K. Teschler, D. Zamorano-Sánchez, A. S. Utada, C. J. A. Warner, G. C. L. Wong, R. G. Linington, and F. H. Yildiz, "Living in the matrix: assembly and control of Vibrio cholerae biofilms.," *Nature reviews. Microbiology* **13**, pp. 255–268, May 2015.

[53] J. C. N. Fong, K. A. Syed, K. E. Klose, and F. H. Yildiz, "Role of Vibrio polysaccharide (vps) genes in VPS production, biofilm formation and Vibrio cholerae pathogenesis," *Microbiology* **156**, pp. 2757–2769, Sep 2010.

[54] L. Houot, S. Chang, B. S. Pickering, C. Absalon, and P. I. Watnick, "The phosphoenolpyruvate phosphotransferase system regulates Vibrio cholerae biofilm formation through multiple independent pathways.," *Journal of bacteriology* **192**, pp. 3055–67, Jun 2010.

[55] A. D. Tischler and A. Camilli, "Cyclic diguanylate (c-di-GMP) regulates Vibrio cholerae biofilm formation," *Molecular Microbiology* **53**, pp. 857–869, Jun 2004.

[56] W. Liang, A. Pascual-Montano, A. J. Silva, and J. A. Benitez, "The cyclic AMP receptor protein modulates quorum sensing, motility and multiple genes that affect intestinal colonization in Vibrio cholerae," *Microbiology* **153**, pp. 2964–2975, Sep 2007.

[57] H. He, J. N. Cooper, A. Mishra, and D. M. Raskin, "Stringent Response Regulation of Biofilm Formation in Vibrio cholerae," *Journal of Bacteriology* **194**, pp. 2962–2972, Jun 2012.

[58] R. C. Charles and E. T. Ryan, "Cholera in the 21st century," *Current Opinion in Infectious Diseases* **24**, pp. 472–477, Oct 2011.

[59] P. A. Blake, "Endemic Cholera in Australia and the United States," in *Vibrio cholerae and Cholera*, pp. 309–319, American Society of Microbiology, Jan 1994.

[60] D. Barua, "History of Cholera," in *Cholera*, pp. 1–36, Springer US, Boston, MA, 1992.

[61] F. Pacini, "Osservazioni microscopiche e deduzioni patologiche sul cholera asiatico - Filippo Pacini - Google Books," *Gazzetta Medica Italiana* , 1854.

[62] J. Snow, *On the mode of communication of cholera*, 1855.

[63] D. Hu, B. Liu, L. Feng, P. Ding, X. Guo, M. Wang, B. Cao, P. R. Reeves, and L. Wang, "Origins of the current seventh cholera pandemic.," *Proceedings of the National Academy of Sciences of the United States of America* **113**, pp. E7730–E7739, Nov 2016.

[64] A. K. Mukhopadhyay, Y. Takeda, and G. Balakrish Nair, "Cholera Outbreaks in the El Tor Biotype Era and the Impact of the New El Tor Variants," in *Current topics in microbiology and immunology*, **379**, pp. 17–47, 2014.

[65] J. B. Kaper, J. G. Morris, and M. M. Levine, "Cholera.," *Clinical microbiology reviews* **8**, pp. 48–86, Jan 1995.

[66] A. S. Faruque, G. J. Fuchs, and M. J. Albert, "Changing epidemiology of cholera due to Vibrio cholerae O1 and O139 Bengal in Dhaka, Bangladesh.," *Epidemiology and infection* **116**, pp. 275–8, Jun 1996.

[67] M. Halder, S. Mookerjee, P. Batabyal, and A. Palit, "Environmental Vibrio cholerae non O1/ non O139 from the Gangetic delta: a diarrhoeal disease purview," *International Journal of Environmental Health Research* , pp. 1–11, Jun 2017.

[68] M. Ali, A. R. Nelson, A. L. Lopez, and D. A. Sack, "Updated global burden of cholera in endemic countries.," *PLoS neglected tropical diseases* **9**(6), p. e0003832, 2015.

[69] D. M. Lin, B. Koskella, and H. C. Lin, "Phage therapy: An alternative to antibiotics in the age of multi-drug resistance," *World Journal of Gastrointestinal Pharmacology and Therapeutics* **8**(3), p. 162, 2017.

[70] H. Brüssow and R. W. Hendrix, "Phage genomics: small is beautiful.," *Cell* **108**, pp. 13–16, Jan 2002.

[71] N. D. Zinder, "RNA Phages," *Annual Review of Microbiology* **19**, pp. 455–473, Oct 1965.

[72] M. R. Clokie, A. D. Millard, A. V. Letarov, and S. Heaphy, "Phages in nature.," *Bacteriophage* **1**, pp. 31–45, Jan 2011.

[73] Y. N. Chiang, J. R. Penadés, and J. Chen, "Genetic transduction by phages and chromosomal islands: The new and noncanonical," *PLOS Pathogens* **15**, p. e1007878, Aug 2019.

[74] J. Bertozzi Silva, Z. Storms, and D. Sauvageau, "Host receptors for bacteriophage adsorption," *FEMS Microbiology Letters* **363**, Feb 2016.

[75] G. P. C. Salmond and P. C. Fineran, "A century of the phage: past, present and future.," Dec 2015.

[76] H. Oliveira, C. São-José, and J. Azeredo, "Phage-derived peptidoglycan degrading enzymes: Challenges and future prospects for in vivo therapy," *Viruses* **10**(6), 2018.

[77] R. Feiner, T. Argov, L. Rabinovich, N. Sigal, I. Borovok, and A. A. Herskovits, "A new perspective on lysogeny: Prophages as active regulatory switches of bacteria," *Nature Reviews Microbiology* **13**(10), pp. 641–650, 2015.

[78] F. M. Stewart and B. R. Levin, "The population biology of bacterial viruses: Why be temperate," *Theoretical Population Biology* **26**, pp. 93–117, Aug 1984.

[79] M. Brown-Jaque, W. Calero-Cáceres, and M. Muniesa, "Transfer of antibiotic-resistance genes via phage-related mobile elements," *Plasmid* **79**, pp. 1–7, 2015.

[80] A. M. Nanda, K. Thormann, and J. Frunzke, "Impact of spontaneous prophage induction on the fitness of bacterial populations and host-microbe interactions," *Journal of Bacteriology* **197**(3), pp. 410–419, 2015.

[81] Z. Erez, I. Steinberger-Levy, M. Shamir, S. Doron, A. Stokar-Avihail, Y. Peleg, S. Melamed, A. Leavitt, A. Savidor, S. Albeck, G. Amitai, and R. Sorek, "Communication between viruses guides lysis–lysogeny decisions," *Nature* , Jan 2017.

[82] J. Maniloff, J. Das, and J. R. Christensen, "Viruses of mycoplasmas and spiroplasmas.," *Advances in virus research* **21**, pp. 343–380, 1977.

[83] S. M. Faruque and J. J. Mekalanos, "Phage-bacterial interactions in the evolution of toxigenic Vibrio cholerae.," *Virulence* **3**, pp. 556–65, Nov 2012.

[84] I. Chirakadze, A. Perets, and R. Ahmed, "Phage typing.," *Methods in molecular biology (Clifton, N.J.)* **502**, pp. 293–305, 2009.

[85] M. Demerec and U. Fano, "Bacteriophage-Resistant Mutants in Escherichia Coli," *Genetics* **30**, pp. 119–136, Mar 1945.

[86] F. W. Studier, "Bacteriophage T7.," *Science (New York, N.Y.)* **176**, pp. 367–376, Apr 1972.

[87] A. Ionel, J. A. Velázquez-Muriel, D. Luque, A. Cuervo, J. R. Castón, J. M. Valpuesta, J. Martín-Benito, and J. L. Carrascosa, "Molecular rearrangements involved in the capsid shell maturation of bacteriophage T7.," *The Journal of biological chemistry* **286**, pp. 234–242, Jan 2011.

[88] P. Kemp, L. R. Garcia, and I. J. Molineux, "Changes in bacteriophage T7 virion structure at the initiation of infection," *Virology* **340**(2), pp. 307–317, 2005.

[89] D. H. Krüger and C. Schroeder, "Bacteriophage T3 and bacteriophage T7 virus-host cell interactions," *Microbiological reviews* **45**, pp. 9–51, Mar 1981.

[90] S. Basu and S. Mukerjee, "Bacteriophage typing of Vibrio eltor.," *Experientia* **24**, pp. 299–300, Mar 1968.

[91] D. J. Chattopadhyay, B. L. Sarkar, M. Q. Ansari, B. K. Chakrabarti, M. K. Roy, A. N. Ghosh, and S. C. Pal, "New phage typing scheme for Vibrio cholerae O1 biotype El Tor strains.," *Journal of clinical microbiology* **31**, pp. 1579–85, Jun 1993.

[92] A. Sen and A. N. Ghosh, "New Vibrio cholerae O1 Biotype ElTor bacteriophages," *Virology Journal* **2**(1), p. 28, 2005.

[93] S. M. Faruque, M. J. Islam, Q. S. Ahmad, A. S. G. Faruque, D. A. Sack, G. B. Nair, and J. J. Mekalanos, "Self-limiting nature of seasonal cholera epidemics: Role of host-mediated amplification of phage," *Proceedings of the National Academy of Sciences* **102**, pp. 6119–6124, Apr 2005.

[94] A. Al-Fendi, R. H. Shueb, M. Ravichandran, and C. Y. Yean, "Isolation and characterization of lytic vibriophage against Vibrio cholerae O1 from environmental water samples in Kelantan, Malaysia," *Journal of Basic Microbiology* **54**, pp. 1036–1043, Oct 2014.

[95] A. Solís-Sánchez, U. Hernández-Chiñas, A. Navarro-Ocaña, J. De la Mora, J. Xicohtencatl-Cortes, and C. Eslava-Campos, "Genetic characterization of ØVC8 lytic phage for Vibrio cholerae O1," *Virology Journal* **13**, p. 47, Dec 2016.

[96] L. B. Gao S., Wu S., "Characteristics of typing phages of Vibrio cholerae biotype El Tor," *Fu Huo Luan Zi Liao Hui Bian* , 1984.

[97] K. D. Seed, K. L. Bodi, A. M. Kropinski, H.-W. Ackermann, S. B. Calderwood, F. Qadri, and A. Camilli, "Evidence of a dominant lineage of Vibrio cholerae-specific lytic bacteriophages shed by cholera patients over a 10-year period in Dhaka, Bangladesh.," *mBio* **2**(1), pp. e00334–10, 2011.

[98] S. C. Hardies, A. M. Comeau, P. Serwer, and C. A. Suttle, "The complete sequence of marine bacteriophage VpV262 infecting vibrio parahaemolyticus indicates that an ancestral component of a T7 viral supergroup is widespread in the marine environment.," *Virology* **310**, pp. 359–71, Jun 2003.

[99] M. Das, R. K. Nandy, T. S. Bhowmick, S. Yamasaki, A. Ghosh, G. B. Nair, and B. L. Sarkar, "Vibrio cholerae typing phage N4: genome sequence and its relatedness to T7 viral supergroup.," *Intervirology* **55**(3), pp. 185–93, 2012.

[100] W. Li, J. Zhang, Z. Chen, Q. Zhang, L. Zhang, P. Du, C. Chen, and B. Kan, "The genome of VP3, a T7-like phage used for the typing of Vibrio cholerae," *Archives of Virology* **158**, pp. 1865–1876, Sep 2013.

[101] M. S. H. Zahid, Z. Waise, M. Kamruzzaman, A. N. Ghosh, G. B. Nair, S. A. M. Khairul Bashar, J. J. Mekalanos, and S. M. Faruque, "An experimental study of phage mediated bactericidal selection & emergence of the El Tor Vibrio cholerae.," *The Indian journal of medical research* **133**, pp. 218–24, Feb 2011.

[102] M. S. H. Zahid, S. M. N. Udden, A. S. G. Faruque, S. B. Calderwood, J. J. Mekalanos, and S. M. Faruque, "Effect of Phage on the Infectivity of Vibrio cholerae and Emergence of Genetic Variants," *Infection and Immunity* **76**, pp. 5266–5273, Nov 2008.

[103] B. R. Levin, F. M. Stewart, and L. Chao, "Resource-Limited Growth, Competition, and Predation: A Model and Experimental Studies," Tech. Rep. 977, 1977.

[104] S. J. Labrie, J. E. Samson, and S. Moineau, "Bacteriophage resistance mechanisms," *Nature Reviews Microbiology* **8**(5), pp. 317–327, 2010.

[105] M. R. Tock and D. T. Dryden, "The biology of restriction and anti-restriction," *Current Opinion in Microbiology* **8**, pp. 466–472, Aug 2005.

[106] R. Barrangou, C. Fremaux, H. Deveau, M. Richards, P. Boyaval, S. Moineau, D. A. Romero, and P. Horvath, "CRISPR provides acquired resistance against viruses in prokaryotes.," *Science (New York, N.Y.)* **315**, pp. 1709–12, Mar 2007.

[107] A. M. Box, M. J. McGuffie, B. J. O'Hara, and K. D. Seed, "Functional Analysis of Bacteriophage Immunity through a Type I-E CRISPR-Cas System in Vibrio cholerae and Its Application in Bacteriophage Genome Engineering.," *Journal of bacteriology* **198**(3), pp. 578–90, 2015.

[108] D. Tan, A. Dahl, and M. Middelboe, "Vibriophages Differentially Influence Biofilm Formation by Vibrio anguillarum Strains.," *Applied and environmental microbiology* **81**, pp. 4489–97, Jul 2015.

[109] I. J. Molineux, "Host-parasite interactions: recent developments in the genetics of abortive phage infections.," *The New biologist* **3**, pp. 230–6, Mar 1991.

[110] T. R. Blower, F. L. Short, F. Rao, K. Mizuguchi, X. Y. Pei, P. C. Fineran, B. F. Luisi, and G. P. C. Salmond, "Identification and classification of bacterial Type III toxin-antitoxin systems encoded in chromosomal and plasmid genomes.," *Nucleic acids research* **40**, pp. 6158–73, Jul 2012.

[111] J. E. Samson, A. H. Magadán, M. Sabri, and S. Moineau, "Revenge of the phages: defeating bacterial defences," *Nature Reviews Microbiology* **11**, pp. 675–687, Oct 2013.

[112] A. Pawluk, A. R. Davidson, and K. L. Maxwell, "Anti-CRISPR: discovery, mechanism and function," *Nature Reviews Microbiology* **16**, pp. 12–17, Jan 2018.

[113] M. M. Doolittle, J. J. Cooney, and D. E. Caldwell, "Tracing the interaction of bacteriophage with bacterial biofilms using fluorescent and chromogenic probes.," *Journal of industrial microbiology* **16**, pp. 331–41, Jun 1996.

[114] R. Briandet, P. Lacroix-Gueu, M. Renault, S. Lecart, T. Meylheuc, E. Bidnenko, K. Steenkeste, M.-N. Bellon-Fontaine, and M.-P. Fontaine-Aupart, "Fluorescence Correlation Spectroscopy To Study Diffusion and Reaction of Bacteriophages inside Biofilms," *Applied and Environmental Microbiology* **74**, pp. 2135–2143, Apr 2008.

[115] L. Vidakovic, P. K. Singh, R. Hartmann, C. D. Nadell, and K. Drescher, "Dynamic biofilm architecture confers individual and collective mechanisms of viral protection," *Nature Microbiology* **3**, pp. 26–31, Jan 2018.

[116] L. Fernández, S. González, A. B. Campelo, B. Martínez, A. Rodríguez, and P. García, "Low-level predation by lytic phage phiIPLA-RODI promotes biofilm formation and triggers the stringent response in Staphylococcus aureus," *Scientific reports* **7**, p. 40965, Jan 2017.

[117] B. Zhang, P. Yu, Z. Wang, and P. J. J. Alvarez, "Hormetic Promotion of Biofilm Growth by Polyvalent Bacteriophages at Low Concentrations," *Environmental Science & Technology* **54**, pp. 12358–12365, Oct 2020.

[118] M. F. Hansen, S. L. Svenningsen, H. L. Røder, M. Middelboe, and M. Burmølle, "Big Impact of the Tiny: Bacteriophage–Bacteria Interactions in Biofilms," *Trends in Microbiology* **27**(9), pp. 739–752, 2019.

[119] J. J. Bull, K. A. Christensen, C. Scott, B. R. Jack, C. J. Crandall, and S. M. Krone, "Phage-Bacterial Dynamics with Spatial Structure: Self Organization around Phage Sinks Can Promote Increased Cell Densities.," *Antibiotics (Basel, Switzerland)* **7**, Jan 2018.

[120] E. L. Simmons, M. C. Bond, B. Koskella, K. Drescher, V. Bucci, and C. D. Nadell, "Biofilm Structure Promotes Coexistence of Phage-Resistant and Phage-Susceptible Bacteria," *mSystems* **5**, pp. e00877–19, Jun 2020.

[121] C. Bleuven and C. R. Landry, "Molecular and cellular bases of adaptation to a changing environment in microorganisms," *Proceedings. Biological sciences* **283**, p. 20161458, Oct 2016.

[122] J. A. Bartell, L. M. Sommer, J. A. J. Haagensen, A. Loch, R. Espinosa, S. Molin, and H. K. Johansen, "Evolutionary highways to persistent bacterial infection," *Nature Communications* **10**(1), p. 629, 2019.

[123] R. S. Galhardo, P. J. Hastings, and S. M. Rosenberg, "Mutation as a Stress Response and the Regulation of Evolvability," *Critical Reviews in Biochemistry and Molecular Biology* **42**, pp. 399–435, Jan 2007.

[124] L. J. Rothschild and R. L. Mancinelli, "Life in extreme environments," *Nature* **409**(6823), pp. 1092–1101, 2001.

[125] J. A. Shapiro, "All living cells are cognitive," *Biochemical and Biophysical Research Communications* , 2020.

[126] F. Poelwijk, M. de Vos, and S. Tans, "Tradeoffs and Optimality in the Evolution of Gene Regulation," *Cell* **146**, pp. 462–470, Aug 2011.

[127] J. Marles-Wright and R. J. Lewis, "Stress responses of bacteria," *Current Opinion in Structural Biology* **17**(6), pp. 755–760, 2007.

[128] J. A. Hoch, "Two-component and phosphorelay signal transduction," *Current Opinion in Microbiology* **3**(2), pp. 165–170, 2000.

[129] D. F. Browning and S. J. W. Busby, "The regulation of bacterial transcription initiation," *Nature Reviews Microbiology* **2**(1), pp. 57–65, 2004.

[130] D. Kalia, G. Merey, S. Nakayama, Y. Zheng, J. Zhou, Y. Luo, M. Guo, B. T. Roembke, and H. O. Sintim, "Nucleotide, c-di-GMP, c-di-AMP, cGMP, cAMP, (p)ppGpp signaling in bacteria and implications in pathogenesis.," *Chemical Society reviews* **42**, pp. 305–41, Jan 2013.

[131] F. C. Fang, E. R. Frawley, T. Tapscott, and A. Vázquez-Torres, "Bacterial Stress Responses during Host Infection.," *Cell host & microbe* **20**, pp. 133–143, Aug 2016.

[132] S. Gottesman, "Trouble is coming: Signaling pathways that regulate general stress responses in bacteria," *The Journal of biological chemistry* **294**, pp. 11685–11700, Aug 2019.

[133] S. Poncet, E. Milohanic, A. Mazé, J. N. Abdallah, F. Aké, M. Larribe, A.-E. Deghmane, M.-K. Taha, M. Dozot, X. De Bolle, J. J. Letesson, and J. Deutscher, "Correlations between carbon metabolism and virulence in bacteria.," *Contributions to microbiology* **16**, pp. 88–102, 2009.

[134] A. Galinier and J. Deutscher, "Sophisticated Regulation of Transcriptional Factors by the Bacterial Phosphoenolpyruvate: Sugar Phosphotransferase System," *Journal of Molecular Biology* **429**(6), pp. 773–789, 2017.

[135] V. D. Gordon and L. Wang, "Bacterial mechanosensing: the force will be with you, always.," *Journal of cell science* **132**, Apr 2019.

[136] M. W. Hahn and M. G. Hoefle, "Grazing of protozoa and its effect on populations of aquatic bacteria," *FEMS Microbiology Ecology* **35**, pp. 113–121, Apr 2001.

[137] C. Matz, J. S. Webb, P. J. Schupp, S. Y. Phang, A. Penesyan, S. Egan, P. Steinberg, and S. Kjelleberg, "Marine Biofilm Bacteria Evade Eukaryotic Predation by Targeted Chemical Defense," *PLoS ONE* **3**, p. e2744, Jul 2008.

[138] C. D. Nadell, K. Drescher, N. S. Wingreen, and B. L. Bassler, "Extracellular matrix structure governs invasion resistance in bacterial biofilms," *The ISME Journal* **9**, pp. 1700–1709, Aug 2015.

[139] L. D. R. Melo, G. Pinto, F. Oliveira, D. Vilas-Boas, C. Almeida, S. Sillankorva, N. Cerca, and J. Azeredo, "The Protective Effect of Staphylococcus epidermidis Biofilm Matrix against Phage Predation," 2020.

[140] J. A. Imlay, "Where in the world do bacteria experience oxidative stress?," *Environmental Microbiology* **21**, pp. 521–530, Feb 2019.

[141] B. Gasser, M. Saloheimo, U. Rinas, M. Dragosits, E. Rodríguez-Carmona, K. Baumann, M. Giuliani, E. Parrilli, P. Branduardi, C. Lang, D. Porro, P. Ferrer, M. L. Tutino, D. Mattanovich, and A. Villaverde, "Protein folding and conformational stress in microbial cells producing recombinant proteins: a host comparative overview," *Microbial cell factories* **7**, p. 11, Apr 2008.

[142] I. R. Booth and C. F. Higgins, "Enteric bacteria and osmotic stress: intracellular potassium glutamate as a secondary signal of osmotic stress?," *FEMS microbiology reviews* **6**, pp. 239–246, Jun 1990.

[143] J. Deutscher, C. Francke, and P. W. Postma, "How Phosphotransferase System-Related Protein Phosphorylation Regulates Carbohydrate Metabolism in Bacteria," *Microbiology and Molecular Biology Reviews* **70**, pp. 939 LP – 1031, Dec 2006.

[144] C. P. Long, J. Au, N. R. Sandoval, N. A. Gebreselassie, and M. R. Antoniewicz, "Enzyme I facilitates reverse flux from pyruvate to phosphoenolpyruvate in Escherichia coli," *Nature Communications* **8**(1), p. 14316, 2017.

[145] J. McCoy, Z. Ren, V. Stanevich, J. Lee, S. Mitra, E. Levin, S. Poget, M. Quick, W. Im, and M. Zhou, "The Structure of a Sugar Transporter of the Glucose EIIC Superfamily Provides Insight into the Elevator Mechanism of Membrane Transport," *Structure* **24**(6), pp. 956–964, 2016.

[146] J. Deutscher, "The mechanisms of carbon catabolite repression in bacteria," *Current Opinion in Microbiology* **11**(2), pp. 87–93, 2008.

[147] P. Joyet, H. Bouraoui, F. M. D. Aké, M. Derkaoui, A. C. Zébré, T. N. Cao, M. Ventroux, S. Nessler, M.-F. Noirot-Gros, J. Deutscher, and E. Milohanic, "Transcription regulators controlled by interaction with enzyme IIB components of the phosphoenolpyruvate:sugar phosphotransferase system," *Biochimica et Biophysica Acta (BBA) - Proteins and Proteomics* **1834**(7), pp. 1415–1424, 2013.

[148] J. Stülke, M. Arnaud, G. Rapoport, and I. Martin-Verstraete, "PRD — a protein domain involved in PTS-dependent induction and carbon catabolite repression of catabolic operons in bacteria," *Molecular Microbiology* **28**, pp. 865–874, Jun 1998.

[149] R. Gao and A. M. Stock, "Biological insights from structures of two-component proteins.," *Annual review of microbiology* **63**, pp. 133–154, 2009.

[150] J. J. Falke, R. B. Bass, S. L. Butler, S. A. Chervitz, and M. A. Danielson, "The two-component signaling pathway of bacterial chemotaxis: a molecular view of signal transduction by receptors, kinases, and adaptation enzymes.," *Annual review of cell and developmental biology* **13**, pp. 457–512, 1997.

[151] J. Perry, K. Koteva, and G. Wright, "Receptor domains of two-component signal transduction systems.," *Molecular bioSystems* **7**, pp. 1388–1398, May 2011.

[152] A. M. Stock, V. L. Robinson, and P. N. Goudreau, "Two-component signal transduction.," *Annual review of biochemistry* **69**, pp. 183–215, 2000.

[153] A. Buschiazzo and F. Trajtenberg, "Two-Component Sensing and Regulation: How Do Histidine Kinases Talk with Response Regulators at the Molecular Level?," *Annual Review of Microbiology* **73**, pp. 507–528, Sep 2019.

[154] T. Mascher, J. D. Helmann, and G. Unden, "Stimulus perception in bacterial signal-transducing histidine kinases.," *Microbiology and molecular biology reviews : MMBR* **70**, pp. 910–938, Dec 2006.

[155] J. B. Stock, M. G. Surette, M. Levit, and P. Park, "Two-Component Signal Transduction Systems: Structure-Function Relationships and Mechanisms of Catalysis," May 1995.

[156] A. J. Ninfa, P. Jiang, M. R. Atkinson, and J. A. Peliska, "Integration of antagonistic signals in the regulation of nitrogen assimilation in Escherichia coli.," *Current topics in cellular regulation* **36**, pp. 31–75, 2000.

[157] T. Nishijyo, D. Haas, and Y. Itoh, "The CbrA-CbrB two-component regulatory system controls the utilization of multiple carbon and nitrogen sources in Pseudomonas aeruginosa.," *Molecular microbiology* **40**, pp. 917–931, May 2001.

[158] L. Shi and F. M. Hulett, "The cytoplasmic kinase domain of PhoR is sufficient for the low phosphate-inducible expression of pho regulon genes in Bacillus subtilis.," *Molecular microbiology* **31**, pp. 211–222, Jan 1999.

[159] D. T. Verhamme, P. W. Postma, W. Crielaard, and K. J. Hellingwerf, "Cooperativity in signal transfer through the Uhp system of Escherichia coli.," *Journal of bacteriology* **184**, pp. 4205–4210, Aug 2002.

[160] R. M. Macnab, "Flagellar Switch," May 1995.

[161] D. Beier and R. Gross, "Regulation of bacterial virulence by two-component systems," *Current Opinion in Microbiology* **9**(2), pp. 143–152, 2006.

[162] V. Sourjik and J. P. Armitage, "Spatial organization in bacterial chemotaxis.," *The EMBO journal* **29**, pp. 2724–2733, Aug 2010.

[163] J. Lacal, C. García-Fontana, F. Muñoz-Martínez, J.-L. Ramos, and T. Krell, "Sensing of environmental signals: classification of chemoreceptors according to the size of their ligand binding regions.," *Environmental microbiology* **12**, pp. 2873–2884, Nov 2010.

[164] C. B. Whitchurch, A. J. Leech, M. D. Young, D. Kennedy, J. L. Sargent, J. J. Bertrand, A. B. T. Semmler, A. S. Mellick, P. R. Martin, R. A. Alm, M. Hobbs, S. A. Beatson, B. Huang, L. Nguyen, J. C. Commolli, J. N. Engel, A. Darzins, and J. S. Mattick, "Characterization of a complex chemosensory signal transduction system which controls twitching motility in Pseudomonas aeruginosa.," *Molecular microbiology* **52**, pp. 873–893, May 2004.

[165] J. R. Kirby and D. R. Zusman, "Chemosensory regulation of developmental gene expression in Myxococcus xanthus.," *Proceedings of the National Academy of Sciences of the United States of America* **100**, pp. 2008–2013, Feb 2003.

[166] A. Corral-Lugo, J. De la Torre, M. A. Matilla, M. Fernández, B. Morel, M. Espinosa-Urgel, and T. Krell, "Assessment of the contribution of chemoreceptor-based signalling to biofilm formation.," *Environmental microbiology* **18**, pp. 3355–3372, Oct 2016.

[167] J. W. Hickman, D. F. Tifrea, and C. S. Harwood, "A chemosensory system that regulates biofilm formation through modulation of cyclic diguanylate levels.," *Proceedings of the National Academy of Sciences of the United States of America* **102**, pp. 14422–14427, Oct 2005.

[168] M. A. Matilla and T. Krell, "Chemoreceptor-based signal sensing.," *Current opinion in biotechnology* **45**, pp. 8–14, Jun 2017.

[169] C. M. Waters and B. L. Bassler, "Quorum sensing: cell-to-cell communication in bacteria.," *Annual review of cell and developmental biology* **21**, pp. 319–346, 2005.

[170] K. Papenfort and B. L. Bassler, "Quorum sensing signal-response systems in Gram-negative bacteria.," *Nature reviews. Microbiology* **14**, pp. 576–588, Aug 2016.

[171] J. A. Freeman, B. N. Lilley, and B. L. Bassler, "A genetic analysis of the functions of LuxN: a two-component hybrid sensor kinase that regulates quorum sensing in Vibrio harveyi.," *Molecular microbiology* **35**, pp. 139–149, Jan 2000.

[172] R. C. Kelly, M. E. Bolitho, D. A. Higgins, W. Lu, W.-L. Ng, P. D. Jeffrey, J. D. Rabinowitz, M. F. Semmelhack, F. M. Hughson, and B. L. Bassler, "The Vibrio cholerae quorum-sensing autoinducer CAI-1: analysis of the biosynthetic enzyme CqsA.," *Nature chemical biology* **5**, pp. 891–895, Dec 2009.

[173] J. M. Henke and B. L. Bassler, "Three Parallel Quorum-Sensing Systems Regulate Gene Expression in Vibrio harveyi," *Journal of Bacteriology* **186**, pp. 6902 LP – 6914, Oct 2004.

[174] G. Brackman, S. Celen, K. Baruah, P. Bossier, S. Van Calenbergh, H. J. Nelis, and T. Coenye, "AI-2 quorum-sensing inhibitors affect the starvation response and reduce virulence in several Vibrio species, most likely by interfering with LuxPQ.," *Microbiology (Reading, England)* **155**, pp. 4114–4122, Dec 2009.

[175] D. A. Rasko, C. G. Moreira, D. R. Li, N. C. Reading, J. M. Ritchie, M. K. Waldor, N. Williams, R. Taussig, S. Wei, M. Roth, D. T. Hughes, J. F. Huntley, M. W. Fina, J. R. Falck, and V. Sperandio, "Targeting QseC Signaling and Virulence for Antibiotic Development," *Science* **321**, pp. 1078 LP – 1080, Aug 2008.

[176] K. Papenfort, J. E. Silpe, K. R. Schramma, J.-P. Cong, M. R. Seyedsayamdost, and B. L. Bassler, "A Vibrio cholerae autoinducer-receptor pair that controls biofilm formation.," *Nature chemical biology* **13**, pp. 551–557, May 2017.

[177] B. G. Coutinho, E. Mevers, A. L. Schaefer, D. A. Pelletier, C. S. Harwood, J. Clardy, and E. P. Greenberg, "A plant-responsive bacterial-signaling system senses an ethanolamine derivative," *Proceedings of the National Academy of Sciences* **115**, pp. 9785 LP – 9790, Sep 2018.

[178] S. A. Jung, L. A. Hawver, and W.-L. Ng, "Parallel quorum sensing signaling pathways in Vibrio cholerae.," *Current genetics* **62**, pp. 255–260, May 2016.

[179] B. N. Lilley and B. L. Bassler, "Regulation of quorum sensing in Vibrio harveyi by LuxO and sigma-54.," *Molecular microbiology* **36**, pp. 940–954, May 2000.

[180] R. Herzog, N. Peschek, K. S. Fröhlich, K. Schumacher, and K. Papenfort, "Three autoinducer molecules act in concert to control virulence gene expression in Vibrio cholerae.," *Nucleic acids research* **47**, pp. 3171–3183, Apr 2019.

[181] J. R. J. Haycocks, G. Z. L. Warren, L. M. Walker, J. L. Chlebek, T. N. Dalia, A. B. Dalia, and D. C. Grainger, "The quorum sensing transcription factor AphA directly regulates natural competence in Vibrio cholerae.," *PLoS genetics* **15**, p. e1008362, Oct 2019.

[182] B. K. Hammer and B. L. Bassler, "Quorum sensing controls biofilm formation in Vibrio cholerae.," *Molecular microbiology* **50**, pp. 101–4, Oct 2003.

[183] P. K. Singh, S. Bartalomej, R. Hartmann, H. Jeckel, L. Vidakovic, C. D. Nadell, and K. Drescher, "Vibrio cholerae Combines Individual and Collective Sensing to Trigger Biofilm Dispersal.," *Current biology : CB* **27**, pp. 3359–3366.e7, Nov 2017.

[184] W.-L. Ng and B. L. Bassler, "Bacterial quorum-sensing network architectures.," *Annual review of genetics* **43**, pp. 197–222, 2009.

[185] J. Mordue, N. O'Boyle, N. Gadegaard, and A. J. Roe, "The force awakens: The dark side of mechanosensing in bacterial pathogens.," *Cellular signalling* **78**, p. 109867, Feb 2021.

[186] L. Turner, A. S. Stern, and H. C. Berg, "Growth of Flagellar Filaments of Escherichia coli is Independent of Filament Length," *Journal of Bacteriology* **194**, pp. 2437 LP – 2442, May 2012.

[187] M. A. Echazarreta, J. L. Kepple, L.-H. Yen, Y. Chen, and K. E. Klose, "A Critical Region in the FlaA Flagellin Facilitates Filament Formation of the Vibrio cholerae Flagellum.," *Journal of bacteriology* **200**, Aug 2018.

[188] H. C. Berg, "The Rotary Motor of Bacterial Flagella," *Annual Review of Biochemistry* **72**, pp. 19–54, Jun 2003.

[189] F. F. V. Chevance and K. T. Hughes, "Coordinating assembly of a bacterial macromolecular machine," *Nature Reviews Microbiology* **6**(6), pp. 455–465, 2008.

[190] X. Fang and M. Gomelsky, "A post-translational, c-di-GMP-dependent mechanism regulating flagellar motility.," *Molecular microbiology* **76**, pp. 1295–1305, Jun 2010.

[191] C. Opoku-Temeng, J. Zhou, Y. Zheng, J. Su, and H. O. Sintim, "Cyclic dinucleotide (c-di-GMP, c-di-AMP, and cGAMP) signalings have come of age to be inhibited by small molecules," *Chem. Commun.* **52**(60), pp. 9327–9342, 2016.

[192] M. Gomelsky, "cAMP, c-di-GMP, c-di-AMP and now cGMP: bacteria use them all!," *Molecular Microbiology* **79**, pp. 562–565, Feb 2011.

[193] M. Cashel and J. Gallant, "Two Compounds implicated in the Function of the RC Gene of Escherichia coli," *Nature* **221**(5183), pp. 838–841, 1969.

[194] R. Tamayo, J. T. Pratt, and A. Camilli, "Roles of cyclic diguanylate in the regulation of bacterial pathogenesis.," *Annual review of microbiology* **61**, pp. 131–148, 2007.

[195] R. M. Corrigan and A. Gründling, "Cyclic di-AMP: another second messenger enters the fray.," *Nature reviews. Microbiology* **11**, pp. 513–24, Aug 2013.

[196] P. Ross, H. Weinhouse, Y. Aloni, D. Michaeli, P. Weinberger-Ohana, R. Mayer, S. Braun, E. de Vroom, G. A. van der Marel, J. H. van Boom, and M. Benziman, "Regulation of cellulose synthesis in Acetobacter xylinum by cyclic diguanylic acid.," *Nature* **325**, pp. 279–281, Jan 1987.

[197] R. Simm, M. Morr, A. Kader, M. Nimtz, and U. Römling, "GGDEF and EAL domains inversely regulate cyclic di-GMP levels and transition from sessility to motility.," *Molecular microbiology* **53**, pp. 1123–1134, Aug 2004.

[198] K. B. Hisert, M. MacCoss, M. U. Shiloh, K. H. Darwin, S. Singh, R. A. Jones, S. Ehrt, Z. Zhang, B. L. Gaffney, S. Gandotra, D. W. Holden, D. Murray, and C. Nathan, "A glutamate-alanine-leucine (EAL) domain protein of Salmonella controls bacterial survival in mice, antioxidant defence and killing of macrophages: role of cyclic diGMP.," *Molecular microbiology* **56**, pp. 1234–1245, Jun 2005.

[199] R. Hengge, "Principles of c-di-GMP signalling in bacteria.," *Nature reviews. Microbiology* **7**, pp. 263–273, Apr 2009.

[200] U. Römling, M. Y. Galperin, and M. Gomelsky, "Cyclic di-GMP: the first 25 years of a universal bacterial second messenger.," *Microbiology and molecular biology reviews : MMBR* **77**, pp. 1–52, Mar 2013.

[201] J. Pei and N. V. Grishin, "GGDEF domain is homologous to adenylyl cyclase.," *Proteins* **42**, pp. 210–216, Feb 2001.

[202] T. R. M. Barends, E. Hartmann, J. J. Griese, T. Beitlich, N. V. Kirienko, D. A. Ryjenkov, J. Reinstein, R. L. Shoeman, M. Gomelsky, and I. Schlichting, "Structure and mechanism of a bacterial light-regulated cyclic nucleotide phosphodiesterase.," *Nature* **459**, pp. 1015–1018, Jun 2009.

[203] V. Stelitano, G. Giardina, A. Paiardini, N. Castiglione, F. Cutruzzolà, and S. Rinaldo, "C-di-GMP Hydrolysis by Pseudomonas aeruginosa HD-GYP Phosphodiesterases: Analysis of the Reaction Mechanism and Novel Roles for pGpG," *PLOS ONE* **8**, p. e74920, Sep 2013.

[204] U. Jenal, A. Reinders, and C. Lori, "Cyclic di-GMP: second messenger extraordinaire," *Nature Reviews Microbiology* **15**(5), pp. 271–284, 2017.

[205] J. G. Conner, D. Zamorano-Sánchez, J. H. Park, H. Sondermann, and F. H. Yildiz, "The ins and outs of cyclic di-GMP signaling in Vibrio cholerae," *Current Opinion in Microbiology* **36**, pp. 20–29, Apr 2017.

[206] J. T. Pratt, R. Tamayo, A. D. Tischler, and A. Camilli, "PilZ domain proteins bind cyclic diguanylate and regulate diverse processes in Vibrio cholerae.," *The Journal of biological chemistry* **282**, pp. 12860–12870, Apr 2007.

[207] N. Sudarsan, E. R. Lee, Z. Weinberg, R. H. Moy, J. N. Kim, K. H. Link, and R. R. Breaker, "Riboswitches in eubacteria sense the second messenger cyclic di-GMP.," *Science (New York, N.Y.)* **321**, pp. 411–413, Jul 2008.

[208] R. Hengge, "High-Specificity Local and Global c-di-GMP Signaling.," *Trends in microbiology* , Feb 2021.

[209] B. W. Davies, R. W. Bogard, T. S. Young, and J. J. Mekalanos, "Coordinated regulation of accessory genetic elements produces cyclic di-nucleotides for V. cholerae virulence.," *Cell* **149**, pp. 358–370, Apr 2012.

[210] G. B. Severin, M. S. Ramliden, L. A. Hawver, K. Wang, M. E. Pell, A.-K. Kieninger, A. Khataokar, B. J. O'Hara, L. V. Behrmann, M. B. Neiditch, C. Benning, C. M. Waters, and W.-L. Ng, "Direct activation of a phospholipase by cyclic GMP-AMP in El Tor Vibrio cholerae," *Proceedings of the National Academy of Sciences* **115**, pp. E6048 LP – E6055, Jun 2018.

[211] D. Cohen, S. Melamed, A. Millman, G. Shulman, Y. Oppenheimer-Shaanan, A. Kacen, S. Doron, G. Amitai, and R. Sorek, "Cyclic GMP-AMP signalling protects bacteria against viral infection.," *Nature* **574**, pp. 691–695, Oct 2019.

[212] F. Li, A. Cimdins, M. Rohde, L. Jänsch, V. Kaever, M. Nimtz, and U. Römling, "DncV Synthesizes Cyclic GMP-AMP and Regulates Biofilm Formation and Motility in Escherichia coli ECOR31," *mBio* **10**, pp. e02492–18, Apr 2019.

[213] L. Sun, J. Wu, F. Du, X. Chen, and Z. J. Chen, "Cyclic GMP-AMP synthase is a cytosolic DNA sensor that activates the type I interferon pathway.," *Science (New York, N.Y.)* **339**, pp. 786–791, Feb 2013.

[214] J. Wu, L. Sun, X. Chen, F. Du, H. Shi, C. Chen, and Z. J. Chen, "Cyclic GMP-AMP is an endogenous second messenger in innate immune signaling by cytosolic DNA.," *Science (New York, N.Y.)* **339**, pp. 826–830, Feb 2013.

[215] H. Maeda, N. Fujita, and A. Ishihama, "Competition among seven Escherichia coli sigma subunits: relative binding affinities to the core RNA polymerase.," *Nucleic acids research* **28**, pp. 3497–3503, Sep 2000.

[216] M. Madan Babu and S. A. Teichmann, "Functional determinants of transcription factors in Escherichia coli: protein families and binding sites.," *Trends in genetics : TIG* **19**, pp. 75–79, Feb 2003.

[217] M. M. Barker, T. Gaal, C. A. Josaitis, and R. L. Gourse, "Mechanism of regulation of transcription initiation by ppGpp. I. Effects of ppGpp on transcription initiation in vivo and in vitro.," *Journal of molecular biology* **305**, pp. 673–688, Jan 2001.

[218] B. Müller-Hill, *The lac Operon*, De Gruyter, 2011.

[219] E. Pérez-Rueda and J. Collado-Vides, "The repertoire of DNA-binding transcriptional regulators in Escherichia coli K-12.," *Nucleic acids research* **28**, pp. 1838–1847, Apr 2000.

[220] A. Martínez-Antonio and J. Collado-Vides, "Identifying global regulators in transcriptional regulatory networks in bacteria.," *Current opinion in microbiology* **6**, pp. 482–489, Oct 2003.

[221] E. Holmqvist and E. G. H. Wagner, "Impact of bacterial sRNAs in stress responses," *Biochemical Society transactions* **45**, pp. 1203–1212, Dec 2017.

[222] J. M. Abduljalil, "Bacterial riboswitches and RNA thermometers: Nature and contributions to pathogenesis," *Non-coding RNA research* **3**, pp. 54–63, Apr 2018.

[223] A. J. McBroom and M. J. Kuehn, "Release of outer membrane vesicles by Gram-negative bacteria is a novel envelope stress response.," *Molecular microbiology* **63**, pp. 545–558, Jan 2007.

[224] V. Pader, S. Hakim, K. L. Painter, S. Wigneshweraraj, T. B. Clarke, and A. M. Edwards, "Staphylococcus aureus inactivates daptomycin by releasing membrane phospholipids," *Nature Microbiology* **2**(October), p. 16194, 2016.

[225] R. Hengge, "The General Stress Response in Gram-Negative Bacteria," Nov 2010.

[226] S. Ozturk and B. Aslim, "Modification of exopolysaccharide composition and production by three cyanobacterial isolates under salt stress," *Environmental Science and Pollution Research* **17**, pp. 595–602, Mar 2010.

[227] D. Ren, L. A. Bedzyk, S. M. Thomas, R. W. Ye, and T. K. Wood, "Gene expression in Escherichia coli biofilms," *Applied Microbiology and Biotechnology* **64**, pp. 515–524, May 2004.

[228] N. Høiby, T. Bjarnsholt, M. Givskov, S. Molin, O. Ciofu, S. Lanng, and E. Al., "Antibiotic resistance of bacterial biofilms.," *International journal of antimicrobial agents* **35**, pp. 322–32, Apr 2010.

[229] T. F. Mah and G. A. O'Toole, "Mechanisms of biofilm resistance to antimicrobial agents.," *Trends in microbiology* **9**, pp. 34–39, Jan 2001.

[230] D. K. H. Rode, P. K. Singh, and K. Drescher, "Multicellular and unicellular responses of microbial biofilms to stress.," *Biological chemistry* **401**, pp. 1365–1374, Nov 2020.

[231] B. Koskella and M. A. Brockhurst, "Bacteria-phage coevolution as a driver of ecological and evolutionary processes in microbial communities.," *FEMS microbiology reviews* **38**, pp. 916–31, Sep 2014.

[232] M. A. Jensen, S. M. Faruque, J. J. Mekalanos, and B. R. Levin, "Modeling the role of bacteriophage in the control of cholera outbreaks," *Proceedings of the National Academy of Sciences of the United States of America* **103**, pp. 4652 LP – 4657, Mar 2006.

[233] E. J. Nelson, A. Chowdhury, J. Flynn, S. Schild, L. Bourassa, Y. Shao, R. C. LaRocque, S. B. Calderwood, F. Qadri, and A. Camilli, "Transmission of Vibrio cholerae Is Antagonized by Lytic Phage and Entry into the Aquatic Environment," *PLoS Pathogens* **4**, p. e1000187, Oct 2008.

[234] E. E. Bernardy, M. A. Turnsek, S. K. Wilson, C. L. Tarr, and B. K. Hammer, "Diversity of clinical and environmental isolates of Vibrio cholerae in natural transformation and contact-dependent bacterial killing indicative of type VI secretion system activity," *Applied and Environmental Microbiology* **82**(9), pp. 2833–2842, 2016.

[235] L. Chao, B. R. Levin, and F. M. Stewart, "A Complex Community in a Simple Habitat: An Experimental Study with Bacteria and," Tech. Rep. 2, 1977.

[236] H. J. Busscher and H. C. van der Mei, "Microbial Adhesion in Flow Displacement Systems," *Clinical Microbiology Reviews* **19**, pp. 127 LP – 141, Jan 2006.

[237] K. Drescher, J. Dunkel, C. D. Nadell, S. van Teeffelen, I. Grnja, N. S. Wingreen, H. A. Stone, and B. L. Bassler, "Architectural transitions in Vibrio cholerae biofilms at single-cell resolution.," *Proceedings of the National Academy of Sciences of the United States of America* **113**, pp. E2066–72, Apr 2016.

[238] S. Vaidya, M. F. Hansen, P. K. Singh, E. Jelli, K. Nosho, and K. Drescher, "Bacterial danger-sensing induces biofilm formation to protect cells against phage predation," 2021.

[239] A. J. Manning and M. J. Kuehn, "Contribution of bacterial outer membrane vesicles to innate bacterial defense.," *BMC microbiology* **11**, p. 258, Jan 2011.

[240] T. Reyes-Robles, R. S. Dillard, L. S. Cairns, C. A. Silva-Valenzuela, M. Housman, A. Ali, E. R. Wright, and A. Camilli, "Vibrio cholerae outer membrane vesicles inhibit bacteriophage infection," *Journal of Bacteriology* , pp. JB.00792–17, Apr 2018.

[241] S. Ripp and R. V. Miller, "Dynamics of the pseudolysogenic response in slowly growing cells of Pseudomonas aeruginosa.," *Microbiology (Reading, England)* **144 (Pt 8**, pp. 2225–2232, Aug 1998.

[242] M. Łoś and G. Węgrzyn, "Chapter 9 - Pseudolysogeny," in *Bacteriophages, Part A*, M. Łobocka and W. T. B. T. A. i. V. R. Szybalski, eds., **82**, pp. 339–349, Academic Press, 2012.

[243] A. Lwoff, "Lysogeny," *Bacteriological reviews* **17**, pp. 269–337, Dec 1953.

[244] R. Bastías, G. Higuera, W. Sierralta, and R. T. Espejo, "A new group of cosmopolitan bacteriophages induce a carrier state in the pandemic strain of Vibrio parahaemolyticus," *Environmental Microbiology* **12**, pp. 990–1000, Apr 2010.

[245] L. M. Jones, C. R. McDuff, and J. B. Wilson, "Phenotypic alterations in the colonial morphology of Brucella abortus due to a bacteriophage carrier state.," *Journal of bacteriology* **83**, pp. 860–866, Apr 1962.

[246] G. Steinbach, C. Crisan, S. L. Ng, B. Hammer, and P. Yunker, "Accumulation of dead cells from contact killing facilitates coexistence in bacterial biofilms," *bioRxiv* , p. 2020.04.03.024158, Jan 2020.

[247] J. G. Morris, M. B. Sztein, E. W. Rice, J. P. Nataro, G. A. Losonsky, P. Panigrahi, C. O. Tacket, and J. A. Johnson, "Vibrio cholerae 01 Can Assume a Chlorine-Resistant Rugose Survival Form that Is Virulent for Humans," *Journal of Infectious Diseases* **174**, pp. 1364–1368, Dec 1996.

[248] F. H. Yildiz and G. K. Schoolnik, "Vibrio cholerae O1 El Tor: Identification of a gene cluster required for the rugose colony type, exopolysaccharide production, chlorine resistance, and biofilm formation," *Proceedings of the National Academy of Sciences* **96**, pp. 4028–4033, Mar 1999.

[249] K. G. Roelofs, C. J. Jones, S. R. Helman, X. Shang, M. W. Orr, J. R. Goodson, M. Y. Galperin, F. H. Yildiz, and V. T. Lee, "Systematic Identification of Cyclic-di-GMP Binding Proteins in Vibrio cholerae Reveals a Novel Class of Cyclic-di-GMP-Binding ATPases Associated with Type II Secretion Systems," *PLoS Pathogens* **11**(10), pp. 1–29, 2015.

[250] H. Szurmant and G. W. Ordal, "Diversity in chemotaxis mechanisms among the bacteria and archaea.," *Microbiology and molecular biology reviews : MMBR* **68**, pp. 301–319, Jun 2004.

[251] UniProt Consortium, "UniProt: a hub for protein information," *Nucleic Acids Research* **43**, pp. D204–D212, Jan 2015.

[252] M. Kanehisa and S. Goto, "KEGG: kyoto encyclopedia of genes and genomes.," *Nucleic acids research* **28**, pp. 27–30, Jan 2000.

[253] P. S. Dehal, M. P. Joachimiak, M. N. Price, J. T. Bates, J. K. Baumohl, D. Chivian, G. D. Friedland, K. H. Huang, K. Keller, P. S. Novichkov, I. L. Dubchak, E. J. Alm, and A. P. Arkin, "MicrobesOnline: an integrated portal for comparative and functional genomics," *Nucleic acids research* **38**, pp. D396–D400, Jan 2010.

[254] R. Lavigne, W. Sun, and G. Volckaert, "PHIRE, a Deterministic Approach to Reveal Regulatory Elements in Bacteriophage Genomes," *Bioinformatics (Oxford, England)* **20**(5), 2004.

[255] E. Balleza, J. M. Kim, and P. Cluzel, "Systematic characterization of maturation time of fluorescent proteins in living cells.," *Nature methods* **15**, pp. 47–51, Jan 2018.

[256] N. C. Shaner, G. G. Lambert, A. Chammas, Y. Ni, P. J. Cranfill, M. A. Baird, B. R. Sell, J. R. Allen, R. N. Day, M. Israelsson, M. W. Davidson, and J. Wang, "A bright monomeric green fluorescent protein derived from Branchiostoma lanceolatum," *Nature Methods* **10**(5), pp. 407–409, 2013.

[257] R. G. Abisado, S. Benomar, J. R. Klaus, A. A. Dandekar, and J. R. Chandler, "Bacterial Quorum Sensing and Microbial Community Interactions," *mBio* **9**, pp. e02331–17, Jul 2018.

[258] C. D. Nadell, K. Drescher, and K. R. Foster, "Spatial structure, cooperation and competition in biofilms," *Nature Reviews Microbiology* **14**(9), pp. 589–600, 2016.

[259] M. LeRoux, S. B. Peterson, and J. D. Mougous, "Bacterial danger sensing.," *Journal of molecular biology* **427**, pp. 3744–3753, Nov 2015.

[260] D. A. Ritchie, "Physical characterization of the DNA released from phage particles by heat inactivation.," *FebS letters* **11**, pp. 257–260, Dec 1970.

[261] Z. Vörös, G. Csík, L. Herényi, and M. Kellermayer, "Temperature-Dependent Nanomechanics and Topography of Bacteriophage T7," *Journal of Virology* **92**, pp. e01236–18, Oct 2018.

[262] S. Ghosh, S. M. Hamdan, T. E. Cook, and C. C. Richardson, "Interactions of Escherichia coli thioredoxin, the processivity factor, with bacteriophage T7 DNA polymerase and helicase," *The Journal of biological chemistry* **283**, pp. 32077–32084, Nov 2008.

[263] D. F. Mark and C. C. Richardson, "Escherichia coli thioredoxin: a subunit of bacteriophage T7 DNA polymerase," *Proceedings of the National Academy of Sciences of the United States of America* **73**, pp. 780–784, Mar 1976.

[264] U. Qimron, B. Marintcheva, S. Tabor, and C. C. Richardson, "Genomewide screens for Escherichia coli genes affecting growth of T7 bacteriophage," *Proceedings of the National Academy of Sciences* **103**, pp. 19039 LP – 19044, Dec 2006.

[265] A. Delgado, R. Arco, B. Ibarra-Molero, and J. M. Sanchez-Ruiz, "Using Resurrected Ancestral Proviral Proteins to Engineer Virus Resistance," *Cell Reports* **19**, pp. 1247–1256, May 2017.

[266] J. Zhang, W. Li, Q. Zhang, H. Wang, X. Xu, B. Diao, L. Zhang, and B. Kan, "The Core Oligosaccharide and Thioredoxin of Vibrio cholerae Are Necessary for Binding and Propagation of Its Typing Phage VP3," *Journal of Bacteriology* **191**, pp. 2622–2629, Apr 2009.

[267] J. Yan, A. G. Sharo, H. A. Stone, N. S. Wingreen, and B. L. Bassler, "Vibrio cholerae biofilm growth program and architecture revealed by single-cell live imaging," *Proceedings of the National Academy of Sciences* **113**, pp. E5337 LP – E5343, Sep 2016.

[268] A. Ito, T. May, K. Kawata, and S. Okabe, "Significance of rpoS during maturation of Escherichia coli biofilms.," *Biotechnology and bioengineering* **99**, pp. 1462–1471, Apr 2008.

[269] F. Smakman and A. R. Hall, "Exposure to lysed bacteria can promote or inhibit growth of neighbouring live bacteria depending on local abiotic conditions," *bioRxiv* , p. 2020.10.23.352005, Jan 2020.

[270] C. B. Whitchurch, T. Tolker-Nielsen, P. C. Ragas, and J. S. Mattick, "Extracellular DNA required for bacterial biofilm formation.," *Science (New York, N.Y.)* **295**, p. 1487, Feb 2002.

[271] U. Alon, L. Camarena, M. G. Surette, B. Aguera y Arcas, Y. Liu, S. Leibler, and J. B. Stock, "Response regulator output in bacterial chemotaxis," *The EMBO journal* **17**, pp. 4238–4248, Aug 1998.

[272] M. A. Boin, M. J. Austin, and C. C. Häse, "Chemotaxis in Vibrio cholerae.," *FEMS microbiology letters* **239**, pp. 1–8, Oct 2004.

[273] P. V. Krasteva, J. C. N. Fong, N. J. Shikuma, S. Beyhan, M. V. A. S. Navarro, F. H. Yildiz, and H. Sondermann, "Vibrio cholerae VpsT Regulates Matrix Production and Motility by Directly Sensing Cyclic di-GMP," *Science* **327**(5967), 2010.

[274] A. L. Goodman, B. Kulasekara, A. Rietsch, D. Boyd, R. S. Smith, and S. Lory, "A signaling network reciprocally regulates genes associated with acute infection and chronic persistence in Pseudomonas aeruginosa.," *Developmental cell* **7**, pp. 745–754, Nov 2004.

[275] C. Reimmann, M. Beyeler, A. Latifi, H. Winteler, M. Foglino, A. Lazdunski, and D. Haas, "The global activator GacA of Pseudomonas aeruginosa PAO positively controls the production of the autoinducer N-butyryl-homoserine lactone and the formation of the virulence factors pyocyanin, cyanide, and lipase.," *Molecular microbiology* **24**, pp. 309–319, Apr 1997.

[276] H. Zhou, C. Zheng, J. Su, B. Chen, Y. Fu, Y. Xie, Q. Tang, S.-H. Chou, and J. He, "Characterization of a natural triple-tandem c-di-GMP riboswitch and application of the riboswitch-based dual-fluorescence reporter," *Scientific Reports* **6**(1), p. 20871, 2016.

[277] J. B. Andersen, C. Sternberg, L. K. Poulsen, S. P. Bjorn, M. Givskov, and S. Molin, "New unstable variants of green fluorescent protein for studies of transient gene expression in bacteria," *Applied and environmental microbiology* **64**, pp. 2240–2246, Jun 1998.

[278] Z. Qin, Y. Ou, L. Yang, Y. Zhu, T. Tolker-Nielsen, S. Molin, and D. Qu, "Role of autolysin-mediated DNA release in biofilm formation of Staphylococcus epidermidis.," *Microbiology (Reading, England)* **153**, pp. 2083–2092, Jul 2007.

[279] M. Carrolo, M. J. Frias, F. R. Pinto, J. Melo-Cristino, and M. Ramirez, "Prophage Spontaneous Activation Promotes DNA Release Enhancing Biofilm Formation in Streptococcus pneumoniae," *PLOS ONE* **5**, p. e15678, Dec 2010.

[280] A. M. T. Barnes, K. S. Ballering, R. S. Leibman, C. L. Wells, and G. M. Dunny, "Enterococcus faecalis Produces Abundant Extracellular Structures Containing DNA in the Absence of Cell Lysis during Early Biofilm Formation," *mBio* **3**, pp. e00193–12, Aug 2012.

[281] M. Okshevsky and R. L. Meyer, "The role of extracellular DNA in the establishment, maintenance and perpetuation of bacterial biofilms," *Critical Reviews in Microbiology* **41**, pp. 341–352, Jul 2015.

[282] J. Gödeke, K. Paul, J. Lassak, and K. M. Thormann, "Phage-induced lysis enhances biofilm formation in Shewanella oneidensis MR-1.," *The ISME journal* **5**, pp. 613–26, Apr 2011.

[283] S. Bhattacharyya, D. M. Walker, and R. M. Harshey, "Dead cells release a 'necrosignal' that activates antibiotic survival pathways in bacterial swarms," *Nature Communications* **11**(1), pp. 1–12, 2020.

[284] S. Westhoff, G. P. van Wezel, and D. E. Rozen, "Distance-dependent danger responses in bacteria," *Current Opinion in Microbiology* **36**, pp. 95–101, 2017.

[285] S. Bruisson, G. Berg, P. Garbeva, and L. Weisskopf, "Volatile Interplay Between Microbes: Friends and Foes BT - Bacterial Volatile Compounds as Mediators of Airborne Interactions," pp. 215–235, Springer Singapore, Singapore, 2020.

[286] D. Tan, S. L. Svenningsen, and M. Middelboe, "Quorum Sensing Determines the Choice of Antiphage Defense Strategy in Vibrio anguillarum.," *mBio* **6**, p. e00627, Jun 2015.

[287] M. LeRoux, R. L. Kirkpatrick, E. I. Montauti, B. Q. Tran, S. B. Peterson, B. N. Harding, J. C. Whitney, A. B. Russell, B. Traxler, Y. A. Goo, D. R. Goodlett, P. A. Wiggins, and J. D. Mougous, "Kin cell lysis is a danger signal that activates antibacterial pathways of Pseudomonas aeruginosa.," *eLife* **4**, Feb 2015.

[288] M. Valentini, D. Gonzalez, D. A. I. Mavridou, and A. Filloux, "Lifestyle transitions and adaptive pathogenesis of Pseudomonas aeruginosa," *Current Opinion in Microbiology* **41**, pp. 15–20, 2018.

[289] K. Lapouge, M. Schubert, F. H.-T. Allain, and D. Haas, "Gac/Rsm signal transduction pathway of gamma-proteobacteria: from RNA recognition to regulation of social behaviour.," *Molecular microbiology* **67**, pp. 241–253, Jan 2008.

[290] D. H. Lenz, M. B. Miller, J. Zhu, R. V. Kulkarni, and B. L. Bassler, "CsrA and three redundant small RNAs regulate quorum sensing in Vibrio cholerae.," *Molecular microbiology* **58**, pp. 1186–1202, Nov 2005.

[291] P. R. Kulkarni, X. Cui, J. W. Williams, A. M. Stevens, and R. V. Kulkarni, "Prediction of CsrA-regulating small RNAs in bacteria and their experimental verification in Vibrio fischeri.," *Nucleic acids research* **34**(11), pp. 3361–3369, 2006.

[292] A. M. Tsou, Z. Liu, T. Cai, and J. Zhu, "The VarS/VarA two-component system modulates the activity of the Vibrio cholerae quorum-sensing transcriptional regulator HapR.," *Microbiology (Reading, England)* **157**, pp. 1620–1628, Jun 2011.

[293] H. Kono and K. L. Rock, "How dying cells alert the immune system to danger.," *Nature reviews. Immunology* **8**, pp. 279–289, Apr 2008.

[294] A. J. Wolf and D. M. Underhill, "Peptidoglycan recognition by the innate immune system," *Nature Reviews Immunology* **18**(4), pp. 243–254, 2018.

[295] O. Irazoki, S. B. Hernandez, and F. Cava, "Peptidoglycan muropeptides: Release, perception, and functions as signaling molecules," *Frontiers in Microbiology* **10**(MAR), 2019.

[296] G. Buist, A. Steen, J. Kok, and O. P. Kuipers, "LysM, a widely distributed protein motif for binding to (peptido)glycans," *Molecular Microbiology* **68**, pp. 838–847, May 2008.

[297] S. Mesnage, M. Dellarole, N. J. Baxter, J.-B. Rouget, J. D. Dimitrov, N. Wang, Y. Fujimoto, A. M. Hounslow, S. Lacroix-Desmazes, K. Fukase, S. J. Foster, and M. P. Williamson, "Molecular basis for bacterial peptidoglycan recognition by LysM domains," *Nature Communications* **5**(1), p. 4269, 2014.

[298] A. Bateman and M. Bycroft, "The structure of a LysM domain from E. coli membrane-bound lytic murein transglycosylase D (MltD).," *Journal of molecular biology* **299**, pp. 1113–1119, Jun 2000.

[299] S. Moorthy and P. I. Watnick, "Genetic evidence that the Vibrio cholerae monolayer is a distinct stage in biofilm development," *Molecular microbiology* **52**(2), pp. 573–587, 2004.

[300] D. R. Ortega, A. Kjaer, and A. Briegel, "The chemosensory systems of Vibrio cholerae.," *Molecular microbiology* **114**, pp. 367–376, Sep 2020.

[301] N. M. Oliveira, K. R. Foster, and W. M. Durham, "Single-cell twitching chemotaxis in developing biofilms.," *Proceedings of the National Academy of Sciences of the United States of America* **113**, pp. 6532–6537, Jun 2016.

[302] Z. Huang, Y.-H. Wang, H.-Z. Zhu, E. P. Andrianova, C.-Y. Jiang, D. Li, L. Ma, J. Feng, Z.-P. Liu, H. Xiang, I. B. Zhulin, and S.-J. Liu, "Cross Talk between Chemosensory Pathways That Modulate Chemotaxis and Biofilm Formation," *mBio* **10**, pp. e02876–18, Feb 2019.

[303] W. Liu, Y. Sun, R. Shen, X. Dang, X. Liu, F. Sui, Y. Li, Z. Zhang, G. Alexandre, C. Elmerich, and Z. Xie, "A Chemotaxis-Like Pathway of Azorhizobium caulinodans Controls Flagella-Driven Motility, Which Regulates Biofilm Formation, Exopolysaccharide Biosynthesis, and Competitive Nodulation.," *Molecular plant-microbe interactions : MPMI* **31**, pp. 737–749, Jul 2018.

[304] R. Allard-Massicotte, L. Tessier, F. Lécuyer, V. Lakshmanan, J.-F. Lucier, D. Garneau, L. Caudwell, H. Vlamakis, H. P. Bais, and P. B. Beauregard, "Bacillus subtilis Early Colonization of Arabidopsis thaliana," *mBio* **7**, pp. e01664–16, Dec 2016.

[305] L. Laganenka, R. Colin, and V. Sourjik, "Chemotaxis towards autoinducer 2 mediates autoaggregation in Escherichia coli," *Nature communications* **7**, p. 12984, Sep 2016.

[306] K. He and C. E. Bauer, "Chemosensory signaling systems that control bacterial survival.," *Trends in microbiology* **22**, pp. 389–398, Jul 2014.

[307] V. M. Suchanek, M. Esteban-López, R. Colin, O. Besharova, K. Fritz, and V. Sourjik, "Chemotaxis and cyclic-di-GMP signalling control surface attachment of Escherichia coli.," *Molecular microbiology* **113**, pp. 728–739, Apr 2020.

[308] M. H. Russell, A. N. Bible, X. Fang, J. R. Gooding, S. R. Campagna, M. Gomelsky, and G. Alexandre, "Integration of the second messenger c-di-GMP into the chemotactic signaling pathway.," *mBio* **4**, pp. e00001–13, Mar 2013.

[309] P. A. Cotter and S. Stibitz, "c-di-GMP-mediated regulation of virulence and biofilm formation," *Current Opinion in Microbiology* **10**(1), pp. 17–23, 2007.

[310] C. M. Waters, W. Lu, J. D. Rabinowitz, and B. L. Bassler, "Quorum Sensing Controls Biofilm Formation in Vibrio cholerae through Modulation of Cyclic di-GMP Levels and Repression of vpsT," *Journal of Bacteriology* **190**, pp. 2527 LP – 2536, Apr 2008.

[311] N. M. Oliveira, E. Martinez-Garcia, J. Xavier, W. M. Durham, R. Kolter, W. Kim, and K. R. Foster, "Biofilm formation as a response to ecological competition," *PLoS Biology* **13**(7), pp. 1–23, 2015.

[312] E. García Véscovi, F. C. Soncini, and E. A. Groisman, "Mg2+ as an extracellular signal: environmental regulation of Salmonella virulence.," *Cell* **84**, pp. 165–174, Jan 1996.

[313] B. Lories, S. Roberfroid, L. Dieltjens, D. De Coster, K. R. Foster, and H. P. Steenackers, "Biofilm Bacteria Use Stress Responses to Detect and Respond to Competitors," *Current Biology* **30**(7), pp. 1231–1244.e4, 2020.

[314] M. K. Paczosa and J. Mecsas, "Klebsiella pneumoniae: Going on the Offense with a Strong Defense.," *Microbiology and molecular biology reviews : MMBR* **80**, pp. 629–661, Sep 2016.

[315] J. K. Rudkin, R. M. McLoughlin, A. Preston, and R. C. Massey, "Bacterial toxins: Offensive, defensive, or something else altogether?," *PLoS pathogens* **13**, p. e1006452, Sep 2017.

[316] A. Ostrowski, F. R. Cianfanelli, M. Porter, G. Mariano, J. Peltier, J. J. Wong, J. R. Swedlow, M. Trost, and S. J. Coulthurst, "Killing with proficiency: Integrated post-translational regulation of an offensive Type VI secretion system.," *PLoS pathogens* **14**, p. e1007230, Jul 2018.

[317] E. T. Granato, T. A. Meiller-Legrand, and K. R. Foster, "The Evolution and Ecology of Bacterial Warfare," *Current Biology* **29**(11), pp. R521–R537, 2019.

[318] E. T. Granato and K. R. Foster, "The Evolution of Mass Cell Suicide in Bacterial Warfare.," *Current biology : CB* **30**, pp. 2836–2843.e3, Jul 2020.

[319] D. M. Cornforth and K. R. Foster, "Competition sensing: the social side of bacterial stress responses.," Apr 2013.

[320] A. Delhaye, J. F. Collet, and G. Laloux, "A Fly on the Wall: How Stress Response Systems Can Sense and Respond to Damage to Peptidoglycan," *Frontiers in Cellular and Infection Microbiology* **9**(November), 2019.

[321] S. Hunke, R. Keller, and V. S. Müller, "Signal integration by the Cpx-envelope stress system," *FEMS Microbiology Letters* **326**, pp. 12–22, Jan 2012.

[322] Z. Baharoglu and D. Mazel, "SOS, the formidable strategy of bacteria against aggressions.," *FEMS microbiology reviews* **38**, pp. 1126–1145, Nov 2014.

[323] B. Ezraty, A. Gennaris, F. Barras, and J.-F. Collet, "Oxidative stress, protein damage and repair in bacteria.," *Nature reviews. Microbiology* **15**, pp. 385–396, Jul 2017.

[324] C. L. Hews, T. Cho, G. Rowley, and T. L. Raivio, "Maintaining Integrity Under Stress: Envelope Stress Response Regulation of Pathogenesis in Gram-Negative Bacteria ," 2019.

[325] S. J. Coulthurst, A. M. L. Barnard, and G. P. C. Salmond, "Regulation and biosynthesis of carbapenem antibiotics in bacteria.," *Nature reviews. Microbiology* **3**, pp. 295–306, Apr 2005.

[326] C. Gabrielsen, D. A. Brede, I. F. Nes, and D. B. Diep, "Circular bacteriocins: biosynthesis and mode of action.," *Applied and environmental microbiology* **80**, pp. 6854–6862, Nov 2014.

[327] S. Coulthurst, "The Type VI secretion system: a versatile bacterial weapon.," *Microbiology (Reading, England)* **165**, pp. 503–515, May 2019.

[328] C. S. Hayes, S. K. Aoki, and D. A. Low, "Bacterial contact-dependent delivery systems.," *Annual review of genetics* **44**, pp. 71–90, 2010.

[329] J. van Gestel, T. Bareia, B. Tenennbaum, A. Dal Co, P. Guler, N. Aframian, S. Puyesky, I. Grinberg, G. G. D'Souza, Z. Erez, M. Ackermann, and A. Eldar, "Short-range quorum sensing controls horizontal gene transfer at micron scale in bacterial communities," *Nature Communications* **12**(1), p. 2324, 2021.

[330] M. E. Bianchi, "DAMPs, PAMPs and alarmins: all we need to know about danger.," *Journal of leukocyte biology* **81**, pp. 1–5, Jan 2007.

[331] E. C. Garcia, A. I. Perault, S. A. Marlatt, and P. A. Cotter, "Interbacterial signaling via Burkholderia contact-dependent growth inhibition system proteins," *Proceedings of the National Academy of Sciences* **113**, pp. 8296 LP – 8301, Jul 2016.

[332] D. A. Mavridou, D. Gonzalez, W. Kim, S. A. West, and K. R. Foster, "Bacteria Use Collective Behavior to Generate Diverse Combat Strategies," *Current Biology* **28**(3), pp. 345–355.e4, 2018.

[333] N. Obeng, A. A. Pratama, and J. D. van Elsas, "The Significance of Mutualistic Phages for Bacterial Ecology and Evolution," *Trends in Microbiology* **24**, pp. 440–449, Jun 2016.

[334] E. Cascales, S. K. Buchanan, D. Duché, C. Kleanthous, R. Lloubès, K. Postle, M. Riley, S. Slatin, and D. Cavard, "Colicin biology.," *Microbiology and molecular biology reviews : MMBR* **71**, pp. 158–229, Mar 2007.

[335] J. W. Arnold and G. B. Koudelka, "The TroJan Horse of the microbiological arms race: phage-encoded toxins as a defence against eukaryotic predators.," *Environmental microbiology* **16**, pp. 454–466, Feb 2014.

[336] J. A. Draghi and P. E. Turner, "DNA secretion and gene-level selection in bacteria.," *Microbiology (Reading, England)* **152**, pp. 2683–2688, Sep 2006.

[337] Y. Deng, H. Xu, Y. Su, S. Liu, L. Xu, Z. Guo, J. Wu, C. Cheng, and J. Feng, "Horizontal gene transfer contributes to virulence and antibiotic resistance of Vibrio harveyi 345 based on complete genome sequence analysis," *BMC Genomics* **20**(1), p. 761, 2019.

[338] K. L. Meibom, M. Blokesch, N. A. Dolganov, C.-Y. Wu, and G. K. Schoolnik, "Chitin induces natural competence in Vibrio cholerae.," *Science (New York, N.Y.)* **310**, pp. 1824–1827, Dec 2005.

[339] N. Matthey, S. Stutzmann, C. Stoudmann, N. Guex, C. Iseli, and M. Blokesch, "Neighbor predation linked to natural competence fosters the transfer of large genomic regions in Vibrio cholerae.," *eLife* **8**, Sep 2019.

[340] B. R. Wucher, M. Elsayed, J. S. Adelman, D. E. Kadouri, and C. D. Nadell, "Bacterial predation transforms the landscape and community assembly of biofilms.," *Current biology : CB* , Apr 2021.

[341] K. H. Thelin and R. K. Taylor, "Toxin-coregulated pilus, but not mannose-sensitive hemagglutinin, is required for colonization by Vibrio cholerae O1 El Tor biotype and O139 strains.," *Infection and immunity* **64**, pp. 2853–6, Jul 1996.

[342] V. de Lorenzo and K. N. Timmis, "Analysis and construction of stable phenotypes in gram-negative bacteria with Tn5- and Tn10-derived minitransposons," in *Methods in enzymology*, **235**, pp. 386–405, 1994.

[343] S. Borgeaud, L. C. Metzger, T. Scrignari, and M. Blokesch, "The Type VI Secretion System of Vibrio Cholerae Fosters Horizontal Gene Transfer," *Science* **347**(6217), 2015.

[344] D. W. Lazinski and A. Camilli, "Homopolymer tail-mediated ligation PCR: a streamlined and highly efficient method for DNA cloning and library construction.," *BioTechniques* **54**, pp. 25–34, Jan 2013.

[345] K. L. Meibom, X. B. Li, A. T. Nielsen, C.-Y. Wu, S. Roseman, and G. K. Schoolnik, "The Vibrio cholerae chitin utilization program," *Proceedings of the National Academy of Sciences of the United States of America* **101**(8), p. 2524, 2004.

[346] F. H. Yildiz and G. K. Schoolnik, "Role of rpoS in Stress Survival and Virulence of Vibrio cholerae," *Journal of Bacteriology* **180**(4), p. 773, 1998.

[347] E. M. Bik, R. D. Gouw, and F. R. Mooi, "DNA fingerprinting of Vibrio cholerae strains with a novel insertion sequence element: a tool to identify epidemic strains.," *Journal of Clinical Microbiology* **34**(6), p. 1453, 1996.

[348] P. K. Singh, D. K. H. Rode, P. Buffard, K. Nosho, M. Bayer, H. Jeckel, E. Jelli, K. Neuhaus, E. Jiménez-Siebert, N. Peschek, T. Glatter, K. Papenfort, and K. Drescher, "Vibrio cholerae biofilm dispersal regulator causes cell release from matrix through type IV pilus retraction," *bioRxiv* , p. 2021.05.02.442311, Jan 2021.

[349] D. O. Serra, A. M. Richter, G. Klauck, F. Mika, and R. Hengge, "Microanatomy at cellular resolution and spatial order of physiological differentiation in a bacterial biofilm.," *mBio* **4**, pp. e00103–13, Mar 2013.

[350] J. G. Malone, T. Jaeger, C. Spangler, D. Ritz, A. Spang, C. Arrieumerlou, V. Kaever, R. Landmann, and U. Jenal, "YfiBNR Mediates Cyclic di-GMP Dependent Small Colony Variant Formation and Persistence in Pseudomonas aeruginosa," *PLOS Pathogens* **6**, p. e1000804, Mar 2010.

[351] L. Friedman and R. Kolter, "Two genetic loci produce distinct carbohydrate-rich structural components of the Pseudomonas aeruginosa biofilm matrix.," *Journal of bacteriology* **186**, pp. 4457–4465, Jul 2004.

[352] N. Vojtov, H. F. Ross, and R. P. Novick, "Global repression of exotoxin synthesis by staphylococcal superantigens.," *Proceedings of the National Academy of Sciences of the United States of America* **99**, pp. 10102–10107, Jul 2002.

[353] K. Drescher, C. D. Nadell, H. A. Stone, N. S. Wingreen, and B. L. Bassler, "Solutions to the public goods dilemma in bacterial biofilms," *Current biology : CB* **24**(1), p. 50, 2014.

[354] K. R. Yamamoto, B. M. Alberts, R. Benzinger, L. Lawhorne, and G. Treiber, "Rapid bacteriophage sedimentation in the presence of polyethylene glycol and its application to large-scale virus purification," *Virology* **40**, pp. 734–744, Mar 1970.

[355] S. Beyhan and F. H. Yildiz, "Smooth to rugose phase variation in Vibrio cholerae can be mediated by a single nucleotide change that targets c-di-GMP signalling pathway," *Molecular Microbiology* **63**, pp. 995–1007, Feb 2007.

[356] J. Jyot, J. K. Gautam, M. Raje, and A. Ghosh, "Localization of DnaK and GroEL in Vibrio cholerae," *FEMS Microbiology Letters* **172**, pp. 165–171, Mar 1999.

[357] T. Dörr, H. Lam, L. Alvarez, F. Cava, B. M. Davis, and M. K. Waldor, "A Novel Peptidoglycan Binding Protein Crucial for PBP1A-Mediated Cell Wall Biogenesis in Vibrio cholerae," *PLOS Genetics* **10**, p. e1004433, Jun 2014.

[358] J. Sambrook, E. Fritsch, and T. Maniatis, *Molecular Cloning: a laboratory manual, 2nd Ed.*, Cold Spring Harbor Laboratory Press, 1989.

[359] K. Skorupski and R. K. Taylor, "Positive selection vectors for allelic exchange," *Gene* **169**, pp. 47–52, Feb 1996.

[360] D. G. Gibson, L. Young, R.-Y. Chuang, J. C. Venter, C. A. Hutchison, and H. O. Smith, "Enzymatic assembly of DNA molecules up to several hundred kilobases," *Nature Methods* **6**, pp. 343–345, May 2009.

[361] S. C. Iyer, D. Casas-Pastor, D. Kraus, P. Mann, K. Schirner, T. Glatter, G. Fritz, and S. Ringgaard, "Transcriptional regulation by σ factor phosphorylation in bacteria," *Nature Microbiology* **5**(3), pp. 395–406, 2020.

[362] J. Cox and M. Mann, "MaxQuant enables high peptide identification rates, individualized p.p.b.-range mass accuracies and proteome-wide protein quantification," *Nature Biotechnology* **26**, pp. 1367–1372, Dec 2008.

[363] J. Cox, N. Neuhauser, A. Michalski, R. A. Scheltema, J. V. Olsen, and M. Mann, "Andromeda: A Peptide Search Engine Integrated into the MaxQuant Environment," *Journal of Proteome Research* **10**, pp. 1794–1805, Apr 2011.

[364] J. Cox, M. Y. Hein, C. A. Luber, I. Paron, N. Nagaraj, and M. Mann, "Accurate Proteome-wide Label-free Quantification by Delayed Normalization and Maximal Peptide Ratio Extraction, Termed MaxLFQ," *Molecular & Cellular Proteomics* **13**, pp. 2513–2526, Sep 2014.

[365] C. E. Jahn, A. O. Charkowski, and D. K. Willis, "Evaluation of isolation methods and RNA integrity for bacterial RNA quantitation.," *Journal of microbiological methods* **75**, pp. 318–324, Oct 2008.

[366] P. H. Culviner, C. K. Guegler, and M. T. Laub, "A Simple, Cost-Effective, and Robust Method for rRNA Depletion in RNA-Sequencing Studies.," *mBio* **11**, Apr 2020.

[367] K. Kearney, "boundedline.m, GitHub.," 2021.

[368] J. Ahrens, B. Geveci, and C. Law, "36 - ParaView: An End-User Tool for Large-Data Visualization," pp. 717–731, Butterworth-Heinemann, Burlington, 2005.